Universiteit Leiden
The Netherlands

Chitin in the fungal cell wall: Towards valorization of spent biomass of Aspergillus niger

Leeuwe, T.M. van

Citation
Leeuwe, T. M. van. (2020, November 4). *Chitin in the fungal cell wall: Towards valorization of spent biomass of Aspergillus niger*. Retrieved from https://hdl.handle.net/1887/138011

Version:	Publisher's Version
License:	Licence agreement concerning inclusion of doctoral thesis in the Institutional Repository of the University of Leiden
Downloaded from:	https://hdl.handle.net/1887/138011

Note: To cite this publication please use the final published version (if applicable).

Cover Page

Universiteit Leiden

The handle http://hdl.handle.net/1887/138011 holds various files of this Leiden University dissertation.

Author: Leeuwe, T.M. van
Title: Chitin in the fungal cell wall: Towards valorization of spent biomass of *Aspergillus niger*
Issue date: 2020-11-04

Chitin in the fungal cell wall: towards valorization of spent biomass of *Aspergillus niger*

Tim M. van Leeuwe

ISBN: 978-94-6416-108-3
Author: Tim M. van Leeuwe
Cover & layout design: Tim M. van Leeuwe
Printing: Ridderprint BV, Ridderkerk, The Netherlands
Funding statement: This work is part of the “FunChi” ERA-IB project with project number ERA-IB-15-080, which is (partly) financed by the Dutch Research Council (NWO).

Copyright © T.M. van Leeuwe, 2020. All rights reserved.

Chitin in the fungal cell wall: towards valorization of spent biomass of *Aspergillus niger*

Proefschrift

ter verkrijging van

de graad van Doctor aan de Universiteit Leiden,

op gezag van Rector Magnificus prof. mr. C.J.J.M. Stolker,

volgens het besluit van het College voor Promoties

te verdedigen op woensdag 4 november 2020

klokke 13:45 uur

door

Tim Marijn van Leeuwe

geboren te Haarlem

in 1990

Promotoren:	Prof. dr. P.J. Punt
	Dr. A.F.J. Ram
Promotiecommissie:	Prof. dr. G.P. van Wezel
	Prof. dr. J.H. de Winde
	Prof. dr. A.H. Meijer
	Prof. dr. H.A.B. Wösten (Universiteit Utrecht)
	Prof. dr. B.M. Moeschbacher (Westfälische Wilhelms Universität)

Contents

CHAPTER 1

General Introduction

Filamentous fungi

Filamentous fungi are commonly found in all sorts of places on earth. Most people have a negative association with these fungi, causing black spots in poorly ventilated bathrooms or as food spoilers; found as green patches on old bread or as white fluffy mold in a jar of pesto that is past the due date. Despite this negative association, filamentous fungi have been used by humans for beneficial purposes. Universal examples are the fermentation of certain cheeses and dried sausages, but they are also used to produce soy sauce and antibiotics (e.g. penicillin). The term "filamentous" applies to these fungi because they grow as hair-like filaments that give them a fluffy appearance. The correct scientific name for these hair-like filaments is hyphae. These hyphae (singular = hypha) contain cells enveloped by a cell wall that extends laterally through cell division and also branches out sideways, similar to a branch from a tree. Hyphal extension and branching together are colloquially referred to as vegetative growth. During vegetative growth, compartmentalization occurs within the hyphae through the formation of walls to separate cells. However, these separating walls (septa, singular = septum) are porous which means that the cells stay physically connected to one another to form a large interconnected network, known as a mycelium. The mycelial lifestyle is very different from yeast-like unicellular fungi, where growth occurs through separation of mother and daughter cells into individual entities. In mushroom-forming fungi, these mycelial networks can grow to an impressive size and form fairy rings (Dutch: heksenkring) that can be characterized by a circle of mushrooms (fruiting bodies). Most filamentous fungi do not form such fruiting bodies and produce either sexual or asexual spores as a means of proliferation (Cole, 1996). Asexual reproduction is commonly found among filamentous fungi and has the upside of not having to invest in finding a mating partner for the production of (sexual) spores. Instead, such as in the case of the filamentous fungus *Aspergillus niger*, asexual spores are formed as genetically identical (clonal) cells from a single vegetative mycelium. To produce these asexual spores, aerial hyphae are formed that extend from the vegetative mycelium below. Then, *A. niger* forms vesicles on top of aerial hyphae that sprout asexual spore chains (Figure 1). The shapes and forms of which these asexual reproduction structures are formed vary greatly between different filamentous fungi and so do the number of spores produced.

Spores are quite easily distributed when a spore-chain is physically disturbed, for example by a breeze of wind or by the touch of an animal, allowing colonization far away from the parental mycelium. Because spores are hardy survival structures, they can remain dormant for quite some

time before they germinate. A spore will germinate upon finding favorable conditions (such as in that pesto jar), forming an initial germ tube that will be the first-formed hyphae (germling). From here on out, germlings grow into a vegetative mycelium that starts the lifecycle all over again. What these favorable conditions are, depends on the type of fungus and its preferred environment. These environments can be rougly categorized into either dead material (saprophytic) or living material (parasitic). Hence, fungi are very efficient in colonizing many different places on earth.

Fungi are in many ways very similar to animal and plant cells, all belonging to the domain of Eukaryotes (true nuclei). In addition to nuclei, eukaryotic cells also harbor other compartments such as endoplasmic reticula, Golgi apparvatus and mitochondria, that can be found in all kingdoms of

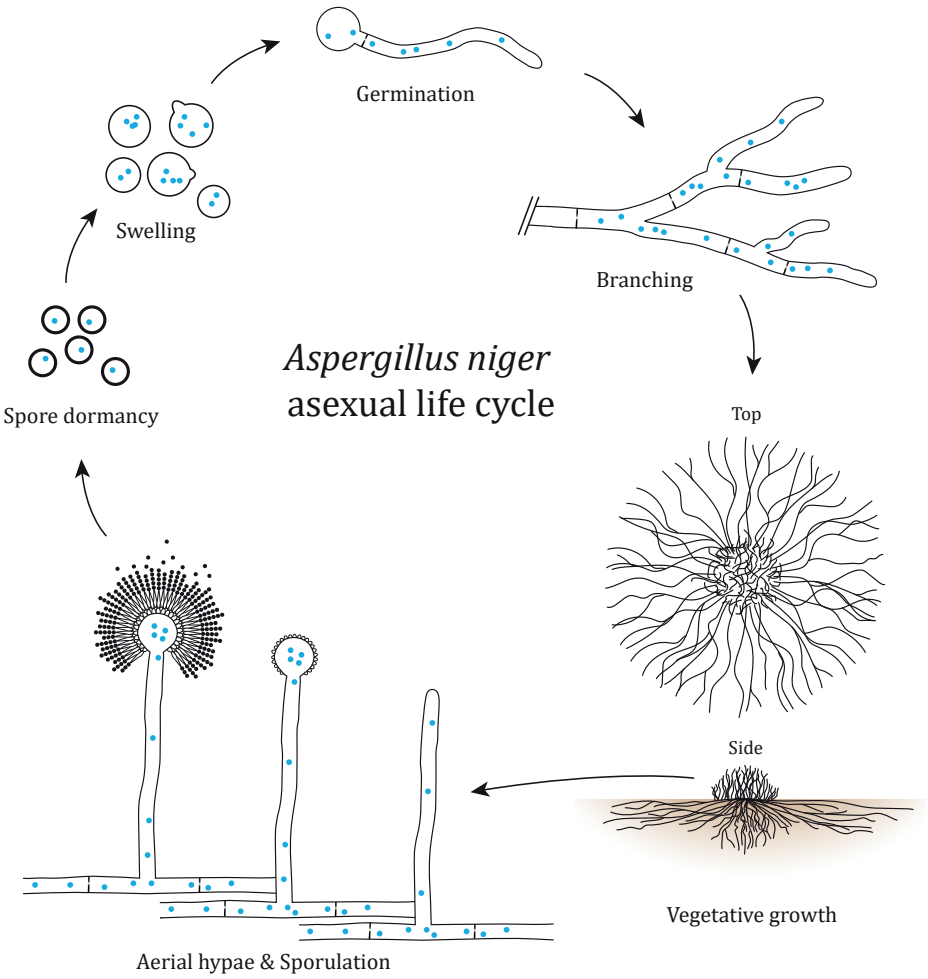

Figure 1. ***Aspergillus niger*** **asexual life cycle.**

Eukaryotes (Animalia, Fungi and Planta). When looking into more detail of what sets apart fungi from animals, we find that fungi possess a unique feature compared to animal cells: the cell wall. This cell wall dictates the shape of fungi and protects them from the outside world. Even though plants also have cell walls, fungal cell walls are very different in their compositional (polymeric) make-up. This difference in composition is one of the characteristics what makes filamentous fungi unique. This unique feature of the fungi is of interest for fundamental studies, but is also relevant for clinical/agricultural sectors to develop anti-fungal compounds (Garcia-Rubio et al., 2020), as infectious colonization of fungi is found in both kingdoms of Animalia and Planta. As mentioned above, the cellular similarity of fungi to both human and plant cells makes it difficult to specifically inhibit growth of fungi with antibiotic drugs, without affecting the host organism. An antibiotic drug that kills fungal cells due to an interaction with one of its cellular mechanisms is also likely to damage or kill the cells of animals, humans or plants crops. The cellular similarity between the kingdoms of Animalia, Planta and Fungi signifies why fungal research is important in the pursuit of finding and designing anti-fungal medication.

Besides infections and their potential danger, fungi have been (and will continue to be) used for the benefit of humanity. Common examples are cheese, beer, wine and fermented soy products, such as soy sauce. Less commonly known, but of high importance to (food)industry, is the use of filamentous fungi to produce different types of enzymes, antibiotics and organic acids. Organic acids, such as those that provide building blocks for other chemicals (Aurich et al., 2012) or those used as natural food flavor enhancers, acidifiers, stabilizers or preservatives (Magnuson and Lasure, 2004). A highly familiar example of citric acid application is in sugar-substituted Cola beverages. These either contain citric acid (light) or trisodium citric acid (zero), both for preservation and flavor and are also known as E330 and E331 food additives, respectively. Annual citric acid production quantities range up to 900,000 metric tons and is by far the largest organic acid made through fermentation, primarily by *A. niger* (Karaffa and Kubicek, 2003). Another organic acid, itaconic acid, is naturally produced by *Aspergillus terreus* (Bentley and Thiessen, 1957), and has its primary application in the polymer industry as a co-monomer, but is additionally used to manufacture coatings, adhesives and synthetic fibers (Magnuson and Lasure, 2004). However, *A. terreus* produces itaconic acid in less than economically feasible quantities (Weastra, 2011). Genetic engineering of *A. niger* has successfully led to production of itaconic acid to respectable titers for industrial production (Hossain et al., 2016). Both the production of plant cell wall degrading enzymes (e.g. to hydrolyze plant biomass to produce sugars which can be converted to bio-ethanol by yeasts) and production of organic acids of *A. niger* are two major exploits used by biotechnological industries (Cairns et al., 2018). Yet, another organic acid, lactic acid, is often used as a food preservative, flavor enhancer and acid regulator and can also be used as a precursor for the production of a biodegradable plastic: Poly Lactic Acid (PLA). The majority of lactic acid is produced by bacteria of the Genera *Lactobacillus* and *Bacillus*, but also fungi are capable of the production of this industrially promising organic acid. One of these is *Rhizopus oryzae*, a fungus traditionally used for the fermentation of soy to create tempeh (Magnuson and Lasure, 2004).

Next to large scale organic acid production, the production of enzymes can also be facilitated by fungi, including recombinant and genetically engineered, optimized enzymes. In 2016, annual world sales of enzymes by filamentous fungi are estimated at ca. 4.7 billion euros, which is expected to double in the next 10 years (Meyer et al., 2016). Both the production of enzymes and the use of cell factories for the biosynthesis of other products require large scale fermentations of micro-organisms, such as bacteria, yeasts, fungi. The best suited organism depends on each different enzyme, but in the case of filamentous fungi, *Aspergillus spp., Penicillium spp., Fusarium spp.* and *Trichoderma spp*. are most commonly used.

Aspergillus niger

The filamentous fungus *Aspergillus niger* is a haploid, saprophytic member of the phylum Ascomycota and is frequently used for industrial purposes as described above. The Genus "*Aspergillus*" was coined by its first discoverer in 1729, Pier Antonio Micheli, who found resemblance between the spore-bearing structure of the fungus and an "aspergillum", an object used by Roman Catholic clergy to sprinkle holy water (Bennett, 2010). The species name "*niger*" owes its name to the black color of the heavily melanized spores, providing protection from harmful UV-radiation. In our daily lives, the most likely place to encounter *A. niger* is in the form of black conidia on the outside of onions (Gherbawy et al., 2015).

A. niger has been reported to produce only asexual spores, but may yet have a cryptic sexual cycle (Dyer and O'Gorman, 2012) as it is also able to produce sclerotia (Frisvad et al., 2014; Jørgensen et al., 2020). Sclerotia are a type of macrostructure of aggregating hyphae that resemble the shape of psychedelic sclerotial "magic truffles" that one can buy in Dutch smartshops. These very hardy sclerotial structures are commonly formed by many fungal species and come in various shapes and sizes. In case of *A. niger*, this is the size of a sesame seed. It has been postulated that sclerotia formation has an evolutionary advantage as a way to survive adverse environmental conditions such freezing, drought, nutrient depletion or microbial attack (Smith et al., 2015). In addition to enhancing survivability in hostile environments, sclerotia formation is considered to be part of the sexual reproduction process in certain filamentous fungi (Smith et al., 2015). For example, in *Aspergillus flavus*, a known opportunistic pathogen and common spoiler of peanuts and peanut butter (Adeyeye, 2016), the sclerotia have been shown to also act as reproductive structures that contain ascospores (Horn et al., 2009). In studies of *A. niger*'s sclerotia (Frisvad et al., 2014; Jørgensen et al., 2020), the correct genetic requirements to induce sexual spore formation (two opposite mating types) have not been met. This means that the existence of a true sexual cycle of *A. niger* remains elusive, for now.

Because the existence of a sexual cycle can be very useful for genetic investigation of *A. niger*, a workaround technique has been developed—which is also used in the research described in this thesis (**Chapter 4** and **Chapter 5**)—known as the parasexual cycle (Pontecorvo et al., 1953). A schematic representation of how this process works is shown in Figure 2. The parasexual cycle

is a technique to redistribute/shuffle the chromosomes from both parents without true meiosis. Crucially, this means that there is no meiotic cross-over, only sparce mitotic cross-over events. In essence, two auxotrophic haploid *A. niger* strains are coerced to fuse (anastomosis) and then undergo cytoplasmic mixing (plasmogamy) based on non-complementary auxotrophic deficiencies (Figure 2A and B). Post-fusion a mycelium with two types of haploid nuclei (heterokaryon) will form, shown in Figure 2C. On low chance occurrence, nuclei in this heterokaryon can undergo karyogamy (nuclear fusion), resulting in a heterozygous diploid. In addition to the auxotrophic markers, the use of visually distinguishable color markers (specific complementation groups of in melanin synthesis, Jørgensen et al., 2011) may be added to visually track karyogamy in time.

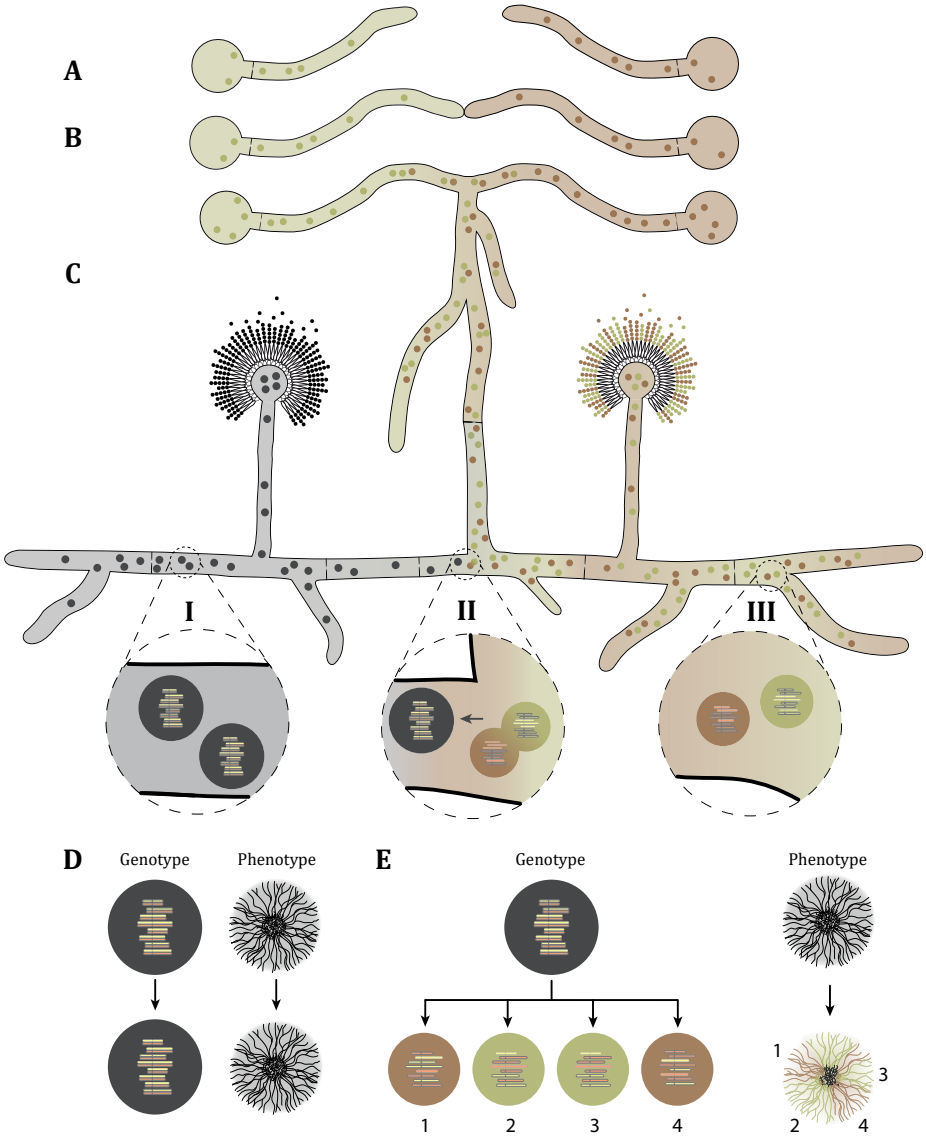

Figure 2. The parasexual cycle of *Aspergillus niger*. (A) Two complementary, haploid auxotrophic strains carrying different spore color mutations, *ΔbrnA* or *ΔolvA*, (Jørgensen et al., 2011b). (B) Initiation of directed hypal fusion, called anastomosis. Complementary auxotrophic strains are coerced to undergo plasmogamy (the fusion of cytoplasm) in absence of nutrients required for either of the two parental strains (C) Following plasmogamy, a heterokaryotic mycelium is formed that contains nuclei from both strains. On rare-chance occurrence, a heterozygous diploid (I) is formed through karyogamy, the fusion of nuclei from both parental strains (II). A heterozygous diploid forms black spores due to complementation of both parental spore color mutations. Without karyogamy, a heterokaryotic mycelium (III) produces the two parental type uninuclear, haploid spores, unable to germinate in the absence of the required nutrient supplementation. (D) The heterozygous diploid has a uniform spore color phenotype. (E) Benomyl induced haploidization of a heterozygous diploid. Benomyl destabilizes chromosome segregation that causes random distribution of chromosomes from either parent into haploid segregants with all different spore color and nutrient phenotypes.

Haploid heterokaryons produce spores of either genotype resulting in different spore colors, based on the fact that spores are generally uninuclear—or at least have clonal nuclei—whereas a heterozygous diploid will have black spores. A diploid is stable (Figure 2D), but can be artificially haplodized into haploid segregants upon addition of benomyl (Arentshorst and Ram, 2018). Benomyl destabilizes chromosome segregation, causing random distribution of chromosomes that result in all different color marker and nutrient phenotypes (Figure 2E).

A. niger is a saprobe, meaning that it thrives on decaying organic matter. As such, it secretes enzymes into its environment to degrade complex plant (cell wall) polysaccharides maily to release either dimeric or monomeric sugars. As described previously, *A. niger* is able to convert these sugars into large amounts of organic acid. These organic acids can then be consumed at later stage after sugar depletion. The conversion of sugar into acid(s)—thereby acidifying the surroundings—has been postulated to act as evolutionary benefit (Andersen et al., 2009), keeping other microbes at bay that would otherwise try to snatch the plant-cell-wall-released sugars from *A. niger*. Contrarily to the natural soil habitat of *A. niger*, industrial profiteering of *A. niger*'s secreted compounds is attained from submerged cultivation in large bioreactors. These bioreactors range in volume from a few hundred to up to more than hundred thousand liters. These (unnatural) liquid growth conditions cause *A. niger* to either grow dispersed, as clumps (germlings sticking together) or even as larger aggregates: pellets (P. Krijgsheld et al., 2013). In these submerged growth conditions, *A. niger* is able to produce large quantities of aforementioned products, while also converting much of the energy into acquisition of fungal biomass. When the secreted products (enzymes or organic acids) have been obtained, the remaining mycelial biomass is a left-over product. Currently, this mycelium is typically used as a low-cost fertilizer for agricultural crop plant production or as cattle feed (NRC, 1983). However, these disposal routes are a significant cost factor in the biotechnological production process, and clearly under-exploit this potentially precious material.

The potential of cell walls in mycelial waste

As the number of industrial scale fungal fermentation increases, so does the accumulation of fungal biomass waste. Most of the dry weight of the mycelial biomass is comprised of polymers from

fungal cells (50-80%) that may be of high value when extracted (Isaza-Pérez et al., 2020). These cell wall polysaccharides are mainly made up of differently linked monomers of either glucose, (*N*-acetyl-)glucosamine, galactose or mannose (Free, 2013; Gow et al., 2017; Ruiz-Herrera and Ortiz-Castellanos, 2019). Glucose residues can be found in either an α-linked or β-linked orientation, such as α-1,3-glucan, mixed α-1,3/1-4-glucans or β-1,3-glucan, β-1,6-glucan and mixed β-1,3/1,4 or β-1,3/1,6 glucan variations, and comprise the major fraction of the fungal cell wall. The second most abundant polymer of fungal cell wall is chitin. Chitin is also found in the exoskeletons of crustaceans (shell fish), insect cuticles and squid gladius/pen (the hard, internal body part that you may find on the beach). As such, chitin also happens to be second-most abundant world-wide, after cellulose (present in the cell walls of plants (Kaur and Dhillon, 2014). Comprised of β-1,4-linked *N*-acetylglucosamine monomers (GlcNAc), chitin naturally occurs as either one of three different crystalline, polymorphic forms: α-chitin, β-chitin or γ-chitin (Rudall and Kenchington, 1973). Fungal cell walls only harbor α-chitin which consists of anti-parallel GlcNAc chains that form the strongest type of intrachain hydrogen bonds of all chitin forms. A small percentage of the cell wall contains de-acetylated chitin (i.e. lack the (*N*-linked) acetyl group on the glucosamine monomer which liberates the amino group NH_2). The definitions of chitin and chitosan are based on the degree of acetylation (DA); any given β-1,4-(*N*-acetyl) glucosamine polymer that contains a DA ≥ 50%, is termed chitin, whereas if the DA < 50%, the term is chitosan (Muzzarelli, 1973; Pillai et al., 2009).

Variation in DA and degrees of polymerization (DP), molecular weight and pattern of charge distribution of chitin/chitosan determine the active properties and solubility of chitosan, giving rise to a wide range of applications in biomedical, pharmaceutical and agricultural sectors (El Gueddari et al., 2014; Rinaudo, 2006). Many (potential) applications have recently been reviewed and include promotion of wound healing, anti-microbial activity, but also anti-tumor, anti-inflammatory, immuno-stimulating, anti-diabetic, anti-Alzheimer's and anti-HIV activity, just to name a few (Naveed et al., 2019). In addition, chitosan can be used to inhibit microbial growth and extend the shelf-life of fresh produce as edible coatings, either by itself or combined with other natural (anti-microbial) biomaterials (Yousuf et al., 2018). Furthermore, chitosan has been shown to be an environmentally-friendly alternative for pesticides in disease control due to antimicrobial activity (Orzali et al., 2017). A broad spectrum of antimicrobial activity of chitosan has been described for both phytopathogenic fungi and bacteria, such as the fungi *Botrytis cinerea,* infectious to grapevine and strawberry (Feliziani et al., 2015; Reglinski et al., 2010), and *Rhizoctonia solani*, infectious to multiple crops, e.g. potatoes, sugar beet, cucumber and rice (Liu et al., 2012), but also bacteria *Agrobacterium tumefaciens* (crown gall disease – formation of tumors) and *Erwinia carotovora* (both multi-crop pathogens) (Badawy et al., 2014). Application of chitosan-mediated antimicrobial defense is often achieved by either amending soil or by coating of plant seeds, both treatments which have been shown in inhibit *Fusarium* infections (Bell et al., 1998; Lafontaine and Benhamou, 1996; Orzali et al., 2014). Aside from anti-microbial activity, chitosan addition to healthy plants enhanced seedling growth, total biomass production, crop yields (Corsi et al., 2015; Kowalski et al., 2006; Lizárraga-Paulín et al., 2013; Utsunomiya et al., 1998; Ziani et al.,

2010), and have also been found to protect plants against abiotic factors such as drought (Zeng and Luo, 2012). The effects of chitosan on plant protection are more extensively reviewed in Hidangmayum et al., 2019. The main mode of action in which chitosan achieves these feats is through electrostatic interactions with other molecules—through their protonated amino (NH_3^+) groups—causing plasma membrane damage, chitosan-DNA/RNA interactions, metal chelation, but also elicit plant defense responses through receptor binding, as well as affecting complex signal transduction networks (Xing et al., 2015). The almost innumerable range of applications that have been shown to positively use chitosan or substitute current plant treatments, signify the likely increase in demand for chitin and chitosan in the future. The large left-over fungal mycelial biomass production that currently being discarded could thus provide a means to close the gap in the market.

Exploitation of fungal chitin – challenges and perspectives

Currently, large scale commercial production of chitosans proceeds almost exclusively from shrimp and crab shell wastes through hot alkali extractions (Aranaz et al., 2009; Roberts, 1992). The chitosan obtained by such treatments shows inconsistent levels of de-acetylation, high molecular weight and protein contamination, which results in variable physico-chemical characteristics (Knorr & Klein, 1986; No and Meyers, 1997). Additional problems associated with these sources concern varying qualities due to seasonal variations, and spoilage during storage and transport (Aranaz et al., 2009). Also, animal origin *per se* poses a problem for certain markets, either due to consumer preferences such as in cosmetics, or due to regulatory issues concerning possible contaminations with allergens or viruses, particularly in the biomedical and pharmaceutical markets (Dhillon et al., 2012). Finally, the limited regional supply of raw material does not allow truly large-scale chitosan production from these sources, and traceability of the material back to the original source is also difficult in most cases.

A. niger provides a valuable source for chitin/chitosan not only because of its large scale production quantities, but also because of its already relatively high (~16%) extractable chitin/chitosan content (Isaza-Pérez et al., 2020). Extraction of chitin/chitosan from fungal cell walls is not too difficult, but necessitates rather harsh alkali extraction conditions (as mentioned above). High molarity alkali exposure can lead to uncontrolled partial de-polymerization and partial de-acetylation (Dhillon et al., 2012; Klis et al., 2007). This translates to low chitosan yields that are of poor quality in terms of polymer size and purity (Dhillon et al., 2012; Maghsoodi et al., 2009). Alkali extraction has only been scaled up to the extent that fungal chitosan is available in limited quantities on the market today (Dhillon et al., 2013). An alternative, but less cost-efficient strategy, involves enzymatic degradation of the cell wall, which can lead up to a 3-fold increase in chitosan yield along with increased polymer size (Cai et al., 2006).

Next to cultivation conditions and extraction methods, we hypothesized that the covalent linkages between chitin and glucans present in the fungal cell walls (Arroyo et al., 2016) may hamper

extraction and may cause impurity in fractionation. In *S. cerevisiae*, this covalent chitin/glucan linkage—the nature of which is not entirely understood in filamentous fungi—has been shown to be removed upon deletion of the genes encoding specific cross-linking enzymes. The genes encoding these cross-linking enzymes were named after their hypersensitivity to Congo Red (Crh), a cell wall disturbing compound, that signified the importance of these enzymes in cell wall integrity (Rodríguez-Peña et al., 2000b). Later, it was shown that removal of the Crh enzymes completely separated the chitin from the glucan fraction in the cell wall (Cabib, 2009; Cabib et al., 2007). As such, cell wall chitin from glucan separation may provide a valuable method of enhancing chitin extraction with both higher quantatiy and purity.

In order to use mycelial biomass waste as an economically feasible source of chitin/chitosan that can compete with the current chitosan production from shrimp waste, two major issues need to be addressed: (i) The overall chitin content in fungal cell walls should be boosted to increase yields. (ii) To enhance the extraction of chitin from the fungal cell walls, removal of covalent linkages between chitin and glucan is required. The work in this thesis addresses both of these topics by using a forward genetics screens to identify high chitin producing fungal strains and through complete removal of the seven *crh* genes encoding chitin-glucan crosslinking enzymes in a single *A. niger* strain.

Outline of the research presented in this thesis

Aspergillus niger is an important industrial producer of organic acids and enzymes producing large amounts of spent fungal biomass. In the European Research Area Industrial Biotechnology (ERA-IB) funded project, we effectively aimed to improve the composition of post-fermentation fungal biomass for extraction of the value-added product chitosan as a derivative of cell wall chitin (FunChi). The chapters of this thesis following this introductory chapter (**Chapter 1**), will discuss the identification of genes that are important for chitin deposition in the cell wall of *A. niger*, and also specifically discuss the genes that facilitate chitin cross-linking to the cell wall.

To enable mutant strain construction, **Chapter 2** describes the development of a very efficient and recyclable, marker free CRISPR/Cas9-based gene-editing system for *A. niger*. Using this system, we generated a complete seven-fold knockout of a cell wall chitin cross-linking enzyme family. By doing so, we aimed to understand the effect of removing Crh enzymes that covalently link chitin to the cell wall on cell wall integrity as a proxy for chitin extractability. The effects on morphology, cell wall composition and transcriptomic response in the seven-fold deletion mutant are discussed in **Chapter 3**. The results show that removal of the *crh* gene family does not affect cell wall composition, and the experiments hint towards an important relation between chitin and α-glucan to compensate for *crh* loss. In addition, we identified and characterized *A. niger* mutant strains with increased cell wall chitin deposition by exploiting the cell wall chitin compensatory response of the cell wall integrity pathway. Using the cell wall stress mutant library (Damveld et al., 2008), we screened mutants for increased cell wall chitin deposition. Two selected mutants

were characterized using classical genetics (parasexual crossing) combined with genome sequencing. Identified SNPs were carefully re-created in a wild type strain using CRISPR/Cas9 gene editing to confirm single gene involvement (discussed in **Chapter 4** and **Chapter 5**, respectively). These genes are a transcriptional repressor of cell wall chitin (*cwcA*) and Rab GTPase dissociation inhibitor (*gdiA*). Next to the cell wall mutant library, an industrially favorable hyperbranching *A. niger* mutant was selected and tested for increased chitin deposition. The mutant strain in question, *ΔkexB*, was chosen for its visibly thicker and shorter hyperbranched hyphae, resulting in a low-viscosity fermentation phenotype, a favorable trait in large scale fermentations. Effects of this gene deletion are discussed in relation to its morphology, transcriptome and cell wall chitin phenotype in **Chapter 6**. The results showed an increase in cell wall chitin content; however, this was not related to its hyperbranching phenotype. An overall discussion of all findings relating to the FunChi project, and an outlook to the future, are presented in **Chapter 7**.

1

CHAPTER 2

Efficient marker free CRISPR/Cas9 genome editing for functional analysis of gene families in filamentous fungi

Tim M. van Leeuwe, Mark Arentshorst, Tim Ernst, Ebru Alazi, Peter J. Punt, Arthur F.J. Ram

ABSTRACT

CRISPR/Cas9 mediated genome editing has expedited the way of constructing multiple gene alterations in filamentous fungi, whereas traditional methods are time-consuming and can be of mutagenic nature. These developments allow the study of large gene families that contain putatively redundant genes, such as the seven-membered family of *crh*-genes encoding putative glucan–chitin crosslinking enzymes involved in cell wall biosynthesis. Here, we present a CRISPR/Cas9 system for *Aspergillus niger* using a non-integrative plasmid, containing a selection marker, a Cas9 and a sgRNA expression cassette. Combined with selection marker free knockout repair DNA fragments, a set of the seven single knockout strains was obtained through homology directed repair (HDR) with an average efficiency of 90%. Cas9–sgRNA plasmids could effectively be cured by removing selection pressure, allowing the use of the same selection marker in successive transformations. Moreover, we show that either two or even three separate Cas9–sgRNA plasmids combined with marker-free knockout repair DNA fragments can be used in a single transformation to obtain double or triple knockouts with 89% and 38% efficiency, respectively. By employing this technique, a seven-membered *crh*-gene family knockout strain was acquired in a few rounds of transformation; three times faster than integrative selection marker (*pyrG*) recycling transformations. An additional advantage of the use of marker-free gene editing is that negative effects of selection marker gene expression are evaded, as we observed in the case of disrupting virtually silent *crh* family members. Our findings advocate the use of CRISPR/Cas9 to create multiple gene deletions in both a fast and reliable way, while simultaneously omitting possible locus-dependent-side-effects of poor auxotrophic marker expression.

This chapter is published as: van Leeuwe, T.M., Arentshorst, M., Ernst, T., Alazi, E., Punt, P.J., Ram, A.F.J., Fungal Biol Biotechnol 6, 13 (2019). doi: 10.1186/s40694-019-0076-7

1. INTRODUCTION

The fungal cell wall is comprised of a series of different polymeric sugars, such as alpha-glucans, beta-glucans, chitin (poly-1,4-linked N-acetyl-glucosamine), galactomannans and mannoproteins. These structural components are synthesized by membrane localized alpha-glucan synthases (Ags-proteins), beta glucan-synthases (Fks- or Bgs-proteins), chitin synthases (Chs-proteins) or are assembled in the secretion pathway (galactomannans and mannoproteins). For an extensive review on cell wall organization and biosynthesis we refer to Free, 2013 (Free, 2013). The individual components are often cross-linked to each other by extracellular transglycosidases including the beta-glucan crosslinking enzymes (Gas or Gas1p/GEL1/Phr1p family-proteins (Fonzi, 1999; Hartland et al., 1996; Mouyna et al., 2000) or beta-glucan-chitin cross linking enzymes (Crh/Utr family-proteins (Cabib et al., 2008, 2007; Rodriguez-Peña et al., 2002; Rodríguez-Peña et al., 2000a). For a comprehensive review on glucan-chitin cross-linking we refer to Arroyo et al., 2016 (Arroyo et al., 2016). The interlinked cell wall matrix forms the physical barrier between the outside world and the inside of the cell, providing structural integrity and protection from biotic and abiotic factors.

Genome sequences of filamentous fungi, including *Aspergillus niger,* have shown that these cell wall related synthases and crosslinking enzymes often consist of large gene families. For example, the *A. niger* genome contains five Ags homologs, nine Chs homologs, seven Gas/GEL homologs and seven Crh-homologs (Pel et al., 2007). The high number of genes in these families may correlate to the complexity of the multicellular, filamentous life style and offers the fungus to regulate the expression of these genes both in time and space during development or in response to stress. To perform functional analysis and determine possible redundancy of genes within a gene family, the construction of a single strain with multiple gene deletions is desirable.

Current methods to create multiple gene deletions in *A. niger* include the use of the *pyrG* or *amdS*-based transformation system combined with the subsequent recycling of *pyrG* or *amdS* via counter selection approach using 5-fluoroorotic acid (5'-FOA) or 5-fluoro-acetamide (5-FAA) (Arentshorst et al., 2015), respectively. Another approach is the use of multiple auxotrophic strains, but limits one to a total of four separate selection markers in *A. niger* (*pyrG, nicB, argB, adeA*) (Niu et al., 2016b). Dominant markers such as hygromycin or phleomycin resistance genes (Punt and van den Hondel, 1992) can additionally be used. The recycling method is time consuming and the use of auxotrophic markers require supplementation when not all auxotrophic markers are used which can influence the growth phenotype of the strain, and both are therefore undesirable.

Alternatively, the CRISPR/Cas9 era has opened up the possibility to target and alter genes in an effective way with the potential to be selection marker free, hypothetically allowing limitless genetic alterations. For *A. niger*, several studies have been published to demonstrate the potential of CRISPR/Cas9, yet many still rely on the integration of selection marker in which the repair DNA fragment either remains integrated (Kuivanen et al., 2016; Sarkari et al., 2017; Zheng et al., 2019) or allows subsequent "pop-out" (*pyrG*) using 5'-FOA counter selection (Dong et al., 2019;

Leynaud-Kieffer et al., 2019). Additionally, some studies have reported the use of marker-free deletion of single genes in one transformation, using repair DNA fragment(s) in combination with either integrative pUC-based plasmids (Zhang et al., 2019) or plasmids with self-replicating extrachromosomal AMA1 elements (Nødvig et al., 2018a; Song et al., 2018). As such, these developments have expedited the possibility to target multiple genes in a single transformation and thereby increase efficiency of strain construction. However, no studies have reported on the ability to multiplex knockouts of different genes in a single transformation without the use of integrative selection markers. To circumvent the time-consuming recycling of markers or the use of multiple auxotrophic strains to generate multiple gene deletion mutants, we demonstrate a marker-free CRISPR/Cas9-based transformation procedure. This procedure allows us to knock out multiple genes in one transformation in which the transformed strain can immediately be reused for subsequent transformations, if desired. Moreover, this marker-free approach excludes the possibility for "position effects" from genomic loci with low overall gene expression causing lack of marker gene expression (Bok et al., 2006; Greenstein et al., 2006; Oestreicher et al., 2008; Robellet et al., 2010). Here, efficiency of multiplex knockout strain construction is demonstrated, using Cas9-sgRNA plasmids together with marker-free repair DNA fragments by knocking out the seven-membered cell wall chitin cross-linking gene family (*crhA-G*), without using an obvious selectable phenotype.

2. METHODS

2.1 Strains, media, growth conditions and transformations

A. niger strains MA234.1 (*cspA1, ΔkusA::DR-amdS-DR*) (Park et al., 2016) and MA169.4 (*cspA1, ΔkusA::DR-amdS-DR, pyrG*)(Carvalho et al., 2010) were used in this study. Strains used in this study can be found in Table 2. All media were prepared as described by Arentshorst et al., 2012. In all cases minimal medium (MM) contained 1% (w/v) glucose, 1.5% agar and was supplemented when required with either uridine (10mM) or hygromycin (100 μg/mL). Complete medium (CM) contained 1% (w/v) glucose, 1.5% agar (Scharlau, Barcelona, Spain), 0.1% (w/v) casamino acids and 0.5% (w/v) yeast extract in addition to MM. To harvest spores, strains were first inoculated from -80°C glycerol stocks onto fresh CM plates and were allowed to grow and sporulate for 5-7 days at 30°C. Spores were harvested by addition of 15 mL of 0.9% (w/v) NaCl to CM spore plates and were gently scraped from the plate surface with a cotton stick. Spore solution was pipetted through sterile cotton filters (Amplitude™ Ecocloth™ Wipes, Contec Inc., Spartanburg, SC, USA) to eliminate large mycelial debris.

Strains were transformed after protoplastation as described previously (Arentshorst et al., 2012). We used 2 μg of Cas9-sgRNA plasmid with approximately 2 μg of repair DNA fragment (1.8 – 2.0kbp) for each transformation. Transformation plates were incubated on MMS containing hygromycin (200 μg/mL) for 6 days at 30°C. Transformed colonies were single streaked on MM containing hygromycin (100 μg/mL) to ensure nuclei of spores harbor the Cas9-sgRNA plasmid, thus

are most likely to be transformed. Next, a single colony was picked and transferred to non-selective MM medium to allow loss of the Cas9-sgRNA plasmid. A third streak of a single colony on both MM containing hygromycin (100 µg/mL) and MM acts as a control for loss of plasmid. DNA from plasmid-cured strains was isolated as described by Arentshorst et al., 2012, using mortar and pestle to grind the mycelium in liquid nitrogen.

2.2 CRISPR/Cas9 plasmid design

To express Cas9 and the guide RNA from the same autonomously replicating vector using hygromycin as a selection marker for fungal transformation, plasmid pFC332 was used (Nødvig et al., 2015). pFC332 contains a unique *Pac*I site which was used to insert a single guide RNA (sgRNA) expression cassette based on the native *A. niger* RNA polymerase type III Pro[1]-promoter and terminator (Song et al., 2018). The PCR strategy to generate sgRNA expression cassettes is schematically shown in Figure 1. The strategy is based on designing overlapping PCR fragments containing the Pro[1]-promoter region followed by the reverse complemented sgRNA target, and a second PCR fragment containing the target followed by the sgRNA and terminator regions. Complementary target sequences of both PCR products allow fusion through PCR with outer primers (pTE1_for and pTE1_rev) to amplify the entire sgRNA expression cassette. These primers introduce a *Pac*I site on either end of the construct for cloning into pFC332 (Figure 1B).

Template plasmids for amplification of new sgRNA expression cassettes were made by amplifying the Pro[1]-promoter from ANEp8_Cas9_sgRNA-albA (Song et al., 2018) with pTE1_for (Figure 1A) to include *Pac*I restriction site with a CC overhang (5' – CCttaattaa – 3') and OTL487. Resulting PCR product (*Pac*I::Pro[1]-promoter) was cloned directly into pJET1.2/blunt cloning vector (Thermo Scientific™) to yield pTLL108.1. Similarly, the sgRNA::Terminator was amplified through PCR from ANEp8_Cas9_sgRNA-albA with OTL488 and pTE1_rev (Figure 1) to include *Pac*I restriction site and CC overhang (sgRNA::Terminator::*Pac*I), and was cloned into pJET1.2/blunt to yield pTLL109.2 (data not shown).

The sgRNA targets were designed using the CHOPCHOP web-tool (Labun et al., 2016). Putative targets were obtained using the *A. niger* NRRL3 genomic sequence of the gene of interest (GOI) submitted in FASTA format with default CRISPR/Cas9 settings. The *A. niger* was used as reference genome for off-target matching. A selected, variable target sequence of 20bp (without 5' NGG 3' PAM sequence) was added as overhang to target specific primer pTarget (Figure 1A) in the identical forward orientation, whereas the reverse complement (RC) target sequence was added as overhang to target specific primer pRC-target (Figure 1A).

The sgRNA expression cassette was acquired through fusion of two PCR products, the 5' flank and the 3' flank. pTE1_for (5' – ccttaattaaACTCCGCCGAACGTACTG – 3') was used in combination with pRC-target on template plasmid pTLL108.1 to produce a 264bp *Pac*I::Pro[1]-promoter::target sequence (5' flank). Combined primer pair pTarget and pTE1_rev (5' – ccttaattaaAAAAGCAAAAAAGGAAGGTACAAAAAAGC – 3') was used on template plasmid pTLL109.2 to create the 133bp target::trRNA::Terminator::*Pac*I sequence (3' flank). After gel purification, the 5' flank was

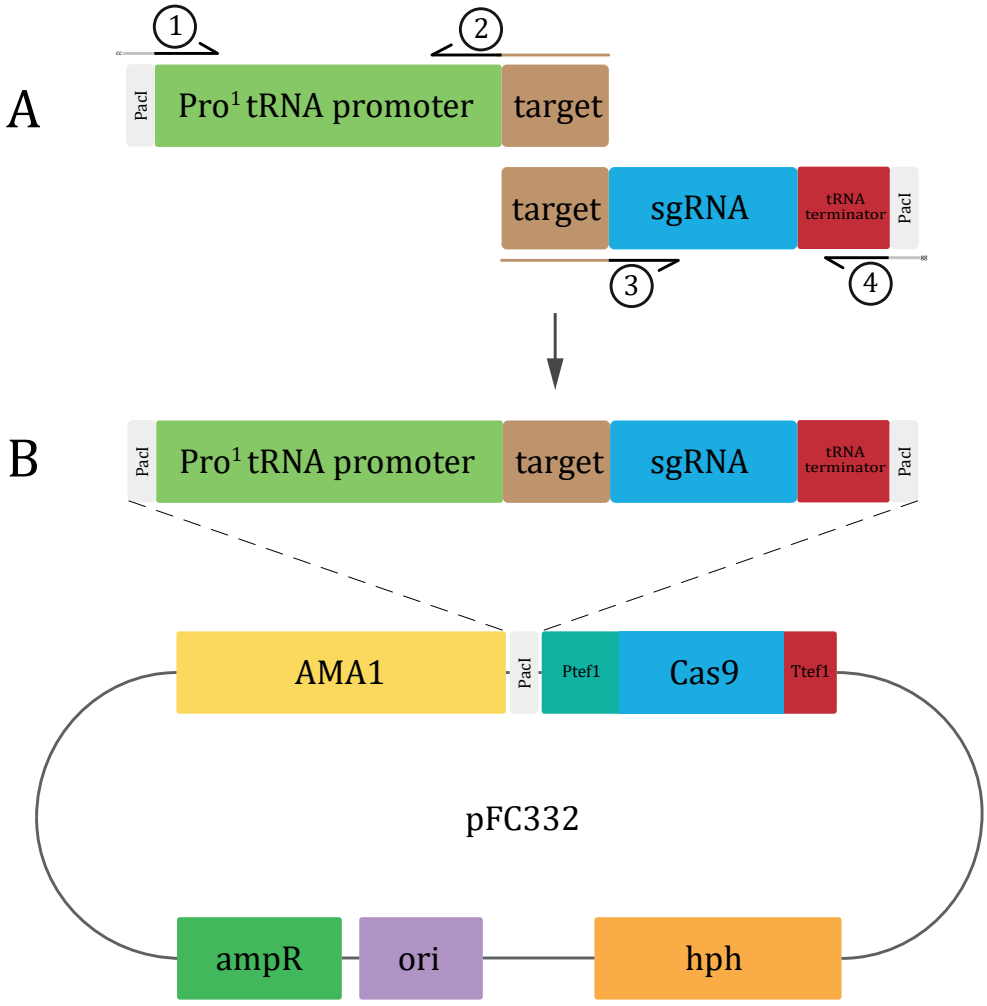

Figure 1. Schematic representation of the pFC332_Pro[1]-sgRNA plasmid construction. (A) Amplification of the two flanks that represent the Pro[1]-sgRNA expression cassette: pTE1_for and pRC-target are used to amplify the Pro[1]-tRNA promoter and target sequence, where pRC-target contains a variable 20bp overhang (indicated by brown color) that represents the reverse complement target sequence of choice. In turn, pTarget and pTE1_rev are used to amplify the target-sgRNA-Pro[1]-tRNA terminator flank. Here, pTarget contains a variable overhang that contains the target sequence of choice. Separate flanks are joined together through fusion PCR by pTE1_for and pTE1_rev, where the overhang sequence (=target) fvacilitates the homologous region between both flanks. (B) Addition of *Pac*I sites to either end of the fusion construct (part of pTE1_for and pTE1_rev sequence) allows ligation of the fusion construct into pFC332. Diagnostic restriction analysis of the cloned plasmid ought to be done with *Cfr*42i (*Sac*II) and shows a fragment of either 497bp or 500bp in addition to 1kb and 14.3kb fragments, for forward or reverse orientation, respectively.

subsequently fused to the 3' flank, facilitated by the unique target as complementary sequence between the two flanks. Amplification of both flanks in one reaction with pTE1_for and pTE1_rev (Figure 1B) results in a 397bp sgRNA construct *Pac*I::Pro[1]-promoter::target::trRNA::Terminator::*Pac*I (Figure 1B). PCR conditions: 5x HF buffer (Phusion), 200 µM dNTP mix (final conc.), 0.2µM of each primer (final conc.), 2 ng template plasmid (pTLL108.1 or pTLL109.2), 0.1 µL/10

µL reaction volume of Phusion Polymerase (Thermo Scientific™). PCR cycle settings: 30 sec. initial denaturation (98°C), 5 sec. denaturation (98°C), 5 sec. annealing (60°C), 6 sec. extension for 5' flank, 2 sec. extension for 3' flank and 12 sec. for fusion PCR of both flanks (72°C), repeat denaturation to extension cycle 30x, final extension 30 sec. for individual flanks, 2 min. for fusion PCR (72°C), hold at 10°C.

2.3 Plasmid construction and repair DNA fragment design

sgRNA constructs that were obtained through PCR were column purified (GeneJET PCR Purification Kit, Thermo Scientific™) and digested with *Pac*I overnight at 37°C for 16h and inactivated for 20 min. at 80°C in a thermocycler (set heated lid to 37°C). Digested samples were column purified and stored on ice prior to ligation. Approximately 1 µg of pFC332 was digested with *Pac*I at 37°C for 1h and heat inactivated at 80°C for 20 min. in a water bath, prior loading the entire sample on gel. Excision of linearized pFC332 plasmid (15.6kb) followed by gel purification (GeneJET Gel purification Kit, Thermo Scientific™) was eluted in 30 µL MQ. Linearized plasmid (17 µL) was dephosphorylated in a total volume of 20 µL with FastAP (FastAP Thermosensitive Alkaline Phosphatase (1 U/µL), Thermo Scientific™) for 10 min. at 37°C, followed by 10 min. inactivation at 75°C. Samples were put directly on ice after inactivation. Treated samples were not purified prior to ligation: 3 µL plasmid together with 12 µL sgRNA construct was used in a ligation reaction for 10 min. (Rapid Ligation Kit, Thermo Scientific™). Entire ligation mix was transformed to competent *E. coli* DH5α cells via heat shock protocol, and cells were plated on LB containing 100 µg/ml ampicillin. Plasmids were isolated from successful transformants according to Miniprep protocol (GeneJET Plasmid Miniprep Kit, Thermo Scientific™). Diagnostic digest with *Cfr*42i (*Sac*II) results in three bands of approximately, 14.3kbp, 1.1kbp and 500bp in case of sgRNA integration, whereas in case of a control digest of pFC332 (or empty transformed vector), the 500bp band will be absent. Confirmed plasmids were sent for Sanger sequencing with pTE1_for (Macrogen Europe, Amsterdam, The Netherlands).

Repair DNA fragments to create gene knockouts were based on a similar concept as producing split marker flanks in bipartite transformation (Arentshorst et al., 2015). Flanking regions on both 5' and 3' end around the gene of interest (GOI) were selected to be approximately 800-1000bp each. The forward primer on the 3' repair flank (Primer 3, Figure 2) was provided with an overhang sequence which is the reverse complement sequence of the reverse primer on the 5' end (Primer 2, Figure 2). This created a 20bp overlap between 5' and 3' repair flanks, required for fusion PCR (Figure 2).

2.4 Cell wall sensitivity assays

Cell wall disturbing compounds Calcofluor White (CFW) and Congo Red (CR) were added in respective concentrations of 400 µg/mL and 800 µg/mL to MM plates (Ram and Klis, 2006). Spores were counted, serially diluted into 2000, 200, 20 and 2 spores/µL and 5 µL of respective dilutions were spotted on MM plates with either CFW or CR. Plates were incubated for 3-5 days at 30°C.

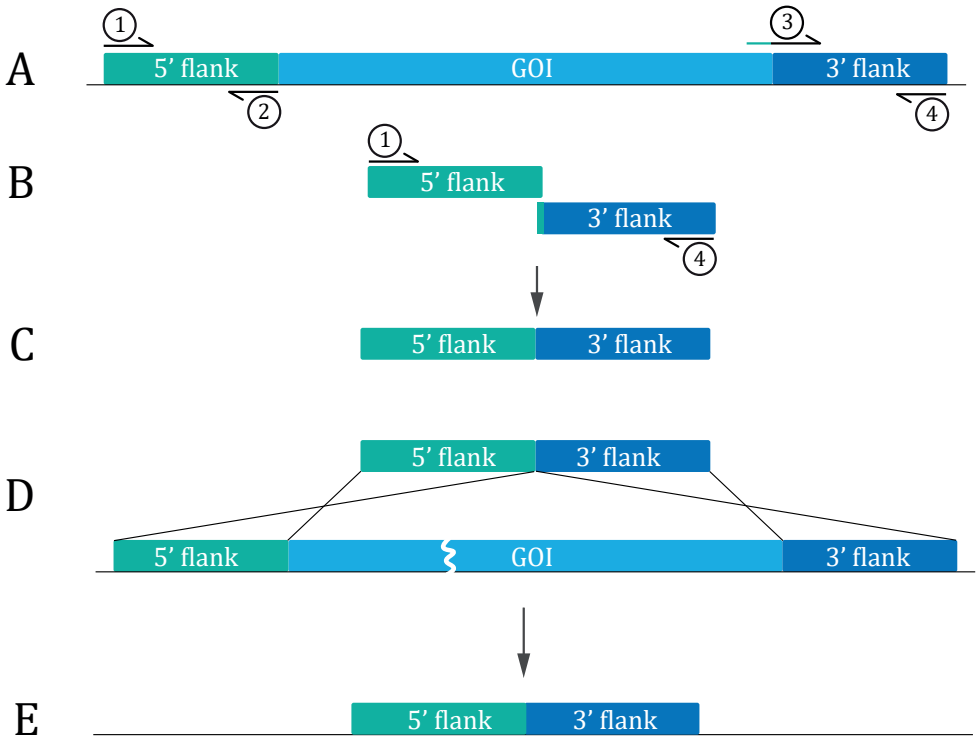

Figure 2. Construction of marker free repair DNA fragment. Amplification of regions upstream (5' flank) and downstream (3' flank) of a gene of interest (GOI): Primer 1 and Primer 3 are used to amplify the 5' flank, typically directly upstream from the start codon of the GOI. Primer 2 and Primer 4 are used to amplify the 3' flank, just downstream of the open reading frame (ORF) stop codon (A). Addition of 20bp reverse complement sequence of Primer 3 to the 5' end of Primer 2 ensures overlap between the 5' and 3' flanks necessary for fusion of the two flanks with primers 1 and 4 (B) to construct the marker free repair DNA fragment (C). Upon introduction of the marker free repair DNA fragment to the fungal cell, repair of the double strand break (DSB) that was created by a Cas9-sgRNA complex, is possible by homology directed repair (HDR) with the marker free repair DNA at the site of the GOI (D). Resultantly, the complete ORF is removed of the GOI (E).

3. RESULTS

3.1 CRISPR/Cas9 plasmid design and proof of functionality

Our CRISPR/Cas9 procedure combines Cas9 expression driven by the constitutive *Aspergillus nidulans tef1*-promoter from an autonomously replicating plasmid (pFC332; Nødvig et al., 2015) with expression of the sgRNA driven by the $tRNA^{Pro1}$ RNAIII polymerase promoter (Song et al., 2018). The sgRNA expression cassette was amplified with extended primers to include *Pac*I restriction sites on both ends of the cassette. A unique *Pac*I restriction site in the pFC-series plasmids (pFC330-333) was used for ligation the sgRNA expression cassette into the vector.

To show functionality of the CRISPR/Cas9 system, we chose to target the *brnA* gene (NRRL3_01040; An14g05370) of *A. niger* which is homologous to *Aspergillus fumigatus abr1* and encodes a multi

copper oxidase that is involved in the synthesis of melanin (Jørgensen et al., 2011b; Tsai et al., 1999). A knockout of *brnA* results in the formation of brown-colored spores, thus providing a direct read-out on transformation plates. A sgRNA target sequence for *brnA* was designed with CHOPCHOP (see Methods). Using fusion PCR, the *brnA*-target was cloned into a sgRNA expressing PCR fragment and ligated into pFC332 to yield pFC332_*brnA*-sgRNA (Table 1).

Table 1. All plasmids used in this study.

Plasmid name	Gene	Name	Target sequence	Reference
pFC332	-	-	-	Nødvig et al., 2015
pFC332_*brnA*-sgRNA	NRRL3_01040	*brnA*	GGAGTGGTACCAATATGTGC	This study
pFC332_*crhA*-sgRNA	NRRL3_10021	*crhA*	GGAGCTACCCATAATGATCC	This study
pFC332_*crhB*-sgRNA	NRRL3_04809	*crhB*	GTAGGTCTTGCTCTCACACA	This study
pFC332_*crhC*-sgRNA	NRRL3_04315	*crhC*	GCTGTCGGTGCTGCAAGTCG	This study
pFC332_*crhD*-sgRNA	NRRL3_02532	*crhD*	GACTGCTGTTGCGTTGGCTG	This study
pFC332_*crhE*-sgRNA	NRRL3_01365	*crhE*	GCTCGTCTTGGCGTGATAGA	This study
pFC332_*crhF*-sgRNA	NRRL3_07085	*crhF*	GTAACGACACATCTTTCGAC	This study
pFC332_*crhG*-sgRNA	NRRL3_03998	*crhG*	GGTGTTGAGGGGGTTGCAAT	This study

To test whether both *cas9* and the *brnA*-sgRNA were expressed (and able to target the *brnA* locus), a series of transformations were performed in a non-homologous-end-joining (NHEJ) deficient strain MA234.1 (*ΔkusA*) (Table 2). The *ΔkusA* (*Δku70* ortholog) mutant cannot repair a Cas9-induced double strand break (DSB) through NHEJ and thus relies on homology directed repair (HDR). As shown in Additional file 1: Figure S1A, the transformation of MA234.1 with pFC332_*brnA*-sgRNA did not yield in any viable transformants, whereas transformation with the control plasmid, lacking a sgRNA (pFC332, Additional file 1: Figure S1B), resulted in 100 viable, black transformants, indicating that the *brnA*-sgRNA generates a DSB which cannot be repaired leading to non-viable cells in a *ΔkusA* background. Co-transformation of homology-containing knockout-repair DNA fragment consisting of fused 5'- and 3'-flanks of the *brnA* gene, together with pFC332_*brnA*-sgRNA yielded 17/17 brown transformants on the transformation plates (Additional file 1: Figure S1C). Brown spores were visible across the entire colony for all transformants, suggesting that no sectors remained untransformed. Hence, no heterokaryotic colonies were observed on the initial transformation plate or found after single streaking. Single streaking of knockout-repair DNA fragment containing transformants on MM plates containing hygromycin showed brown coloration more clearly (Additional file 1: Figure S1E). In addition, a control co-transformation with plasmid pFC332 and knockout-repair DNA fragment did not yield brown colonies (0/63, Additional file 1: Figure S1D), showing that repair DNA fragment does not integrate autonomously at the site of homology without the assistance of a Cas9-sgRNA targeting plasmid (Single streak shown in Additional file 1: Figure S1F for clarity of coloration).

Both brown transformants (pFC332_*brnA*-sgRNA + knockout-repair DNA fragment) and black

Table 2. All strains used in this study.

Name	Genotype	Reference
N402	cspA1	Bos et al., 1988
MA234.1	cspA1, *ΔkusA::DR-amdS-DR*	Park et al., 2016
MA169.4	cspA1, *ΔkusA::DR-amdS-DR, pyrG*$^{-}$	Carvalho et al., 2010
TLF57	cspA1, *ΔkusA::DR-amdS-DR, ΔcrhA*	This study
TLF58	cspA1, *ΔkusA::DR-amdS-DR, ΔcrhB*	This study
TLF59	cspA1, *ΔkusA::DR-amdS-DR, ΔcrhC*	This study
TLF60	cspA1, *ΔkusA::DR-amdS-DR, ΔcrhD*	This study
TLF61	cspA1, *ΔkusA::DR-amdS-DR, ΔcrhE*	This study
TLF62	cspA1, *ΔkusA::DR-amdS-DR, ΔcrhF*	This study
TLF63	cspA1, *ΔkusA::DR-amdS-DR, ΔcrhG*	This study
TLF65	cspA1, *ΔkusA::DR-amdS-DR, ΔcrhDEF*	This study
TLF66	cspA1, *ΔkusA::DR-amdS-DR, ΔcrhABDEF*	This study
TLF67	cspA1, *ΔkusA::DR-amdS-DR, ΔcrhADEFG*	This study
TLF68	cspA1, *ΔkusA::DR-amdS-DR, ΔcrhABDEFG*	This study
TLF39	cspA1, *ΔkusA::DR-amdS-DR, ΔcrhABCDEFG*	This study
MA628.1	cspA1, *ΔkusA::DR-amdS-DR, pyrG*$^{-}$*, ΔcrhA::DR-AOpyrG-DR*	This study
MA629.1	cspA1, *ΔkusA::DR-amdS-DR, pyrG*$^{-}$*, ΔcrhB::DR-AOpyrG-DR*	This study
MA630.2	cspA1, *ΔkusA::DR-amdS-DR, pyrG*$^{-}$*, ΔcrhC::DR-AOpyrG-DR*	This study
MA631.2	cspA1, *ΔkusA::DR-amdS-DR, pyrG*$^{-}$*, ΔcrhD::DR-AOpyrG-DR*	This study
MA632.2	cspA1, *ΔkusA::DR-amdS-DR, pyrG*$^{-}$*, ΔcrhE::DR-AOpyrG-DR*	This study
MA633.2	cspA1, *ΔkusA::DR-amdS-DR, pyrG*$^{-}$*, ΔcrhF::DR-AOpyrG-DR*	This study
MA634.3	cspA1, *ΔkusA::DR-amdS-DR, pyrG*$^{-}$*, ΔcrhG::AOpyrG*	This study

transformants (pFC332 + repair DNA fragment) were single streaked on MM without hygromycin as described in Methods to assess whether the transformants could lose the plasmid without selection pressure. About 80% of the transformants were confirmed to lose their plasmid (data not shown).

Genomic DNA (gDNA) of successfully plasmid-cured transformants was isolated to genotype the *brnA* locus via a diagnostic PCR. A primer set was designed that prime outside of the repair DNA fragment (Additional file 2: Figure S2A). Amplification on gDNA of the wild type strain is expected to generate a PCR fragment of 4012 bp whereas the seamless ORF removal in the mutants is expected to generate a PCR fragment of 2411bp. Additional file 2: Figure S2B shows the result of the diagnostic PCR. All brown transformants show a smaller PCR product at the expected size compared to both wild type strain and black transformants (pFC332 + knockout-repair DNA). Therefore, we conclude that our combined system of the pFC332 plasmid and a Pro^{1}-promoter expression driven sgRNA construct are efficient, and can be successfully used in future gene editing.

Table 3. *A. niger* colony expression levels of *crh* genes in different zones grown on xylose. Seven-day old sandwiched colonies grown on xylose were used for RNA isolation and subsequent microarray analysis (Levin et al., 2007). Distinct zones of the mycelium (zone 1, 3, and 5) harvested form the colony. Zone 1 represents the oldest or central part of the colony. Zone 5 represents the youngest or peripheral part of the colony, whereas zone 3 represents the intermediate zone. Expression levels are represented as percentage of actin expression.

	crhA	*crhB*	*crhC*	*crhD*	*crhE*	*crhF*	*crhG*
N402 zone 1	3.49	6.18	19.90	7.12	5.20	4.99	0.85
N402 zone 3	3.18	8.50	19.23	7.46	4.59	7.03	0.93
N402 zone 5	2.39	39.65	8.63	10.84	2.11	11.50	1.25

3.2 Multiplexing *crh* gene knockouts in successive transformation cycles

To assess the use of the multiplex CRISPR/Cas9 approach, we selected the seven-membered gene *crh* family. As shown in Table 3, this gene family consists of genes with a largely different expression levels, including both significantly expressed genes (e.g. *crhB, crhC* and *crhD*) and genes with very low expression levels (i.e. *crhG*) in different zones an *A. niger* colony under plate growth conditions grown on xylose (Levin et al., 2007). Additionally, we looked into expression data of liquid fermentation conditions on both xylose and glucose to find that the expression of *crh* genes is independent of the carbon source. Also, under these growth conditions the expression of *crhG* was consistently low (Braaksma et al., 2009). Expression of *crhA* and *crhC* also shows to be lower than during plate growth, whereas *crhD* is overall most highly expressed, followed by *crhB* and *crhF* (data not shown).

To target the individual *crh* genes, we constructed seven Cas9-sgRNA plasmids (pFC332_*crhA-G*-sgRNA). Targets of each *crh* gene were designed using CHOPCHOP and listed in Table 1. The *crh* targeting plasmids were co-transformed with PCR-amplified repair DNA fragments that consisted of a fused 5' flank upstream of the *crh* ORF with a 3' flank downstream of the *crh* ORF, similar as described for *brnA*. All transformations were performed in a *ΔkusA* background (MA234.1, Table 2).

Plasmid and repair DNA fragment combinations were transformed successfully to create single gene knockout mutants. Transformants were purified and cured of their plasmids through single streaks (see Methods). Knockouts were confirmed using diagnostic PCR, validating the functionality of all seven plasmids (Additional file 3: Figure S3). Out of thirty transformants tested, we observed twenty-seven with the correctly deleted gene; resulting in a frequency of repair DNA integration of 90% across seven independent transformations (Table 4). Transformation with plasmids pFC332_*crhC*-sgRNA, pFC332_*crhD*-sgRNA and pFC332_*crhE*-sgRNA and respective knockout-repair DNA fragments were both found to have a single tested transformant that did not display the deleted ORF (Table 4, Additional file 3: Figure S3). These transformants were likely able to evade the Cas9-sgRNA complex mediated DSBs, and were not investigated any further.

In addition, control sgRNA-plasmid transformations of the *ΔkusA* background without knockout-repair DNA fragments did not yield transformants for *crhB*, *crhD*, *crhF* and *chrG*. The *crhA* sgRNA-plasmid transformation showed 90% fewer transformants without knockout-repair DNA fragment compared to when the knockout-repair DNA fragment was added (data not shown). In only two cases (*crhC* and *crhE*), close to equal numbers (Table 4) of transformants were observed, either with or without knockout-repair DNA fragments, indicating that these guides were less efficient in creating DSBs. This type of control sgRNA-plasmid transformation without repair DNA fragment provides a good control for sgRNA functionality, and may help to predict the knockout

Table 4. Gene knockout efficiency per target in *Aspergillus niger*.

Gene target	Knockout efficiency (%)*	*ΔkusA* protoplast survival (%) knockout repair DNA fragment (with/without)
brnA	100% (9/9)	0% (17/0)
crhA	100% (5/5)	6.9% (72/5)
crhB	100% (5/5)	0% (12/0)
crhC	83% (5/6)	82% (56/46)
crhD	66.7% (2/3)	0% (6/0)
crhE	80% (4/5)	87.5% (280/245)
crhF	100% (2/2)	0% (2/0)
crhG	100% (4/4)	0% (18/0)

*Knockout efficiency among transformants checked by diagnostic PCR

efficiency among transformants.

In order to examine whether multiple genes could be deleted in a single transformation, we transformed the cured *ΔcrhE* strain (TLF61) with pFC332_*crhD*-sgRNA and pFC332_*crhF*-sgRNA (Table 1). Plasmids were transformed together with both knockout-repair DNA fragments for *crhD* and *crhF* and yielded eight colonies. Control transformation without any knockout-repair DNA fragment showed no colonies (data not shown). All eight transformants were plasmid-cured and were tested for the knockout of both *crhD* and *crhF* by diagnostic PCR. Six out of the eight transformants were found to have a double deletion of both *crhD* and *crhF* (Additional file 3: Figure S3). Subsequently, we continued using *ΔcrhDEF* (TLF65) for a successive round of transformation.

Inspired by the successful transformation with two separate plasmids harboring the same hygromycin selection marker, we decided to perform both additional double and also triple gene targeting transformations. To construct quintuple mutants *(ΔcrhABDEF)* and *(ΔcrhADEFG)* or sextuple mutant (*ΔcrhABDEFG*), TLF65 *(ΔcrhDEF*) was co-transformed with respective pFC332_*crh*-sgRNA plasmids and corresponding knockout-repair DNA fragments. Simultaneous deletion of either *crhA* and *crhB* or *crhA* and *crhG* were both found to be 100% efficient in the tested transformants (*crhA* and *crhB* (7/7) and *crhA* and *crhG* (4/4), Additional file 3: Figure S3). Concurrent deletion of *crhA, crhB* and *crhG* resulted in eight transformants that were all tested for successful knock-

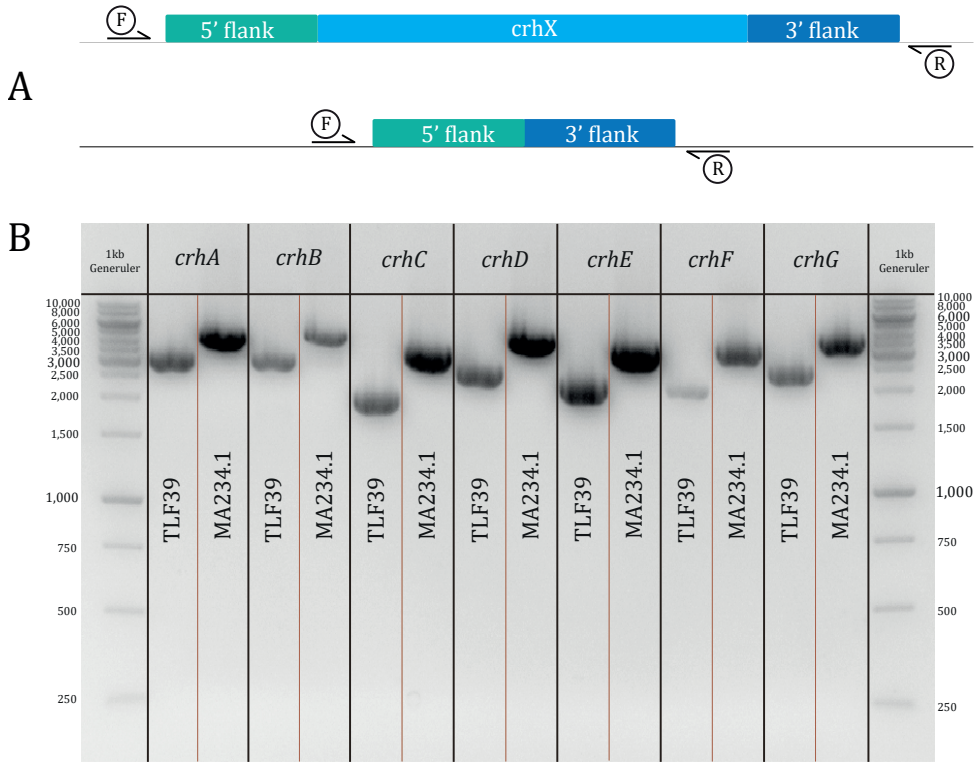

Figure 3. Diagnostic PCR of *crhA-G* in the *A. niger* TLF39 and wild type (MA234.1) strains. ORFs removed for each *crh* gene in TLF39 show a downward band shift compared to MA234.1. (A) Exact band sizes are listed. (B) gDNA of TLF39 and MA234.1 was amplified with primer pairs for each *crh* gene (listed in Additional file 4: Table S1); PCR samples were loaded on 1% agarose gels.

outs of all three genes. Three out of eight transformants were found to be *ΔcrhA*, *ΔcrhB* and *ΔcrhG* (*ΔcrhABDEFG*). In one transformant both *ΔcrhB* and *ΔcrhG* were deleted (*ΔcrhBDEFG*), whereas the four other transformants were deleted for *ΔcrhA* (Additional file 3: Figure S3). The observed reduction in knockout efficiency among transformants marks a tipping point at which the attempt can be considered worthwhile. Note however that, despite a significantly lower efficiency score compared to double knockouts, the set-up with three individual gene targeting plasmids—each with identical selection markers and separate knockout-repair DNA fragment—remains within practically manageable numbers of strains to be analyzed.

Lastly, *ΔcrhABDEFG* (TLF68) was transformed with pFC332_*crhC*-sgRNA and respective knock-out-repair DNA fragment yielding a septuple *ΔcrhABCDEFG* knockout (TLF39) of the whole *crh* gene family. A diagnostic PCR (primers used are listed in Additional file 4: Table S1) of the each *crh* gene shows a band size difference between wild type strain and TLF39 (Figure 3A). Results of the diagnostic PCR of both the mutant (TLF39) and wild type (MA234.1) strains are shown in Figure 3B, where all ORFs of the seven *crh* genes are removed resulting in a size difference.

All single, intermediate triple, quintuple and final septuple CRISPR/Cas9 derived *crh* knockouts

were spotted on MM 1% glucose. As is evident from Figure 4, there is no difference in growth between the different knockouts. However, there is a subtle difference in compactness of the colony morphology between the wild type and the septuple *crh*-knockout (Figure 4A and 4B).

3.3 *Crh* gene knockouts via split marker and effects of the integrated *AOpyrG* marker

At the time of setting up CRISPR/Cas9 based gene editing in *A. niger,* we used traditional split marker (i.e. bipartite) transformation to assess the effects of single gene deletions of the *crh* gene family. All seven single knockouts of *crhA-G* were obtained using the auxotrophic *Aspergillus oryzae pyrG* (*AOpyrG*) selection marker in a *ΔkusA, pyrG*- background (MA169.4, Table 2). To allow possible future transformation of single gene knockouts we opted to use direct-repeat (DR) split marker flanks required for looping-out the marker via counter selection (see Methods). However, synthesis of DR split marker flanks proved to be problematic for *crhG* and forced us to refrain from creating a *ΔcrhG::*DR-*AOpyrG*-DR type construct (data not shown) and to use a *Δcrh*G*::AOpyrG* deletion construct instead. Transformant colonies were single streaked for purification, and genotyping through diagnostic PCR showed correct replacement of the ORF by *AOpyrG* for all seven genes (data not shown). During single streaking for strain purification it became evident that *ΔcrhG*::*AOpyrG* transformants already showed poor growth on MM (Additional file 5: Figure S4), whereas CRISPR/Cas9 constructed *ΔcrhG* was not found to display a growth phenotype (Figure 2B). Supplementation of the medium with 10mM uridine (auxotrophic *pyrG*- supplementation) abolished the poor growth phenotype for *ΔcrhG::AOpyrG* compared to wild type strain MA234.1 (Additional file 5: Figure S4), indicating that poor growth was due to

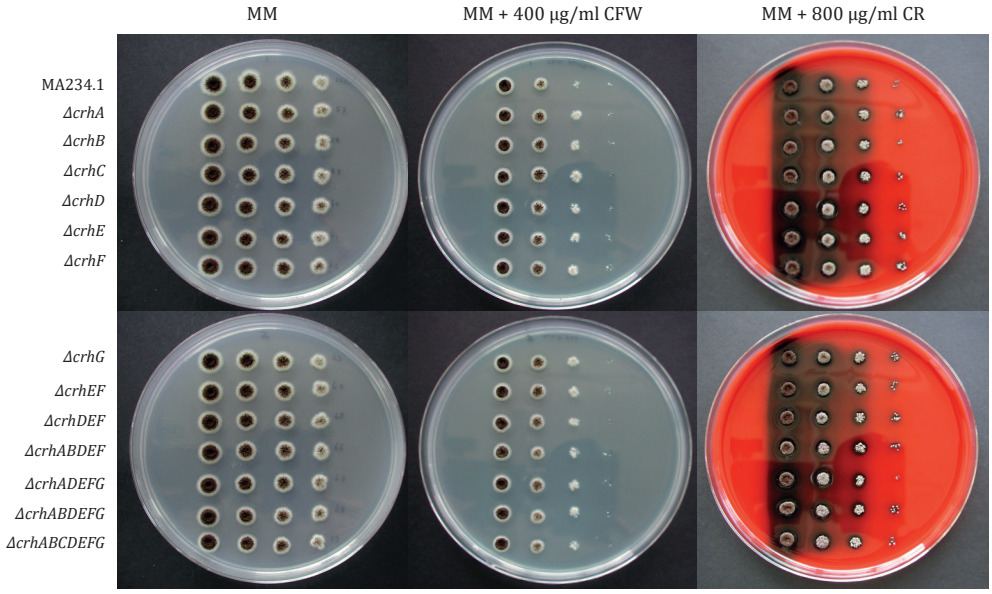

Figure 4. Growth morphology of *crh* knockouts in MA234.1 (Δ*kusA*) obtained using CRISPR/Cas9. MA234.1, *ΔcrhA, ΔcrhB, ΔcrhC, ΔcrhD, ΔcrhE, ΔcrhF, ΔcrhG, ΔcrhEF, ΔcrhDEF, ΔcrhABDEF, ΔcrhADEFG, ΔcrhABDEFG* and *ΔcrhABCDEFG* on MM (A and B), MM + 400 µg/ml CFW (C and D) or MM + 800 µg/ml CR (E and F).

insufficient levels of endogenously synthesized uridine/uracil.

All remaining single knockouts (*ΔcrhA*-F) were cultured to obtain fresh spore solutions and were spotted in equal spore numbers on MM with cell wall disturbing compounds Calcofluor White (CFW) and Congo Red (CR), to assess phenotypic effects (MM + CFW and MM + CR). Wild type MA234.1 and mutants were cultured under equal conditions (Additional file 6: Figure S5). No growth effects were found for *ΔcrhA*::DR-*AOpyrG*-DR, *ΔcrhB*::DR-*AOpyrG*-DR, *ΔcrhC*::DR-*AOpyrG*-DR, *ΔcrhD*::DR-*AOpyrG*-DR and *ΔcrhF*::DR-*AOpyrG*-DR on both MM, MM + CFW and MM + CR. However, *ΔcrhE*::DR-*AOpyrG*-DR only displayed a growth phenotype on MM containing either CFW or CR, but not on MM alone (Additional file 6: Figure S5). Similar to the situation of *ΔcrhG*::*AOpyrG*, uridine supplementation to MM + CFW and MM + CR plates abolished the growth phenotype for *ΔcrhE*::DR-*AOpyrG*-DR (Additional file 7: Figure S6). Set aside, our data show that single knockouts of *crh* genes do not affect growth or morphology per se, analogous to CRISPR/Cas9 obtained single mutants.

3.4 Effects on cell wall sensitivity in *crh*-knockouts derived from CRISPR/Cas9 mediated transformation

To follow up on the phenotypic analysis of *crh* knockouts in bipartite-obtained transformants, CRISPR/Cas9-derived transformants were also tested for cell wall sensitivity in accordance with yeast literature on *crh* functionality (Cabib et al., 2007), using MM with CFW or MM with CR. In addition to previously reported expression data on plates (Table 3), we checked expression of *crh* genes in the *ΔugmA* (UDP-galactopyranose mutase A) strain (Park et al., 2016). The *ΔugmA* strain is known to exhibit a constitutive state of cell wall stress and may therefore resemble conditions similar to cell wall stress induced by either CFW or CR. Expression data of the *ΔugmA* strain indicates a 2.91 log2 fold-change of *crhE* under cell wall stress conditions, whereas additional positive differential expression of both *crhA* and *crhF* and negative differential expression of *crhB* are noticeable, but not scored as significant (data not shown). Consequently, we postulate that *crh* genes are required in the cell wall stress response and that deletion mutants' phenotypes reflect this in a cell wall stress assay with CFW or CR. Phenotypes on MM with either CFW or MM with CR of CRISPR/Cas9 derived single knockouts and the septuple knockout of *crhA-G* are shown in Figure 4C-F. It is clear from the assay that both single knockouts and the septuple knockout of *crhA-G* do not show a disturbed growth phenotype on MM, and show no sensitivity towards either of the tested compounds. These data suggest that the knockouts—both in singular cases and in septuple combination—do not affect the ability of *A. niger* to grow. Moreover, *crhA-G* do not appear to be required for the survival when the cell wall is stressed with either CFW or CR.

4. DISCUSSION

This study demonstrates an efficient CRISPR/Cas9 based gene-editing procedure for *A. niger* using a combination of the previously described methods (Nødvig et al., 2015; Song et al., 2018).

Our approach combines the use of the pFC332 Cas9-AMA1 vector with the Pro[1]-sgRNA expression cassette. Due to a unique *Pac*I site located on the pFC332 plasmid, newly synthesized sgRNA expression cassettes could easily be ligated to generate pFC332_sgRNA plasmids both quickly and effectively. These plasmids have been shown to generate either single, double or triple knockouts in combination with homologous knockout-repair DNA fragments in high frequencies, allowing fast and efficient construction of multiple gene knockouts in a marker-free way. Such gene alterations can be performed in any strain devoid of a hygromycin selection marker, and circumvents the reliance on auxotrophic mutant strains (e.g. *pyrG*-). Moreover, the curability of these hygromycin containing AMA1-vectors in the absence of selection pressure as an intrinsic property warrants the recyclability of this system for putative recurrent transformations, without the need to use of possibly mutagenic counter selection strategies.

An often overlooked limitation of CRISPR/Cas9 based gene editing is that Cas9-sgRNA functionality is difficult to predict. In our approach, the use of the *ΔkusA* strain allows for sufficient assessment of this functionality; in the absence of a repair DNA fragment, an efficient sgRNA does not result in any transformants on the transformation plates due to the inability to repair a Cas9 induced DSB. This was observed for six out of the eight sgRNAs presented here. In two instances, transformants were observed when no knockout-repair DNA fragment was supplied, which may suggest less efficient generation of DSBs. However, in these two occasions the knockout efficiency was still 80-83% through integration of the knockout-repair DNA fragment (Table 4). These data show that sgRNAs are effectively expressed using our procedure.

As an alternative strategy to homology directed DNA repair editing, gene disruptions can be made in a *kusA+* wild type strain without the addition of repair DNA fragment. Selection for indels is enforced by recurrent recognition and cutting by the Cas9-gRNA complex of the targeted DNA. As such, this would provide a more simplistic model for gene disruption. Song et al. (2018) have previously shown the occurrence of differently sized indels in either *fwnA* (NRRL3_00462, An09g05730) or *olvA* (NRRL3_01039, An14g05350) in *A. niger* NRRL3, ranging from 88 bp insertions up to 1096 bp deletions across 30 individual mutants. In this study, while targeting the *brnA* gene, we observed even larger deletions that potentially range over 2 kb (data not shown). The DSB in *brnA* in the wild type strain N402 caused by pFC332_*brnA*-sgRNA lies 2.0 kb upstream from the *olvA* start codon. *OlvA* is epistatic over *brnA* in the melanin synthesis pathway (Jørgensen et al., 2011b; Tsai et al., 1999), and a knockout of *olvA* becomes olive-colored. N402 transformed with pFC332_*brnA*-sgRNA occasionally (2.8%, n=580) showed olive-colored transformants (data not shown), suggesting that deletions extend over previously reported 1 kb. As a result, we avoid this type of gene disruption due to the unpredictable outcome, and instead, highly recommend to perform gene edits with targeted repair DNA fragments in *ΔkusA* background.

In addition to creating single knockouts with Cas9-sgRNA plasmids, we have shown to efficiently multiplex two or three knockouts using identical vectors (pFC332-Cas9 backbone), harboring separate gRNAs, in a single transformation. These results suggest that multiple, different AMA1-vector copies with the same selection marker can successfully create knockout combinations in *A.*

niger. This positive result contradicts findings in *A. oryzae* where multiplexing with two different sgRNA on separate AMA1-vectors only resulted in single knockouts (Katayama et al., 2019). Only when both sgRNA constructs were cloned into a single vector, similar double knockout efficiencies observed as described here. It remains to be tested to what extent this number of simultaneous gene edits can be achieved in *A. niger*, but may ultimately be limited to the maximum copy number of approximately 10-20 AMA1 plasmids per nucleus (Aleksenko, I. Nikolaev, Y. Vinetski, 1996).

The CRISPR/Cas9 procedure presented here provides evidence that multiplexing up to three targets does not require expression of three different sgRNAs on a single plasmid. High knockout efficiencies can be acquired by combining individual gene targeting plasmids with respective knockout-repair DNA fragments. This allows to combine different gene targeting plasmids as desired. Hence, existing plasmids can be used in various combinations without the need for reconstruction of complex cassettes, such as described by Nødvig et al., 2018. In addition, we show that multiple genetic alterations, such described for multiple gene knock-ins (Dong et al., 2019), do not need integrative selection markers to ensure efficient genome editing. This work has addressed the current limitations of creating marker-free multiplex knockouts of separate genes in *A. niger*, without the reliance on either integrative plasmids (Zhang et al., 2019; Zheng et al., 2019) or integrative (albeit recyclable) selection markers (Dong et al., 2019; Kuivanen et al., 2016; Leynaud-Kieffer et al., 2019; Sarkari et al., 2017), and can directly be re-transformed for additional gene editing if desired. Therefore, it can be concluded that the use of singular sgRNA expression cassettes provides a flexible system in which both single, double and triple marker-free knockouts can efficiently be made.

CRISPR/Cas9 based genome editing is now a relevant technique in addition to conventional split marker transformations. The benefit of using CRISPR/Cas9 is multiplex ability, independence of integrative selection markers and the option to reuse the identical selection marker in follow-up gene-editing steps. Currently, recyclable systems do exist for *pyrG* and *amdS* in both CRISPR/Cas9 gene editing (Dong et al., 2019; Leynaud-Kieffer et al., 2019) and conventional split marker transformation (Arentshorst et al., 2015). This process can be induced with the counter-selectable compounds, either 5'-FOA or 5-FAA, for *pyrG* and *amdS* markers respectively. Exposure to 5'-FOA/FAA selects for either loop-out in case of direct repeat elements or loss (of function) of *pyrG/amdS*, as the active gene metabolizes 5'-FOA/FAA to a toxic compound. Consequently, the *pyrG/amdS* gene can be recycled to target a different GOI. In this way, any gene can be systematically knocked out in a relatively time consuming single-step fashion. In addition to being more labor intensive, successive use of 5'-FOA/FAA may be undesirable due to their mutagenic nature. To put this in perspective, we estimate that construction of a septuple knockout strain can be obtained 3 times faster with CRISPR/Cas9 gene editing than split marker *pyrG* recycling due to the high efficiency of multiplexing and the omission of the counter selection procedure.

In addition to CRISPR/Cas9 obtained *crh* knockouts, single knockouts were constructed using the recyclable *pyrG* marker to test *crh* functionality. We observed an effect from the locus of integration for the *AOpyrG* selection marker in case of *crhG,* which is most likely related to low

baseline expression (Table 3). Deletion of *crhG* via *AOpyrG* integration resulted in a poor growth phenotype on MM, and was shown to be complemented with the addition of uridine (Additional file 5: Figure S4). Additionally, unlike *crhG*, *ΔcrhE*::DR-*AOpyrG*-DR shows normal growth on MM, but shows impaired growth on MM with either cell wall disturbing compounds CFW or CR. Cell wall stressing compounds CFW and CR are known disrupt fungal cell wall assembly (Roncero and Duran, 1985), triggering the cell wall integrity (CWI) response (Levin, 2005). In addition to chemical disruption, the CWI pathway is constitutively activated in the *ΔugmA* mutant, lacking cell wall galactofuranose (Damveld et al., 2008). This condition resembles exposure to CFW or CR, and transcriptomic analysis of the *ΔugmA* mutant showed upregulation of *crhE,* suggesting its importance during the CWI stress response. However, parallel phenotypic analysis of MA632.2 (*ΔcrhE*::DR-*AOpyrG*-DR) with the CRISPR/Cas9 derived TLF61 (*ΔcrhE*) showed no affected growth phenotype for TLF61 when exposed to either CFW or CR, whereas MA632.2 showed sensitivity toward both compounds. Only when the medium was supplemented with uridine, we observed the same wild type like phenotype as TLF61 (Additional file 7: Figure S6). Despite the projected hypothesis on the requirement of *crhE* in the CWI response, these findings indicate an effect on the *AOpyrG* marker during the CWI response rather than the lack of *crhE*. A possible explanation may be the locus activity of *crhE* (e.g. chromatin remodeling) during cell wall stress, affecting expression of ectopically integrated genes such as *AOpyrG* in MA632.2.

Ectopic expression of auxotrophic markers have previously been described to be affected by the locus of integration. Specifically, the use of *pyrG* marker was reported to have a negative effect on either the ability to have a proper sexual cycle in *A. nidulans* (Robellet et al., 2010) or during vegetative growth in *Aspergillus flavus* (Luo et al., 2016). In case of *A. nidulans*, Robellet and colleagues clearly showed lower expression of *pyrG* at the *alcS* locus (required for ethanol utilization) compared to other ectopic integration sites of *pyrG.* This was tested in both *alcS*-locus inducing and non-inducing conditions, and may thus not only be related to an active or silent locus, but also where the position of the locus resides on the genome. These “position effects”, where the expression of the selectable marker highly depends on the genetic elements at the locus of integration (Miki et al., 2009), have been also been reported for *pyr4* (*pyrG* ortholog) in *N. crassa*, *nadA* and *argB* in *A. nidulans* (Bok et al., 2006; Greenstein et al., 2006; Oestreicher et al., 2008) and *URA3* (*pyrG* ortholog) in *Candida albicans* (Lay et al., 1998; Staab and Sundstrom, 2003). Taken together, these reports highlight that the expression of integrative selection markers, and specifically *pyrG*/*pyr4*/*URA3*, are sensitive to the locus of integration. In this study, we found that the auxotrophic *AOpyrG* selection marker is affected by the locus of integration. Therefore, caution must be taken in interpreting the phenotypic and/or pleiotropic effects that arise from this artifact in strains that harbor integrative selection markers. We propose to use either alternative, dominant selection markers such as hygromycin for construction of single knockouts or use non-integrative CRISPR/Cas9 selection procedures such as the one presented here.

5. CONCLUSION

We have demonstrated the efficiency of marker-free multiplex gene knockout construction, using Cas9-sgRNA plasmids with marker-free repair DNA fragments, in parallel to split marker fragment transformation to knockout the cell wall chitin cross-linking gene family (*crhA-G*). The use of multiple Cas9-sgRNA plasmids harboring the same selection marker can be achieved 3 times faster than *AOpyrG* recycling; showing that double or even triple knockouts are possible at relatively high efficiency using CRISPR/Cas9. Moreover, removal of selection medium allows the loss of Cas9-sgRNA plasmids while the gene knockout remains present. In turn, this grants the recurrent use of plasmids with the same selection marker in future transformations without prior need to recycle *pyrG/amdS*-type integrative selection markers. Additionally, it became evident that the expression of the integrated *AOpyrG* selection marker was affected in two of the seven *crh* knockout strains generated by a classical split marker approach compared to the same gene knockouts in CRISPR/Cas9 obtained mutants. Therefore, the marker-free CRISPR/Cas9 procedure presented here clearly favors over integrative selection marker-based transformations for multiplex knockout strain construction.

Acknowledgements

We would like to thank professor Uffe Mortensen (Technical University of Denmark, Denmark) for sharing plasmids and professor Adrian Tsang (Concordia University, Toronto, CA) for kindly providing us with the Pro[1]-sgRNA expression cassette prior to publication. In addition, we want to thank Sjoerd J. Seekles for scoring brown and olive transformants in CRISPR/Cas9 transformations without knockout repair DNA fragments in the wild type N402 background.

Availability of data and material

All dataset(s) supporting the results of this article are included within this article and its additional files. Plasmids and strains are available upon request.

Funding

This work is part of the “FunChi” ERA-IB project with project number ERA-IB-15-080, which is (partly) financed by the Dutch Research Council (NWO).

SUPPLEMENTARY FIGURES

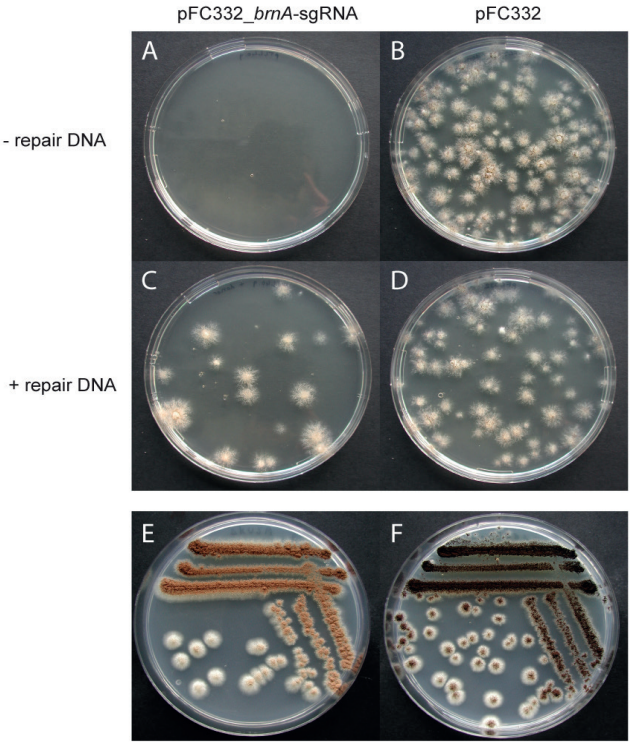

Additional file 1: Figure S1. PEG-mediated transformation of the *A. niger ΔkusA* strain targeting the *brnA* gene. Protoplasts were transformed with a pFC332-Cas9 vector, either with a sgRNA expression cassette (pFC332-brnA_sgRNA; A and C) or without any sgRNA expression cassette (pFC332; B and D), and were grown on MM containing 32.5% (w/v) sucrose (MMS) and 200 µg/ml hygromycin B. Knockout-repair DNA fragment was either left out (A and B) or added (C and D) to the protoplasts in addition to the plasmid. (E) Single streak of a *ΔbrnA* transformant taken from the plate shown in C and (F) a transformant taken from the plate shown in D.

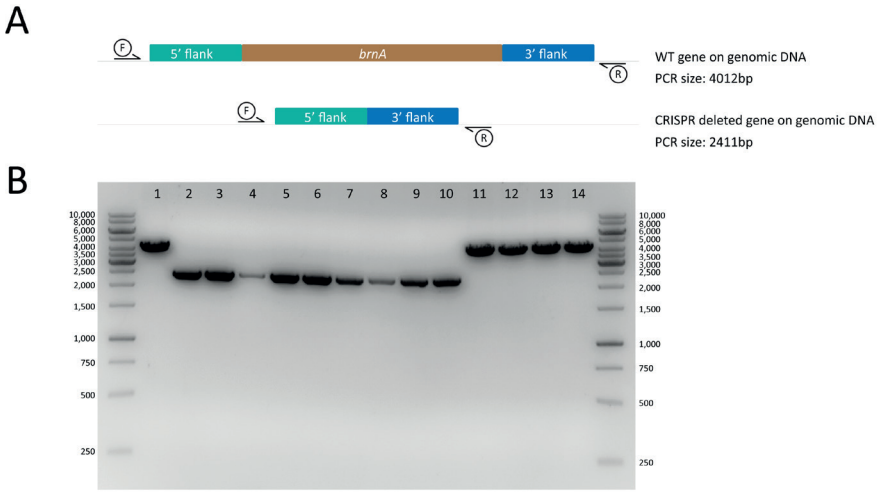

Additional file 2: Figure S2. Diagnostic PCR of the *brnA* locus. (A) Shows the forward (F) and reverse (R) primers used to amplify the *brnA* on the gDNA of *A. niger*. The PCR amplified brnA locus in the wild type strain is 4012bp, whereas that in the ΔbrnA is expected to be 2411bp. (B) A. niger gDNA was isolated and amplified with F and R primers from both MA234.1 (1), ΔbrnA transformants (2-10, Additional file 1: Figure S1C) and black transformants (pFC332 + knockout-repair DNA) (11-14, Additional file 1: Figure S1D). PCR samples were loaded on 1% agarose gels. Ladder: 1kb Generuler.

	crhA	*crhB*	*crhC*	*crhD*	*crhE*	*crhF*	*crhG*
Wild type (MA234.1) size (bp)	4507	4549	3432	4207	3461	3331	3748
Δ*crh* size (bp)	3183	3035	2046	2662	2304	2060	2484
Size difference (bp)	**1324**	**1514**	**1386**	**1545**	**1157**	**1271**	**1264**

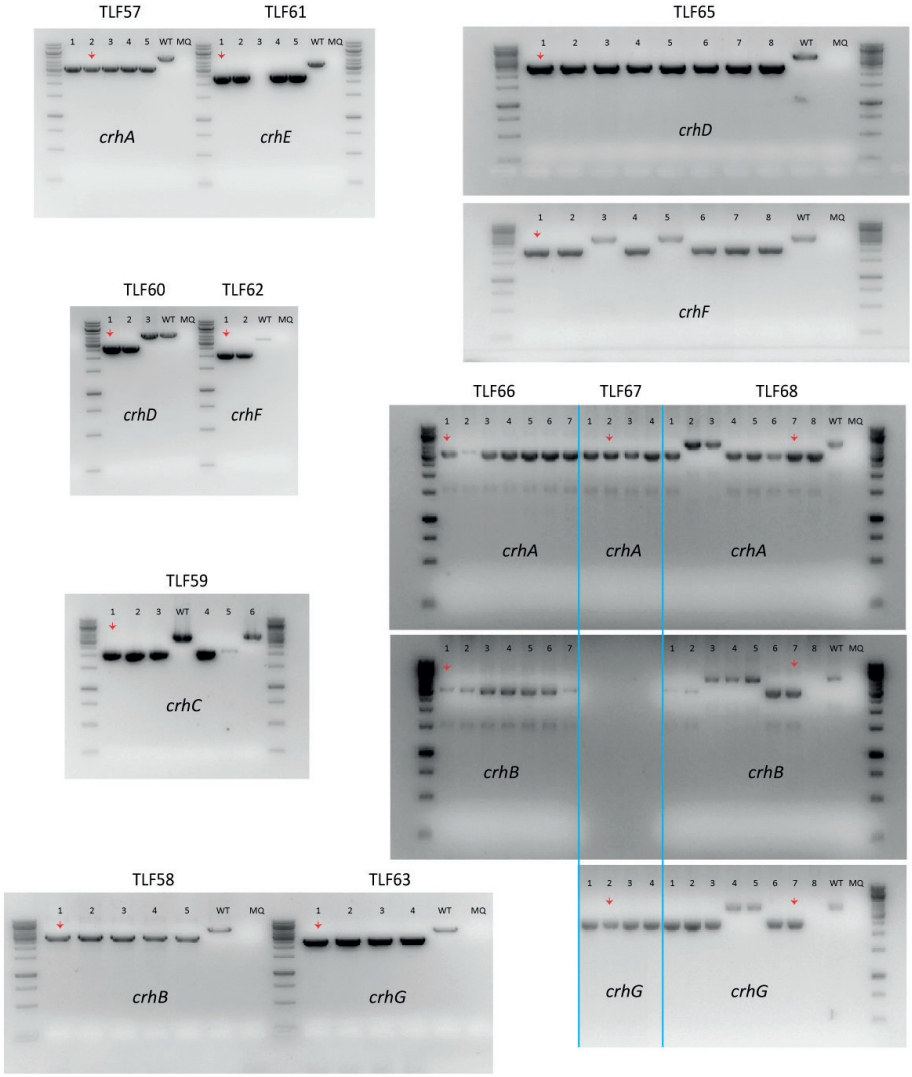

Additional file 3: Figure S3. Diagnostic PCR of all knockout mutants created in the *A. niger* MA234.1 (*ΔkusA*) background. Single (TLF57-63), double (TLF65-67) and triple (TLF68) gene. The table on the top shows the expected PCR product sizes based on the ORFs removed with the knockout repair DNA fragments for each *crh* gene. gDNA of all mutants, wild type and a negative water control (MQ) was amplified with primer pairs for each crh gene listed in Table S1 ("HDR check" primers). Different mutants from the same transformation plate are indicated by a number, ranging from 1-8. PCR samples were loaded on 1% agarose gels with 1kb Generuler ladder. All correctly removed ORFs show a downward band shift compared to MA234.1 (WT). Red arrows indicate the selected mutants which are included in this study.

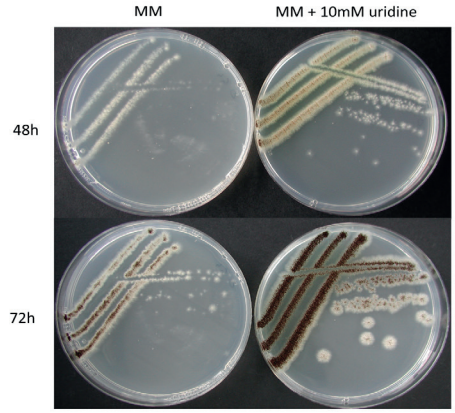

Additional file 5: Figure S4. Growth morphology of ΔcrhG::AOpyrG knockout strain on MM and MM containing 10mM uridine.

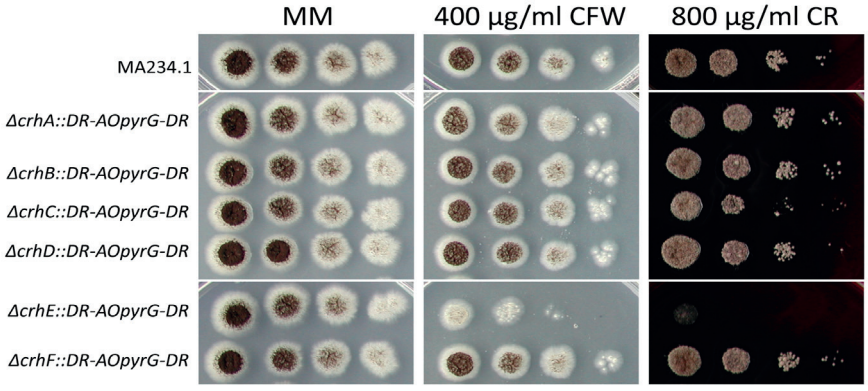

Additional file 6: Figure S5. Growth morphology of single crh knockout strains obtained via replacing the respective crh gene with DR-split marker AOpyrG in MA169.4; ΔcrhA-F on MM, MM + 400 µg/ml CFW or MM + 800 µg/ml CR.

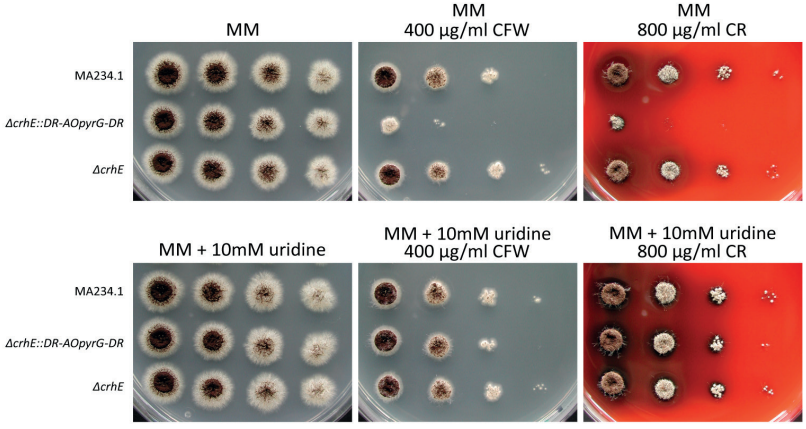

Additional file 7: Figure S6. Growth morphology of MA234.1, ΔcrhE::DR-AOpyrG-DR and ΔcrhE. (A) Strains were grown on MM, MM + 400 µg/ml CFW or MM + 800 µg/ml CR. (B) Additionally, strains were grown on MM + 10mM uridine, MM + 10mM uridine + 400 µg/ml CFW)and MM + 10mM uridine + 800 µg/ml CR.

CHAPTER 3

A seven-membered cell wall related transglycosylase gene family in *Aspergillus niger* is relevant for cell wall integrity in cell wall mutants with reduced α-glucan or galactomannan

Tim M. van Leeuwe, Jasper Wattjes, Anna Niehues, Gabriel Forn-Cuni, Mark Arentshorst, Nicholas Geoffrion, Hugo Mélida, Antonio Molina, Adrian Tsang, Annemarie H. Meijer, Bruno M. Moerschbacher, Peter J. Punt, Arthur F.J. Ram

ABSTRACT

Chitin is an important fungal cell wall component that is cross-linked to β-glucan for structural integrity. Acquisition of chitin to glucan cross-links have previously been shown to be performed by transglycosylation enzymes in *Saccharomyces cerevisiae*, called Congo Red hypersensitive (*CRH*) enzymes. Here, we characterized the impact of deleting all seven members of the *crh* gene family (*crhA-G*) in *Aspergillus niger* on cell wall integrity, cell wall composition and genome-wide gene expression. In this study, we show that the seven-fold *crh* knockout strain shows slightly compact growth on plates, but no increased sensitivity to cell wall perturbing compounds. Additionally, we found that the cell wall composition of this knockout strain was virtually identical to that of the wild type. In congruence with these data, genome-wide expression analysis revealed very limited changes in gene expression and no signs of activation of the cell wall integrity response pathway. However, deleting the entire *crh* gene family in cell wall mutants that are deficient in either galactofuranose or α-glucan, mainly α-1,3-glucan, resulted in a synthetic growth defect and an increased sensitivity towards Congo Red compared to the parental strains, respectively. Altogether, these results indicate that loss of the *crh* gene family in *A. niger* does not trigger the cell wall integrity response, but does play an important role in ensuring cell wall integrity in mutant strains with reduced galactofuranose or α-glucan.

This chapter is published as: van Leeuwe, T.M., Wattjes, J., Niehues, A., Forn-Cuni, G., Arentshorst, M., Geoffrion, N., Mélida, H., Molina, A., Tsang, A., Meijer, A.H., Moerschbacher, B.M., Punt, P.J., Ram, A.F.J. ,2020. Cell Surf., 6, 100039. doi: 10.1016/j.tcsw.2020.100039

1. INTRODUCTION

The fungal cell wall is a rigid, yet dynamic structure that dictates cell shape, provides protection from other microbes, helps to colonize new environments and is required for virulence in pathogenic fungi. The fungal cell wall consists of different polymeric sugars, including α-1,3-glucans, mixed α-1,3/1-4-glucans, β-1,3-glucans, β-1,6-glucans and mixed β-1,3/1,4 or β-1,3/1,6 glucan varieties, chitin (β-1,4-*N*-acetyl glucosamine polymer), galactomannan and glycoproteins (Free, 2013; Gow et al., 2017; Ruiz-Herrera and Ortiz-Castellanos, 2019). In filamentous fungi, β-1,3-glucans and chitin comprise the majority of these polymers, forming intrachain hydrogen bonds that can assemble into microfibrils to form a scaffold around the cell (Gow et al., 2017). Additionally, β-1,3-glucans act as a backbone structure wherefrom branching, through β-1,6-glucan linkages that constitute 3% to 4% of the total glucan linkages (Latgé, 2007), creates multiple β-1,3-glucan non-reducing end acceptor sites. These non-reducing ends can be used for covalent cross-links for other β-1,3-glucans, chitin and mannan, facilitated by Gel/Gas/Php, Crh and Ktr/Mnt/Mnn families, respectively (Cabib et al., 2008, 2007; Fontaine et al., 2000; Fonzi, 1999; Hartland et al., 1996; Henry et al., 2016; Mouyna et al., 2000; Rodríguez-Peña et al., 2000a; Samalova et al., 2017).

Prior to cross-linking, both β-1,3-glucan and chitin are synthesized at the plasma membrane by β-glucan and chitin synthases using UDP-glucose and UDP-*N*-acetyl-glucosamine, respectively. Polymers are extruded into the periplasmic space, where chitin becomes cross-linked to glucan by GPI-anchored Crh transglycosylases (Arroyo et al., 2016). Crh enzymes exhibit both chitinase and transglycosylation activity, effectively hydrolyzing a chitin donor molecule followed by subsequent (re-)attachment to acceptor substrates. These acceptor substrates are either chitin (homotransglycosylation) or β-1,3 and β-1,6-glucans (heterotransglycosylation), respectively (Mazáň et al., 2013). Crh enzymes can be classified as part of either of the fungal specific GH16_18/19 subfamilies (Viborg et al., 2019). These chitin to β-1,3-glucan cross-linking enzymes have been most extensively studied in *Saccharomyces cerevisiae* on both functional and structural level (Blanco et al., 2015; Cabib et al., 2008, 2007; Rodríguez-Peña et al., 2000a). Named Congo Red Hypersensitive (*CRH*), *CRH1* and *CRH2* showed redundant function in the covalent attachment of chitin to glucan, and exhibited sensitivity towards Congo Red (CR) and Calcofluor White (CFW) in both single and double knockouts strains. *CRH1* and *CRH2* were found to be induced during vegetative growth whereas a third, *CRH*-related gene 1 (*CRR1*) encoding an additional transglycosylase, was only induced during sporulation, concomitantly with *CRH1.* A single knockout of *CRR1* did not result in hypersensitivity to either CR or CFW (Rodríguez-Peña et al., 2000a), but was shown to have a role in formation of the ascospore cell wall (Gómez-Esquer et al., 2004). In *Candida albicans,* single, double and triple knockouts of the three *CRH* paralogues, *UTR2*, *CRH11* and *CRH12* resulted in sensitivity towards CR, and avirulence in mouse models (Pardini et al., 2006). Furthermore, overexpression of either *CRH1* or *UTR2* in *C. albicans* led to protection against osmotic shock as a result of reduced cell wall elasticity, whereas a triple deletion resulted in increased osmo-sensitivity (Ene et al., 2015).

In contrast to yeast-like fungi, relatively little is known on the function of the Crh enzymes in filamentous fungi. A phylogenetic analysis showed that Crh enzymes are very well conserved in fungal genomes with noticeably more orthologs found in filamentous fungi compared to yeast-like fungi (Arroyo et al., 2016). *Neurospora crassa* and *Aspergillus fumigatus* both encode five orthologs, whereas *A. niger* contains seven orthologs (Pel et al., 2007). All these three fungi displayed wild type growth morphology for all single knockouts strains (Fang et al., 2019; Patel and Free, 2019, **Chapter 2**). In case of *A. fumigatus, Af*Crh5 was structurally and functionally characterized as a true transglycosylase with both homo- and heterotransglycosylation activity, additionally identifying both donor and acceptor substrate binding kinetics and moieties (Fang et al., 2019). Unlike the situation in *S. cerevisiae* and *C. albicans,* the quintuple *crh* knockout strain of *A. fumigatus* only showed slight sensitivity towards CR, similar to some of the single knockouts. We previously showed that both single knockouts and seven-fold *crh* gene family knockout in *A. niger* did not display a significant sensitivity towards CR (**Chapter 2**). These data indicate that either Crh enzymes play a different physiological role or that *crh* gene loss is compensated by other cell wall components and/or cross-links in filamentous fungi.

A specific difference in cell wall composition between *Aspergilli* and other organisms that have been studied for Crh functionality, *S. cerevisiae* and *C. albicans,* is the presence of α-glucan in filamentous fungi. Recently, the molecular architecture of *A. fumigatus* cell walls was studied in more detail, revealing the importance of α-1,3-glucan for structural integrity (Kang et al., 2018). It was shown that α-1,3-glucan, in addition to the outer cell wall layer, plays an important structural role in the cell wall by forming a rigid hydrophobic core by interaction with chitin. Additionally, they showed that β-glucans have a more mobile and dynamic role in the cell wall, challenging the prevailing paradigm that the chitin-β-glucan matrix provides the load-bearing scaffold of the fungal cell wall (Gow et al., 2017). These findings led us to form a new hypothesis with respect to the function of Crh enzymes in α-glucan containing cell walls of filamentous fungi. In α-glucan containing filamentous fungi, chitin is likely tethered to the cell wall through both β-glucan cross-linking and chitin-α-1,3-glucan hydrophobic interactions, forming a reciprocal and redundant mechanism for chitin-to-cell-wall "anchoring". As such, removal of all *crh* genes would affect the integrity of the filamentous fungal cell wall to a much lesser extent, than observed in yeasts, which lack α-glucans (Yoshimi et al., 2017).

We previously reported on the construction of a *crh* family knockouts (*crhA-G*) in *A. niger* by seamlessly excising the corresponding ORFs, using CRISPR/Cas9 gene editing (**Chapter 2**). Initial phenotypic analysis on cell wall stressing compounds CalcoFluor White (CFW) and CR showed no effects on cell wall integrity. Here, we report on a more extensive analysis of the seven-fold *crh* mutant by analyzing multi-condition gene expression data sets, additional cell stress assays, bioreactor growth, transcriptomic analysis and cell wall composition. Moreover, we analyzed the role of Crh enzymes in the process of cell wall deficiency, by introducing a mutation in a gene required for cell wall galactomannan synthesis (*ΔugmA*) in the seven-fold *crh* knockout strain. A deletion of *ugmA* was previously shown to compromise cell wall integrity caused by

a galactofuranose deficiency (Damveld et al., 2008), and revealed upregulation of *crhE* in transcriptomic studies (Park et al., 2016). Additionally, we assessed the relation between chitin to β-glucan cross-linking and α-1,3-glucan, by reducing cell wall α-glucan synthesis in both wild type and the seven-fold *crh* mutant. We disrupted both the most actively expressed α-glucan synthase E (*agsE*), and cell wall stress induced α-glucan synthase A (*agsA*) (Damveld et al., 2005b). Taken together, our data indicate that Crh enzymes play a significant role in cell wall integrity when galactofuranose is absent and when cell wall α-1,3-glucan levels are reduced.

2. MATERIALS AND METHODS

2.1 Strains, media, growth conditions

Strains used in this study can be found in Table 1. All media were prepared as described by Arentshorst et al., 2012. In all cases, minimal medium (MM) contained 1% (w/v) glucose, 1.5% agar (Scharlau, Barcelona, Spain) and was not supplemented unless otherwise specified. Complete medium (CM) contained 0.1% (w/v) casamino acids and 0.5% (w/v) yeast extract in addition to MM. Strains were inoculated from -80°C glycerol stocks onto fresh CM plates and were allowed to grow and sporulate for 5-7 days at 30°C, prior to spore harvesting. Spores were harvested by addition of 15 mL of 0.9% (w/v) NaCl to CM spore plates and were carefully scraped from the surface with a cotton swab. In case of harvesting spore plates for bioreactor cultivations, 0.05% Tween-80 was added to the 0.9% (w/v) NaCl to prevent spore clumping. Spore solutions were poured over sterile cotton filters (Amplitude™ Ecocloth™ Wipes, Contec Inc., Spartanburg, SC, USA) to remove large mycelial debris. Spore solutions were counted using Bio-Rad TC20™ Automated Cell Counter (Bio-Rad Laboratories, Inc. USA) using Counting Slides, Dual Chamber for Cell Counter (Cat#145-0011, Bio-Rad Laboratories, Inc. USA).

Table 1. All strains used in this study

Name	Genotype	Reference
N402	cspA1	Bos et al., 1988
MA234.1	cspA1, *ΔkusA::DR-amdS-DR*	Park et al., 2016
TLF39	cspA1, *ΔkusA::DR-amdS-DR, ΔcrhA-G*	van Leeuwe et al., 2019
MA613.1	cspA1, *ΔkusA::DR-amdS-DR, ΔugmA::hygB*	This study
TLF70	cspA1, *ΔkusA::DR-amdS-DR, ΔcrhA-G, ΔugmA::hygB*	This study
TLF93	cspA1, *ΔkusA::DR-amdS-DR, ΔagsA*	This study
TLF94	cspA1, *ΔkusA::DR-amdS-DR, ΔagsE*	This study
TLF95	cspA1, *ΔkusA::DR-amdS-DR, ΔagsA, ΔagsE*	This study
TLF96	cspA1, *ΔkusA::DR-amdS-DR, ΔcrhA-G, ΔagsA*	This study
TLF97	cspA1, *ΔkusA::DR-amdS-DR, ΔcrhA-G, ΔagsE*	This study
TLF98	cspA1, *ΔkusA::DR-amdS-DR, ΔcrhA-G, ΔagsA, ΔagsE*	This study

2.2 Cell wall sensitivity assays

Cell wall disturbing compounds Congo Red (CR), Caspofungin (CA, 0-0.25 μM), sodium dodecyl sulfate (SDS, 0.004% and 0.005%), H_2O_2 (0-50 mM) and tunicamycin (0-10 μg/mL) were added to MM plates. Spores were harvested as described above, counted, serially diluted into 2000, 200, 20 and 2 spores/μL and 5 μL of respective dilutions were spotted on MM plates containing cell wall disturbing compounds. Plates were incubated for 3-5 days at 30°C.

2.3 Cell wall isolation and fractionation

2.3.1 Cell wall isolation

Cell wall samples were isolated as described in **Chapter 5**. In short, dried mycelium was frozen in liquid N_2 and were ground to break open the cells. Samples were washed to remove intracellular debris and proteins, three times with 1M NaCl and three times with Milli-Q ultrapure water (MQ). Supernatant was carefully discarded prior to the next washing step. Cell wall samples were lyophilized after washing steps for 48h.

2.3.2 Cell wall fractionation and dialysis

Lyophilized cell wall samples were weighed using a fine balance (d = ± 0.1 mg) using 50 mL plastic tubes. To fractionate cell walls to the first alkali soluble fraction (ASF-I), 1 mL solvent of 80% (v/v) methanol, 5% KOH and 0.1% $NaBH_4$ was added per 10 mg cell wall sample. Samples were agitated at 200 rpm at RT for 24h. Next, samples were spun down for 10 minutes at 1500 rpm. Harvested supernatant makes up fraction ASF-Ia. A second addition of 1 mL solvent of 80% (v/v) methanol, 5% KOH and 0.1% $NaBH_4$ was added to the pellet per original 10 mg cell wall sample, and was incubated at 100°C for 30 min. Supernatant was harvested after centrifugation (ASF-Ib) and was pooled with ASF-Ia to form the ASF-I fraction. The remaining pellet was taken up in 1 mL solvent of 80% (v/v) methanol, 24% KOH and 0.1% $NaBH_4$ per 10 mg cell wall, and repeated in the same way as described above to obtain the ASF-II. The remaining pellet was deemed the alkali insoluble fraction (AIF) and was washed three times with 0.5M acetic acid, followed by three washes with MQ prior to lyophilization. ASF-I and II supernatants were pH-adjusted (6.0) using glacial acetic acid and freeze-dried after a dialysis step (Spectra/Por MWCO 1000 Daltons, Spectrum Laboratories) against deionized water to remove solutes of a small molecular mass (dialysis tubings were thoroughly washed before use to eliminate any contaminants potentially associated to the membranes) and constituted the alkali-soluble fractions (ASF) I and II respectively.

2.4 Monosaccharide Analysis by Reversed Phase UHPLC-ESI-MS/MS

2.4.1 Hydrolysis and sample preparation:

For each sample ~ 100 μg of freeze-dried and dialyzed cell wall material were treated with either 200 μl 6 M HCl for 180 min at 100°C (amino sugar analysis) or submitted to autoclaving (60 min, 121°C) after the addition of 1 mL 2 M TFA (neutral sugar analysis). For solvent removal, samples

were initially air-dried at 40°C. Afterwards samples for neutral sugar analysis were washed once with 1 mL MeOH and twice with 2 mL MeOH (air-drying between and after washing steps). Samples for amino sugar analysis were washed only once with 2 mL MeOH and air-dried. Before derivatization, samples for both amino sugar and neutral sugar analysis were suspended in 400 µL H_2O each. Subsamples of 25 µL were incubated with a mixture of 100 µL 25 % (v/v) ammonia and 100 µL 1-phenyl-3-methyl-5-pyrazolone (PMP) for 100 min at 70°C and 300 rpm before being cooled down to room temperature. Subsequently, samples were neutralized by adding 75 µL 100% acetic acid. Finally, excess PMP was removed by 3 steps of chloroform extraction (400 µL each). Before being measured by UHPLC-ESI-MS/MS, the aqueous phase (after extraction) was filtered through 3 kDa filters. Standards for all analyzed monomers (mannose, galactose, glucose, arabinose and glucosamine) were treated equally and included in every hydrolysis batch in the following amounts: 3 µg, 6.25 µg, 12.5 µg, 25 µg, 50 µg, 75 µg, 100 µg.

2.4.2 Detection using UHPLC-ESI-MS/MS:

Samples were measured on a Dionex Ultimate 3000RS UHPLC system (Thermo Scientific, Milford, USA) equipped with a Zorbax Eclipse Plus C18 column (1.8 µm, 2.1 mm × 100 mm; Agilent, Santa Clara, USA) and an Eclipse Plus guard column (1.8 µm, 2.1 mm × 5 mm; Agilent, Santa Clara, USA). The LC-system was coupled to an amaZon speed ESI-MSn detector (Bruker Daltonik, Bremen, Germany). PMP derivatized monosaccharides were separated based on a method previously described (Xu et al., 2018), using the following 14 min gradient elution profile: 0-1 min isocratic 95% A (95% H_2O, 5% acetonitrile, 25 mM ammonium acetate, pH 7.8); 1 - 9 min linear from 5% to 25% B (5% H_2O, 95% acetonitrile); 9 - 9.5 min linear from 25% B to 99% B; 9.5 - 12 min isocratic 99% B; column re-equilibration: 12 - 12.5 min linear from 99% B to 95% A; 12.5-14 min isocratic 100% A. 2 µl of sample were injected into the system and samples were measured in UltraScan mode and negative ion mode (Auto MS^2) with the following parameters: capillary voltage 4000 V; plate offset voltage = 500 V; isolation width = 4 m z-1; nebulizer pressure = 1.03 bar. Dry gas = 8 L · min^{-1}; dry temperature = 200°C ICC target = 100000; max. accumulation time 50 ms; CID fragmentation; For each derivatized monosaccharide (monosaccharide-PMP_2), one of the most abundant fragment ions of the precursor ion $[M-H]^-$ was used for quantification as previously described (Xu et al., 2018) (see Table 2). To minimize fragmentation of non-target molecules, we included only precursor masses in the following m/z ranges (Figure S1): 474 – 484 (covering Arabinose-PMP_2) and 503 – 514 (covering Mannose-PMP_2, Glucosamine-PMP_2, Glucose-PMP_2, Galactose-PMP_2).

2.4.3 Data analysis

Fragment ion intensities of given precursor ions were integrated over a pre-defined retention time window, allowing a mass error of 2 Da for both precursor and fragment ion m/z. See Table 2 for m/z values and retention times. Measurements of derivatized monosaccharide standards in different concentration were used to determine power calibration curves (Figure S2). The µg amount of each monosaccharide per mg (dry weight) cell wall ($C_{mono/CW}$) was calculated as follows:

$w_{CWF}\frac{m_{mono}w_{mono}}{m_{CWF}}$, where the mass w_{CWF} fraction is the mass of dialyzed cell wall fraction [mg] divided by the mass of total cell wall [mg] (dry weight). m_{mono} is the mass of a monosaccharide [µg] determined by mass spectrometry $m_{mono} = \left(\frac{I}{a}\right)^{\frac{1}{b}}$ with I = arbitrary intensity of the fragment ion; a and b are coefficients determined by fitting a power function to a measured series of monosaccharide standards. The weight fraction $w_{mono} = \frac{M_{mono}-M_{H2O}}{M_{mono}}$, with M_{mono} = molar mass of monosaccharide, and M_{H2O} = molar mass of water, is used to compensate for the gain of mass due to hydrolysis of glycosidic linkages in cell wall polysaccharides. The mass m_{CWF} is the dry weight [mg] of dialyzed cell wall fraction that was subjected to hydrolysis and derivatization. For further details, see supplementary figures S1 and S2.

Table 2: m/z values of precursor and fragment ions of derivatized monosaccharides.

Molecule	Precursor ion (m/z)	Fragment ion (m/z)	Retention time (min)
Mannose-PMP_2	509.19	214.975	~ 6.3 - 6.6
Glucosamine-PMP_2	508.25	213.97	~ 6.9 - 7.2
Glucose-PMP_2	509.19	214.975	~ 7.8 – 8.05
Galactose-PMP_2	509.19	214.975	~ 8 - 8.25
Arabinose-PMP_2	479.17	214.975	~ 8.2 - 8.5

2.5 Bioreactor cultivation

Controlled batch fermentations for *A. niger* strains MA234.1 and TLF39 were performed in 6.6L BioFlo bioreactors (New Brunswick Scientific), as previously described (Jørgensen et al., 2010). A batch of 21 L MM containing 0.75% D-glucose was made by adding 1 L filter-sterilized (0.2 µm pore) glucose (15.75% w/v) solution to a freshly autoclaved volume of 20 L MM (no carbon source) as described above. Allowing 1 day of dissolving and a check for contamination, 5 L MM 0.75% glucose was added to each bioreactor directly after autoclaving. Temperature, acidity and stir speed were set to and kept at 30°C, pH 3 and 250 rpm, respectively. The pH was controlled by addition of titrants (2M NaOH and 1M HCl). Sparger aeration of 1 L/min was left on to allow oxygen saturation of the medium prior to inoculation. Next, aeration was set to headspace only and 1.5 mL 10% w/v Yeast Extract was added to the medium to promote homogeneous germination for the to-be-added spores. Subsequently, a total of $5x10^9$ (10^6 sp/mL) spores were added to the medium using a concentrated spore solution. Germination time of approximately 4-5h was maintained, preceding the addition of polypropyleneglycol P2000 anti-foam agent, increasing agitation to 750 rpm and changing aeration from headspace to sparger only (1 L/min). Oxygen, base and acid consumption were monitored and samples were taken at regular intervals to obtain biomass, culture filtrate and microscopy samples. Biomass was harvested by applying a vacuum over Whatman™ Glass Microfiber Filter (GF/C™) (diameter 47 mm, CAT No.1822-047, Buckinghamshire, UK). Samples were all quickly frozen in liquid nitrogen prior to storage at -80°C. Biomass accumulation through time was gravimetrically determined by lyophilizing designated samples from the corresponding broth culture mass.

2.6 RNA isolation and RNA-sequencing

RNA was isolated from mycelial biomass samples obtained from batch cultivated *A. niger* strains MA234.1 and TLF39, using TRIzol (Invitrogen). RNA was purified afterwards with NucleoSpin RNA Clean-up kit (Macherey-Nagel) with DNase treatment. Concentration and quality of the RNA was determined using a NanoDrop 2000 spectrophotometer (Thermo Scientific) and by gel-electrophoresis, respectively. RNA samples were sent to Genome Québec for sequencing using the HiSeq4000 technology. Sequencing data is available under GEO accession number GSE142461.

2.7 Transcriptomic analysis

Raw RNA-seq read sets were retrieved from the Génome Québec's Nanuq portal, and pre-processed with BBDuk from the BBTools package (https://sourceforge.net/projects/bbmap) to trim sequencing adapters and remove reads derived from PhiX and ribosomal RNA. The transcriptome of *A. niger* NRRL3 (v. 20140311) was retrieved from the *jgi* Genome portal (Aguilar-Pontes et al., 2018), and the libraries were mapped to the transcriptome using Salmon v0.14.1 (Patro et al., 2017). The libraries were imported in RStudio 1.2.5001 (RStudio: Integrated Development for R. RStudio, Inc., Boston, 2016) running R 3.6.1 (R Development Core Team 3.6.1., 2019) using txtimport v.1.12.3 (Soneson et al., 2016). Initial data exploration showed that the major source of difference between the libraries was due to the strain (Figure S3), although the time-point of sampling was also an important factor to consider. However, both strains behaved in the same way between the 70% and 90% biomass time-points (Figure S4). That is, there was no significant interaction between the 70 and 90% biomass growth and the mutation. Based on this information, we considered the biomass time-points as biological duplicates, thereby increasing the statistical power. Differential gene expression was assessed via pairwise comparisons using DESeq2 v1.24.0 (Love et al., 2014), using the design ~ biomass + mutation ($p$adj ≤ 0.05). Data was manipulated using tidyverse (Wickham, 2017a) and plotted in ggplot2 (Wickham, 2017b). Gene ontology enrichment ($p$adj ≤ 0.05) was performed with goseq v1.36.0 (Young et al., 2010). Updated gene length and Gene Ontology data for the NRRL3 genome was retrieved from the *jgi* Genome portal. The full code is available at github.com/gabrifc/TLF39_transcriptome.

2.8 Single and double gene knockouts

A deletion of *ugmA* was introduced in the seven-fold *crh* knockout strain (TLF39) using a split marker approach as described below. To target α-1,3-glucan synthesis, we disrupted both α-glucan synthase A (NRRL3_07454) and α-glucan synthase E (*agsE*, NRRL3_00248) separately, and constructed a double *agsA, agsE* knockout using CRISPR/Cas9 and repair fragments (see below).

2.8.1 Split marker fragments

MA234.1 and TLF39 (Table 1) were transformed after protoplastation as described previously (Arentshorst et al., 2015). Using the split marker approach for single gene knockouts, entire

ORFs were deleted by replacement with the hygromycin B selection marker (Arentshorst et al., 2015). Flanks were generated via PCR using N402 genomic DNA as template and primers as described in Primer Table. *AOpyrG* fragments were obtained from plasmid pAN7-1 (Punt et al., 1987) with primers as described in Primer Table. Fusion PCR was used to generate split marker fragments containing *AOpyrG.* Approximately 2 µg of DNA per flank was added to protoplasts for transformation. Transformation plates were incubated on MMS for 6 days at 30°C. Transformed colonies were single streaked on MM twice for purification and were genotyped using diagnostic PCR (data not shown).

2.8.2 CRISPR/Cas9 and repair DNA fragments

CRISPR/Cas9 plasmid transformations were performed after protoplastation as described previously (**Chapter 2**). Plasmids were constructed using a pFC332 (*hph*) plasmid (Nødvig et al., 2015) backbone and repair fragment were generated using fusion PCR with N402 genomic DNA as template as described in Primer Table. For transformations 2 µg of Cas9-sgRNA plasmid with 2 µg of repair DNA fragment were used. Transformation plates were incubated on MMS with 200 µg/mL hygromycin for 7 days at 30°C. Transformed colonies were single streaked on selectable MM with 100 µg/mL hygromycin to select for the presence of the Cas9-sgRNA plasmid. Next, a single colony was picked and transferred to non-selective MM medium to allow loss of the Cas9-sgRNA plasmid. A third streak of a single colony on both MM and MM with 100 µg/mL hygromycin uridine was performed as a control for loss of plasmid. DNA from plasmid-cured strains was isolated as described by Arentshorst et al., 2012, using mortar and pestle to grind the mycelium in liquid nitrogen. Genotypes were confirmed using diagnostic PCR to check for open reading frame removal.

3. RESULTS

3.1 *Aspergillus niger* possesses seven *crh* gene orthologs

Crh enzymes have most extensively been studied in yeast, but are well conserved in fungal genomes (Arroyo et al., 2016). In *A. niger,* seven *crh* genes (*crhA* to *crhG*) have been annotated based on homology with both *CRH1, CRH2* and *CRR1* (Pel et al., 2007 and Table 3). Using SignalP 4.1 (Nielsen, 2017), N-terminal signal sequences were predicted for all seven enzymes. Aside from CrhF and CrhG, the Crh enzymes in *A. niger* were also predicted to contain Glycosylphosphatidylinositol (GPI) anchors by the PredGPI server (Pierleoni et al., 2008), whereas CrhF and CrhG were predicted to contain a single transmembrane helix (TMH) using TMHMM 2.0 (Krogh et al., 2001; Sonnhammer et al., 1998). Using ScanProsite (de Castro et al., 2006), we identified that all seven Crh enzymes carry a catalytic active site E-I-D-[WFL]-E, similar to the previously reported common catalytic motif (E-[ILV]-D-[IVAF]-[VILMF](0,1)-E), in which the first glutamic acid, central aspartic acid and final glutamic acid act as nucleophile, auxiliary residue and the general acid/base, respectively (Gaiser et al., 2006; Hahn et al., 1995; Johansson et al., 2004; Keitel et al., 1993). Additionally, all

Crh enzymes carry the essential substrate-binding pocket GTIXWXGG motif for transglycosylation activity as reported in *Aspergillus fumigatus Af*Crh1-5 (Fang et al., 2019), whereas CrhG was found to have another polar amino acid at the conserved second position of this motif (GNIXWXGG). In addition to these seven members of the GH16 family, six other GH16 enzymes are reported for *A. niger* in the CAZy database (NRRL3_06188, NRRL3_02000, NRRL3_02614, NRRL3_05937, NRRL3_01051 and NRRL3_05408). However, these do not show up as reciprocal BLAST hits with Crh1p, Crh2p and Crr1p. Despite a GH16 active site in these GH16 enzymes (E-[IS]-D-[IV]-[ILV]-E), these non-Crh GH16 enzymes of *A. niger* do not have the consensus GTIXWXGG motif of Crh enzymes, as is also not the case for the yeast GH16 enzymes Kre6p and Skn1p.

Table 3. GH16 enzymes in *A. niger* and properties thereof.

NRRL3 ID	Gene	GH16 catalytic motif*	Consensus crh motif**	Signal peptide	GPI anchor	TMH
NRRL3_10021	*crhA*	EIDWE	GTIDWAGG	yes	yes	0
NRRL3_04809	*crhB*	EIDFE	GTIEWAGG	yes	yes	0
NRRL3_04315	*crhC*	EIDLE	GTIEWAGG	yes	yes	0
NRRL3_02532	*crhD*	EIDWE	GTIEWAGG	yes	yes	0
NRRL3_01365	*crhE*	EIDWE	GTIEWAGG	yes	yes	0
NRRL3_07085	*crhF*	EIDWE	GTIVWAGG	yes	no	1
NRRL3_03998	*crhG*	EIDWE	GNIEWGGG	yes	no	1
NRRL3_06188	-	EIDIIE	n.d.	yes	yes	0
NRRL3_02000	-	EIDIIE	n.d.	yes	no	0
NRRL3_02614	-	EIDVLE	n.d.	no	no	1
NRRL3_05937	-	EIDVIE	n.d	no	no	1
NRRL3_05408	-	EIDVVE	n.d	no	no	0
NRRL3_01051	-	ESDIE	n.d.	yes	no	1

*Hits for E-[IS]-D-x-[VILMF](0,1)-E
**Hits for G-[TN]-I-x-W-x-G-G
n.d. (not detected)

3.2 Multi-condition expression data shows *crh* genes activity during different stages of development

In yeast, *CRH1* and *CRH2* are both expressed during vegetative growth, whereas *CRR1* is only induced upon sporulation. This suggests diversification of Crh enzymes to fulfill a role in different stages of growth. As a first step in our studies on the *crh* gene family in *A. niger* we analyzed expression levels of *crh* genes in a gene-expression dataset, covering 155 different cultivation and developmental conditions (Paege et al., 2016; Schäpe et al., 2019). We previously reported on a sub-set of these conditions where we looked into *crh* expression under plate growth conditions and during exponential growth from liquid fermentation (**Chapter 2**). Here, we expanded this study for different growth and developmental phases, including germination (Novodvorska et al., 2013;

van Leeuwen et al., 2013), exponential vegetative growth, starvation and sporulation conditions (Jørgensen et al., 2010; van Munster et al., 2015) as well as sclerotium formation (Jørgensen et al., 2020), spore maturation (Teerstra et al., 2017) and exposure to cell wall disturbing compounds (Meyer et al., 2007; Fiedler et al., 2014). An overview of these gene expression data expressed as a percentage of actin expression is shown in Table 4.

From the analysis it is clear that during conidial germination, in particular *crhB* and *crhC* are expressed upon swelling, initial germ tube formation, and early branching (t = 1-6h). In non-germinated, resting conidia (t = 0h), we find very low levels of *crh* gene transcripts, the highest being *crhF* (Novodvorska et al., 2013). These low levels of *crh* gene transcript are in congruence RNA-seq data from maturing spores (Teertstra et al., 2017), and also show the highest relative number of transcripts for *crhF* followed by *crhB* (Table S1), similar as found in Table 4 (t = 0h). Upon exposure to antifungal compounds caspofungin (β-1,3-glucan synthase inhibitor, CA) and aureobasidin A (sphingolipid biosynthesis inhibition, AbaA) in germlings, both *crhB* and *crhC* were reported to be higher than in control (no drug added) experiments (Fiedler et al., 2014; Meyer et al., 2007b), whereas only *crhD* was induced in the presence of fenpropimorph (sterol biosynthesis inhibition, FP) (Table 4).

During exponential growth, *crhD* is the highest expressed *crh* gene. Nonetheless, both *crhB* and *crhC* are also expressed. Carbon starvation showed to induce the expression of *crhD* even further. Because the increase of *crhD* is not observed during carbon starvation of non-sporulating *ΔbrlA* and *ΔflbA* mutants, the induction of *crhD* is likely to relate to spore formation. No other *crh* genes were specifically expressed during the starvation time points, suggesting that *crhD* is the main *crh* gene involved in spore formation and maturation. We noticed the high expression of *crhB* and *crhC* in the *ΔflbA* mutant which might explain the different cell wall morphology observed in the *ΔflbA* mutant (Pauline Krijgsheld et al., 2013). The involvement of *crh* genes in spore development was also analyzed by examining gene expression in retentostat cultures. During the later time points, massive conidiation was observed evidenced by black pigmentation in the effluent (Jorgensen et al., 2010), but no apparent strong induction of any of the *crh* genes was found, again with the exception of *crhD*.

A. niger mutants have been isolated to form sclerotia (Jørgensen et al., 2011a). During sclerotium formation, *crhA* is specifically induced, suggesting a role for *crhA* during sclerotium development. Finally, in the study by Park et al, it was observed that *crhE* was the only significantly induced (7.51 FC) *crh* gene upon cell wall stress in the galactofuranose cell wall deficient *ΔugmA* (UDP-galactopyranose mutase A) mutant (Park et al., 2016).

In conclusion, the expression analysis suggests that different *crh* genes are expressed under different conditions. Most noticeable is the expression of *crhA* during sclerotia formation, *crhB* and *crhC* during germination, *crhD* during vegetative growth and sporulation and *crhE* during cell wall stress caused by the absence of cell wall galactofuranose. Expression of *crhF* and especially *crhG* were low across all tested conditions, though *crhF* may be involved in spore maturation.

3.3 Cell wall integrity is not disturbed by loss of the *crh* gene family

Loss of *crh* genes in *S. cerevisiae* and *C. albicans* has previously been reported to affect cell wall integrity when exposed to the cell wall stressing compound CR, but displayed normal growth under non-stressing conditions (Rodriguez-Pena et al., 2000; Pardini et al., 2006). A quintuple *crh* knockout strain in *A. fumigtus* was recently shown to have a much lesser effect on growth when exposed to CR compared to yeasts (Fang et al., 2019). In line with the results observed for *A. fumigatus*, we also showed that single knockouts strains of either *crhA, crhB, crhC, crhD, crhE, crhF* or *crhG*, as well as a double, triple, quintuple and seven-fold knockouts strains of *crhA-G* (TLF39), were unaffected by the presence of cell wall disturbing compounds CR and CFW (**Chapter 2**). Additional assays were conducted to assess the impact of a full *crh* gene family knockout in this study, and include sensitivity assays towards SDS (cell wall/cell membrane disturbing), H_2O_2 (oxidative stress), tunicamycin (N-glycosylation, unfolded protein response) and CA. However, both the wild type and the seven-fold deletion strain (*ΔcrhA-G*) showed the same levels of sensitivity towards all these tested compounds (data not shown).

In addition to these cell wall stress assays, closer examination of colony morphology during vegetative growth was carried out showing that there is a minor difference between wild type (MA234.1) and TLF67 (*ΔcrhADEFG*), TLF68 (*ΔcrhABDEFG*) and TLF39 (*ΔcrhABCDEFG*) in radial growth, causing a slightly more compact colony, but not for single, double, triple and quintuple (*ΔcrhABDEF*) mutants (Figure 1). This result indicated that *crh* activity is at least to some extent involved in surface growth behavior, but no differences in hyphal thickness, branching or other aberrant growth behavior were observed when looking into the edges of these colonies.

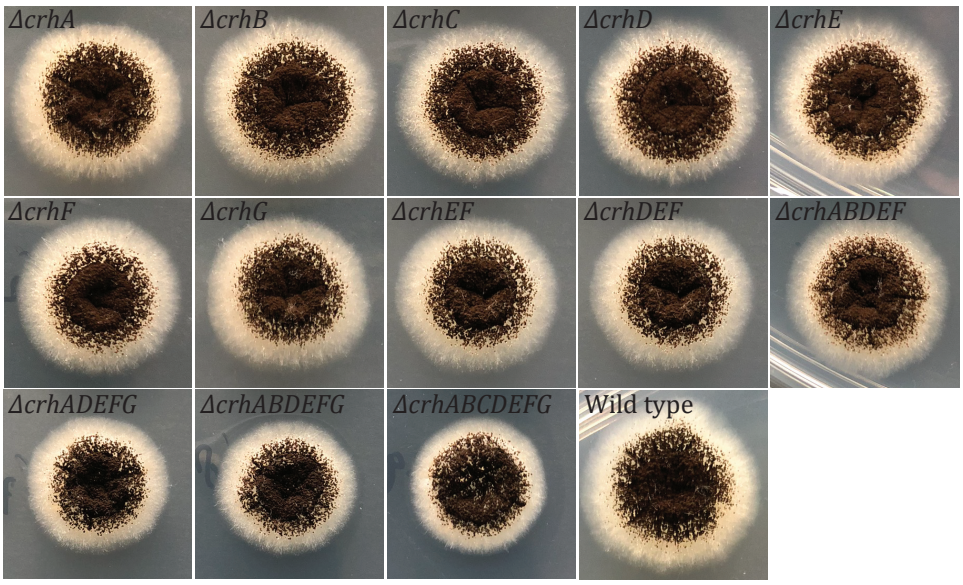

Figure 1. Colony morphology of *crh* mutants and wild type (MA234.1) on MM. All strains were grown equally as described in section 2.1, and were spotted to contain 10^4 spores. Plates were incubated at 30°C for 3 days.

Table 4. Microarray expression data of crh genes (as percentage of actin expression, scale 0% - 100%). Color coding ranges from white to green, representing low and high gene expression, respectively.

Condition	*crhA*	*crhB*	*crhC*	*crhD*	*crhE*	*crhF*	*crhG*	Reference
Germination of conidia								
0h	0.5	2	1	1	0.9	3.3	0.5	Novodvorska et al., 2013
1h	0.5	6	1.5	6	1	0.8	0.5	
2h	0.5	21	10	9	1.5	1.1	0.5	
4h	0.5	18	21	2	1.5	0.8	0.5	
6h	0.5	12	13	2	1.5	1.2	0.5	
Germlings (5h) response to either Caspofungin (CA), Fenpropimorph (FP), Aureobasidin A (AbaA) or FK506, 1h post-incubation								
CA/FP ctrl	0.5	7.5	21	5.6	1.1	0.9	0.4	Meyer et al., 2007; Fiedler et al., 2014
CA	0.6	14	38	4.4	1.2	1.9	0.3	
FP	0.6	7.1	22	8.9	1.4	1	0.3	
AbaA ctrl	0.7	15	36	4.5	1.9	1v.3	0.5	
AbaA	0.9	20	46	3.7	1.9	1.6	0.4	
FK506 ctrl	1.3	21	34	3.6	1.8	2.1	0.6	
FK506	0.8	14	34	3.3	1.5	2.5	0.5	
Retentostat culture of N402 approaching zero growth rate on maltose								
0 days	1	4.3	2.8	20	1.6	1	0.2	Jørgensen et al., 2010
2 days	1.5	4.5	1.6	39	1.1	2.1	0.1	
8 days	0.6	3.2	1.6	20	1.3	2	0.2	
Carbon starvation and sporulation onset on maltose								
N402 exponential growth	0.9	4.4	2.4	18	1.4	1.2	0.4	van Munster et al., 2015
ΔbrlA exponential growth	2.2	6	5	9	3	1.5	0.5	
ΔflbA exponential growth	2.8	21	18	11	1.5	3.5	0.5	
N402 carbon starvation day 1	1.9	3.3	0.9	87.8	0.9	0.8	0.4	
ΔbrlA carbon starvation day 1	1	3	2	17	1.5	1.1	0.5	
ΔflbA carbon starvation day 1	1	10	10	25	1.2	1.1	0.5	
N402 carbon starvation day 3	1	3.6	2	57.3	0.9	3.7	0.4	
ΔbrlA carbon starvation day 3	1.5	8	6.8	7	1.5	1.5	0.5	
ΔflbA carbon starvation day 3	0.7	9	6	13.5	1.5	1.5	0.5	
N402 carbon starvation day 6	0.5	4.3	2.4	38.9	0.8	2.5	0.3	
ΔbrlA carbon starvation day 6	0.9	7	10	2	1.5	1	0.5	
ΔflbA carbon starvation day 6	1	8.5	11	7.5	1.7	1.5	0.5	
Sclerotia formation on glucose plates								
ΔsclB mycelium	2	8.2	8.5	5	1.2	3.2	0.5	Jørgensen et al., 2020
ΔsclB sclerotia	10	3.4	1.5	0.9	0.9	1.5	0.5	

0%

100%

3.4 Genome-wide expression profiling reveals high similarity between mutant and wild type

To further study the effect of deleting the *crh* family, we performed controlled batch fermentations followed by genome wide gene expression analysis by RNA-sequencing in the seven-fold *crh* mutant (TLF39) and the wild type strain (MA234.1). Both strains were cultivated in 0.75% glucose batch-fermentations in bioreactors as described in section 2.5. Dry weights of fermentations were used to determine the maximal specific growth rate. Both MA234.1 ($0.224 \pm 0.013 \cdot h^{-1}$) and TLF39 ($0.219 \pm 0.005 \cdot h^{-1}$) were found to exhibit equal growth rates, maximum biomass acquisition (MA234.1 g_{DW} $6.4 \pm 0.5 \cdot kg^{-1}$ and TLF39 g_{DW} $6.4 \pm 0.15 \cdot kg^{-1}$) and similar base consumption (data not shown). In addition, morphological analysis of culture samples showed that both wild type and mutant display a very similar growth phenotype (Figure S5).

RNA was isolated from culture samples in the exponential growth phase at both 70% and 90% of the maximum attained biomass. Duplicate batch-culture cultivations for both wild type and mutant were used to obtain a total of 8 RNA-sequencing samples. RNA sequencing was performed as described in section 2.6, followed by transcriptomic analysis (section 2.7). We found 230 transcripts—approximately 2% of the 11846 total transcripts—to be differentially expressed

Table 4. Putative cell wall biosynthetic related genes upregulated in the TLF39 mutant. Listed reads are the average of 70% and 90% biomass DESeq2 normalized (by library and gene length) reads.

Gene ID	Gene	Description	WT reads	Mutant reads	FC	P-adj
NRRL3_10372	-	aldose 1-/glucose-6-phosphate 1-epimerase family protein	607	2045	3.27	5.38E-09
NRRL3_00240	-	carbohydrate-binding module family 50 protein (LysM)	30	78	2.64	4.35E-04
NRRL3_02950	*pirA*	putative cell wall protein with internal repeats	4982	7950	1.48	3.16E-04
NRRL3_00771	*cwpA*	glycosylphosphatidylinositol-anchored cell wall mannoprotein	322	464	1.44	5.47E-05
NRRL3_04222	-	carbohydrate-binding module family 50 protein (LysM)	156	221	1.41	2.60E-03
NRRL3_00251	-	cell-wall synthesis Kre9/Knh1 family protein	1115	1541	1.38	2.62E-14
NRRL3_04221	-	chitinase-like protein	138	189	1.37	1.99E-02
NRRL3_00249	*agtA*	GPI-anchored α-glucanosyltransferase	1811	2311	1.28	1.31E-07
NRRL3_08822	-	cell-wall synthesis Kre9/Knh1 family protein	1316	1675	1.27	2.00E-08
NRRL3_08347	*gfaB*	glutamine-fructose-6-phosphate aminotransferase	1001	1224	1.23	1.41E-02

between the mutant strain and the wild type (adjusted *p*-value ≤ 0.05) (Table S2). First, we found that wild type expression of *crh* genes is in line with previous transcript levels observed in Table 4, where *crhD* is most highly expressed during exponential growth, followed by *crhB, crhC* and *crhA* (Figure S6). Contrarily in the mutant, the deleted *crh*-family genes were no longer expressed, thus validating their knockout, whereas for the other GH16 family members no significant difference was observed between the mutant and the wild type (Figure S6). In accordance to this result, most of the observed variation between mutant and wild type was explained by the difference in expression in these 7 *crh* genes.

Table 5. Putative cell wall biosynthetic genes downregulated in the TLF39 mutant. Listed reads are the average of 70% and 90% biomass DESeq2 normalized (by library and gene length) reads.

Gene ID	Gene	Description	WT reads	Mutant reads	FC	P-adj
NRRL3_02532	*crhD*	glycoside hydrolase family 16 protein	3170	0	∞	4.71E-35
NRRL3_04809	*crhB*	glycoside hydrolase family 16 protein	991	0	∞	4.32E-30
NRRL3_10021	*crhA*	glycoside hydrolase family 16 protein	548	0	∞	4.27E-26
NRRL3_04315	*crhC*	glycoside hydrolase family 16 protein	489	0	∞	3.36E-25
NRRL3_03998	*crhG*	glycoside hydrolase family 16 protein	262	0	∞	4.13E-21
NRRL3_07085	*crhF*	glycoside hydrolase family 16 protein	168	0	∞	1.90E-18
NRRL3_01365	*crhE*	glycoside hydrolase family 16 protein	60	0	∞	9.59E-13
NRRL3_08490	-	carbohydrate-binding module family 63 protein (expansin-like)	1578	1178	-1.34	2.43E-07
NRRL3_06700	*dfgG*	mannan endo-1,6-alpha-mannosidase	781	644	-1.21	1.31E-02
NRRL3_00523	*ctcA*	chitinase-like protein	18371	15208	-1.21	2.44E-03
NRRL3_03954	-	alpha-1,3-mannosyltransferase-like protein	1079	921	-1.17	1.22E-02
NRRL3_07862	*cfcC*	chitinase	1570	1372	-1.15	1.34E-02
NRRL3_04653	*chsA*	chitin synthase	1527	1356	-1.13	2.85E-02

Gene Ontology (GO) analysis of the differentially expressed genes suggests very few processes are significantly affected between wild type and mutant (Table S3). Three enriched processes pertaining to cell wall biosynthesis (lichenase activity (GO:0042972), hydrolase activity/ hydrolyzing O-glycosyl compounds (GO:0004553), and carbohydrate metabolic process (GO:0005975)), were identified based solely on the differential expression of the *crh* genes present in these three GO categories. Therefore, we also decided to specifically analyze differential gene expression in the datasets of genes involved in cell wall biosynthesis. In this manual search we used a list of all annotated cell wall biosynthetic genes described by Pel et al. 2007 and an overview of all cell wall integrity (CWI) response-related genes as previously described (Meyer et al., 2007b; Park et al., 2016). Significantly upregulated and significantly downregulated cell wall biosynthetic genes are shown in Table 5 and Table 6, respectively. For the upregulated genes, the

highest fold change was found for an aldose 1-/glucose-6-phosphate 1-epimerase family protein (NRRL3_10372), responsible for interconversion between α-glucose and β-glucose. Noticeably, this gene is part of a previously uncharacterized putative secondary metabolite gene cluster for which the expression of all genes was upregulated in TLF39 (NRRL3_10368 – NRRL3_10375), suggesting that this gene is not related to a genuine cell wall related function. As mentioned previously, besides the *crh* gene family, no differential expression of other GH16 enzymes was found and no clear signs for cell wall stress were observed. We only found slight up-regulation for both *gfaB* and *pirA,* yet no induction of other CWI pathway related genes such as *agsA*, *phiA*, *gfaA* (CWI genes highlighted in Table S2), confirming that the CWI pathway is not activated in the seven-fold deletion strain.

3.5 Cell wall fractionation shows identical composition between wild type and mutant

Previous results showed no increased sensitivity towards to cell wall disturbing compounds and no indications for a cell wall stress response, exemplified by lack of induction of *agsA* and *gfaA* in the seven-fold *crh* mutant. Notwithstanding these results, we analyzed whether the seven-fold deletion affected the cell wall composition. To do so, we isolated cell walls from maximum biomass samples of both wild type (MA234.1) and seven-fold *ΔcrhA-G* mutant (TLF39), using aforementioned batch fermentation cultures. Cell walls were fractionated using a 5% (w/v) KOH and 24% (w/v) KOH alkali treatment (see section 2.3.2) to obtain alkali soluble fraction I (ASF-I) and alkali soluble fraction II (ASF-II), respectively. Residual cell wall material after fractionation represents the alkali-insoluble fraction (AIF). ASF-I and ASF-II were dialyzed and weighed. Relative amounts of recovered cell wall dry weight per fraction were found to be of equal proportion for both MA234.1 and TLF39 (Table S4). The unaccounted fraction after recovery is likely attributable to the presence of both (cell wall) proteins and cell debris in the fractionated samples, and partially because of loss of material during transfer in fractionation and dialysis. Next, each fraction was hydrolyzed with either TFA or HCl (see section 2.4.1), followed by derivatization and analysis to detect both neutral and amino sugars with UHPLC-ESI-MS (section 2.4.2). The total cell wall composition as the sum of all fractions is displayed as relative amounts of sugar monomers per mg cell wall prior to fractionation, in Figure 2A. Here, we found that there is no difference in the cell wall sugar composition between MA234.1 and TLF39 for galactose, glucose, mannose and (*N*-acetyl) glucosamine (arabinose was not detected). As β-1,3-glucan has been reported to become alkali insoluble due to its covalent linkage with chitin in the wild type cell wall (Hartland et al., 1994; Mol and Wessels, 1987; Sietsma and Wessels, 1979), we specifically looked in detail whether deletion of the *crh* genes resulted in a shift of the amount of β-1,3-glucan in the AIF to the ASFs of the cell wall, as shown before in yeast (Rodríguez-Peña et al., 2000a). The AIF, shown in Figure 2B, showed that the relative difference between MA234.1 and TLF39 of both glucose and chitin is slightly lower in TLF39. Additionally, we did not observe a significant increase in glucose in either ASF-I or ASF-II fractions (Figure 2B), indicating the lack of *crh* genes neither affected the cell wall composition nor the extractability of glucans out of the AIF.

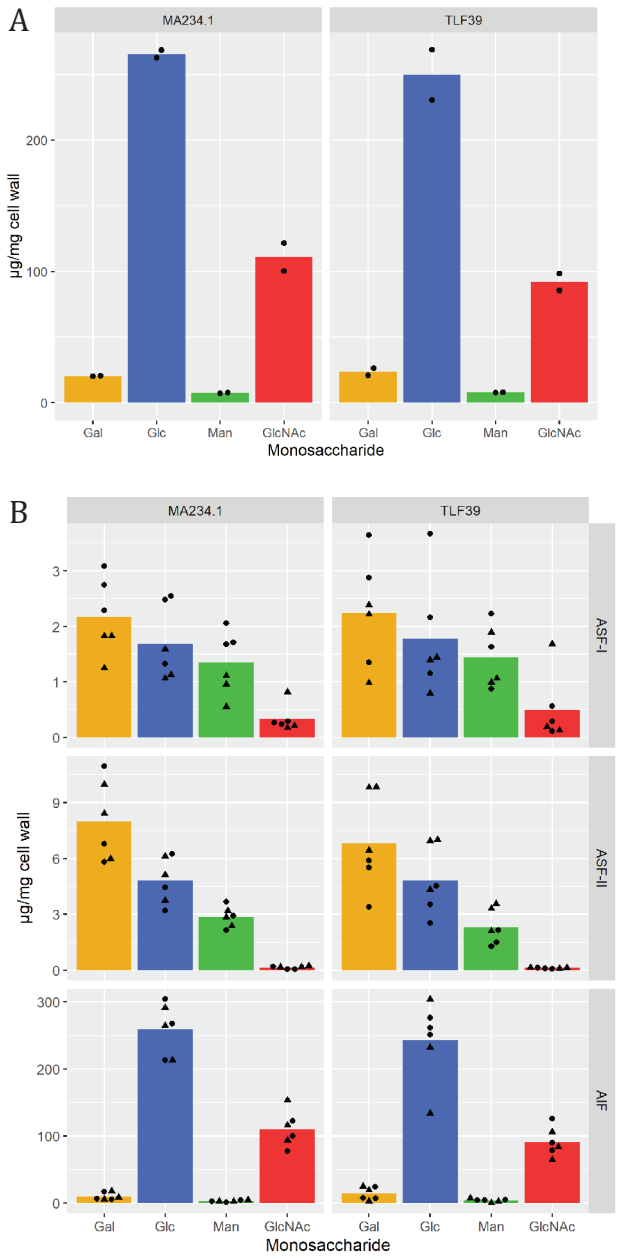

Figure 2. Monosaccharide cell wall composition of wild type strain (MA234.1) and the seven-fold *crh* mutant (TLF39). Cell wall isolation, fractionation, hydrolysis, monosaccharide detection and data processing are described in sections 2.3 and 2.4. Measured monosaccharides include galactose (Gal), glucose (Glc), mannose (Man) and *N*-acetyl-glucosamine (GlcNAc), respectively shown as yellow, blue green and red colored bars. Fractions were obtained from two biological replicate bioreactor (BR) cultivations (maximum biomass) of both wild type (MA234.1), BR_TvL_15 and BR_TvL_18, and seven-fold *crh* mutant (TLF39), BR_TvL_16 and BR_TvL_17. Individual cell wall fractions are alkali soluble fraction I (ASF-I), alkali soluble fraction II (ASF-II) and alkali insoluble fraction (AIF). (A) Total monosaccharide composition per total cell wall dry weight (µg/mg cell wall) from combined fractions (Table S4). Data points are shown as either filled circles (BR_TvL_15 and BR_TvL_16) or filled triangles (BR_TvL_17 and BR_TvL_18), and represent averages of technical triplicate measurements per biological replicate. (B) Monosaccharide composition of each separate fraction as part of the total cell wall dry weight (µg/mg cell wall). Data points are indicated as either empty circles (BR_TvL_15 and BR_TvL_16) or empty triangles (BR_TvL_17 and BR_TvL_18), and represent technical triplicates per biological sample.

3.6 The *crh* gene family is relevant for cell wall integrity in the absence of galactofuranose and α-glucan biosynthesis

Phenotypic analysis, transcriptional data and cell wall composition analysis revealed that the *crh* gene family appears dispensable for growth and does not lead to reduced integrity of the cell wall itself. However, to assess the importance of Crh enzymes in strains with reduced cell

wall integrity, we introduced a mutation causing galactofuranose deficiency (*ΔugmA*) which was previously reported to have reduced integrity of the cell wall, accompanied by increased chitin levels (Damveld et al., 2008; Park et al., 2016). Cell wall chitin compensation has also been reported to occur by deletion of α-1,3-glucan synthases in *A. fumigatus* (Henry et al., 2012) and *A. nidulans* (Yoshimi et al., 2013). We hypothesized that disturbed cell wall integrity involving a chitin compensatory response also increases the importance of Crh-facilitated chitin cross-linking. Additionally, we wanted to assess the role of Crh enzymes in relation to both chitin-α-1,3-glucan interaction and chitin to β-glucan cross-linking. Therefore, knockouts of *ugmA*, *agsE*, *agsA* and double *agsA/E* were performed in both wild type (MA234.1) and seven-fold *crh* mutant (TLF39) genetic backgrounds. All strains were verified by using diagnostic PCR (data not shown).

To assess the level of cell wall integrity, both wild type (MA234.1) and *ΔcrhA-G* (TLF39) strains with additionally introduced knockouts (either *ΔugmA*, *ΔagsE*, *ΔagsA* or *ΔagsA/E*) were exposed to CR, shown in Figure 3. On MM, the *ΔugmA* (Figure 3B) mutant grows and sporulates poorly

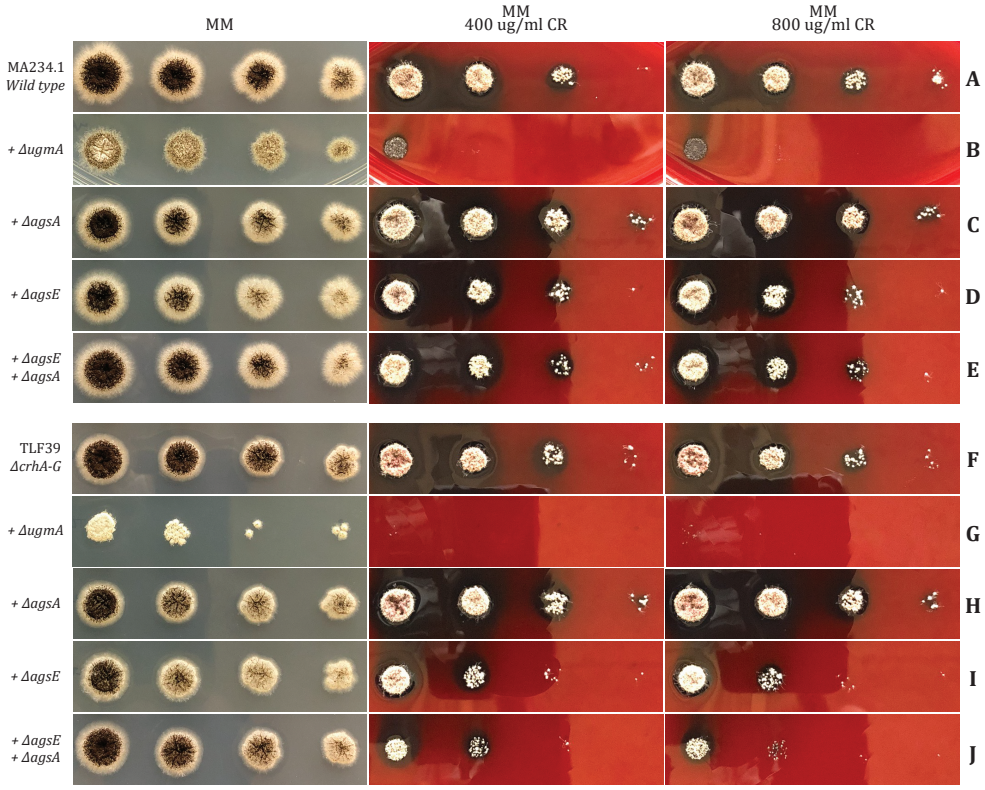

Figure 3. Growth morphology and Congo Red (CR) sensitivity assay. (A) Wild type (MA234.1) and introduced deletions (B) *ΔugmA* (MA613.1), (C) *ΔagsA* (TLF93), (D) *ΔagsE* (TLF94) and (E) *ΔagsA, ΔagsE* (TLF95) on the top five rows. (F) TLF39 (*Δ*crhA-G) and the introduced deletions (G) *ΔugmA* (TLF70), (H) *ΔagsA* (TLF96), (I) *ΔagsE* (TLF97) and (J) *ΔagsA, ΔagsE* (TLF98) on the bottom five rows. Left column shows growth on MM, middle column shows growth on MM with 400 µg/mL CR and right column shows growth on MM with 800 µg/mL CR. All strains were spotted to contain equal amounts of spores from left to right: 10^4, 10^3, 10^2 and 10^1 spores. Plates were incubated at 30°C for 65h.

compared to the wild type strain (Figure 3A). Introduction of *ΔugmA* in the seven-fold *crh* mutant (TLF70, lane G) has an even more drastic effect on both colony size and sporulation compared to both *ΔugmA* (Figure 3B) and *Δcrh*A-G (Figure 3F). It became evident that there is an additive effect of removing cell wall galactofuranose in the background of the seven-fold *crh* gene family knockout on both colony morphology and sporulation, by comparing individual colonies of *ΔugmA* with *Δcrh*A-G/*ΔugmA* (Figure S7). Additionally, Figure 3 shows that sensitivity towards CR, while already much lower for *ΔugmA* compared to wild type, was also exacerbated in the background of the seven-fold *crh* mutant.

Contrarily to galactofuranose deficiency, neither growth nor sporulation defects were observed on MM by deleting either *agsA*, *agsE* or in the *agsA/agsE* double mutant in both wild type (Figure 3C, D and E, respectively) and seven-fold *crh* mutant backgrounds (Figure 3H, I and J, respectively). However, a knockout of *agsE* was found to increase CR sensitivity in the seven-fold *crh* mutant (Figure 3F), but not in the wild type (Figure 3A). Moreover, a double knockout of both *agsA* and *agsE* in the seven-fold *crh* mutant (Figure 3J) resulted in an even more sensitive CR phenotype. The seven-fold *crh* mutants lacking either α-glucan or galactofuranose have also been tested for sensitivity towards CFW, CA and SDS. Similar to CR sensitivity, we found that double mutants were more sensitive to CFW. Susceptibility to both CA and SDS was identical between strains.

4. DISCUSSION

The fungal cell wall matrix is a complex structure that shows large diversity among different species. It is subjected to continuous changes during growth and development, but also in response to environmental cues, mycelial age, available nutrients and cultivation conditions, hypoxia and other stresses (Free, 2013; Lord and Vyas, 2019; Pochanavanich and Suntornsuk, 2002). It is well established that the β-1,3-glucan-chitin core is the load-bearing structure of the cell wall and is essential for survival (Gow et al., 2017). As such, it is under continuous monitoring to ensure its integrity. Despite this importance, relatively few studies have investigated the covalent assembly of the β-1,3-glucan-chitin complex that was first shown to be facilitated by the Crh enzymes in *S. cerevisiae* (Rodríguez-Peña et al., 2000a). Since then, Crh enzymes have been characterized to be solely responsible for this cross-linking activity and recently, advances have been made to investigate and characterize the role of these enzymes in filamentous fungi (Fang et al., 2019; **Chapter 2**). Notwithstanding the same enzymatic activity of Crh enzymes in both yeasts and filamentous fungus *A. fumigatus* (Fang et al., 2019), the cell wall sensitivity phenotypes of *crh* gene family knockouts in *Aspergillus* species do not resemble results obtained in yeast species. In this study, we have investigated the impact of a seven-fold knockout of the *crh* gene family in *A. niger* in more detail.

First off, we investigated an existing, multi-condition expression data set for transcriptional activity of *crh* genes. Analysis of transcriptional activity revealed three majorly active members, namely *crhB, crhC* and *crhD*, whereas the remainder of the family members are expressed at much

lower levels under all conditions tested. In addition to vegetative growth, we observed that *crhD* is likely to be involved during sporulation, yet we did not observe a reduction in sporulation activity in either single *crhD* or seven-fold *crh* gene family knockout strains (Figure 1). Neither did we observe a difference in heat sensitivity of spores (Seekles and van Leeuwe, data not shown). Both *crhB* and *crhC* were found to be expressed upon germination, but neither germination nor growth rate were affected by the loss of the *crh* gene family. In addition, *crhB, crhC* and *crhD* were all shown to be induced upon exposure to differing cell wall stressing compounds, but appear to be dispensable for cell wall integrity based on previous sensitivity assays (**Chapter 2**) and data presented here.

Regarding lowly expressed *crh* genes, *crhA* showed induced expression in sclerotial structures compared to the surrounding mycelium. This may suggest CrhA to play very specific role in this type of structural development, whereas expression levels of all other *crh* genes were relatively low (Table 4, Jørgensen et al., 2020). A single deletion of *crhA* (TLF57) and the seven-fold *crh* mutant (TLF39) were both tested for sclerotium formation and compared to sclerotium formation in the wild type. Both mutants and wild type were able to produce sclerotia, suggesting a non-essential role of *crh* genes during sclerotia formation (data not shown). Despite poor expression in all microarray data, we did find expression of *crhA*, *crhF* and *crhG* during vegetative growth in our batch fermentations using RNA-seq. In addition to observed expression of *crhG* in *A. niger*, we also found that the introduction of a *crhG* deletion (combined with deleting either *crhA* or *crhA* and *crhB* simultaneously) in *Δcrh*DEF, resulted in a small but significant compact colony phenotype (Figure 1), but not as a single *ΔcrhG* knockout. Despite minor differences in growth on plate, we were not able to identify such changes in liquid conditions during submerged batch fermentations because of *crh* loss, nor did we find expressive differences in pellet morphology. For now, the complexity of these genetic interactions as to when and whether other combinations of *crh* knockouts give rise to this compact phenotype have not been investigated and mechanisms of redundancy towards submerged growth remain unknown.

Due to the seemingly expendable nature of *crh* genes in *A. niger*, we performed RNA sequencing to assess whether the seven-fold *crh* deletion triggered a genome-wide transcriptional response. First, we did not find high fold changes in differentially expressed genes. Specifically, some cell wall related enzymes showed small fold-changes (maximum 3.27 < FC > -1.34), and no clear evidence of CWI pathway induction was observed upon deletion of the seven *crh* genes. Furthermore, absence of Crh enzymes in the seven-fold *crh* deletion mutant did not trigger in a transcriptional response of other non-Crh GH16 enzymes in *A. niger*. Recently, a non-Crh GH16 family member of *Trichoderma harzianum, gluc31* described as an endo-β-1,3-glucanase, was shown to have a role in cell wall biogenesis (Ribeiro et al., 2019). The authors argue that a deletion of *gluc31* causes thicker cell walls and a cell wall compensatory response by increased glucan and chitin deposition. A BLAST search with *gluc31* in the *A. niger* genome does not yield clear orthologous hits, the closest ortholog being a GH16 encoding gene (NRRL3_02000) with only 14% query coverage, 48.84% identity. A closer related species to *T. harzianum* and a Sodariomycete, *N. crassa*, revealed a BLAST-based ortholog NCU04431 to *gluc31* (96% query coverage, 56.74%

identity), also encoding a GH16 member. A knockout of NCU04431 was recently shown to exhibit a wild type growth morphology (Patel and Free, 2019), which may suggest that *gluc31* only plays a specific role in cell wall biogenesis of *T. harzianum*. Taken together with transcriptional data from *A. niger*, we do not expect that other non-Crh GH16 enzymes of *A. niger* act in chitin to glucan transglycosylation.

Lack of differential gene expression relating to cell wall biogenesis suggests that the CWI pathway is not induced. However, as mentioned above, some cell wall related enzymes showed small fold-changes in the seven-fold *crh* mutant. These upregulated genes encode two Kre9/Knh1 like proteins, an α-glucanosyltransferase (*agtA*), cell wall proteins *cwpA* and *pirA,* and two LysM (CBM50) binding domain proteins. CBM50 binds with high affinity to chitin, but both proteins identified here (NRRL3_00240: 1 CBM50 domain, and NRRL3_04222: 5 CBM50 domains) lack catalytic domains. Lack of catalytic domains can be indicative of effector proteins that can either protect against chitinolytic activity or capture chitooligosaccharides that are released from the cell wall (Akcapinar et al., 2015). Previously, the cell wall protein *pirA* was identified to be induced upon caspofungin exposure, causing cell wall stress (Meyer et al., 2007b), albeit at much higher levels (FC 23.03) than observed in the seven-fold *crh* mutant (FC 1.48). The *cwpA* gene was also found to be upregulated in the seven-fold *crh* mutant (FC 1.44), but in contrast to *pirA*, *cwpA* was not found to be induced upon cell wall stress. However, a deletion of *cwpA* was reported affect cell wall integrity, indicated by increased sensitivity towards CFW (Damveld et al., 2005a). CwpA belongs to the class of GPI anchored cell wall proteins (GPI-CWP). GPI-CWPs are cross-linked to cell wall β-1,3-glucan via a flexible β-1,6-glucan moiety through a phosphodiester linkage with the GPI-anchor (Frieman et al., 2002; Kapteyn et al., 1996; Kollár et al., 1997; Lu et al., 1995, 1994). The presence of β-1,6-glucosylated cell wall proteins has been reported in *A. niger* (Brul et al., 1997), yet presence of linear β-1,6-glucan chains such as in *S. cerevisiae* remains elusive in filamentous fungi, and is known to be absent in both *A. fumigatus* and *N. crassa* (Free, 2013). The putative synthesis of β-1,6-glucan (moieties), however, may be increased as a result of the two Kre9/Knh1 like proteins found upregulated in the seven-fold *crh* mutant and encode homologs of KRE9 and KNH1 that known to synthesize β-1,6-glucan in *S. cerevisiae* (Brown and Bussey, 1993; Dijkgraaf et al., 1996). The increased presence of both CBM50 effector proteins—with putative chitinolytic protection and chitin tethering—combined with CwpA, PirA, AgtA and Kre9/Knh1 like proteins, may suggest an unknown cell wall stabilizing mechanism through which chitin release is prevented and additional protein to cell wall cross-linking occurs, resulting from the absence of Crh enzymes.

In line with minor changes in expression of some cell wall metabolic genes (Table 5 and 6), we did not find evidence for differences in overall cell wall composition. A more detailed analysis of the fractionated cell wall using alkali fractionation only resulted in a small drop in both glucose and glucosamine in the AIF. However, no increase of glucose in either of the ASF-I or ASF-II fractions was observed, as previously reported upon a double deletion of *CRH1* and *CRH2* in *S. cerevisiae* (Rodríguez-Peña et al., 2000a). Based on these data it is possible either that cross-links between chitin and glucan still exist or that other glucan linkages indirectly (e.g. β-1,4-glucan and β-1,6-

glucan) connect to chitin and result in alkali insolubility. Recently, an *in situ* cell wall assessment of intact *A. fumigatus* cells, using solid state NMR, revealed the cell wall architecture and polymer interactions in great detail (Kang et al., 2018). Interestingly, they show presence of α-1,3-glucan in both the highly (alkali soluble) mobile outer shell and in the rigid hydrophobic core of the cell wall, tightly packed together with chitin. Their findings suggest that β-1,3/-1,6-glucans do not form the rigid backbone structure due to high levels of hydration and mobility, but instead enclose the rigid hydrophobic core that consists of chitin and α-1,3-glucan. Thus, chitin and α-1,3-glucan form the anchor to which β-glucans are proposed to be covalently attached to, while evidence for covalent interactions between α-1,3-glucan and β-glucan or chitin are still lacking. Nonetheless, these findings on intact cells shed new light on the way that we look at the filamentous fungal cell wall. Until now, no cell wall composition assessments have been performed to characterize the impact of removing the *crh* gene family in filamentous fungi. It is important to note that both species that have been studied for cell wall composition in relation to *CRH* loss, *S. cerevisiae* and *C. albicans,* do not possess cell wall α-1,3-glucans and have drastically lower relative amounts of cell wall chitin (Free, 2013). In a different yeast, *Schizosaccharomyces pombe,* vegetative cells neither possess cell wall chitin nor Crh enzymes, but do contain α-1,3-glucan which has been shown to be essential for growth (Grün et al., 2004; Hochstenbach et al., 1998). In filamentous fungi, absence of cell wall α-1,3-glucan has previously been reported to be non-lethal for *A. fumigatus, A. oryzae* and *A. nidulans* (Henry et al., 2012; Miyazawa et al., 2018, 2016), as chitin may suffice for structural integrity. Presence of both chitin and α-1,3-glucan is unique for these filamentous fungi and may create an entirely different dynamic interplay of cell wall integrity. Therefore, based on the reported tight interaction between chitin and α-1,3-glucan and results from our studies, it is possible that loss of chitin to β-glucan cross-linking may not affect cell wall integrity of *A. niger* and *A. fumigatus* in the same way as in either of the aforementioned yeast studies.

Interestingly, we showed an important relation between α-1,3-glucan and chitin to β-glucan cross-linking for maintaining cell wall integrity. When exposed to CR, neither the seven-fold *crh* mutant nor the α-glucan synthase knockouts were negatively affected in growth, separately. However, when both *crh* and *ags* deletions were combined, a synthetic growth defect on CR was observed, showing the importance of Crh enzymes when α-glucan levels are reduced. Additionally, we showed that Crh enzymes are important when galactofuranose biosynthesis is abolished. A deletion of *ugmA* in the seven-fold *crh* family knockout resulted in heavily reduced growth a sporulation and increased sensitivity to CR. Previously reported expression data of the *ΔugmA* strain already revealed increased levels of *crhE* transcript, confirming the importance of Crh enzymes in maintaining cell wall integrity in absence of galactofuranose. In summary, these results suggest that Crh enzymes play an auxiliary role in maintaining cell wall integrity in the absence of other cell wall components.

Because α-1,3-glucan is lacking in cell walls of both *S. cerevisiae* and *C. albicans,* our findings are significant in explaining the discrepancy of the *A. niger* seven-fold *crh* mutant phenotype on CR with the literature on *crh* knockouts in both *S. cerevisiae* and *C. albicans*. We propose that, in α-glucan-containing filamentous fungi, the chitin-α-1,3-glucan interaction and Crh enzymes may

act as reciprocal backup systems to ensure cell wall integrity by anchoring chitin to the cell wall: Reduced α-glucan synthesis is remediated by Crh-facilitated cross-linking of chitin to β-glucans, whereas absence of chitin to β-glucan cross-linking in the seven-fold *crh* knockout strain may be compensated by the tight packing of chitin with α-1,3-glucan.

In contempt of the reported dispensable nature of Crh enzymes in *A. niger*, we are not able to rule out the existence of other cell wall chitin cross-links that may fortify the cell wall. However, we were able to show the importance of Crh enzymes in relation to both α-glucan and galactofuranose, assuming at least in-part loss of cell wall integrity by *crh* family disruption. For now, it remains difficult to explain why there are so many different *crh* genes in *A. niger* and other filamentous fungi. Especially if filamentous fungi possess an α-1,3-glucan-chitin-interaction redundancy mechanism that renders the *crh* gene family dispensable. Paradoxically, filamentous fungi possess more *crh* gene copies than yeast-like fungi that are devoid of cell wall α-glucan and such a putative redundancy mechanism. Despite this, α-glucan synthases most likely evolved post hyphal multicellularity, whereas the *crh*-facilitated β-glucan to chitin transglycosylation coincided with the evolution of hyphae (Kiss et al., 2019). As such, this chronological order of development would allow selection pressure to drive the diversification of Crh enzymes during different growth phases of filamentous fungi, prior to the introduction of cell wall α-glucan. Apart from its role in pathogenesis and conidial aggregation (Yoshimi et al., 2017), α-glucan may thus have the added benefit of aiding chitin-to-cell-wall anchorage—next to Crh-facilitated chitin-β-glucan cross-links—in order to fortify cell wall structure.

5. CONCLUSIONS

Fungi show a high level of complexity with various mechanisms of redundancy to ensure integrity of the cell wall. Not just on the level of multiple gene copies in a single family, but also in terms of inter-connected architectural layers within the macrostructure of the cell wall itself. The complete removal of the *crh* gene family affected neither growth rate nor did it increase the sensitivity towards cell wall stressing compounds, suggesting dispensability of Crh enzymes for cell wall integrity. However, we showed that removal of other cell wall components—through interference of either α-glucan or galactofuranose synthesis—increased susceptibility to cell wall stressing compounds in the seven-fold *crh* deletion mutant compared to the same disruptions in the wild type. Reduced levels of either α-glucans or galactofuranose may increase the cell wall's dependence on chitin for integrity which, in turn, may require Crh-facilitated crosslinks to warrant cell wall stability. Taken together, these findings suggest that inter-structural mechanisms of redundancy are present in filamentous fungi, and only just scratch the surface in understanding cell wall complexity. With special regard to identification of new anti-fungal compounds and strategizing anti-fungal treatments, understanding these mechanisms beckons the need to continue cell wall research in filamentous fungi.

Acknowledgements

We would like to thank Prof. Dr. Bruno M. Moerschbacher for the coordination of the FunChi project.

Funding

This work is part of the "FunChi" ERA-IB project with project number ERA-IB-15-080, which is (partly) financed by the Dutch Research Council (NWO) and PCIN-2015-142 (Ministerio de Economía y Competitividad, Spain). G. Forn-Cuní was funded by the European Marie Skłodowska-Curie fellowship H2020-COFUND-2015-FP-707404, HM was funded by an IEF grant (SignWALLINg-624721) from the European Union.

SUPPLEMENTARY TABLES

Supplementary Table S2 and Table S3 are too larg and can be found online at https://doi.org/10.1016/j.tcsw.2020.100039.

Table S1. Expression data of *crh* genes. Expression data (in FPKMs) during spore maturation at 2 days, 5 days and 8 days. Data from Teertstra et al., 2017.

Gene	NRRL3 ID	ATCC1015 ID	FPKM		
			2 days	5 days	8 days
crhA	NRRL3_10021	Aspni7|1178171	2.54	0.78	0.90
crhB	NRRL3_04809	Aspni7|1134881	10.22	6.51	5.94
crhC	NRRL3_04315	Aspni7|1164138	1.92	1.28	1.32
crhD	NRRL3_02532	Aspni7|1142635	5.85	5.66	3.97
crhE	NRRL3_01365	Aspni7|1141960	0.12	0.09	0.28
crhF	NRRL3_07085	Aspni7|1166076	54.71	63.58	83.35
crhG	NRRL3_03998	Aspni7|40692	0.22	0.34	0.46

Table S4. Batch-cultivation fractionation percentages of initial dry weight. Yield percentages (dry weight/starting dry weight) after alkali fractionation and dialysis from individual bioreactor samples (BR_TvL_#). Biological replicate cell wall samples from both wild type (MA234.1; BR_TvL_15 and BR_TvL_18) and seven-fold *crh* mutant (TLF39; BR_TvL_16 and BR_TvL_18) were fractionated as described in section 2.4.1.

Strain (bioreactor batch)	ASF-I (%)	ASF-II (%)	AIF (%)	Total recovery (%)
MA234.1 (BR_TvL_15)	13	3	36	52
MA234.1 (BR_TvL_18)	12	3	39	54
TLF39 (BR_TvL_16)	13	2	40	55
TLF39 (BR_TvL_17)	13	3	38	54

SUPPLEMENTARY FIGURES

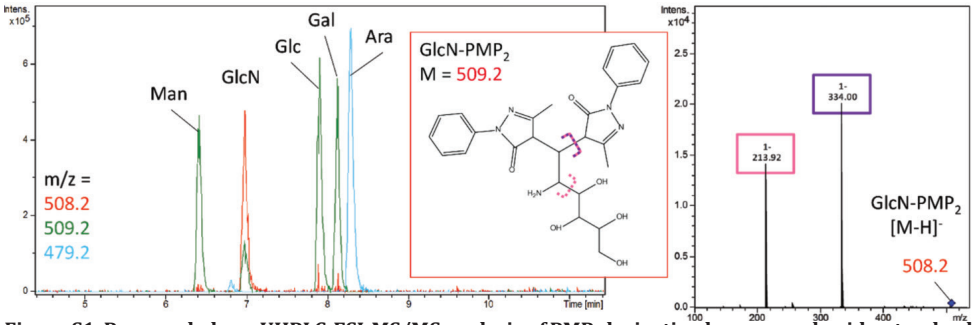

Figure S1. Reversed phase UHPLC-ESI-MS/MS analysis of PMP-derivatized monosaccharide-standards. (A) Extracted-ion chromatograms of the derivatized neutral sugars mannose-PMP2 (Man), glucose-PMP2 (Glc), galactose-PMP2 (Gal) and arabinose-PMP2 (Ara) as well as the amino sugar glucosamine-PMP2 (GlcN) (MS1, negative ion mode), (B) Example MS2 spectrum of glucosamine-PMP2. Fragmentation behavior of derivatized monosaccharide precursor ions is illustrated with GlcN-PMP2 as an example (A). The fragment with m/z = 213.9 is used for quantification.

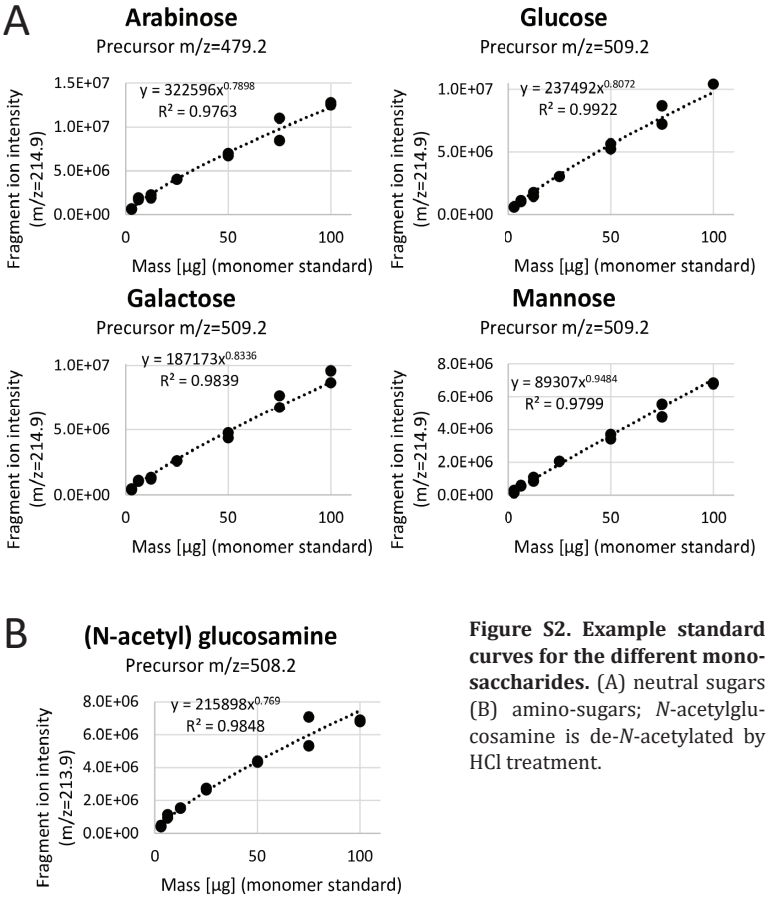

Figure S2. Example standard curves for the different monosaccharides. (A) neutral sugars (B) amino-sugars; *N*-acetylglucosamine is de-*N*-acetylated by HCl treatment.

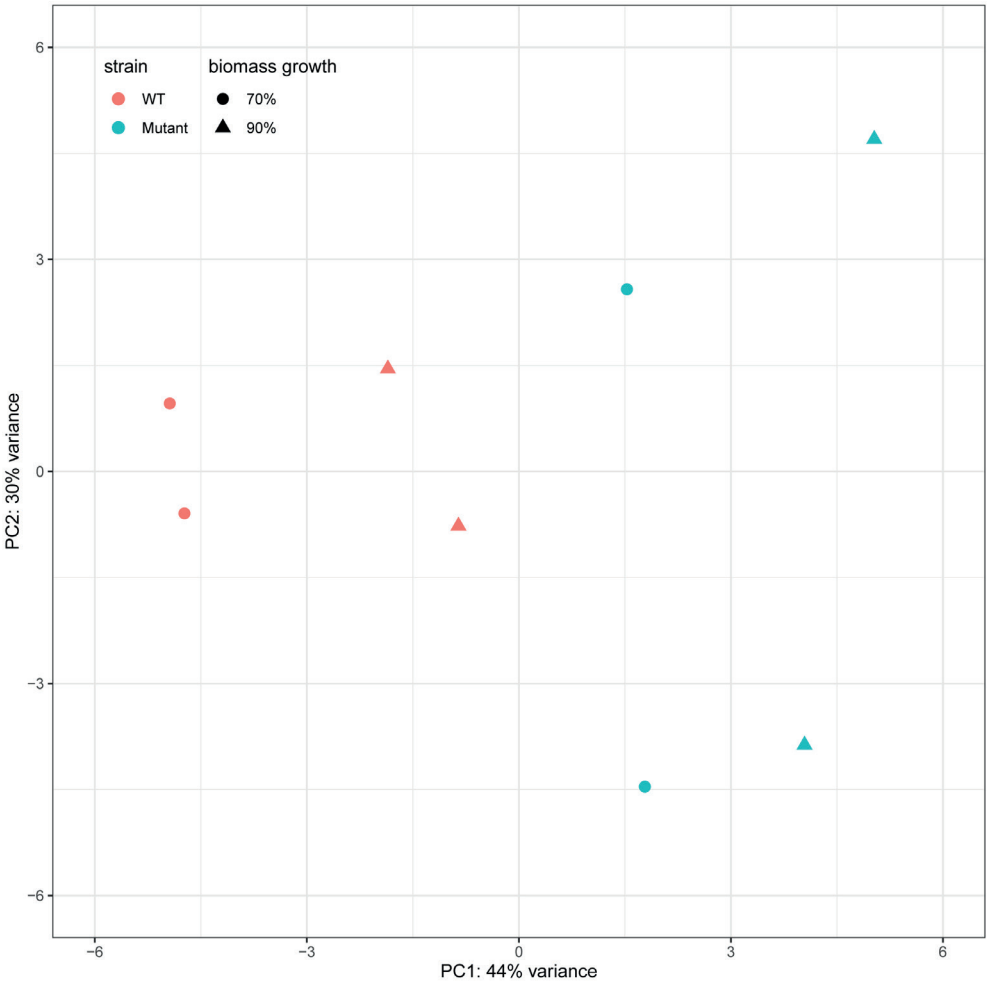

Figure S3. Principal component analysis of the gene expression data obtained by RNA sequencing. The RNA sequencing libraries were separated in the first-dimension axis according to the mutation of the *crh* genes.

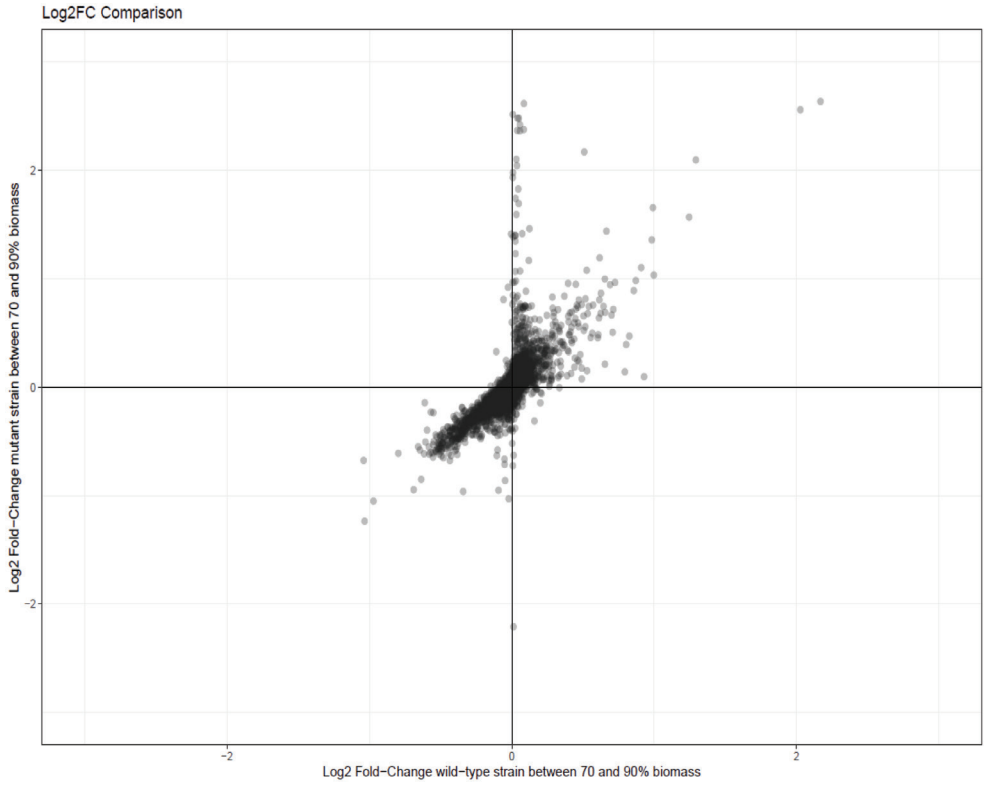

Figure S4. Correlation of fold-change between 70 and 90% biomass. Growth in the WT (x-axis) and the *crh* genes mutated strain (y-axis). Each dot represents a gene.

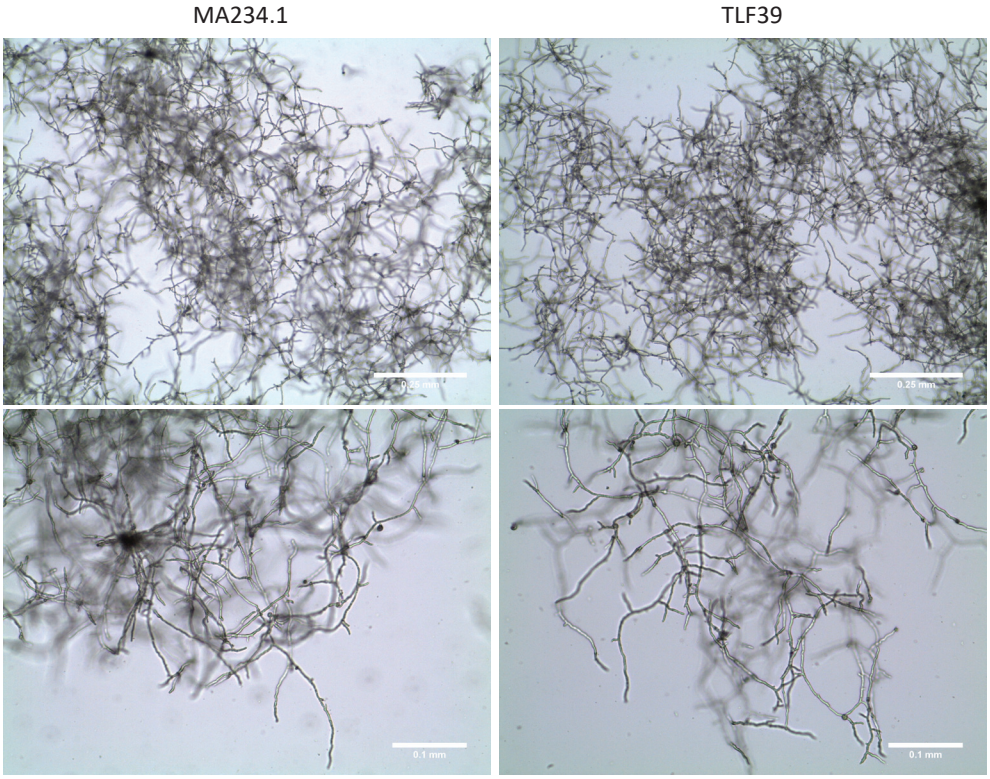

Figure S5. Hyphal and pellet morphology of glucose batch cultures during exponential growth. Wild type, MA234.1 (left) and *ΔcrhA-G*, TLF39 (right). 70% biomass.

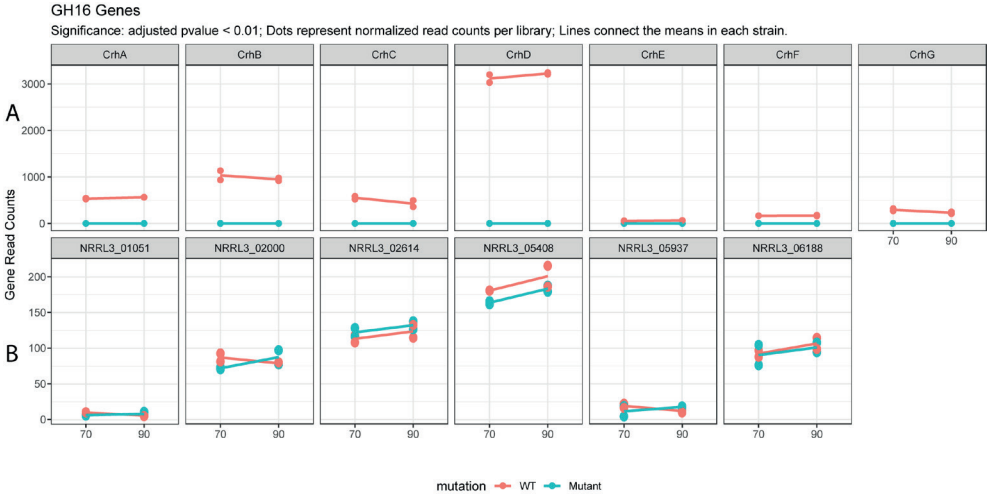

Figure S6. Normalized gene read counts for the *crh* and other GH16 genes. WT (red) and mutant (teal) libraries. While there is a complete decrease of detectable expression of the mutated genes, the expression of other GH16-family genes is not affected.

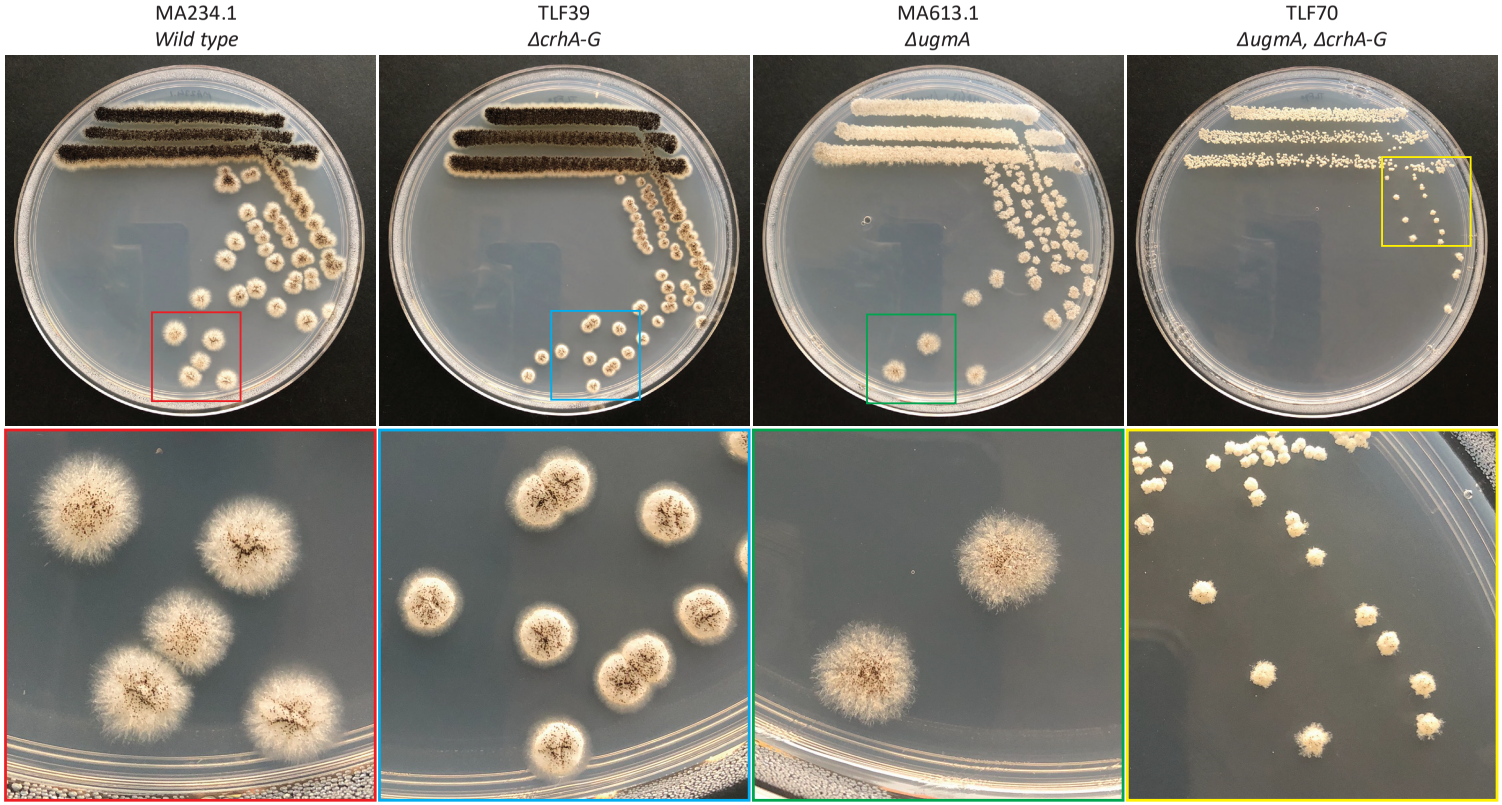

Figure S7. Growth of individual colonies on minimal medium (MM). Wild type (MA234.1), TLF39 (*ΔcrhA-G*), MA613.1 (*ΔugmA*) and TLF70 (*ΔugmA, ΔcrhA-G*) were single streaked on MM and were incubated at 30°C for 3 dayst.

CHAPTER 4

Interrogation of the cell wall integrity pathway in *Aspergillus niger* identifies a putative negative regulator of transcription involved in chitin deposition

Tim M. van Leeuwe, Mark Arentshorst, Peter J. Punt, Arthur F.J. Ram

ABSTRACT

Post-fermentation fungal biomass waste provides a viable source for chitin. Cell wall chitin of filamentous fungi, and in particular its de-*N*-acetylated derivative chitosan, has a wide range of commercial applications. Although the cell wall of filamentous fungi comprises 10-30% chitin, these yields are too low for cost-effective production. Therefore, we aimed to identify the genes involved in increased chitin deposition by screening a collection of UV-derived cell wall mutants in *Aspergillus niger*. This screen revealed a mutant strain (RD15.4#55) that showed a 30-40% increase in cell wall chitin compared to the wild type. In addition to the cell wall chitin phenotype, this strain also exhibited sensitivity to SDS and produces an unknown yellow pigment. Genome sequencing combined with classical genetic linkage analysis identified two mutated genes on chromosome VII that were linked with the mutant phenotype. Single gene knockouts and subsequent complementation analysis revealed that an 8 bp deletion in NRRL3_09595 is solely responsible for the associated phenotypes of RD15.4#55. The mutated gene, which was named *cwcA* (*cell wall chitin A*), encodes an ortholog of *Saccharomyces cerevisiae* Bypass of *ESS1* (*BYE1*), a negative regulator of transcription elongation. We propose that this conserved fungal protein is involved in preventing cell wall integrity signaling under non-inducing conditions, where loss of function results in constitutive activation of the cell wall stress response pathway, and consequently leads to increased chitin content in the mutant cell wall.

This chapter is published as: van Leeuwe, T.M., Arentshorst, M., Punt, P.J., Ram A.F.J., Gene X 5, 100028 (2020). doi: 10.1016/j.gene.2020.100028

1. INTRODUCTION

Aspergillus niger is a filamentous fungus widely used in industrial fermentations to produce organic acids, enzymes and pharmaceuticals (Meyer et al., 2011; Pel et al., 2007; Punt et al., 2002; Wösten et al., 2013). Specifically, *A. niger* is renowned for its citric acid yields and is able to produce up to 95 kg of citric acid per 100 kg of carbon source, contributing the majority of the worldwide estimate annual yield: 9,000,000 metric tons (Karaffa and Kubicek, 2003). Large scale fermentations result, in addition to the desired product, in accumulation of fungal biomass; a product that is either incinerated or used as a low cost fertilizer for agriculture (Ghormade et al., 2017). However, post-fermentation fungal cell wall biomass waste contains many different sugar polymers that could provide an added-value product. Due to the high levels of post-mycelial biomass produced annually, *A. niger* is considered a fungus of interest to be used of post-fermentation harvesting for cell wall products, such the important biopolymer chitosan with its broad range of applications in different fields (Dhillon et al., 2012).

The fungal cell wall consists of α-glucans (α-1,3-glucans, mixed α-1,3/1-4-glucan and α-1,6-glucans), β-glucans (β-1,3-glucans, β1,6-glucans, mixed β-1,3/1,4 and β-1,3/1,6 varieties), chitin (β-1,4-linked *N*-acetyl-2-amino-2-deoxy-D-glucose), chitosan (β-1,4-linked 2-amino-2-deoxy-D-glucose), galactomannan and glycoproteins (Gow et al., 2017; Ruiz-Herrera and Ortiz-Castellanos, 2019). All fungal cell walls most commonly contain β-1,3-glucans that forms a backbone structure to which other β-glucans, galactomannans or chitin can be cross-linked. Total polymer content and relative composition differs among species and, in addition, is dependent on environmental cues such as nutrients, cultivation conditions, mycelial age, stress or hypoxia (Free, 2013; Lord and Vyas, 2019; Pochanavanich and Suntornsuk, 2002).

Among all cell wall components, chitin and its de-*N*-acetylated derivative chitosan are especially of industrial interest. Chitosan has been reported to have many applications across fields of medicine, cosmetics, agriculture and food industry (Ribeiro et al., 2009; Shen et al., 2009; Takai et al., 2001; Zou et al., 2016). Varying degrees of de-acetylation (DD) and degrees of polymerization (DP) of chitosan regulate its active properties and determine its wide range of applications (El Gueddari et al., 2014). Naturally occurring, cell wall chitosan is most often found among pathogenic species, and is required for both virulence and as a means of avoiding recognition of the immune system in the opportunistic human pathogen *Cryptococcus neoformans* (Baker et al., 2011; Bose et al., 2003). Similarly, phytopathogenic fungi convert cell wall chitin to chitosan that is required for infection. This results in evasion of the plant-host defense response, while simultaneously reducing susceptibility to plant-produced chitinases (Geoghegan et al., 2017). In *A. niger*, chitin and chitosan content have been shown to be dependent on strain, mycelial age, cultivation medium, conditions and extraction methods (Kumaresapillai et al., 2011; Pochanavanich and Suntornsuk, 2002; White et al., 1979). Chitin content has been reported in the range from 10% up to 42% (Knorr, 1991) of the cell wall dry weight, whereas chitosan yields are reported between 5 and 11%, with DD ranging from 73 to 90% (Dhillon et al., 2013; Muñoz et al., 2015; Pochanavanich and Suntornsuk, 2002).

Given the interesting properties of chitin and chitosan, the use filamentous fungi for chitin and chitosan production has been considered. Obviously to make this a profitable option, high levels of cell wall chitin and optimization of chitin extraction are required (Cai et al., 2006; Dhillon et al., 2012). One approach is to improve the overall chitin content in fungal cell walls. As such, efforts have been made to optimize the production of chitin and its de-*N*-acetylated derivative chitosan through genetic modification of the chitin biosynthetic pathway or through alterations of fermentation conditions (Deng et al., 2005; Hammer and Carr, 2006; Ja'afaru, 2013; Nwe and Stevens, 2004). Alternatively, increased cell wall chitin deposition has been reported to coincide with cell wall stress (CWS) in filamentous fungi (Fortwendel et al., 2010; Guest et al., 2004; Ram et al., 2004). Consequently, CWS could result in an increased extractable yield of chitin. Cell wall stress induced signaling of the cell wall integrity (CWI) pathway in *A. niger* is known to induce expression of genes involved in α-glucan and chitin synthesis, *agsA* (alpha-glucan synthase A) (Damveld et al., 2005b) and *gfaA* (glutamine-fructose-6-phosphate-amidotransferase A), respectively (Ram et al., 2004). Consequently, CWS could be used to increase the extractable yield of chitin and chitosan.

We previously reported about a set of cell wall mutants that showed constitutive high levels of *agsA* expression: strains were equipped with a dual reporter system where both an *amdS* and a Histone 2B-GFP (H2B-GFP) construct were fused to the *agsA* promoter (*PagsA*). UV-mutagenesis followed by selection for improved growth on acetamide as a sole nitrogen source, containing H2B-GFP labeled nuclei (selection against *cis*-mutations), allowed to obtain cell wall mutants with a constitutively activated CWI pathway (Damveld et al., 2008). In the study reported here, we specifically screened for cell wall mutants from this collection for increased chitin deposition. Consequently, UV mutant RD15.4#55 was identified that showed constitutive expression of *agsA* and a 30-40% increase in cell wall chitin content. Additional phenotypes of this strain are sensitivity to SDS, also suggesting an effect on cell wall or cell membrane, and the production of an unknown yellow compound. Genome sequencing combined with a classical genetics approach identified mutations in two genes that could be responsible for the mutant phenotypes. Single gene knockouts and complementation studies were used to show that the disruption of NRRL3_09595 (An11g06750), an ortholog of *BYE1* encoding a negative regulator of transcription elongation in *Saccharomyces cerevisiae,* causes an increase in cell wall chitin deposition.

2. MATERIALS AND METHODS

2.1 Strains, media, growth conditions

Strains used in this study can be found in Table 1. MA169.4 (*cspA1, ΔkusA::DR-amdS-DR, pyrG*)-(Carvalho et al., 2010) was used for all single knockout transformations. All media were prepared as described by Arentshorst et al., 2012. In all cases (unless otherwise specified) minimal medium (MM) contained 1% (w/v) glucose, 1.5% agar and was supplemented with uridine (10mM), when required. Complete medium (CM) contained 1% (w/v) glucose, 1.5% agar (Scharlau, Barcelona,

Spain), 0.1% (w/v) casamino acids and 0.5% (w/v) yeast extract in addition to MM. To harvest spores, strains were first inoculated from -80°C glycerol stocks onto fresh CM plates and were allowed to grow and sporulate for 5-7 days at 30°C. Spores were harvested by addition of 15 mL of 0.9% (w/v) NaCl to CM spore plates and were gently scraped from the plate surface with a cotton stick. Spore solution was pipetted through sterile cotton filters (Amplitude™ Ecocloth™ Wipes, Contec Inc., Spartanburg, SC, USA) to eliminate large mycelial debris. Spore solutions were counted using Bio-Rad TC20™ Automated Cell Counter (Bio-Rad Laboratories, Inc. USA) using Counting Slides, Dual Chamber for Cell Counter (Cat#145-0011, Bio-Rad Laboratories, Inc. USA).

Table 1. All strains used in this study.

Name	Genotype	Reference
N402	cspA1	Bos et al., 1988
MA169.4	cspA1, *ΔkusA::DR-amdS-DR, pyrG-*	Carvalho et al., 2010
RD15.4	cspA1, *pyrG-, PagsA-H2B-GFP-TtrpC-pyrG*, PagsA-amdS-TamdS + pAN7-1 (hph+)*	Damveld et al., 2008
RD15.8	cspA1, *pyrG-, PagsA-H2B-GFP-TtrpC-pyrG*, PagsA-amdS-TamdS + pAN7-1 (hph+)*	Damveld et al., 2008
RD15.4#55	UV-mutant RD15.4	Damveld et al., 2008
RD15.8#16	UV-mutant RD15.8	Damveld et al., 2008
RD15.8#35	UV-mutant RD15.8	Damveld et al., 2008
RD15.8#36	UV-mutant RD15.8	Damveld et al., 2008
RD6.13#6	UV-mutant RD6.13	Damveld et al., 2008
RD6.13#7	UV-mutant RD6.13	Damveld et al., 2008
RD6.13#8	UV-mutant RD6.13	Damveld et al., 2008
RD6.13#16	UV-mutant RD6.13	Damveld et al., 2008
RD6.47#56	UV-mutant RD6.47	Damveld et al., 2008
TLF55	RD15.4UV#55, *pyrG-* (5'-FOA selected)	This study
TLF51	RD15.4UV#55, *pyrG-* (5'-FOA selected), *ΔbrnA*	This study
JN6.2	cspA1, *nicB::hygB, olvA::AOpyrG*	Niu et al., 2016
TLF91	Diploid strain: JN6.2xTLF51(3)	This study
MA841.1	*cspA1, ΔkusA::DR-amdS-DR, pyrG-, Δ*An04g04020*::AOpyrG*	This study
MA842.1	*cspA1, ΔkusA::DR-amdS-DR, pyrG-, Δ*NRRL3_03052*::AOpyrG*	This study
MA843.1	*cspA1, ΔkusA::DR-amdS-DR, pyrG-, Δ*NRRL3_09002*::AOpyrG*	This study
MA844.1	*cspA1, ΔkusA::DR-amdS-DR, pyrG-, Δ*NRRL3_09595*::AOpyrG*	This study
TLF83	RD15.4UV#55, *pyrG-* (5'-FOA selected), restored NRRL3_09595	This study

2.2 Calcofluor White staining and confocal laser scanning microscopy

Strains for microscopy were cultured as described above. Spore solutions were diluted and 10^4 spores were spotted on plates containing 20mL MM 1% agarose, and were incubated for 8h at

30°C to allow germination. Agar cubes of approximately 1 cm^2 were excised containing the spot of germlings, and were inverted on top a 24 x 60 mm cover slide containing a 20 µL droplet of 5µg/mL CalcoFluor White (CFW). Following 5 min of incubation, samples were imaged for CFW fluorescence with a 405 nm laser in a Zeiss Observer confocal laser-scanning microscope (Zeiss, Jena, Germany). Images were processed and analyzed using FIJI (ImageJ) software (Schindelin et al., 2012). To all images, background subtraction was applied (Rolling ball radius 50.0 pixels) prior to processing into Z-project with Max Intensity settings. Look-up table used was Cyan Hot.

2.3 SDS sensitivity assays

Cell wall disturbing compound SDS was added to MM agar plates from a 10% stock to obtain final concentrations of either 0.004%, 0.0045% or 0.005% SDS. Spores were counted, serially diluted into 2000, 200, 20 and 2 spores/µL and 5 µL of respective dilutions were spotted on MM SDS plates. Plates were incubated for 3-5 days at 30°C prior to scoring.

2.4 Cell wall isolation and chitin analysis

Cell wall isolation, hydrolysis and chitin content analysis, measured as total glucosamine, have been performed as described in **Chapter 5**. Cell wall glucosamine measurements from independent replicate experiments are expressed as means ± SEM. The statistical analysis was carried out using software R studio (Version 1.1.456) (RStudio: Integrated Development for R. RStudio, Inc., Boston, 2016). For total cell wall glucosamine experiments, we used one-way ANOVA. When there was significant difference between groups, we ran a posthoc Tukey multiple-comparisons analysis. Significance is indicated as $p > 0.05$, not significant (n.s.) $p \leq 0.05$ (*), $p \leq 0.005$ (**), $p \leq 0.001$ (***) and $p \leq 0.0001$ (****).

2.5 DNA isolation, Illumina sequencing and SNP analysis

Genomic DNA was isolated as described by Arentshorst et al., 2012. In case of genome sequencing, this procedure was followed by column purification using the Nucleospin Plant II kit (Machery-Nagel), according to the manufacturer's instructions. Genome sequencing was executed by GenomeScan B.V (Leiden, The Netherlands). The NEBNext® Ultra DNA Library Prep kit for Illumina (cat# NEB #E7370S/L) was used to process the samples. Fragmentation of the DNA using the Biorupor Pico (Diagenode), ligation of sequencing adapters, and PCR amplification of the resulting product was performed according to the procedure described in the NEBNext Ultra DNA Library Prep kit for Illumina Instruction Manual. The quality and yield after sample preparation was measured with the Fragment Analyzer. The size of the resulting product was consistent with the expected size of approximately 500-700 bp. Clustering and DNA sequencing using the Illumina cBot and HiSeq 4000 was performed according to manufacturer's protocols. A concentration of 3.0 nM of DNA was used. HiSeq control software HCS v3.4.0 was used. Image analysis, base calling, and quality check was performed with the Illumina data analysis pipeline RTA v2.7.7 and Bcl2fastq v2.20. SNP calling was performed according to GenomeScan Guidelines Small Variant Analysis v3.0. The Variant Call Format (VCF) files were manually analyzed by the

authors. Frequency score of identical SNP call boundary was set to ≥ 0.75, while sequencing depth was left unselected.

2.6 Parasexual cycle and segregant analysis

Formation of heterokaryons and selection for diploids was performed as described previously (Arentshorst and Ram, 2018). To obtain an auxotrophic haploid derivative of RD15.4#55, this strain was subjected to 5'-FOA counter selection to lose the *pyrG* marker (Arentshorst et al., 2015), resulting in strain TLF55 (Table 1). TLF55 was subsequently than transformed with pFC330_*brnA*-sgRNA (pTLL37.1) and a knockout repair DNA fragment as described previously (**Chapter 2**).

The RD15.4#55, *pyrG-, ΔbrnA* strain, TLF51 (Table 1), was cured of the pTLL37.1 plasmid to ensure TLF51 was *pyrG-* for a parasexual cross. Wild type derivative JN6.2 (Table 1) was used as second haploid auxotrophic strain for the parasexual cross. For the parasexual cross, these two haploid strains are coerced to fuse without supplementation for their respective auxotrophic deficiencies. This process yields a heterokaryotic, prototrophic mycelium in which karyogamy can occur at a very low frequency, resulting in a diploid strain. Due to the primarily uninuclear nature of *A. niger* asexual spores, color markers help identify whether nuclei have fused, and become black as a result of complementing alleles from the other chromosome, or remain unfused as one of the individual colors in the heterokaryotic mycelium. An obtained diploid contains both chromosome-sets and can be haploidized to allow random distribution of each chromosome by exposure to benomyl, creating auxotrophic, brown- or olive-colored segregants. Segregation of diploid TLF91 was performed at 0.4 μg/mL benomyl on complete medium (CM) supplemented with 10mM uridine and 2.5 μg/mL nicotinamide, haplodizing into brown and olive colored segregants. Segregants were single streaked twice on MM with uridine and nicotinamide prior to phenotypic characterization of segregants. Segregation analysis of the cell wall mutant phenotype and auxotrophic markers was performed on MM, MM + uridine and MM + uridine + nicotinamide + 0.005% SDS.

2.7 Construction of single gene deletions

MA169.4 (Table 1) was transformed after protoplastation as described previously (Arentshorst et al., 2012) to remove the entire ORF, generating split marker fragments using the split marker approach for single gene knockouts (Arentshorst et al., 2015) with *Aspergillus oryzae pyrG* (*AOpyrG*) as selection marker. Flanks were generated via PCR using N402 genomic DNA as template and primers as described in Supplementary Table 1. *AOpyrG* fragments were obtained using plasmid pAO4-13 (de Ruiter-Jacobs et al., 1989) as template and primers as described in Supplementary Table 1. Through fusion PCR, split marker fragments were created containing *AOpyrG* as selection marker. For transformation, approximately 2 μg of DNA per flank was added to protoplasts. Transformation plates were incubated on MMS for 6 days at 30°C. Transformed colonies were single streaked on MM twice for purification and were genotyped using diagnostic PCR (data not shown).

2.8 Complementation of RD15.4#55 with wild type NRRL3_09595 allele

Complementation of NRRL3_09595 was employed using CRISPR/Cas9 mediated gene editing with a marker-free repair DNA fragment (**Chapter 2**). Primers OTL464 and OTL465 were used in combination with pTE1_rev and pTE1_for, respectively, to obtain a sgRNA construct to target the mutant allele NRRL3_09595 in RD15.4#55. Plasmids pTLL108.1 and pTLL109.2 were used as template DNA for sgRNA flanks (**Chapter 2**). Cloning of the sgRNA into pFC330 resulted in pFC330_NRRL3_09595-*mut*-sgRNA. Marker-free repair DNA fragment of 449 bp was obtained with OTL385 and OTL386, using N402 as template DNA. Repair DNA fragment contained 308 bp overlap upstream and 141 bp downstream of the double strand break (DSB). CRISPR/Cas9 plasmid transformations were performed after protoplastation of TLF55: 2 µg of Cas9-sgRNA plasmid with 2 µg of repair DNA fragment was used for transformation. Transformation plates were incubated on MMS for 6 days at 30°C. Transformed colonies were single streaked on selectable medium to select for the presence of the Cas9-sgRNA plasmid. Next, a single colony was picked and transferred to non-selective MM 10mM uridine medium, allowing loss of the Cas9-sgRNA plasmid. A third streak of a single colony on both MM and MM 10mM uridine was performed as a control for loss of plasmid. DNA from plasmid-cured strains was isolated as described by Arentshorst et al., 2012, using mortar and pestle to grind the mycelium in liquid nitrogen. Genotypes were confirmed using diagnostic PCR for the 8 bp deletion in the mutant allele of NRRL3_09595. Diagnostic PCR fragments from RD15.4, RD15.4#55 and TLF55 transformants (complemented with the wild type NRRL3_09595 allele) were sequenced to check for either absence or presence of the 8 bp deletion in the mutant allele (Macrogen Europe, Amsterdam, The Netherlands).

3. RESULTS

3.1 RD15.4#55 shows increased cell wall chitin, SDS sensitivity and yellow pigment production

A previously obtained cell wall stress UV-mutant library (Damveld et al., 2008) was used to screen for mutants with a higher cell wall chitin content, initially using Calcofluor white (CFW) staining followed by chemical quantification of total glucosamine content (see section 2.4.2). Nine candidates that exhibited increased CFW staining were analyzed for cell wall glucosamine content. Both RD15.4#55 (283 ± 11.6 µg/mg) and RD15.8#16 (312 ± 20.9 µg/mg) showed a significantly increased cell wall glucosamine content compared to both N402 (221 ± 13.8 µg/mg) and parental strain RD15.4 (205 ± 10.2 µg/mg), displayed in Figure 1A. Strain RD15.4#55 was selected for further phenotypic assessment, whereas RD15.8#16 is discussed in **Chapter 5**. The germination process was analyzed in conjunction Calcofluor White (CFW) staining during the mutant screen. This showed that the hyphal morphology of RD15.4#55 was similar to the parental strain, indicating that its constitutive condition of cell wall stress does not affect growth (Figure 1B). Although no controlled growth experiments have been conducted to determine growth rates,

also under submerged conditions no obvious growth differences were observed. In addition to glucosamine content, we also tested the effect of cell wall disturbing compounds with Calcofluor White (CFW) and SDS (De Groot et al., 2001; de Nobel et al., 2000; Delley and Hall, 1999). Figure 1C shows single streaks of N402 and RD15.4#55 on MM and MM + 0.005% SDS. As is evident from these sensitivity assays, RD15.4#55 displays sensitivity towards SDS, indicating that either cell wall membrane or cell wall synthesis is perturbed in this mutant. RD15.4#55 did not show clear sensitivity to CFW (data not shown). Lastly, an indicative feature of RD15.4#55 observed on MM plates was the production of a yellow compound into the surrounding agar. Strain RD15.4#55 was selected for genotypic characterization in an attempt to find the underlying mutation(s) causing an increase in cell wall chitin deposition.

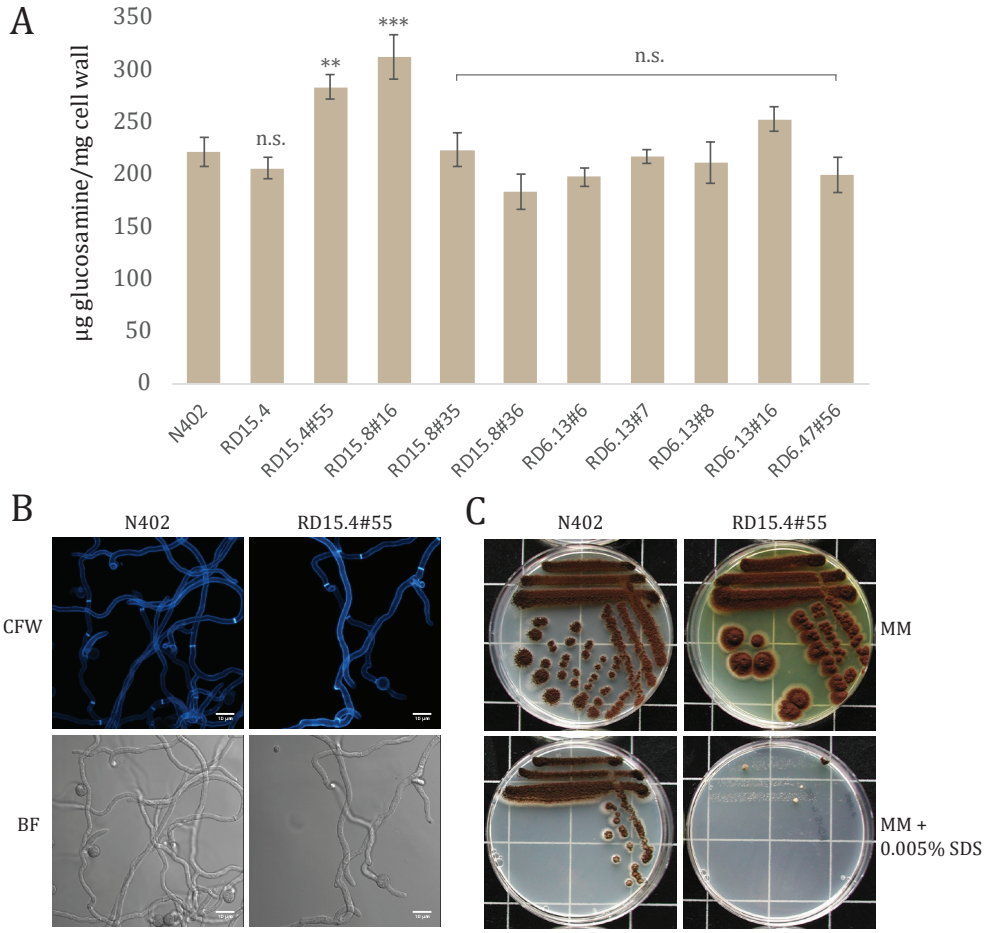

Figure 1. Glucosamine content analysis and candidate selection from UV-mutant collection. (A) Chitin content measured as total glucosamine and normalized to wild type (N402) levels to indicate percentage differences between wild type and listed mutants. Asterisks refer to statistical difference (section 2.4.2). (B) CLSM of N402 and RD15.4#55. Strains were grown as described (section 2.2), top images show chitin staining with Calcofluor White (CFW) and bottom images show bright field (BF) setting. Bars indicate 10 µm (C) Single streak of N402 and RD15.4#55 on MM and MM with 0.005% SDS grown for 96h at 30°C. Statistical methods and significance are described in section 2.4.2. Listed significant differences are compared to N402.

Table 2. Genomic single nucleotide polymorphisms (SNPs) of TLF51. SNPs found inside open reading frame (ORF) of TLF51 (derivative of RD15.4#55)

Chr	NRRL3 ID	CBS513.88 ID	Gene description	ORF strand	WT	TLF51	Effect of SNP on codon sequence
III	NRRL3_03052	An12g08790	Phospholipid translocating ATPase (flippase)	-	G	A	Codon change: $Ser^{1426/1519} \rightarrow Phe^{1426/1519}$
III	NRRL3_03881	An12g04630	Oxalate decarboxylase	+	C	CT	insertion at the +21 position of intron 2 (129bp)
V	NRRL3_06613	An16g09230	Putative fungal transcription factor	-	G	GA	insertion at the +32 position of intron 7 (85bp)
VI	N/A	An04g04020	Unknown protein	-	T	A	Codon change: $Phe^{77/136} \rightarrow Ile^{77/136}$
VII	NRRL3_09002	An12g02450	α-glucan synthase C (*agsC*)	+	C	T	Codon change: $Gln^{1599/2407} \rightarrow Stop^{1599/2407}$
VII	NRRL3_09595	An11g06750	*BYE1* ortholog (Transcription Elongation Factor SII)	-	CGCGGAGGA	G	Frameshift → $stop^{642/943}$
VIII	NRRL3_10506	An18g04180	40S ribosomal protein S19	+	G	GA	insertion at the +31 position of intron 3 (78 bp)
VIII	NRRL3_11411	An08g08570	Hypothetical protein (DNA binding)	-	G	A	Synonymous substitution: GTC to GTT (Valine)

3.2 Genome sequencing and segregant analysis of RD15.4#55 shows linkage of the phenotype to chromosome VII

To identify the responsible mutation(s) that cause(s) the phenotype of RD15.4#55, we sequenced the genomic DNA of the parental strain RD15.4 and strain TLF51, a *pyrG*⁻, *ΔbrnA* derivative of RD15.4#55 (see section 2.6). Post data processing as described in section 2.5 revealed a total of 9 SNPs and 31 indels in TLF51 compared to RD15.4. Indels were found in the *pyrG* and *brnA* markers as expected (data not shown). The remaining 9 SNPs and 29 indels are listed in Supplementary Table 2. A total of 5 SNPs and 24 indels were scored to either be intergenic (26) or present in telomeric regions (3). In addition to intergenic SNPs and indels, four SNPs and five indels were found to be inside ORFs and are described in Table 2.

Strain TLF51 was also used to set up a parasexual cross with JN6.2 (*ΔnicB::hygB, ΔolvA::AOpyrG*, Table 1). The diploid strain (TLF91) was haploidized using benomyl to obtain haploid segregants (see section 2.6). In an initial segregant screen for SDS sensitivity, 26 segregants were found to be SDS sensitive, 23 of which were scored as *nicB*⁺ suggesting linkage to the *nicB* (NRRL3_09250) locus. Analysis of an additional 80 *nicB*⁺ segregants showed that 79/80 were SDS sensitive, confirming this linkage analysis of the SDS sensitive phenotype of RD15.4#55 to *nicB*, located on chromosome VII. Because of the parasexual cross (i.e. no meiosis), crossover events are rare (mitotic) and chromosomes are generally fully inherited from either wild type or mutant.

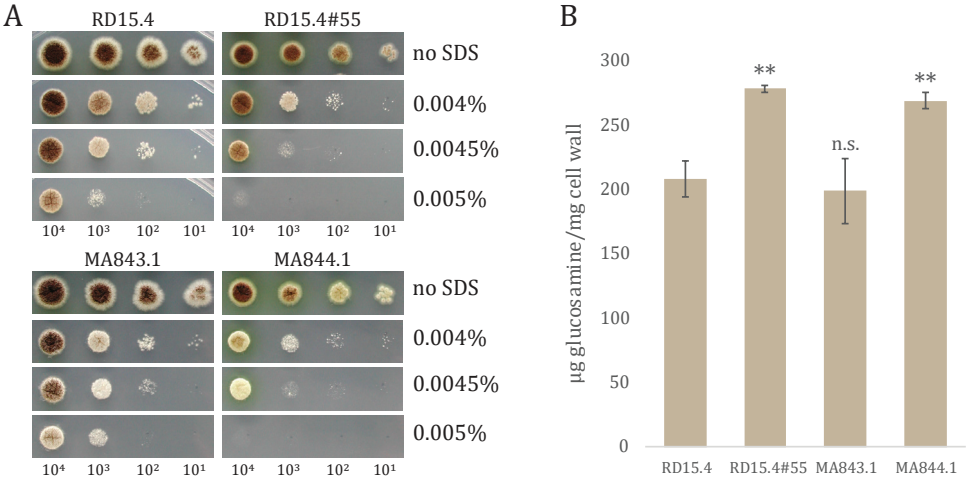

Figure 2. SDS sensitivity and cell wall glucosamine phenotypes of single knockout strains. (A) Growth phenotype and SDS sensitivity of parental strain RD15.4, UV-mutant RD15.4#55 and knockout strains of *agsC* (MA843.1) and NRRL3_09595 (MA844.1) on MM with 10mM uridine (U). Strains were grown on either 0.004%, 0.0045% or 0.005% SDS plates. All plates were incubated for 72h at 30°C. Spore amounts (#) per spot from left to right are 10^4, 10^3, 10^2 or 10^1, and are listed below the figure. (B) Total cell wall glucosamine determination of single knockouts. Parental strain RD15.4, UV-mutant RD15.4#55 and knockout strains MA843.1 and MA844.1. Cell wall glucosamine of all strains grown in Complete medium (CM) with 10mM uridine at 30°C for 17h (n=3). Statistical methods and significance are described in section 2.4.2. Listed significant differences are compared to RD15.4.

Linkage to *nicB*+ (TLF51 chromosome VII) therefore suggests involvement of SNPs located on this chromosome. SNP analysis of TLF51 revealed that both *agsC* and NRRL3_09595 were mutated, resulting in premature translation stop, and are located on chromosome VII (Table 2).

3.3 Single gene knockouts show that ΔNRRL3_9595 displays the same phenotype as RD15.4#55

Based on the linkage analysis we opted to construct full gene knockouts of chromosome VII located genes alpha glucan synthase C (*agsC*) and NRRL3_09595, and test how they relate to the phenotypes of RD15.4#55. An additional 3 indels in intergenic regions (Supplementary table 2) of chromosome VII were left out for consideration. Strain MA169.4 (Table 1) was transformed with split marker flanks, harboring the *AOpyrG* selection marker as described in section 2.7, resulting in knockout strains MA843.1 (*ΔagsC*) and MA844.1 (*Δ*NRRL3_09595) (Table 1). Strains were confirmed to have replaced ORFs through diagnostic PCR (data not shown).

Parental strain RD15.4 and UV-mutant RD15.4#55 were cultured together with knockout strains and were plated on MM + uridine containing either 0.004%, 0.0045 or 0.005% SDS plates. Figure 2A shows that knockout strain MA843.1 (*ΔagsC*) grows similar to the parental RD15.4 strain on both MM and MM + SDS (Figure 2A), whereas the growth of MA844.1 (*Δ*NRRL3_09595) is affected by the presence of SDS, similar to RD15.4#55.

Next, all strains were cultured for cell wall isolation and determination of total glucosamine content (see section 2.4.2). Evidently, parental strain RD15.4 was measured to contain a glucosamine content of 208±5.5 µg/mg cell wall, whereas the UV-mutant RD15.4#55 showed a glucosamine content of 278±4.4 µg/mg cell wall: a 33.6% increase in overall glucosamine (Figure 2B). Single knockout strains MA843.1 (*ΔagsC*) and MA844.1 (ΔNRRL3_09595) were measured to have a glucosamine content of 199±6.2 and 269±5.2 µg/mg cell wall, respectively. Statistical analysis showed that there is a significant difference between RD15.4 and RD15.4#55 and MA844.1, but not between RD15.4 and MA843.1. Neither do RD15.4#55 and MA844.1 differ significantly from each other, suggesting they produce equal, yet increased, levels of cell wall glucosamine.

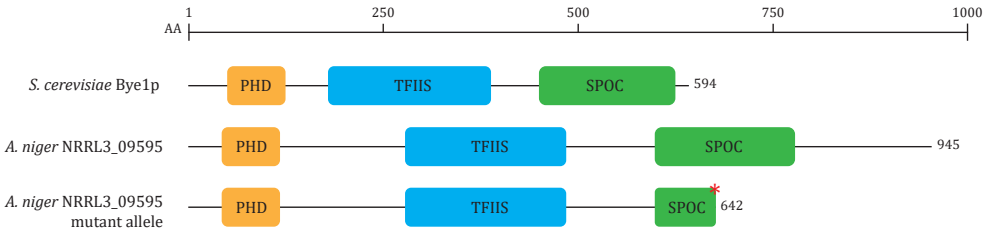

Figure 3. Schematic representation of NRRL3_09595 and respective domains and the yeast ortholog *BYE1*. Proteins contain a Plant Homeo Domain (PHD, orange), Transcription elongation Factor S-II (TFIIS) superfamily domain (blue) and a Spen paralogue and ortholog C-terminal (SPOC) domain (green). Red asterisk shown for mutant allele of NRRL3_09595 represents an early STOP codon as a result of a frameshift leading to truncation of NRRL3_09595 (see section 3.4). An amino acid (aa) scale indicates length of proteins.

3.4 Complementation of RD15.4#55 with the wild type NRRL3_09595 allele restores all associated phenotypes

The 8 bp deletion found in NRRL3_09595 (*BYE1* ortholog) causes an initial aa change of $Ser^{636/945}$ to $Gln^{636/945}$, followed by a frameshift 5 amino acids (aa) downstream, ultimately leading to stop codon at aa642/945 (Figure 3). We showed that a full knockout of NRRL3_09595 results in the same phenotype as the RD15.4#55 including SDS sensitivity, cell wall glucosamine and yellow pigment production. To rule out the involvement of other SNPs in RD15.4#55 that may contribute to the phenotype, complementation was performed in the RD15.4#55 strain by introducing the wild type allele of NRRL3_09595 through transformation. CRISPR/Cas9 mediated genome editing was used to introduce the wild type allele at the location of the mutant allele of NRRL3_09595 in RD15.4#55. The 8 bp deletion in the mutant allele of NRRL3_09595 provided a location for the design of a sgRNA target (5' – AGTTTACTCAAGCATGTCGG – 3') that is unique for the RD15.4#55

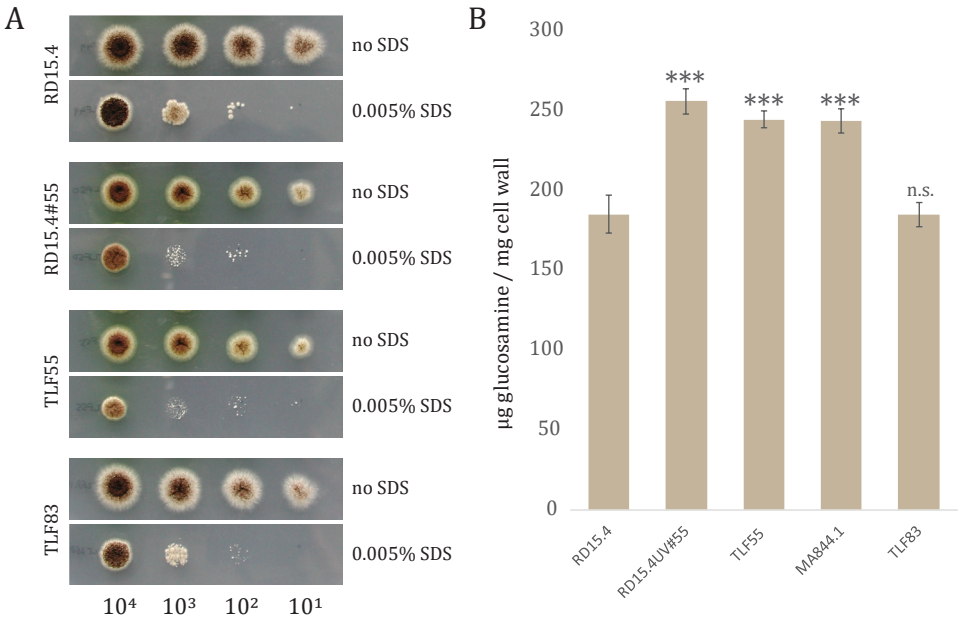

Figure 4. SDS sensitivity and cell wall glucosamine phenotypes. Parental strain RD15.4, UV-mutant RD15.4#55, *pyrG*⁻ derivative of RD15.4#55 (TLF55), single knockout of NRRL3_09595 (MA844.1) and TLF55 with complemented with wild type NRRL3_09595 (TLF83) Absolute spore amounts per spot are listed below the figure (i.e. 10^4, 10^3, 10^2 and 10^1). (A) Growth on MM with 10mM uridine and MM with 10mM uridine and 0.005% SDS. Grown for 72h at 30°C. (B) Total cell wall glucosamine strains (n=3). Statistical methods and significance are described in section 2.4.2. Listed significant differences are compared to RD15.4.

strain. PAM site 5' – AGG – 3' is present in both RD15.4 and RD15.4#55, but the target sequence only matches the first PAM-adjacent 11 bp in the RD15.4 (5' – nnnnnnnnnnAAGCATGTCGG – 3') due to the deletion. Contrarily, the full target sequence is only found at mutant allele of NRRL3_09595 in RD15.4#55, allowing specific targeting of the mutant allele without recognition of the wild type NRRL3_09595 allele presented as repair DNA fragment (See Supplementary Figure 1 for a

detailed visual representation). The designed target was cloned into a sgRNA expression cassette to obtain pFC330_NRRL3_09595-*mut*-sgRNA (pTLL103.2) as described in section 2.8, and a 449 repair DNA fragment was amplified from the wild type allele of NRRL3_09595 in RD15.4. A *pyrG*- derivative of RD15.4#55 (TLF55) was transformed with both plasmid pFC330_NRRL3_09595-*mut*-sgRNA and repair DNA fragment.

Single streaks of transformed colonies were checked for the presence of the yellow pigmentation. Yellow pigment production was expected to be absent for transformed strains that successfully incorporated the repair DNA fragment at the NRRL3_09595 locus, whereas the yellow pigment remained visible for transformed strains that did not incorporate the repair DNA fragment. Fifteen transformants were picked from the initial transformation plate, four of which were found to lack yellow color production. Single streaking on MM with uridine removed selection pressure to cure the Cas9 plasmid. This was successful for two out of the four transformants. A diagnostic PCR of the NRRL3_09595 locus, followed by sequencing revealed that the wild type NRRL3_09595 allele had correctly replaced the mutant allele in the TLF83 transformant.

To show that restoration of NRRL3_09595 in RD15.4#55 (TLF83) restores all associated phenotypes, we cultured RD15.4, RD15.4#55, RD15.4#55, *pyrG*- (TLF55) and TLF83 to create spore solutions of equal age. Spores were diluted and plated on MM with uridine and MM with uridine + 0.005% SDS (Figure 4A) The complemented strain (TLF83) resembles the phenotype of RD15.4, in terms of colony morphology, yellow pigment production and SDS sensitivity. Next, all four strains were cultured together with MA844.1 (*Δ*NRRL3_09595) to check the total cell wall glucosamine content. Strains were grown for 17h on CM with uridine as biological triplicates and cell walls were isolated and lyophilized. Figure 4B shows cell wall glucosamine levels of all tested strains. It is clear from the graph that RD15.4#55, TLF55 and MA844.1 show that there is a significant increase in glucosamine content compared to the parental RD15.4 strain, as previously confirmed. However, all these strains also show a significant difference in cell wall glucosamine compared to TLF83 (restored NRRL3_09595 in RD15.4#55), whereas RD15.4 and TLF83 display identical levels of glucosamine. Taken together with the morphology and SDS sensitivity data, this confirms that NRRL3_09595 is responsible for all the associated phenotypes of RD15.4#55. Based on its effects on levels of cell wall chitin, the NRRL3_09595 gene is named *cwcA* (***c***ell ***w***all ***c***hitin).

4. DISCUSSION

In this study, we describe the mutant RD15.4#55 that was selected from a previously obtained forward genetics screen. UV mutagenesis was used in combination with a dual-reporter system, based on *agsA* expression during the CWI response, to screen for mutants that displayed a continuous state of cell wall stress (Damveld et al., 2008). In addition to alpha-glucan, increases of cell wall chitin deposition have been also been reported in fungi through induction of the CWI signal transduction pathway (Fortwendel et al., 2010; Heilmann et al., 2013; Ram et al., 2004; Walker et

al., 2015, 2008). In *A. niger*, both *agsA* and *gfaA* have been shown to be induced in response to cell wall stress in an *rlmA* dependent way (Damveld et al., 2005). In the attempt to identify mutants with increased chitin deposition, we screened a set of mutants with increased *agsA* expression for concomitant increases in cell wall chitin. Cell wall analysis showed that RD15.4#55 has increased glucosamine levels compared to wild type strains. Next to an approximate increase in glucosamine content (here, chitin and chitosan) of about 30-40%, RD15.4#55 was found to display sensitivity towards SDS and showed the secretion of an unknown yellow pigment (Figure 1).

To identify the genotype related to RD15.4#55's phenotypic traits, we carried out a classical genetics approach: RD15.4#55 was prepared for a parasexual cross (Arentshorst and Ram, 2018) with a wild type strain (JN6.2, Table 1) by introducing the *pyrG*⁻ auxotrophic deficiency and disruption of the *brnA* gene as a color identifier (TLF51, Table 1). Segregants from the parasexual cross showed 96.2% linkage of the SDS sensitive phenotype to chromosome VII (*nicB* auxotrophic marker). Chromosome VII harbors both a SNP in NRRL3_09002 (*agsC*) and an 8 bp deletion in NRRL3_09595, now named *cwcA,* that were identified by whole genome sequencing of strain TLF51. Interestingly, SDS sensitivity assays showed that a full deletion of *cwcA* resembled the phenotype of RD15.4#55, whereas a deletion of *agsC* did not. In addition, total cell wall glucosamine analysis revealed that a deletion of *cwcA* causes elevated levels of cell wall glucosamine. The lack of involvement of *agsC* in the cell wall mutant phenotype, although it encodes a potential cell-wall modifying enzyme, is corroborated by the fact that *agsC* shows low expression during vegetative growth, and is not induced by activation of the cell wall integrity pathway (Damveld et al., 2005b).

To confirm that only a mutation in *cwcA* was responsible for the chitin disposition phenotype of RD15.4#55, the *cwcA* mutant allele in RD15.4#55 was restored by introducing the wild type allele using CRISPR/Cas9 gene editing at the endogenous genomic location, leaving all other SNPs intact. A SDS sensitivity assay showed that complementation in TLF83 results in wild type sensitivity, and that the SDS phenotype is attributable to *cwcA* (Figure 4A). Moreover, also cell wall glucosamine analysis clearly showed that *cwcA* is solely responsible for the increase in glucosamine content of RD15.4#55 (Figure 4B).

Despite a relatively late truncation of the CwcA protein as a result of the frameshift in the mutant allele (Figure 3), a full knockout resembles the phenotype of RD15.4#55 suggesting that the C-terminal domain is critical for complete function of the protein. DELTA-BLAST analysis revealed that CwcA encodes a 945aa protein that is a putative ortholog of *BYE1* in *S. cerevisiae* (Bypass of ESSential gene 1), containing three functional domains: a Plant Homeo Domain (PHD) finger (aa59-108), a Transcription elongation Factor S-II (TFIIS) superfamily domain (aa269-482) and a Spen (*Split Ends*) Paralogue and Orthologue C-terminal (SPOC) domain (aa617-771). The latter domain is largely absent for the protein product of mutant allele *cwcA,* and may be of importance for the function of this protein. To the best of our knowledge, no literature exists on the function of SPOC domains in filamentous fungi. Spen proteins or SPOC domain containing proteins were first described in *Drosophila melanogaster* and are involved in developmental

signaling in embryonic development, where either deletion or mutation of the SPOC domain results in severe perturbation of cell fate specification (Kolodziej et al., 1995; Wiellette et al., 1999). Since then, structural studies have revealed the SPOC domain contains a β-barrel that resembles the *ku80* protein. This domain has been shown to be implicated in protein-protein interactions, also harboring a conserved, relatively basic surface and is suggested to interact with DNA (Ariyoshi and Schwabe, 2003; Lee and Skalnik, 2012). DELTA-BLAST alignment shows that both Pezizomycotina and Saccharomycotina species contain a single ortholog of *cwcA* with all three PHD, TFIIS and SPOC domains, whereas other hits encompassing putative paralogues are evidently deficient in SPOC domains, but still harbor either PHD and TFIIS domains together or either one separately. To date, the function of these single or bi-domain proteins in filamentous fungi is unknown.

In yeast, *BYE1*, the ortholog of CwcA (DELTA-BLAST, 98% query coverage, 16.29% protein identity), has been studied in detail; however, no studies have reported on its role in CWS or chitin deposition. Genetic interaction studies have shown Bye1p can act as a multi-copy suppressor on prolyl isomerase *ESS1* (Hanes et al., 1989). *ESS1* is an essential gene required for the phosphorylation of RNA polymerase II (RNAPII) C-terminal domain and affects co-factor binding through conformationally induced changes that may facilitate proper transcription initiation, elongation and termination (Ma et al., 2012). It was shown that Ess1p opposes the positive effects of known elongation factors Dst1p and the Spt4p-Spt5p complex, and it was found that high levels of Bye1p (as multi-copy suppressor) eliminate the requirement of Ess1p, hence Bypass of *ESS1*, suggesting they both act as negative regulators in transcription (Wu et al., 2003). Bye1p interacts with RNAPII through its TFIIS domain and occupies the 5'-region of active genes, and binds post-translationally modified histone H3 lysine 4 tri-methylation tails (H3K4-3me) of active transcription, using the PHD domain (Kinkelin et al., 2013; Pinskaya et al., 2014). Although *BYE1* is a non-essential gene, it is associated with a very pleiotropic phenotype both when disrupted and when overexpressed (Breslow et al., 2008; Cai et al., 2006; Kapitzky et al., 2010; Pir et al., 2012; Sopko et al., 2006). Deletion did not cause impaired growth rate (Breslow et al., 2008), similar as we observed for RD15.4#55 (section 3.1), whereas overexpression in yeast caused slower vegetative growth compared to wild type (Sopko et al., 2006; Yoshikawa et al., 2011). Based on the available data of *BYE1* we propose that CwcA is also involved in DNA binding and has a general function in transcription repression. In this work, we show for the first time that *A. niger BYE1* ortholog, *cwcA*, may act as a transcriptional repressor of the CWI pathway. Additionally, CwcA may be involved in the repression of secondary metabolite clusters as is suggested by the unscheduled production of an unknown yellow compound in the mutant strain.

Previously, the cell wall mutant library as described by Damveld et al, 2008 has provided a rich research tool to discover proteins involved in the CWI pathway of *A. niger*. Genes required for the synthesis of galactofuranose (*ugmA and ugeA*) vacuolar H(+)-ATPase (*vmaD*), and general transcription repressor *tupA* (yeast Tup1 homolog) were all identified from this cell wall mutant library (Damveld et al., 2008; Park et al., 2014; Schachtschabel et al., 2013, 2012). In case of

ugmA, it was also found that cell wall chitin was increased by activation of the CWI pathway as consequence of losing cell wall galactofuranose (Afroz et al., 2011; Park et al., 2016). Contrarily, the *tupA* mutant included in the initial cell wall chitin screen presented here (RD15.8#36, Figure 1A), did not show an increase in cell wall glucosamine. Essentially, *cwcA* and identified genes from these previous studies can be categorized as either cell wall biosynthesis, remodeling/ recycling proteins or as regulatory elements. Similar to TupA, CwcA appears to be involved in transcriptional regulation rather than cell wall biosynthesis directly. In addition, both deletion strains display distinct pigment production, indicative of secondary metabolite cluster activation. Despite this generalized comparison, it appears as if these regulatory proteins are most likely involved at different levels of regulation in (repression of) production of multiple cellular processes, including the deposition of cell wall chitin.

5. CONCLUSION

In summary, we show that deletion of CwcA results in a 30-40%increase in total cell wall glucosamine, making a *cwcA* mutant a potential candidate for improved chitin and chitosan production as value added by-product from fungal biomass derived from industrial fungal fermentation.

Acknowledgement
We would like to thank Prof. Dr. Bruno M. Moerschbacher for the coordination of the FunChi project.

Funding
This work is part of the "FunChi" ERA-IB project with project number ERA-IB-15-080, which is (partly) financed by the Dutch Research Council (NWO).

Availability of data and materials
All data are available on request by contacting the corresponding author.

Supplemental information
Supplementary tables to this article can be found online at https://doi.org/10.1016/j.gene.2020.100028.

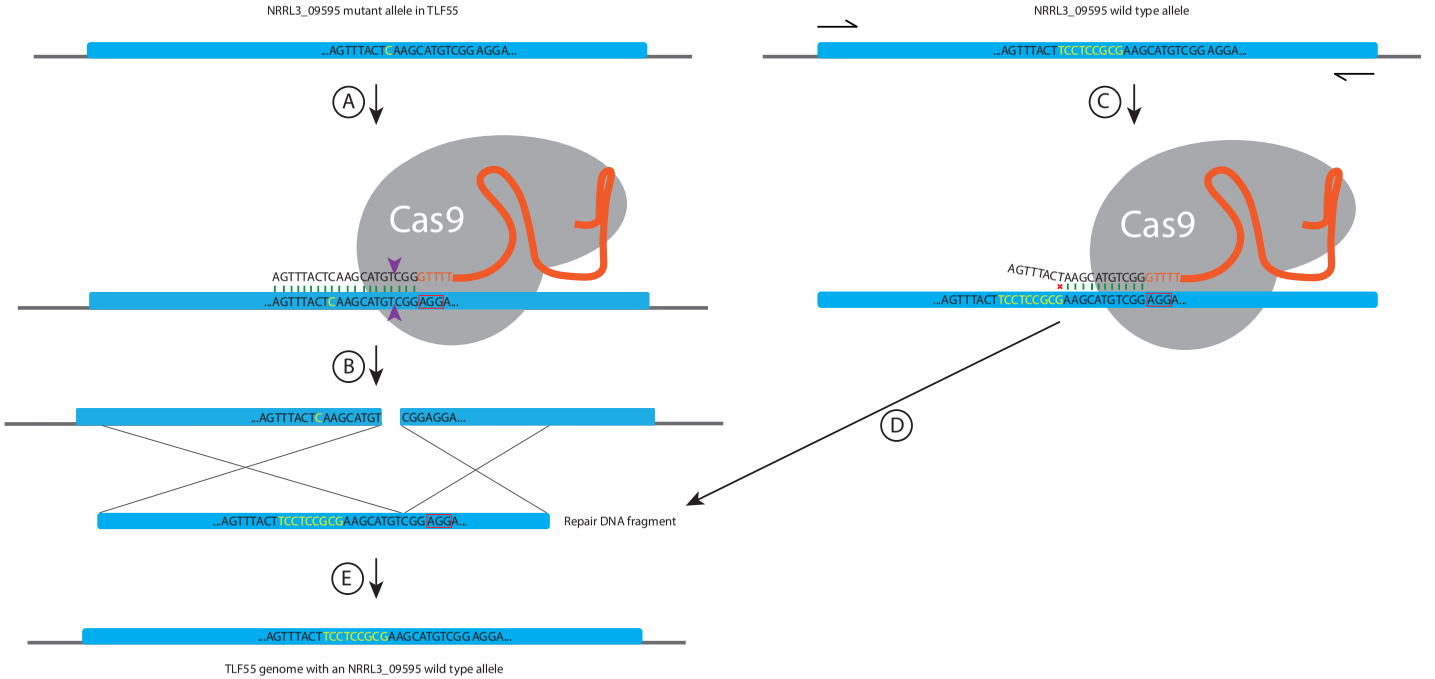

Supplementary figure 1. CRISPR/Cas9 design for targeting of the NRRL3_09595 mutant allele for complementation in the TLF55 (RD15.4#55, *pyrG*-) background. (A) NRRL3_09595-*mut*-sgRNA-Cas9 ribonucleoprotein (RNP) complex binds the genomic DNA of the TLF55 strain. Green bars represent matching of bps between the sgRNA target and genomic sequence. PAM site is highlighted by a red box (AGG). Purple arrows indicate the site of the double stranded break (DSB). (B) Creation of a DSB in mutant allele NRRL3_09595. (C) PCR amplification of the NRRL3_09595 wild type allele to generate a repair DNA fragment from that contains 8 bps that are not present in the NRRL3_09595 mutant allele, shown in yellow. As such, the repair DNA fragment is not recognized by the NRRL3_09595-*mut*-sgRNA-Cas9 RNP due to mismatches succeeding from the 12th nucleotide (nt) upstream from the PAM site, displayed by a red cross. (D) The repair DNA fragment from the NRRL3_09595 wild type allele remains intact and allows repair of the NRRL3_09595 mutant allele through homology directed repair. (E) The resultant transformation restores the NRRL3_09595 mutant allele in TLF55 to a wild type allele at the endogenous locus.

CHAPTER 5

Rab GDP-dissociation inhibitor *gdiA* is an essential gene required for cell wall chitin deposition in *Aspergillus niger*

Tim M. van Leeuwe, Anne Gerritsen, Mark Arentshorst, Peter J. Punt, Arthur F.J. Ram

ABSTRACT

The cell wall is a distinctive feature of filamentous fungi, providing them with structural integrity and protection from both biotic and abiotic factors. Unlike plant cell walls, fungi rely on structurally strong hydrophobic chitin core for mechanical strength together with alpha- and beta-glucans, galactomannans and glycoproteins. Cell wall stress conditions are known to alter the cell wall through the signaling cascade of the cell wall integrity (CWI) pathway and can result in increased cell wall chitin deposition. A previously isolated set of *Aspergillus niger* cell wall mutants were screened for increased cell wall chitin deposition. UV-mutant RD15.8#16 was found to contain approximately 60% more cell wall chitin than the wild type. In addition to the chitin phenotype, RD15.8#16 exhibits a compact colony morphology and increased sensitivity towards SDS. RD15.8#16 was subjected to classical genetic approach for identification of the underlying causative mutation, using co-segregation analysis and SNP genotyping. Genome sequencing of RD15.8#16 revealed eight SNPs in open reading frames (ORF) which were individually checked for co-segregation with the associated phenotypes, and showed the potential relevance of two genes located on chromosome IV. *In situ* re-creation of these ORF-located SNPs in a wild type background, using CRISPR/Cas9 genome editing, showed the importance Rab GTPase dissociation inhibitor A (*gdiA*) for the phenotypes of RD15.8#16. An alteration in the 5' donor splice site of *gdiA* reduced pre-mRNA splicing efficiency, causing aberrant cell wall assembly and increased chitin levels, whereas gene disruption attempts showed that a full gene deletion of *gdiA* is lethal.

This chapter is published as: van Leeuwe, T.M., Gerritsen A., Arentshorst, M., Punt, P.J., Ram A.F.J., Fungal Genet. Biol. 136, 103319 (2020). doi: 10.1016/j.fgb.2019.103319

1. INTRODUCTION

The fungal cell wall is an essential structure that sets apart filamentous fungi from other eukaryotes. Mainly comprised of α-1,3-glucans, β-1,3-glucans, β-1,6-glucans and mixed β-1,3/1,4 varieties, chitin (β-1,4-linked-*N*-acetyl glucosamine), galactomannan and glycoproteins, the cell wall is continuously being built, remodeled, broken down and re-built to accommodate various stages and challenges of the filamentous lifestyle. For extensive review on cell wall organization and biosynthesis we refer to both Free, 2013 and Gow et al., 2017, with the references therein. In addition to the majority of glucans, chitin plays a structurally important part of the fungal cell wall for mechanical strength. At the plasma membrane, chitin synthases assemble the UDP-*N*-acetyl-glucosamine monomers into chitin polymers by extrusion of nascent chitin chains into the periplasmic space. Careful coordination of sufficient precursor and available chitin synthases at the plasma membrane, determine both the rate of which chitin is deposited into the cell wall and chitin chain length (Kang et al., 1984; Keller and Cabib, 1971; Orlean and Funai, 2019; Peter, 1987; Sburlati and Cabib, 1986). Seven clearly defined classes of chitin synthases (CHSI-CHSVII) are known to exist in filamentous fungi, some of which have been studied in detail, and have been shown to be correlated with morphogenesis and adaptation to ecological niches (Liu et al., 2017). Encompassing many different classes of chitin synthases, fungi temporally and spatially regulate expression during different stages of development. Additional post-translational activation of certain chitin synthases, involving glycosylation (Santos and Snyder, 1997; Trilla et al., 1999), phosphorylation (Valdivia and Schekman, 2003) and proteolytic cleavage of zymogenic chitin synthases (Choi et al., 1994) all contribute to tight regulation of chitin deposition in the cell wall.

As a result of this complex organization, levels of cell wall chitin are generally well maintained, and fluctuations in chitin content mainly differ depending differing stages of life cycle, environmental cues, mycelial age, available nutrients and cultivation conditions, hypoxia and stress (Lord and Vyas, 2019; Pochanavanich and Suntornsuk, 2002). Cell wall stress often results in increased cell wall chitin content through activation of the cell wall integrity (CWI) signal transduction pathway (Fortwendel et al., 2010; Heilmann et al., 2013; Ram et al., 2004; Walker et al., 2015, 2008). This conserved, natural response in filamentous fungi often involves a compensatory increase in both cell wall chitin and alpha-glucan deposition. Specifically, under cell wall stress conditions in *A. niger* it was reported that levels of both *agsA* (alpha-glucan synthase A) (Damveld et al., 2005b) and *gfaA* (glutamine-fructose-6-phosphate-amidotransferase A) (Ram et al., 2004) are induced. The expression of the former was previously used in a cell wall stress reporter system to identify mutants with a constitutively activated cell wall stress response in a UV-screen (Damveld et al., 2008). We identified mutants from this cell wall mutant library that display an increased cell wall chitin content (**Chapter 4**). Resultant from this screen, mutant RD15.8#16 was identified as a strain with increased cell wall chitin levels.

In the quest to identify the genotype related to the cell wall phenotype of RD15.8#16, we took a classical genetics approach combined with genome sequencing. A lacking established sexual cycle of *A. niger* prevents traditional type crossings, however, a parasexual cross was used instead

to obtain segregants (Arentshorst and Ram, 2018; Pontecorvo et al., 1953; Swart et al., 2001). Is important to note in this approach that, unlike a conventional sexual cycle, cross-over events are singularly mitotic and are therefore relatively rare. When cross-over events are absent, co-segregation analysis is only indicative of the linked chromosome, rather than a specific gene or genomic region.

In this study, we performed co-segregation analysis of the RD15.8#16 phenotype by selecting segregants that displayed either wild type or the RD15.8#16 phenotypes. Segregants with either of the two phenotypes were checked for presence of SNPs that are unique to RD15.8#16. Comparative SNP analysis revealed the chromosomal distribution among segregants and identified the exclusive co-segregation of markers on chromosome IV with the RD15.8#16 phenotype. With the use of a previously reported CRISPR/Cas9 gene editing system (**Chapter 2**), we performed *in situ* SNP editing of the endogenous wild type allele to re-create the respective mutant alleles on chromosome IV. Re-creation of mutant alleles in a wild type genetic background revealed that inefficient and/or aberrant splicing of Rab GDP-dissociation inhibitor (*gdiA*) is responsible for the phenotype of RD15.8#16.

2. MATERIALS AND METHODS

2.1 Strains, media, growth conditions

Strains used in this study can be found in Table 1. All media were prepared as described by Arentshorst et al., 2012. In all cases, minimal medium (MM) contained 1% (w/v) glucose, 1.5% gar and was supplemented when required with 10mM uridine and 2.5 µg/mL nicotinamide. To test the presence or absence of the *amdS* gene, MM acetamide agar (MM-AA) was used as described by Arentshorst et al., 2012. Complete medium (CM) contained 1% (w/v) glucose, 1.5% agar (Scharlau, Barcelona, Spain), 0.1% (w/v) casamino acids and 0.5% (w/v) yeast extract in addition to MM. Strains were inoculated from -80°C glycerol stocks onto fresh CM plates and were allowed to grow and sporulate for 5-7 days at 30°C, prior to spore harvesting. Spores were harvested by addition of 15 mL of 0.9% (w/v) NaCl to CM spore plates and were carefully scraped from the surface with a cotton swab. Spore solutions were poured over sterile cotton filters (Amplitude™ Ecocloth™ Wipes, Contec Inc., Spartanburg, SC, USA) to remove large mycelial debris. Spore solutions were counted using Bio-Rad TC20™ Automated Cell Counter (Bio-Rad Laboratories, Inc. USA) using Counting Slides, Dual Chamber for Cell Counter (Cat#145-0011, Bio-Rad Laboratories, Inc. USA).

2.2 SDS sensitivity assays

Wild type, mutants and segregants were tested on different concentrations of SDS. Using a 10% (w/v) SDS stock, MM plates (when required, supplemented with either or both uridine and nicotinamide) to create final SDS concentrations of 0.004%, 0.0045% and 0.005% SDS. Spore stocks were created as described above. Spores were counted, serially diluted into 2000, 200, 20

and 2 spores/µL and 5 µL of respective dilutions were spotted on MM SDS plates. The plates were incubated for 96h at 30 °C prior to scoring phenotypes.

SDS sensitivity was tested with un-normalized spore concentrations during the segregants screen. A total of 200 segregants and controls were streaked twice on MM + U + N and spores were harvested from a single colony using a pre-wetted (0.9% NaCl) cotton swab. Cotton swab containing spores was dipped and swirled in 0.5 mL 0.9% NaCl to dissolve spores. For each segregant and control strain, 5 µL spore solution was spotted on plates for testing phenotypes (see section 2.4).

Table 1. All strains used in this study

Name	Genotype	Reference
N402	cspA1	Bos et al., 1988
MA234.1	cspA1, *ΔkusA::DR-amdS-DR*	Park et al., 2016
MA169.4	cspA1, *ΔkusA::DR-amdS-DR*, *pyrG*$^{-}$	Carvalho et al., 2010
RD15.8	cspA1, *pyrG*$^{-}$, *PagsA-H2B-GFP-TtrpC-pyrG*, PagsA-amdS-TamdS + pAN7-1 (hph+)*	Damveld et al., 2008
RD15.8#16	UV-mutant of RD15.8	Damveld et al., 2008
TLF56	RD15.8#16, *pyrG*$^{-}$ (5'-FOA selected)	This study
TLF54	RD15.8#16, *pyrG*$^{-}$ (5'-FOA selected), *ΔbrnA*	This study
JN6.2	cspA1, *ΔkusA::DR-amdS-DR, pyrG-, nicB::hygB, olvA::AOpyrG*	Niu et al., 2016
TLF92	Diploid strain: JN6.2 x TLF54	This study
AG1	NRRL3_05482 mutant allele in MA234.1	This study
AG3	*gdiA* mutant allele in MA234.1	This study
ΔolvA#8	Segregant of TLF92, *ΔolvA::AOpyrG*, *nicB*$^{-}$, *amdS*$^{+}$	This study
ΔolvA#27	Segregant of TLF92, *ΔolvA::AOpyrG*, *nicB*$^{-}$, *amdS*$^{-}$	This study
ΔolvA#41	Segregant of TLF92, *ΔolvA::AOpyrG*, *nicB*$^{+}$, *amdS*$^{-}$	This study
ΔolvA#50	Segregant of TLF92, *ΔolvA::AOpyrG*, *nicB*$^{+}$, *amdS*$^{+}$	This study
ΔolvA#67	Segregant of TLF92, *ΔolvA::AOpyrG*, *nicB*$^{+}$, *amdS*$^{+}$	This study
ΔbrnA#4	Segregant of TLF92, *ΔbrnA*, *pyrG*$^{-}$, *nicB*$^{+}$, *amdS*$^{+}$	This study
ΔbrnA#11	Segregant of TLF92, *ΔbrnA*, *pyrG*$^{-}$, *nicB*$^{+}$, *amdS*$^{+}$	This study
ΔbrnA#25	Segregant of TLF92, *ΔbrnA*, *pyrG*$^{-}$, *nicB*$^{-}$, *amdS*$^{+}$	This study
ΔbrnA#33	Segregant of TLF92, *ΔbrnA*, *pyrG*$^{-}$, *nicB*$^{+}$, *amdS*$^{-}$	This study
ΔbrnA#53	Segregant of TLF92, *ΔbrnA*, *pyrG*$^{-}$, *nicB*$^{+}$, *amdS*$^{+}$	This study
ΔbrnA#77	Segregant of TLF92, *ΔbrnA*, *pyrG*$^{-}$, *nicB*$^{-}$, *amdS*$^{-}$	This study
ΔbrnA#90	Segregant of TLF92, *ΔbrnA*, *pyrG*$^{-}$, *nicB*$^{+}$, *amdS*$^{-}$	This study

2.3 Cell wall isolation and chitin analysis

2.3.1 Cell wall isolation

Strains were cultured to obtain equally aged spores as described above. To 25mL of liquid CM (100mL Erlenmeyer flask), a final concentration of 10^6 spores/mL was added and grown overnight for 17h at 30°C, 200 rpm. Mycelium was harvested by applying a vacuum over a Whatman™ Glass Microfiber Filter (GF/C™) (diameter 47 mm, CAT No.1822-047, Buckinghamshire, UK) to remove medium and capture and dry the mycelium. Dried mycelium was frozen in liquid N_2 prior to grinding in order to break open the cells with mortar and pestle into a fine powder. Next, samples were washed to remove intracellular debris and proteins: washing occurred by addition of 50 mL 1M NaCl, followed by three washing steps with 50mL MQ. In both cases washing involves vigorous shaking and vortexing with 25 mL volume in 50 mL plastic tubes (114x28mm, Sarstedt AG & Co. KG, 62.547.254). Subsequently, the remaining 25 mL volume was added followed by repeated shaking and vortexing. Cell wall suspensions were centrifuged at 3,500 rpm for 10 min. to pellet cell walls. Supernatant was carefully discarded prior to the next washing step. Cell walls were lyophilized after washing steps for 48h.

2.3.2 Cell wall hydrolysis and chitin analysis

Chitin was measured as total glucosamine and was performed based on the principle of the Morgan-Elson protocol (Elson and Morgan, 1934) and was adapted for higher through-put analysis, using a 96-well plate reader. See appendix (Supplementary document 1) for a detailed description of the protocol. Due to variability between separate experiments in absolute glucosamine content, a wild type control was always included every time to compare relative differences. Cell wall glucosamine measurements from independent replicate experiments are expressed as means ± SEM. The statistical analysis was carried out using software R studio (Version 1.1.456) (RStudio: Integrated Development for R. RStudio, Inc., Boston, 2016). For total cell wall glucosamine experiments, we used one-way ANOVA. Significant differences between groups were subjected to posthoc Tukey multiple-comparisons analysis. Significance levels are indicated as $p < 0.05$ (*), $p < 0.005$ (**), $p < 0.001$ (***) and $p < 0.0001$ (****).

2.4 Parasexual cycle and segregant analysis

Formation of heterokaryons and selection for diploids was performed as described previously described (Arentshorst and Ram, 2018). Requirements for this procedure are for each strain to have separate auxotrophic deficiencies and different color markers from one of the three known complementation groups involved in melanin production: fawn (*fwnA*, NRRL3_00462, An09g05730), olive (*olvA*, NRRL3_01039, An14g05350) or brown (*brnA*, NRRL3_01040, An14g05370) colored (Jørgensen et al., 2011). As such, two haploid strains are coerced to fuse without supplementation for their respective auxotrophic deficiencies. This process yields a heterokaryotic, prototrophic mycelium in which karyogamy can occur at a very low frequency, resulting in a diploid strain. Due to the primarily uninuclear nature of *A. niger* asexual spores, color

markers help identify whether nuclei have fused, and become black as a result of complementing alleles from the other chromosome, or remain unfused as one of the individual colors in the heterokaryotic mycelium. An obtained diploid contains both chromosome-sets and can be haploidized to allow random distribution of each chromosome by exposure to benomyl, creating auxotrophic, brown- or olive-colored segregants. To obtain an auxotrophic haploid derivative of RD15.8#16, this strain was subjected to 5'-FOA counter selection to lose the *pyrG* (Arentshorst et al., 2015; Boeke et al., 1984), resulting in strain TLF56 (Table 1). TLF56 was subsequently than transformed with pFC330_*brnA*-sgRNA (pTLL37.1) and a knockout repair DNA fragment as described previously (**Chapter 2**).

Segregation of diploids was performed at 0.4 µg/mL benomyl on complete medium (CM) supplemented with 10mM uridine and 2.5 µg/mL nicotinamide. Segregants were single streaked twice on MM with uridine and nicotinamide prior to segregation analysis. Auxotrophic marker distribution and SDS sensitivity were tested for all 200 segregants. Spores were taken from a single colony of the second single streak with a pre-soaked cotton swab (using 0.9% w/v NaCl solution) and taken up into 500 µL 0.9% (w/v) NaCl. For each segregant, 5 µL spore solution was spotted on MM + uridine + nicotinamide, MM + uridine and MM-AA + uridine + nicotinamide and on MM + uridine + nicotinamide + 0.005% SDS. These were incubated for 144h at 30 °C.

2.5 DNA isolation, Illumina sequencing and SNP analysis

Genomic DNA was isolated as described by Arentshorst et al., 2012. In case of genome sequencing, this procedure was followed by column purification using the Nucleospin Plant II kit (Machery-Nagel), according to the manufacturer's instructions. Genome sequencing was executed by GenomeScan B.V (Leiden, The Netherlands). The NEBNext® Ultra DNA Library Prep kit for Illumina (cat# NEB #E7370S/L) was used to process the samples. Fragmentation of the DNA using the Biorupor Pico (Diagenode), ligation of sequencing adapters, and PCR amplification of the resulting product was performed according to the procedure described in the NEBNext Ultra DNA Library Prep kit for Illumina Instruction Manual. The quality and yield after sample preparation was measured with the Fragment Analyzer. The size of the resulting product was consistent with the expected size of approximately 500-700 bp. Clustering and DNA sequencing using the Illumina cBot and HiSeq 4000 was performed according to manufacturer's protocols. A concentration of 3.0 nM of DNA was used. HiSeq control software HCS v3.4.0 was used. Image analysis, base calling, and quality check was performed with the Illumina data analysis pipeline RTA v2.7.7 and Bcl2fastq v2.20. SNP calling was performed according to GenomeScan Guidelines Small Variant Analysis v3.0. The Variant Call Format (VCF) files were manually analyzed by the authors. Frequency score of identical SNP call boundary was set to ≥ 0.75, while sequencing depth was left unselected.

2.6 Co-segregation analysis of SNPs

Approximately 400-500 bp long PCR products surrounding the SNP in question were amplified with primers listed in Primer Table. An additional nested primer was designed for each PCR

product used for sequencing. Sequencing of individual SNPs was performed using Sanger sequencing (Macrogen Europe, Amsterdam, The Netherlands). Analysis of sequencing data and alignments were performed in Benchling [Biological Software] 2019.

2.7 Single gene knockouts using split marker fragments

MA169.4 (Table 1) was transformed after protoplastation as described previously (Arentshorst et al., 2012). Using the split marker approach for single gene knockouts, entire ORFs were deleted by replacement with the *Aspergillus oryzae pyrG* (*AOpyrG*) selection marker (Arentshorst et al., 2015). Flanks were generated via PCR using N402 genomic DNA as template and primers as described in Primer Table. *AOpyrG* fragments were obtained from plasmid pAO4-13 (de Ruiter-Jacobs et al., 1989) with primers as described in Primer Table. Fusion PCR was used to generate split marker fragments containing *AOpyrG*. Approximately 2 µg of DNA per flank was added to protoplasts for transformation. Transformation plates were incubated on MMS for 6 days at 30°C. Transformed colonies were single streaked on MM twice for purification and were genotyped using diagnostic PCR (data not shown).

2.8 SNP re-creation in a wild type background using CRISPR/Cas9 gene editing

SNPs were introduced in a wild type (MA234.1) background using CRISPR/Cas9 mediated gene editing with a marker-free repair DNA fragment (**Chapter 2**). All primers are listed in Primer Table. Primers OTL479 and OTL480 were used in combination with pTE1_rev and pTE1_for, respectively, to obtain a sgRNA construct to target the wild allele NRRL3_05482 in MA234.1. Similarly, for NRRL3_06010, primers OTL477 and OTL476 were used in combination with pTE1_rev and pTE1_for, respectively, to obtain a sgRNA construct to target the wild allele NRRL3_06010 in MA234.1. Plasmids pTLL108.1 and pTLL109.2 were used as template DNA for sgRNA flanks. Flanks were fused through PCR to obtain sgRNAs, and cloning of the sgRNAs into pFC332 resulted in pFC332_NRRL3_05482-sgRNA and pFC332-NRRL3_06010-sgRNA. Marker-free repair DNA fragment for NRRL3_05482 was obtained through fusion PCR, 5' flank was amplified using OTL481 and OTL482, whereas 3' flank was amplified with OTL483 and OTL484. OTL482 and OTL483 contained a single mismatch to introduce a point mutation (see section 3.5) and allowed sufficient overhang for generation of a fusion construct. Marker-free DNA fragment repair for NRRL3_06010 was amplified from RD15.8 as template DNA, using OTL485 and OTL486. CRISPR/Cas9 plasmid transformations were performed after protoplastation as described previously (**Chapter 2**), using a pFC332 (*hph*) plasmid (Nødvig et al., 2015): 2 µg of Cas9-sgRNA plasmid with approximately 2 µg of repair DNA fragment for transformation. Transformation plates were incubated on MMS with 200 µg/mL hygromycin for 7 days at 30°C. Transformed colonies were single streaked on selectable MM with 100 µg/mL hygromycin to select for the presence of the Cas9-sgRNA plasmid. Next, a single colony was picked and transferred to non-selective MM medium to allow loss of the Cas9-sgRNA plasmid. A third streak of a single colony on both MM and MM with 100 µg/mL hygromycin uridine was performed as a control for loss of plasmid. DNA from plasmid-cured strains was isolated as described by Arentshorst et al., 2012, using mortar

and pestle to grind the mycelium in liquid nitrogen. Genotypes were confirmed using diagnostic PCR. Diagnostic PCR fragments from wild type (RD15.8), mutant (RD15.8#16) and transformants were sent for sequencing to check for SNP alterations (Macrogen Europe, Amsterdam, The Netherlands).

2.9 RNA isolation and RT-PCR for cDNA

RNA was isolated and column purified according to Park et al., 2016. Complementary DNA (cDNA) was obtained using the QuantiTect Reverse Transcription Kit (Qiagen). In short, 1 µg of RNA was added to 2 µL of gDNA Wipeout Buffer and RNAse-free water was added to a total volume of 14 µL. After incubation for 2 min at 42 °C, the reactions were placed on ice. Then Reverse-transcription master mix (1 µL), Quantiscript RT Buffer (4 µL) and RT Primer Mix (1 µL) were added and the RT-reaction was performed for 15 min at 42 °C, followed by a heat inactivation step of 3 min at 95 °C. 1 µL of the resulting cDNA library was used as template in subsequent PCR experiments.

3. RESULTS

3.1 RD15.8#16 displays a compact colony morphology, SDS sensitivity and increased cell wall chitin

RD15.8#16 was selected from a previously obtained set of cell wall stress mutants (Damveld et al., 2008), and was found in a screen for strains with an increased cell wall chitin content (**Chapter 4**). Increased cell wall chitin was suggested by increased Calcofluor White (CFW) staining (Figure 1A). Next, total glucosamine content from cell wall dry weight was measured for the wild type strain N402 (159 µg/mg ± 5.01, n=3), parental strain RD15.8 (163 µg/mg ± 8.73, n=3) and UV-mutant RD15.8#16 (263 µg/mg ± 7.80, n=3) and is depicted in Figure 1B. Whereas the wild type and parental reporter strain have equal amount of cell wall glucosamine, RD15.8#16 shows a respective increase of 61% chitin. In addition to the cell wall phenotype, the mutant has a compact colony morphology and has increased sensitivity towards SDS (Figure 1C).

3.2 A parasexual cross and segregation analysis to isolate linkage to SDS sensitivity

To perform a parasexual cross and subsequent detection of segregation of diploid strains, we used a derivative strain of RD15.8#16 harboring *ΔbrnA, pyrG-,* strain TLF54 (see section 2.4). A previously obtained olive-colored, *nicB*$^{-}$ wild type strain JN6.2 (*ΔnicB*::*AOpyrG*, *ΔolvA::hygB,* (Niu et al., 2016b), Table 1) was used to perform a parasexual cross with TLF54.

Figure 1C shows an SDS sensitivity phenotype for RD15.8#16 used for segregants screening. Prior to segregant analysis, both parental strains JN6.2 and TLF54 were checked against their non-auxotrophic, non-color deficient counterparts RD15.8 and RD15.8#16, respectively. As is evident from Figure 2, both parental strains for the parasexual cross show the same level of SDS sensitivity as their parental counterparts. Additionally, colony morphologies of RD15.8#16 and TLF54 are identical and show a more compact growth style than both JN6.2 and RD15.8.

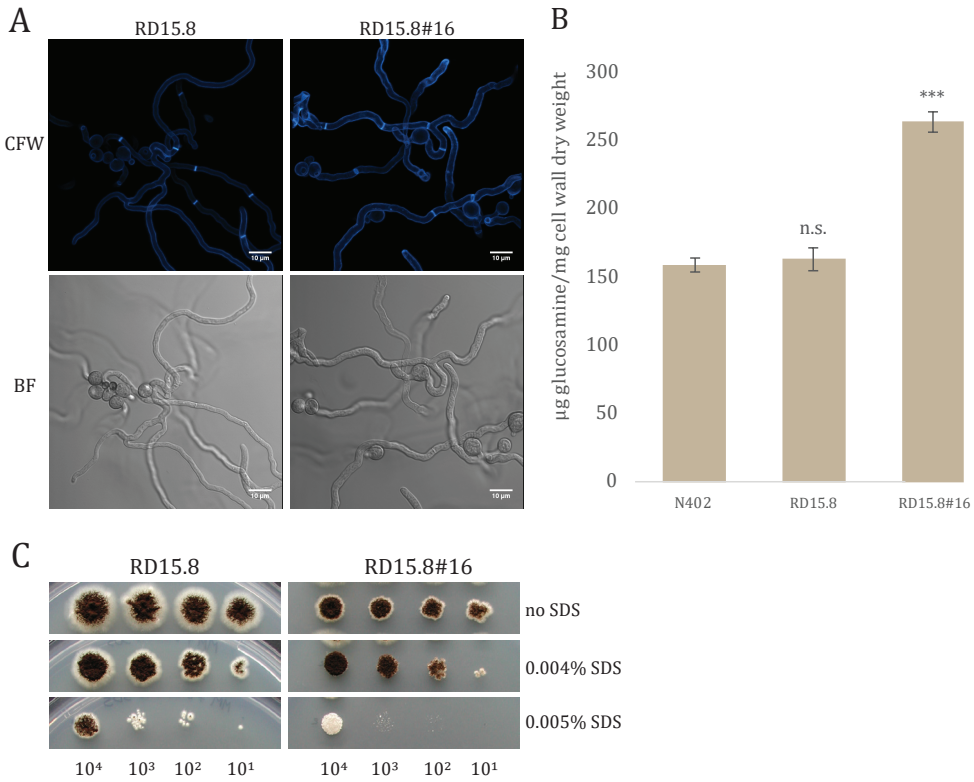

Figure 1. Chitin content and morphology of UV-mutant and wild types. (A) Chitin content of N402, RD15.8 (parent) and RD15.8#16 are shown (n=3). (B) Growth morphology on MM, and SDS sensitivity on MM + SDS for RD15.8 and RD15.8#16. Statistical methods and significance is described in section 2.3.2. Listed significant differences are compared to N402. Abbreviation n.s. refers to not significant. (C) SDS sensitivity of RD15.8 and RD15.8#16 on minimal medium (described in section 2.1) with either no SDS, 0.004% SDS or 0.005% SDS. (section 2.2). Spore amounts (#) per spot from left to right are 10^4, 10^3, 10^2 or 10^1, and are listed below the figure. Strains were incubated 96h at 30°C.

Morphologies of wild type JN6.2, TLF54, original mutant RD15.8#16 and diploid TLF92 are shown on CM and CM + 0.5 µg/mL benomyl in Supplementary figure 1. The diploid strain TLF92 forms black spores, indicating that all spores contain two sets of chromosomes by color complementation of *brnA* and *olvA*. On CM + 0.5 µg/mL benomyl, the diploid strain forms sectors of both brown and olive colors that represent chromosomal loss from diploid to haploid (Supplementary figure 1).

In total 200 segregants were screened for SDS sensitivity by spotting spores on MM + U + N + 0.005% SDS, and for colony morphology resembling TLF54. Only two out of 200 segregants were found to display the same compact phenotype of TLF54 and were prone to SDS sensitivity (Supplementary figure 2A and B, segregants *ΔbrnA*#53 and *ΔbrnA*#90). Two randomly picked segregants, *ΔolvA*#27 and *ΔolvA*#41 resembling both wild type-like morphology and wild type-like SDS sensitivity, were taken in addition to *ΔbrnA*#53 and *ΔbrnA*#90 for a closer comparative analysis SDS sensitivity with normalized spore concentrations (Figure 3A). Evidently, we confirmed that *ΔbrnA*#53 and *ΔbrnA*#90 are indeed equally sensitive to SDS as TLF54. The chitin content of the cell wall was analyzed by determining the total cell wall glucosamine content of

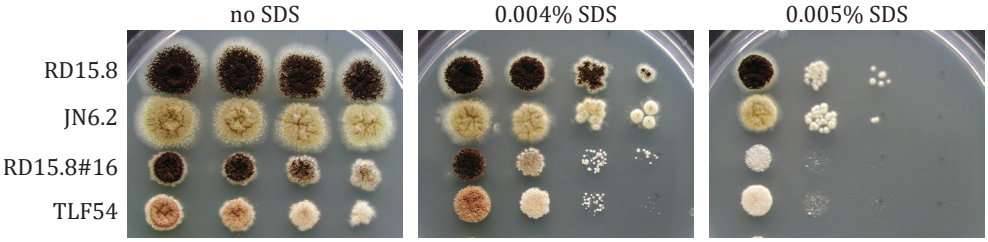

Figure 2. Morphology of strains involved in parasexual cross. SDS sensitivity spot assay of RD15.8, JN6.2, RD15.8#16 and TLF54 on 0.004% and 0.005% SDS in Minimal Medium (MM) with 10mM uridine (U) and 2.5 µg/mL Nicotinamide (N). From left to right, spore count equals 10^4, 10^3, 10^2 and 10^1. Strains were incubated 96h at 30°C.

ΔbrnA#53 and *ΔbrnA*#90, parental strains JN6.2, TLF54 and segregants *ΔolvA*#27, *ΔolvA*#41. Figure 3B shows a comparative analysis of glucosamine content of the aforementioned strains versus the wild type parent JN6.2. Both *ΔbrnA*#53 and *ΔbrnA*#90 showed a significant increase in cell wall glucosamine versus JN6.2, but were not significantly different from TLF54. In addition, segregants *ΔolvA*#27 and *ΔolvA*#41 do not differ significantly from JN6.2. These data suggest that both *ΔbrnA*#53 and *ΔbrnA*#90 inherited all the associated phenotypes of TLF54 and that the SDS sensitivity and increased cell wall chitin are caused by the same mutation.

Due to very unequal segregation of mutant traits, we checked for chromosome distribution among segregants based on the other available genetic markers. As *brnA* and *olvA* are located adjacent to each other on chromosome I, we initially picked a total of 100 brown and 100 olive segregants segregating TLF92 diploid strain to obtain equal numbers of segregants in which one of the copies of chromosome I was present. Equal distribution of wild type and mutant of chromosomes was also checked for chromosome III and VII using the markers located on either chromosome

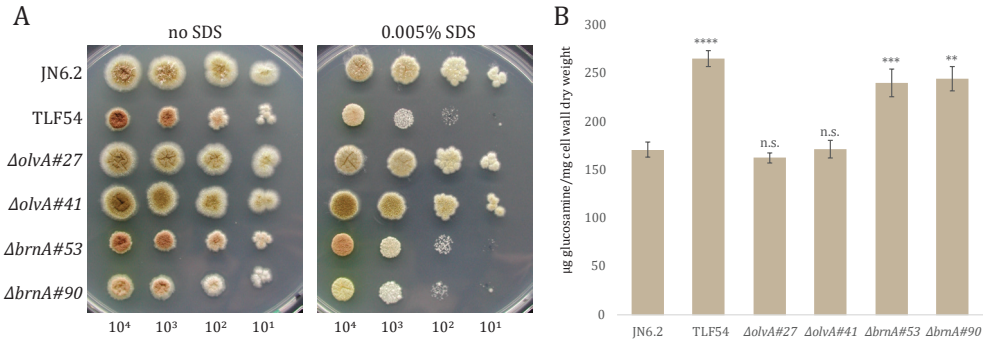

Figure 3. Phenotypes of parental strains JN6.2, TLF54, and segregants thereof. (A) Parents from parasexual cross JN6.2 and TLF54, two non-SDS sensitive segregants (*ΔolvA#27* and *ΔolvA#41*) and two SDS sensitive strains (*ΔbrnA#53* and *ΔbrnA#90*). Colony morphology and SDS sensitivity (0.005%) on Minimal Medium (MM) with 10mM uridine (U) and 2.5 µg/mL nicotinamide (N) grown at 30°C for 96h. (B) Cell wall glucosamine of all strains grown in Complete medium (CM) with U and N at 30°C for 17h (n=3-6)*. Statistical methods and significance are described in section 2.3.2. Listed significant differences are compared to JN6.2. Abbreviation n.s. refers to not significant. *variable sample size.

Table 2. Genomic single nucleotide polymorphisms (SNPs) of TLF54. SNPs located inside open reading frames (ORFs) of TLF54.

Chr	NRRL3_ID	CBS513.88 ID	Gene description	ORF strand	WT	TLF54	Effect of SNP on codon sequence
I	NRRL3_01084	An14g05970	Multi antimicrobial extrusion family protein	-	C	G	Codon change: $Glu^{382/504}$ --> $Gln^{382/504}$
II	NRRL3_01535	An13g00450	Hypothetical protein	-	C	T	Codon change: $Leu^{305/347}$ --> $Val^{305/347}$
II	NRRL3_01607	An01g00340	Solute carrier family 35 member	+	C	CCTT	13^{th} base of 1^{st} intron (CT rich region)
III	NRRL3_03466	An12g03570	*pyrG*	+	G	GGATC	Frameshift: $Pro^{255/277}$ --> $Arg^{255/277}$
IV	NRRL3_05482	An02g09460	C2H2-type and FYVE-type zinc finger containing protein (Yeast ortholog PEP7; adaptor protein involved in vesicle-mediated vacuolar protein sorting)	+	C	T	Codon change: $His^{299/675}$ --> $Tyr^{299/675}$ (between two FYVE-type zinc fingers)
IV	NRRL3_06010	An02g03120	Rab GDI family protein (*gdiA*)	-	T	C	7^{th} base of intron 2 (A>G)
IV	NRRL3_06010	An02g03120	Rab GDI family protein (*gdiA*)		A	C	2^{nd} base of intron 2 (GT>GG)
VII	NRRL3_09701	An11g05430	Hypothetical protein	-	G	A	Codon change: $Arg^{16/365}$ --> $Cys^{16/365}$
VIII	NRRL3_11721	An06g00500	Hypothetical protein	+	CA	TC	Codon change: $Gln^{72/492}$ --> $Ser^{72/492}$

III (*ΔkusA::amdS, JN6.2)* or chromosome VII (*nicB*, TLF54), by scoring all 200 segregants for presence or absence of *nicB*$^{+}$ and *amdS*$^{+}$. Segregation of *nicB*$^{+/-}$ was found to be 102/98, whereas *amdS*$^{+/-}$ segregation was scored to be 84/116 (Supplementary Table 1). These data suggested that the segregation of TLF92 occurred at an approximate 50/50 ratio of chromosomal co-segregation for the genetically marked chromosomes.

3.3 Genome sequencing reveals eight ORF-located SNPs in RD15.8#16

To identify the genotypic relation of the cell wall phenotype of RD15.8#16, we performed genome sequencing of TLF54; the derivative of RD15.8#16 used as mutant parent in the parasexual cross and compared it with the genome sequence of RD15.8. SNP calling was performed as described in section 2.5; a total of 44 SNPs and 9 indels were identified across the genome of TLF54 (Supplementary table 2). Eight SNPs and two insertions were identified to be inside ORFs and nucleotide changes and their respective effect on in protein sequence are listed in Table 2. In addition to coding sequence changes, two genes were found to harbor intron-located mutations.

3.4 Co-segregation analysis of SNPs reveals importance of chromosome IV

Due to the low number of segregants with the mutant phenotype of TLF54, we were unable to perform bulk segregant analysis (BSA) and decided to identify relevant SNPs by performing a SNP co-segregation analysis. VInitially, SNPs were determined by sequencing the ORF-located SNPs (Table 2, with the exception of *pyrG*) in mutant segregants *ΔbrnA*#53 and *ΔbrnA*#90, and two segregants that did not display the mutant phenotype (*ΔolvA*#27 and *ΔolvA*#41).

Sequenced SNPs of parental strains and segregants are displayed schematically in Figure 4. Yellow bars represent the SNPs of the wild type, whereas green bars indicate the SNP identified for TLF54. The co-segregation analysis indicated that SNPs associated with chromosome I and IV co-segregate with the mutant phenotype (Figure 4). However, note that the SNP on chromosome I (NRRL3_01084) is located on the same chromosome arm as either color marker *ΔolvA* (wild type SNP) or *ΔbrnA* (mutant SNP), making co-segregation of the *ΔbrnA* color marker, and not the cell wall mutant phenotype, a possible consequence of genetic linkage.

To check whether mutant SNPs on chromosome I (NRRL3_01084) or on chromosome IV (NRRL3_05482 and NRRL3_06010) are co-segregating with the phenotypes, a second set of segregants with wild type-like phenotypes was included for SNP sequencing shown in Figure 4. Only wild type SNPs were found for both NRRL3_05482 and NRRL3_06010 on chromosome IV in segregants that do not display the TLF54 phenotype. These data suggest that the SNPs found on chromosome IV are associated with the phenotypes of RD15.8#16.

3.5 SNPs re-creation shows that the mutant allele of NRRL3_06010/*gdiA* is responsible for the phenotype of RD15.8#16

The SNP co-segregation analysis showed the SNPs on chromosome IV to be associated with either the wild type or mutant phenotype. In addition to NRRL3_05482 and NRRL3_06010, TLF54

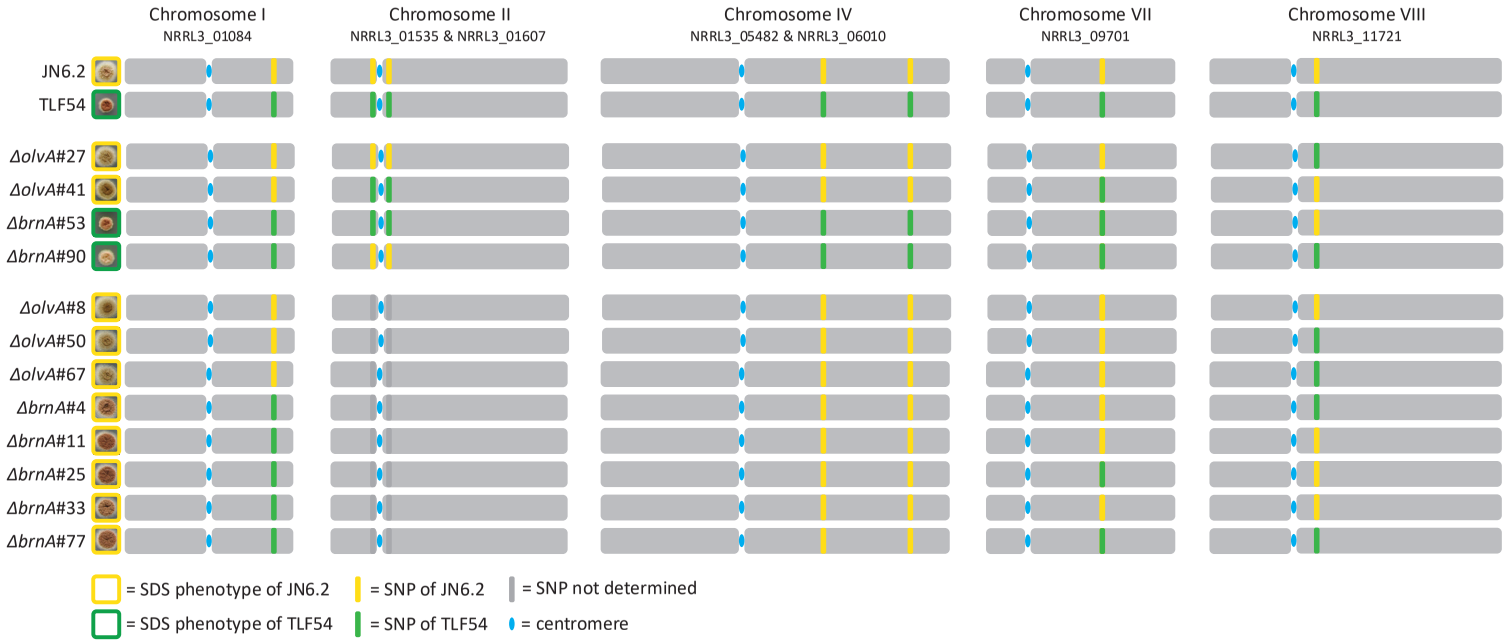

Figure 4. Overview of identified SNPs in JN6.2, TLF54 and 12 segregants based on local sequencing. Parental strains of parasexual cross are listed above; olive colored wild type (JN6.2) and brown colored RD15.8#16 derivative (TLF54). An initial set of four segregants was used to sequence all ORF-related SNPs, previously shown to resemble either the phenotype of RD15.8 #16 or wild type (Figure 3, *ΔbrnA #53* and *ΔbrnA #90*, and *ΔolvA #27* and *ΔolvA #41*, respectively). A second set of segregants that resemble the wild type phenotype (*ΔolvA#8*, *ΔolvA#50*, *ΔolvA#67*, *ΔbrnA#4*, *ΔbrnA#11*, *ΔbrnA#25*, *ΔbrnA#33* and *ΔbrnA#77*) was sequenced for ORF-related SNPs for chromosome I, IV, VII and VIII. Strains and respective colony morphology are shown on Minimal Medium (MM). Only chromosomes I, II, IV, VII and VIII are shown as they harbor the ORF targeted SNPs (see Table 2). Sizes of chromosomes and SNPs are not to scale, and represent both the approximate length of the chromosomes and the SNP locations. Colored bars are indicative for the inherited SNP; yellow represents the wild type (JN6.2) SNP, whereas the green SNP represents the mutant (TLF54). Gene ID of targeted ORFs are listed below the chromosome number in respective order. Genes NRRL3_06010 (*gdiA*) and NRRL3_11721 both harbor two SNPs within 5bp of one another and are displayed in this figure as a single yellow or green bar (for details see Table 2).

harbors three additional SNPs on chromosome IV (Supplementary table 2), but were all found to be outside of promoter or coding regions. Therefore, we considered the two genes NRRL3_05482 and NRRL3_06010 as candidates for causing the observed cell wall phenotype of RD15.8#16.

Using a split marker approach as described in section 2.7, we attempted to create full gene knockouts. Transformants of both ΔNRRL3_05482*::AOpyrG* and ΔNRRL3_06010*::AOpyrG* in MA169.4 showed low levels of sporulation and single streaking on either selective or non-selective medium often did not show colony forming units derived from single spores, suggesting these genes are essential for growth and the null allele only allows growth through heterokaryotic rescue (Osmani et al., 2006). Transformants that did grow after re-streaking were expected to contain ectopically integrated selection markers, as diagnostic PCR did not show correct deletion of ORF (data not shown).

Based on these results we opted to re-create the mutant SNPs in a wild type background using CRISPR/Cas9 genome editing. This was achieved by targeting either NRRL3_05482 or NRRL3_06010 in the wild type MA234.1 (Table 1) with respective plasmids pFC332_NRRL3_05482-sgRNA and pFC332 NRRL3_06010-sgRNA, and simultaneously present a linear repair DNA fragment from TLF54 that contains the SNPs in question, for homologous recombination.

For NRRL3_06010, we exploited the location of the +2 intronic SNP to create a sgRNA target that targets the wild type SNP, but does not recognize the mutant SNP located on the DNA repair fragment. The +2 intronic G/G<u>T</u> --> G/G<u>G</u> mutation of the NRRL3_06010 mutant allele is situated at the second nucleotide upstream from the PAM site of the NRRL3_06010-sgRNA target sequence. A schematic representation of this approach for NRRL3_06010 is shown in Supplementary figure 3A and 3B. MA234.1 was transformed with pFC332_NRRL3_ NRRL3_06010-sgRNA and a 2142bp linear DNA repair fragment (amplified from genomic DNA of TLF54, with primers OTL485 and OTL486 (Primer Table). Sequencing of the NRRL3_06010 locus in transformants revealed the successful integration of the linear repair DNA fragment (data not shown), yielding strain AG3 with the NRRL3_06010 mutant allele SNPs at the +2 and +7 intronic position (Table 1).

The SNP located in NRRL3_05482 mutant allele did not provide a favorable target site for sgRNA design. Instead, a target that lies 317 bp downstream was used to create plasmid pFC332_ NRRL3_05482-sgRNA. To omit recognition of the NRRL3_05482-sgRNA-Cas9 ribonucleoprotein (RNP) complex of the linear DNA repair fragment obtained from NRRL3_05482 mutant allele, we introduced a silent mutation (AC<u>G</u> --> AC<u>A</u>, Thr) in the target site at the 10th nucleotide upstream from the PAM site (5' – TGG – 3'). This was achieved by *in situ* single mismatch PCR, creating two flanks that were subsequently fused by fusion PCR. A schematic overview of this approach is displayed in Supplementary figure 3C. Using the genomic DNA of TLF54, we used primers to introduce a G to A transition using primers listed in Primer Table. The combined flanks yield a 2499bp linear DNA repair fragment from NRRL3_05482 mutant allele with an additional SNP in Thr^{318} (ACG to ACA: NRRL3_05482$^{Thr318(ACA)}$) at the target site of NRR3_05482-sgRNA, and was sequenced to confirm this addition (data not shown). MA234.1 was transformed with pFC332_

NRRL3_05482-sgRNA and repair DNA fragment NRRL3_05482$^{Thr318(ACA)}$. Transformants were confirmed using sequencing (data not shown), yielding strain AG1.

Equally aged spore stocks of strains RD15.8, RD15.8#16, AG1 and AG3 were harvested, counted and diluted for a SDS sensitivity spot assay. On MM, it is evident that RD15.8 and AG1 show a similar growth phenotype, whereas AG3 displays the same compact colony phenotype as RD15.8#16 (Figure 5). Moreover, AG3, harboring the mutant allele of NRRL3_06010, also shows sensitivity towards SDS as seen for RD15.8#16 across a range of SDS concentrations, whereas AG1 showed wild type like sensitivity. In addition, measured glucosamine content from isolated cell walls were found to be identically increased for both RD15.8#16 and AG3 over RD15.8 (data not shown). Interestingly, NRRL3_06010 encodes a homolog of the previously identified *Aspergillus nidulans gdiA* (AN5895), a Rab GDI dissociation inhibitor (Abenza et al., 2010; MacKenzie et al., 2005).

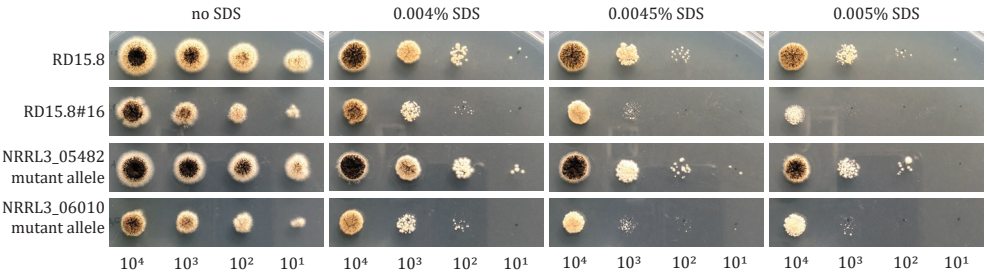

Figure 5. Phenotypes of RD15.8, RD15.8#16, NRRL3_05482 mutant allele (AG1) and NRRL3_06010 mutant allele (AG3). Colony morphology and SDS sensitivity (0.004%, 0.0045% and 0.005%) on Minimal Medium (MM) grown at 30°C for 72h. Spore amounts (#) per spot from left to right are 10^4, 10^3, 10^2 or 10^1, and are listed below the figure. Strains were incubated 96h at 30°C.

3.6 Analysis of *gdiA* mRNA from RD15.8#16 reveals both inefficient and alternative splicing

SNPs in the *gdiA* mutant allele of RD15.8#16 are intronic, showing two SNPs near the 5'donor splice site of intron 2. To assess effects of these mutations on splicing of *gdiA* pre-mRNA (SNPs at the +2 and +7 position, G/GTAGGGA to G/GGAGGGG of the second intron) in RD15#8#16, RNA was isolated from shake flask cultures of both RD15.8 and RD15.8#16 and cDNA was generated using RT-PCR as described in section 2.9. The cDNA of *gdiA* was amplified using PCR (Primer Table) and revealed PCR products for both RD15.8 and RD15.8#16 (data not shown). Next, the purified PCR products were cloned into a pJET1.2/blunt vector. Fourteen clones of RD15.8#16 and of two clones of RD15.8 *gdiA* mRNA (as control) were sequenced using primer 6010_P12r (Primer Table). The two cDNA clones from RD15.8 both carried the fully processed cDNA (https://gb.fungalgenomics.ca/portal/view/geneModelView.php?fullName=NRRL3_06010). Visualization of splicing in wild type and mutant *gdiA* is schematically shown in Figure 6A. For the *gdiA* mutant allele, four different transcripts are observed (Figure 6B). Out of fourteen individual cDNA clones of RD15.8#16, we found that nine carried an un-spliced intron 2, which would result in a premature STOP codon (TGA) located in intron 2, truncating translation of GdiA at 38AA. We also found three instances in which intron 2 was successfully spliced, leading to wild type transcripts. Additionally, two cases of alternative splicing were observed: exon 2 skipping (exon

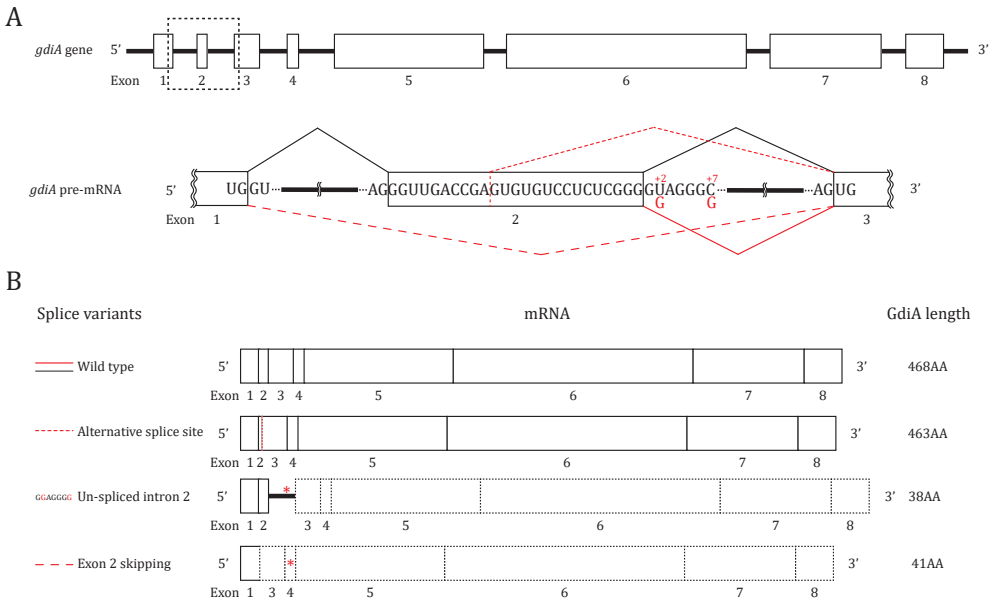

Figure 6. Schematic representation of the *gdiA* gene and the splicing events. (A) The *gdiA* gene consists of 8 exons and 7 introns. Black dashed lines show the region where splicing of *gdiA* pre-mRNA introns 1 and 2 is affected for RD15.8#16 compared to wild type. RD15.8#16 SNPs in *gdiA* of intron 2 at the +2 and +7 position are shown in red. Connecting lines between exons are either shown in black for wild type splicing or red for RD15.8#16 splicing. For RD15.8#16, the solid red line indicates wild type splicing of intron 2, densely interspaced red dashed line represents intron 2 splicing from alternative splice site inside exon 2, and widely interspaced red dashed lines indicate exon 2 skipping. (B) Visualization of resultant mRNA splice variations that have been recorded for both wild type and RD15.8#16 *gdiA* alleles and their corresponding protein length. Red asterisk represents a premature stop-codon. Black dashed line indicates out of frame transcript.

1 joining exon 3) and an alternative splice site in exon 2. Exon 2 (25nt) skipping results in a frameshift that leads to a premature STOP codon (TGA), truncating the protein during translation after 41AA. Interestingly, the alternative splice site found inside exon 2 (GA/GTGTGTCC) results in an in-frame splicing event. This splice variant effectively deletes 5AA (CVLSG) from the 3' end of exon 2, due an alternative splice site upstream from the wild type exon/intron border. Moreover, because of a new exon 2 boundary, the linkage between exon 2 and exon 3 subsequently yields a single nucleotide change that translates in an E19D substitution.

4. DISCUSSION

This work describes the characterization cell wall chitin mutant RD15.8#16 that was obtained from a previously reported cell wall stress mutant library (Damveld et al., 2008). Disturbance of cell wall integrity has been reported to induce cell wall chitin deposition in filamentous fungi (Fortwendel et al., 2010; Heilmann et al., 2013; Ram et al., 2004; Walker et al., 2015, 2008), and was exploited for a screen to identify high chitin producing strains. RD15.8#16 produces 60% more cell wall chitin than wild type *A. niger* and, in addition, displays sensitivity to SDS which is known to disturb the cell wall at low concentrations (De Groot et al., 2001; de Nobel et al.,

2000; Delley and Hall, 1999). These phenotypes, along with a compact colony morphology, were used in a classical genetics approach by employing co-segregation analysis to identify causative mutations.

For co-segregation analysis, a diploid was obtained from a wild type derivative JN6.2 (*Δ*nicB::*AOpyrG*, *ΔolvA::hygB*) and mutant TLF54 (a *pyrG*- and *ΔbrnA* derivative of RD15.8#16) in a parasexual cross to mix wild type and mutant chromosomes, followed by subsequent segregation. Co-segregation of the mutant phenotype among the acquired segregants was scored using sensitivity to SDS. Prior to this, we confirmed similar SDS sensitivity of both TLF54 and JN6.2 compared to their respective prototrophic counterparts, RD15.8#16 and RD15.8. Initial observations on auxotrophic marker segregation suggested equal co-segregation of chromosomes from wild type and mutant, however, unequal segregation of the RD15.8#16 phenotype was observed, resulting in only 2 SDS sensitive segregants from 200 segregants (*ΔbrnA*#53 and *ΔbrnA*#90). Low frequency of mutant phenotype segregation could not be explained by benomyl sensitivity for haploid parents, as RD15.8#16 was affected similarly to benomyl as JN6.2 (Supplementary figure 1). Though, certain mutant SNP(s) can be unfavorable during diploid to haploid segregation, either related or unrelated to the SDS sensitivity phenotype. In extension of this observation, we wanted to ensure that there was no disconnect between cell wall chitin and SDS sensitivity for these segregants. This was done by comparing glucosamine content of parental strains JN6.2 and TLF54 with *ΔbrnA*#53, *ΔbrnA*#90 and two randomly picked non-SDS sensitive segregants *ΔolvA*#27 and *ΔolvA*#41 (Figure 3B). Results showed that the plate phenotypes (SDS sensitivity and colony morphology) are linked to increased cell wall glucosamine content. SNP co-segregation analysis revealed inherited SNPs from either wild type or mutant in both SDS sensitive and non-SDS sensitive segregants. We were able to identify that ORF-located SNPs recur randomly across segregants, with the exception of SNPs on chromosome IV (Figure 4), only found in segregants *ΔbrnA*#53 and *ΔbrnA*#90.

Chromosome IV located mutant SNPs lay within NRRL3_05482 (Yeast *PEP7* ortholog, putative fungal transcription factor) and NRRL3_06010, now identified as *gdiA* (Rab GDP dissociation inhibitor) based on homology with *A. nidulans gdiA* (Abenza et al., 2010). Attempts to create single knockouts of both genes was unsuccessful and suggests them to be essential for growth. In congruence with yeast literature, the ortholog of *gdiA* (*GDI1*) is a known essential gene (Garrett et al., 1994), whereas *PEP7* was previously described as a nonessential gene (Webb et al., 1997). As clean knockout strains could not be obtained, we re-recreated SNPs found in both NRRL3_05482 and *gdiA* for RD15.8#16 in a wild type background, in order to study their phenotypic effects. Re-creation of SNPs in NRRL3_05482 and *gdiA* through CRISPR/Cas9 gene editing resulted in viable mutants AG1 and AG3, respectively. Interestingly, only AG3 showed the same level of SDS sensitivity as RD15.8#16, suggesting that the SNPs in the *gdiA* mutant allele at the conserved 5' splice site (+2 and +7position, G/GTAGGGA to G/GGAGGGG) of the second intron, facilitates both the SDS and cell wall chitin phenotype. The data also indicates that the SNP in the NRRL3_05482 mutant allele co-segregated with the *gdiA* mutant allele as a result of chromosome IV linkage, but is not causative for the RD15.8#16 phenotype.

The T to G SNP in the *gdiA* mutant allele causes a mutated 5' donor splice site. The canonical donor-acceptor splice site pair in fungal introns is 5' GU-AG 3' (Kupfer et al., 2004). In addition, non-canonical splice sites are observed sporadically being either 5' GC-AG 3' or 5' AU-AC 3', the former of which represents approximately 90% of non-canonical type splice sites (Burset et al., 2000). This non-canonical splice site was reported to represent 1.2% of all introns in *Neurospora crassa* with similar ratios for filamentous fungi *Fusarium oxysporum* and *Aspergillus nidulans* (Rep et al., 2006). The 5' GG-AG 3' type splice sites in intron 2 of the *gdiA* mutant allele is different from either of these canonical or non-canonical splice sites. Specifically, a G at second position of the 5' donor splice site (G/GG) has previously been shown to result in failure of proper lariat formation for correct transcript processing (Aebi et al., 1987). However, here we show that the 5' donor splice site in the *gdiA* mutant allele can result in correct pre-mRNA processing. However, failure of intron 2 splice site recognition was more frequently observed. Interestingly, we also found two cases of alternative splicing: exon skipping and an alternative splice site. The latter variant results in a full-length protein that combines a five amino acids deletion with a single amino acid substitution of glutamic acid to aspartic acid. For now, it remains unknown whether this mRNA yields a functional protein and whether other splice variants may exist. Nevertheless, we have found wild type mRNA transcripts for *gdiA*—that are derivative of the mutant allele, suggesting that RD15.8#16 still produces intact, albeit less GdiA. These findings comply with the fact that total loss of *gdiA* mRNA is lethal.

Rab *gdiA* encodes a GDP-dissociation inhibitor that functions as a regulator in Rab GTPase cycling. Known orthologs are conserved and have been reported as essential genes in both yeast and *Drosophila* (Garrett et al., 1994; Ricard et al., 2001). Rab (*ras* from rat brain (Touchot et al., 1987)) GTPases are involved in regulation of intracellular vesicular transport, continuously cycling between and active GTP-bound, and inactive GDP-bound form (Pfeffer, 1992). In the active GTP-bound form, a GTPase is able to interact with downstream effector proteins, assist in cargo selection, transport vesicles, form vesicles from membranes and assist fusion of vesicles with the target membranes (Oesterlin et al., 2014). Once an active GTPase has performed a downstream trafficking cycle at a specific target site, it is subsequently hydrolyzed to a GDP-form. Here, Rab GDIs can solubilize GDP-bound GTPases from membranes into the cytosol prior to re-deposition at new target membranes. Solubilization by GDIs also prevents turnover of GDP to GTP by GEFs, helping to keep an intracellular steady-state balance of active/inactive GTPases (Pfeffer and Aivazian, 2004; Ullrich et al., 1993). Due to the essential role of GdiA in this balancing act, we propose that a reduction in available GdiA—resultant from inefficient pre-mRNA processing—causes a cytosolic imbalance of soluble GTPases.

Obviously, the essential role that GDP dissociation inhibitors have in cellular processes make them difficult to study their function. In *A. niger*, *gdiA* was reported to be repressed by the during exposure of dithiothreitol (DTT), known to disturb cellular redox homeostasis and trigger the unfolded protein response (MacKenzie et al., 2005). In yeast, a conditional mutant *sec19-1* (allelic to *GDI1*) has been studied and has helped to understand its biological function (Garrett

et al., 1994). Resultant phenotypes include accumulation of ER, Golgi and secretory vesicles as well as defects in protein transport and loss of soluble Rab GTPase Sec4p. Although no cell wall phenotypes have been described for the *sec19-1* mutant directly, a conditional mutant of *SEC4* (*sec4-8*), showed random budding patterning, suggesting loss of secretion polarity, an enlarged bud neck and displayed abnormal chitin deposition (Finger and Novick, 1997). Sec4p is an essential protein required for vesicle-mediated exocytic secretion and autophagy (Guo et al., 1999), and relies on the ability to continuously cycle between GTP and GDP, rather than absolute levels of GTP-bound form for proper function (Novick et al., 1993). Unsuccessful release of GDP-bound Sec4p from target membranes as a result of loss or depletion of *GDI1* depletes the soluble pool required for re-activation and re-positioning on new target membranes, rendering Sec4p dysfunctional. Consequentially, putative GDP to GTP exchange of old, *in situ* membrane-bound Sec4p may misallocate protein trafficking, including putative cell wall chitin biosynthesis enzymes. Despite Sec4p and *GDI1* involvement in vesicle trafficking, to the best of our knowledge no reports have investigated its role in cell wall biosynthesis or the cell wall integrity pathway.

In *A. niger*, the closest homolog of Sec4p is secretion related GTPase A (*srgA*, 58% protein identity) and, unlike in yeast, was found to be a non-essential gene (Punt et al., 2001). The *srgA* gene was unable to complement a *sec4* mutant, suggesting the presence of an additional SEC4 homolog or that SEC4 in yeast governs more vesicle sorting processes than in *A. niger*. Overall *srgA* may be related to a more complex multicellular growth behavior (Punt et al., 2001). Interestingly, a deletion of *srgA* resulted in changes of colonial and peripheral hyphae morphology, similar to RD15.8#16. The compact colony morphology caused by the mutant allele of *gdiA* in RD15.8#16 may be indirectly related to a regulatory imbalance caused by less GdiA, possibly affecting SrgA cycling. Whether or not there is a relation between *srgA* and *gdiA*, we observe an effect of the *gdiA* mutant allele on cell wall chitin deposition. The fact that *A. niger* only contains a single genomic copy of a Rab GDI we conclude that less available GdiA as observed in RD15.8#16 affects the Rab GTPase-mediated vesicle trafficking. Consequently, disturbance of these regulatory elements in Rab GTPase cycling most likely causes multiple pleiotropic effects, among which is cell wall chitin biosynthesis.

5. CONCLUSIONS

RD15.8#16 was initially isolated in a screen for strains with a continuous state of cell wall stress and, upon further analysis, was found to have increased chitin levels and an increased sensitivity to SDS. Using classical genetics combined with co-segregation analysis and CRISPR/Cas9 gene editing, we showed the involvement of two intronic mutations in *gdiA* that give rise to this phenotype. It was found that a full gene disruption of *gdiA* was lethal, and that the observed mutations in the *gdiA* mutant allele affect intron splicing resulting in reduced levels of functional *gdiA* transcript. Therefore, we propose that reduced levels of GdiA affect the balance of Rab GTPase cycling. As such, this either influences cell wall chitin deposition directly through increased

(ectopic) secretion or indirectly, by general misconstruction (and recycling) of fungal cell wall components that triggers the CWI pathway with a compensatory chitin deposition response. Both hypotheses are not mutually exclusive, but are in congruence with an asymmetrical distribution in GTPase cycling. To address the issue in more detail, the reported *gdiA* mutant allele may provide a valuable candidate to study the role of GdiA in secretion-related processes of *A. niger* and other filamentous fungi.

Acknowledgements

We would like to thank Prof. Dr. Bruno M. Moerschbacher for the coordination of the FunChi project.

Funding

This work is part of the "FunChi" ERA-IB project with project number ERA-IB-15-080, which is (partly) financed by the Dutch Research Council (NWO).

Availability of data and materials

The DNA reads described in this study will be deposited in the short read archive upon request. All other data are available on request by contacting the corresponding author.

SUPPLEMENTARY TABLES

Supplementary tables to this article can be found online at https:// doi: 10.1016/j.fgb.2019.103319

Primer Table. All primers used during this study.

Supplementary table 1. All *ΔolvA#* and *ΔbrnA#* segregants scored for *pyrG*$^{+/-}$, *nicB*$^{+/-}$ and *amdS*$^{+/-}$ selection marker inheritance.

Supplementary table 2. All 53 SNPs found for TLF54 (VARIANT 004, Mutant) compared to RD15.8 (VARIANT 003, Parent). Frequency cut-off of mutant was performed as described in section 2.5.

SUPPLEMENTARY DOCUMENTS

Supplementary document 1. Detailed protocol for cell wall isolation and total glucosamine determination.

Cell wall hydrolysis and chitin analysis

Cell walls of fungal strains were carefully weighed on a fine balance (d = ±0.1 mg) to be exactly 1.0 mg in a 2 mL Eppendorf tube. Tubes were supplied with a lid cap to secure a closed lid, and were wrapped with PARAFILM® M (Sigma Aldrich). Hydrolysis was performed in triplicate per biological replicate with 1 mL 6M HCl for 4h at 110°C, using a pressure cooker. After cooling down, PARAFILM® M and lid caps were removed and HCl was evaporated at RT for 64h, using an airstream with a Sample Concentrator (Techne Ltd, Cambridge, UK) in the fume hood. To

measure total glucosamine in samples, a Glucosamine HCl standard was included, performed in triplicate*: using a 10 mg/mL stock dilutions of 2000 µg/ml, 1500 µg/ml, 1000 µg/ml, 500 µg/ml, 250 µg/ml, 100 µg/ml, 50 µg/ml and 0 µg/ml (in triplicates) were made. Dried, hydrolyzed cell walls were rehydrated in 500 µL MQ (2 mg/mL cell wall) and incubated for 1h at 37°C, 1,000 rpm, simultaneously with standards. Post-incubation, 20 µL sample (40 µg cell wall hydrolysate) and freshly prepared standards (40, 30, 20, 10, 5, 2, 1 and 0 µg glucosamine) were taken in triplicate and added to freshly prepared 20 µL 1.5N Na_2CO_3 in 4% acetylacetone** in PCR tubes (250 µL), followed by 20 min. incubation at 100°C. Next, 140 µL 96% EtOH was added to cooled down samples and standards. In the fume hood, 20 µL 4-dimethylaminobenzoaldehyde solution (0.64g 4-dimethylaminobenzoaldehyde in 12 ml 96% EtOH and 12 ml concentrated HCl**) was added to samples and standards which colors the solution pink. To allow the reaction to reach optimal coloring intensity, samples and standards were incubated 1h prior to transferring 100 µL solution to a 96-well plate, and OD520 was measured in a plate reader. Standard curve samples range from OD520 = 0 (set intercept) to OD520 = 1 for the highest concentration (2000 µg/mL, i.e. 40 µg glucosamine). Plotting a linear standard curve, total glucosamine content in each sample was inferred.

*NOTE: 6M HCl hydrolysis liberates chitin from the cell wall, but also removes acetyl groups. Essentially, this protocol looks at total glucosamine instead of just free N-acetylglucosamine monomers (no differentiation between chitin and chitosan). Glucosamine monomers can be reactive with surfaces and undergo reactions with other chemicals that may skew the colorimetric read-out. Therefore, it is important to create fresh stocks of glucosamine standards, and that both standards and dissolved cell walls are incubated for an equal amount of time under the same conditions.

** NOTE: It is of very high importance to create fresh solutions every single time this experiment if performed for the sake of reproducibility. Na_2CO_3 (1.5N) in 4% acetylacetone tends to discolor quickly over the course of a couple of days and alters the outcome of the read-out. The degrading effect of 4-dimethylaminobenzoaldehyde in concentrated HCl and EtOH is not completely clear. However, to avoid variation between experiments creating fresh, small volumes of both solutions every single time ensures good reproducibility. This is based on personal experience and that was reflected in standard curves.

SUPPLEMENTARY FIGURES

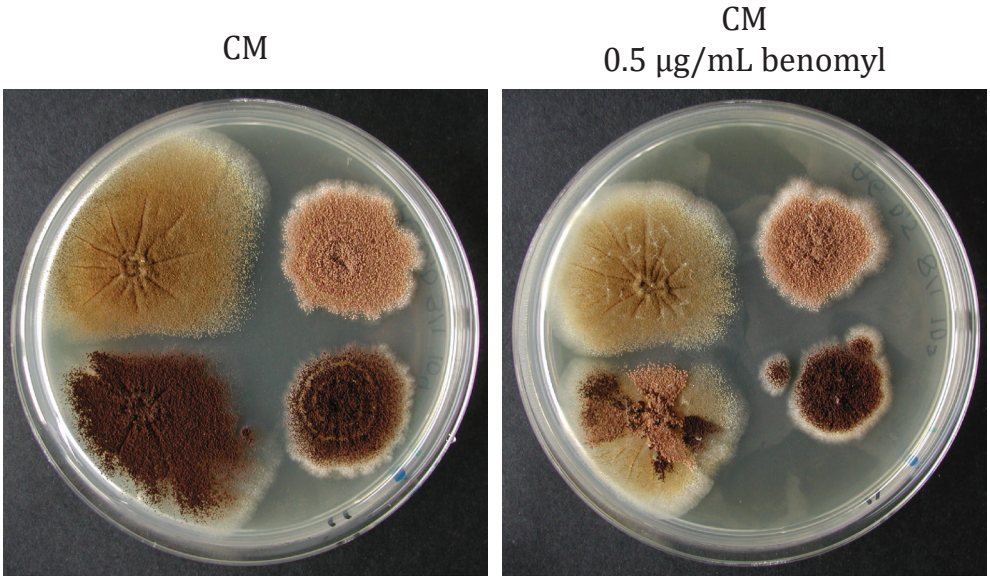

Supplementary figure 1. Growth on CM and CM with benomyl. From left to right, top to bottom: JN6.2, TLF54, TLF92 diploid and RD15.8#16 on CM and 0.5 µg/mL benomyl. Note segregation of diploid phenotype into brown and olive colored sectors.

A

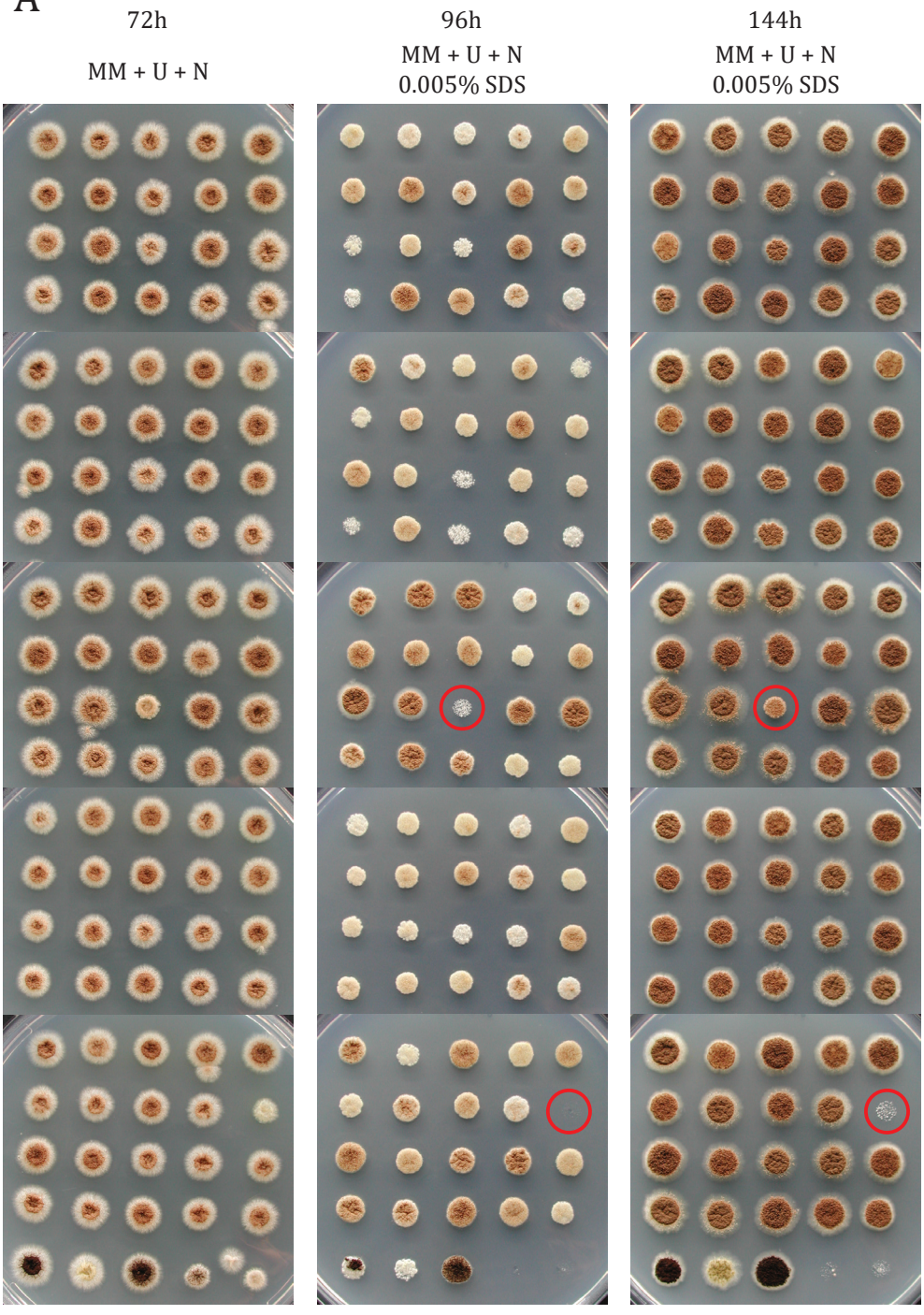

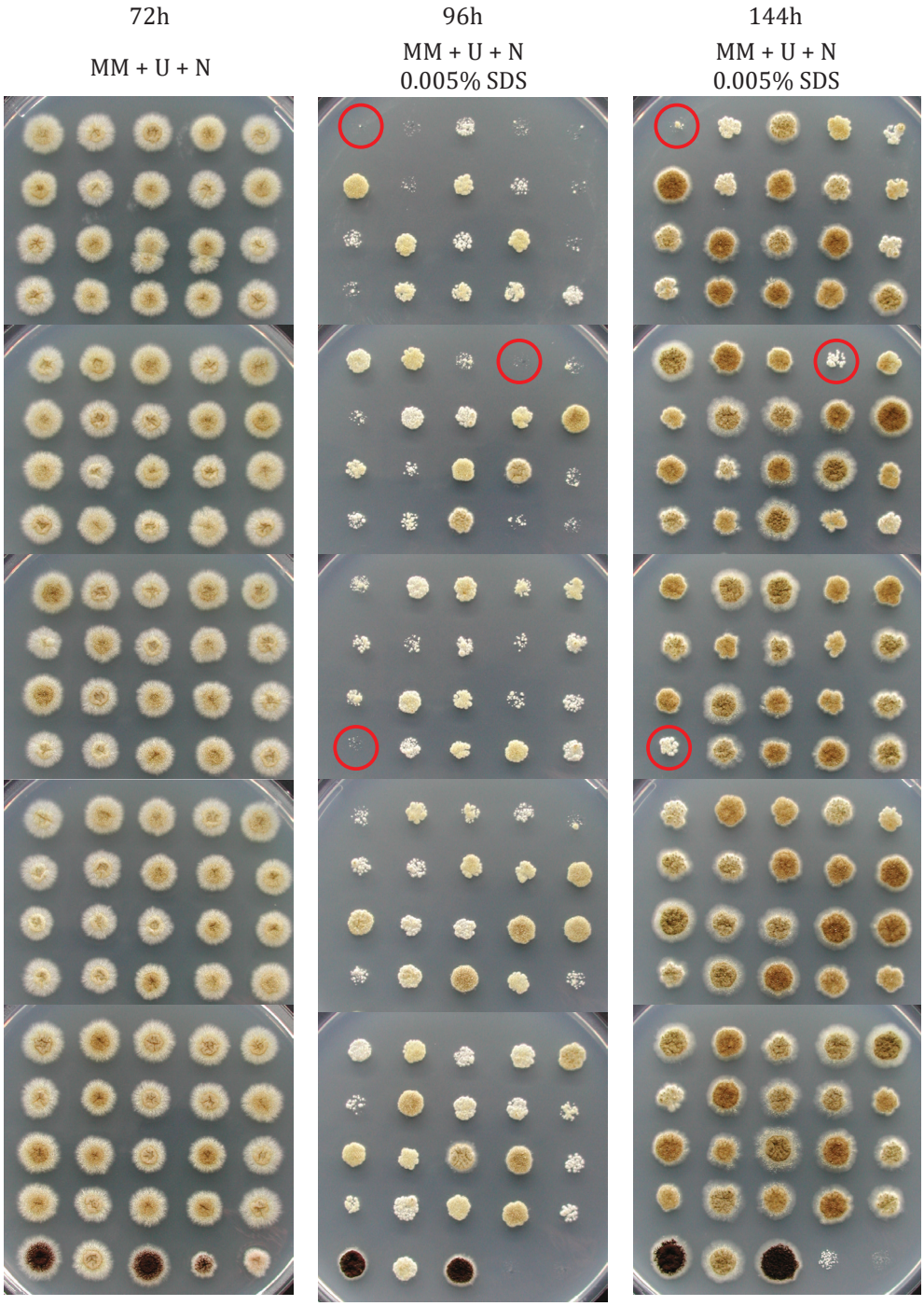
72h
MM + U + N
96h
MM + U + N
0.005% SDS
144h
MM + U + N
0.005% SDS

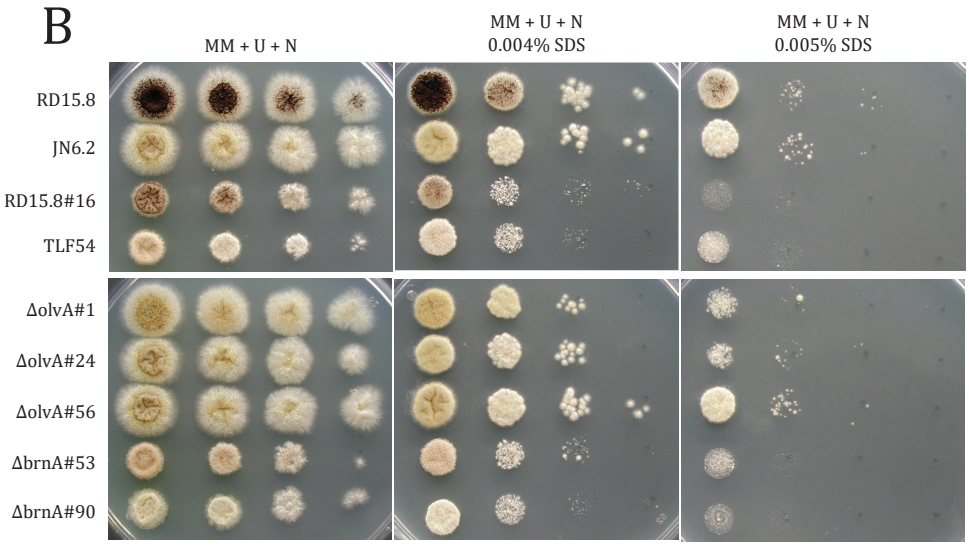

Supplementary figure 2. Screen of 200 segregants and control strains with un-normalized spore concentrations. All plates contain Minimal Medium (MM) with 10mM uridine (U) and 2.5 µg/mL nicotinamide (N) + 0.005% SDS. (A) A total of 200 segregants and controls were spotted (5 µL) with controls at the bottom (from left to right on bottom of each plate: (N402, JN6.2, RD15.8, RD15.8#16 and TLF54). Segregant IDs are brnA#1-100, followed by olvA#1-100 from left to right, top to bottom. Red encircled spore spots resemble putative candidates that exhibit SDS sensitivity. (B) Putative SDS sensitive candidates on a normalized spore SDS spot assay. Plates were incubated for 72h at 30°C.

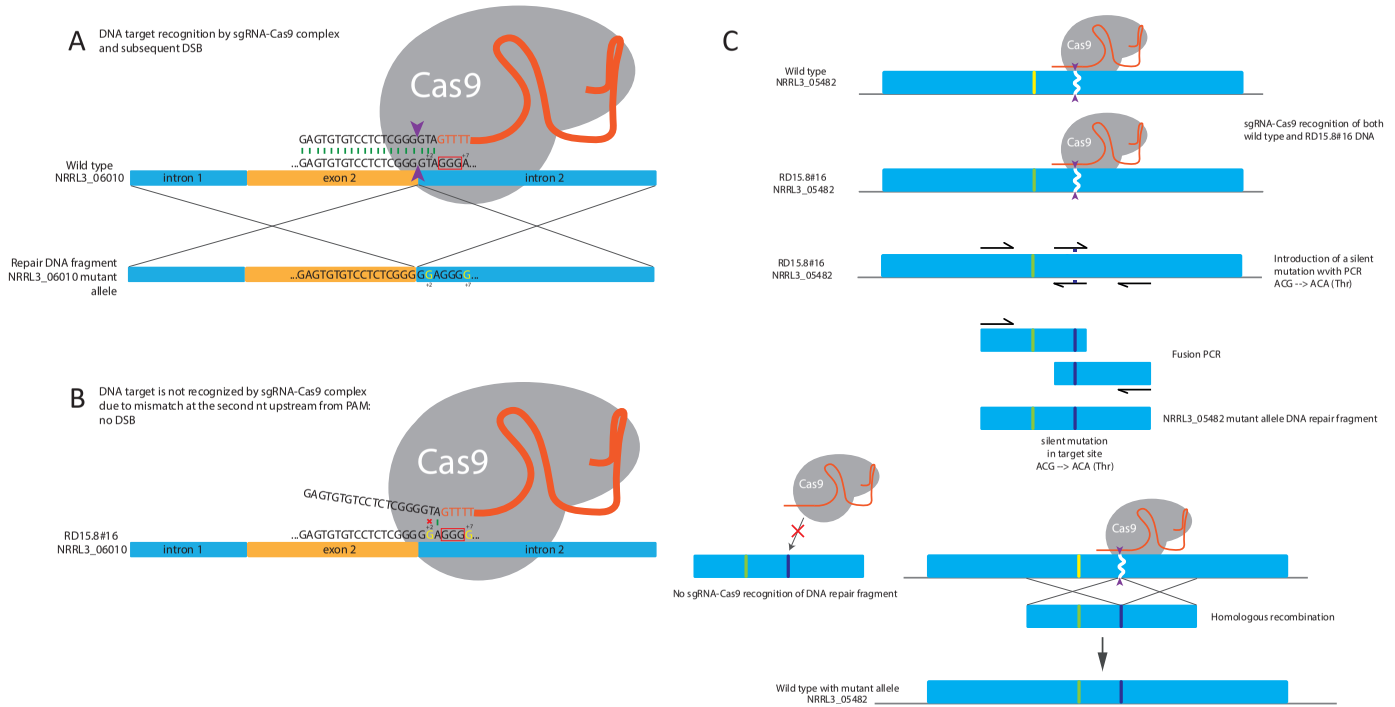

Supplementary figure 3. CRISPR/Cas9 design for targeting of NRRL3_06010 and NRRL3_05482 to re-create SNPs in a wild type background. (A) NRRL3_NRRL3_06010-sgRNA-Cas9 ribonucleoprotein (RNP) complex binds the genomic DNA of the wild type strain, creating a DSB in *gdiA*. PAM site is highlighted by a red box (GGG). Green bars represent matching of bp between the sgRNA target and genomic sequence. Purple arrows indicate the site of the double stranded break (DSB). Repair DNA fragment contains the two point mutations found in RD15.8#16 and are shown in yellow. (B) The mutant allele NRRL3_06010 sequence from RD15.8#16 shows a mismatch at the second nucleotide (nt) upstream from the PAM site, displayed by a red cross, preventing the NRRL3_*gdiA*-sgRNA-Cas9 RNP complex to bind and create a DSB. (C) NRRL3_05482-sgRNA-Cas9 RNP complex targets a region outside of the NRRL3_05482 SNP location. SNPs are shown as either yellow (wild type) or green (RD15.8#16). To prevent recognition and cutting of the DNA repair fragment a silent mutation (ACG --> ACA (Thr)) is introduced at the target site of NRRL3_05482-sgRNA, with fusion PCR. The NRRL3_05482-sgRNA RNP complex creates an in vivo DSB at the wild type locus, but not at the presented DNA repair fragment, allowing repair of the DSB through homologous recombination.

CHAPTER 6

Deletion of the *Aspergillus niger* pro-protein processing protease gene *kexB* results in a pH-dependent morphological transition during submerged cultivations and increases cell wall chitin content

Tim M. van Leeuwe, Mark Arentshorst, Gabriel Forn-Cuní, Nicholas Geoffrion, Adrian Tsang, Frank Delvigne, Annemarie H. Meijer, Arthur F.J. Ram, Peter J. Punt

ABSTRACT

There is a growing interest for the use of post-fermentation mycelial waste to obtain cell wall chitin as an added-value product. In the pursuit to identify suitable production strains that can be used for post-fermentation cell wall harvesting, we turned to an *Aspergillus niger* strain in which the *kexB* gene was deleted. Previous work has shown that deletion of *kexB* causes hyper-branching and thicker cell walls, traits that may be beneficial for reduction of fermentation viscosity and lysis. Hyper-branching of *ΔkexB* was previously found to be pH-dependent on solid medium at pH 6.0, but was absent at pH 5.0. This phenotype was reported to be less pronounced during submerged growth. Here, we show a series of controlled batch cultivations at a pH range of 5, 5.5, and 6 to examine the pellet phenotype of *ΔkexB* in liquid medium. Morphological analysis showed that *ΔkexB* formed wild type-like pellets at pH 5.0 whereas the hyper-branching *ΔkexB* phenotype was found at pH 6.0. Transition of phenotypic plasticity was found in cultivations at pH 5.5, seen as an intermediate phenotype. Analyzing the cell walls of *ΔkexB* from these controlled pH-conditions showed an increase in chitin content compared to wild type across all three pH values. Surprisingly, the increase in chitin content was found to be irrespective of the hyper-branching morphology. Evidence for alterations in cell wall make-up are corroborated by transcriptional analysis that showed a significant cell wall stress response in addition to upregulation of genes encoding other unrelated cell wall biosynthetic genes.

Manuscript submitted

1. INTRODUCTION

Filamentous fungi are industrially used to produce a range of products, from organic acids, antibiotics and other metabolites to enzymes and (heterologous) proteins. However, the industrial scale fermentation using filamentous fungi is typically limited by limited oxygen supply due to the high viscosity of the fermentation broth at high mycelial growth densities. These conditions impair homogeneous mixing, are very energy demanding, and cause stress to the fungus due to the high amounts of hyphal shearing. Fluctuation in nutrient and oxygen levels caused by sub-optimal mixing within the large scale fermentation vessels can subsequently lead to additional metabolic stress and shifts, diminishing batch-to-batch consistency and product quality (Cai et al., 2014; Papagianni, 2004).

In addition to high viscosity problems, intensive use of filamentous fungi as cell factories at an industrial scale produces large amounts of spent mycelium left over as a by-product. Spent mycelium has been suggested to be a source of chitin and chitosan products by extracting this from the fungal cell wall to be used for many applications in medicine and agriculture (Dhillon et al., 2012; Naveed et al., 2019; Orzali et al., 2017). To both outcompete the current supply of chitin from crustacean shell waste and to make chitin yields a profitable option, optimization of extraction and high chitin levels are required (Cai et al., 2006; Dhillon et al., 2012). Efforts have been made do so by genetic modification of the chitin biosynthetic pathway or through alterations of fermentation conditions (Deng et al., 2005; Hammer and Carr, 2006; Ja'afaru, 2013; Nwe and Stevens, 2004). Additionally, we recently reported on the identification of two *Aspergillus niger* UV-mutants that showed increased cell wall chitin (van Leeuwe et al., 2020b, 2020a). These efforts contribute to explore the use of spent mycelium as an added-value product rather than waste output.

In the endeavor to address both the issue of fermentation (mycelial) viscosity and increase chitin production, we turned to an *A. niger kexB* deletion strain that is already known for impaired pro-protein processing. A deletion of *kexB* has already been shown to be beneficial for secretion of fusion proteins consisting of a well secreted carrier and proteolytically sensitive proteins (Punt et al., 2003). In *A. niger*, *kexB* (also named *pclA* in literature) was shown to be implicated in the processing of dibasic cleavage sites of secretory proteins (Jalving et al., 2000, Punt et al., 2003). The *A. niger* KexB protein is the homologue of *Saccharomyces cerevisiae* Kex2p, a Ca^{2+}-dependent serine protease that is responsible for processing dibasic Lys-Arg or Arg-Arg cleavage sites for maturation of secreted proteins (Fuller et al., 1989). Designated proteins that pass through the secretory pathway are processed in the Golgi apparatus where kexin proteins reside due to their Golgi-retention signal (Bryant and Stevens, 1997; Wilcox and Fuller, 1991). These Kex enzymes are important in ascomycete alpha-pheromone processing (Le Marquer et al., 2019; Martin et al., 2011), first discovered in yeast, where 2 to 4 copies are the alpha-pheromone are processed into peptides by *kex2* (Achstetter, 1989; Leibowitz and Wickner, 1976; Wagner and Wolf, 1987). Additionally, Kex2 was shown to be important in subsequent steps of mating during cell fusion

(Heiman et al., 2007). Furthermore, in filamentous fungi, KexB is implicated in the processing of cyclic and modified peptides (Ding et al., 2016; Nagano et al., 2016). Previous reports have also shown that the *A. niger ΔkexB* strain displayed shorter, visibly thicker hyphae and a hyper-branching morphology (Jalving et al., 2000; Punt et al., 2003; te Biesebeke et al., 2005). Shorter hyphae and smaller pellets are ideal traits in order to reduce stirring viscosity in fermenter conditions, but the actual performance of this strain under fermentation conditions has not been fully explored. Also, cell wall compositional assessments have never been performed in any *kexB* mutant strain in *A. niger*. Besides the above-mentioned processing targets of yeast and fungal kexins, many more putatively kexin-processed proteins can be found in fungal proteomes and inferred from the corresponding genomes.

A knockout of *KEX2* in *Candida albicans* resulted in reduced virulence with an acclaimed 147 putatively predicted proteins that were identified as potential Kex2p targets that relate to cell wall construction and modification, including hydrolases, adhesins, cell wall components, and outer membrane proteins (Newport et al., 2003). Previous work in *A. oryzae* has also shown that deletion of *kexB* affects cell wall synthesis and activation of the CWI pathway by MAPK phosphorylation assays (Mizutani et al., 2016, 2004; te Biesebeke et al., 2005). Using Prediction algorithms such as ProP (v.1.0b ProPeptide Cleavage Site Prediction), a plethora of putative KexB targets can be identified which are only indicative for potential targets and lack biological interpretation of any relation to the observed pleiotropic effects, such as shorter hyphae and a hyperbranching phenotype. Interestingly, this growth phenotype has clearly been shown on plates at pH 6.0, but not at pH 5.0, suggesting a pH-dependent phenotype (Jalving, 2005), but a detailed study how the *ΔkexB* strain behaves during submerged growth is lacking. Here, we investigated the role of KexB on hyphal morphology in pH-controlled batch cultivations. In doing so, we aimed to investigate the impact of deleting *kexB* in *A. niger* on the cell wall composition with respect to its shorter and thicker hyphae.

2. MATERIALS AND METHODS

2.1 Strains, media, growth conditions

Strains used in this study can be found in Table 1. All media were prepared as described by Arentshorst et al., 2012. In all cases, minimal medium (MM) contained 1% (w/v) glucose, 1.5% agar (Scharlau, Barcelona, Spain) and was not supplemented unless otherwise specified. Complete medium (CM) contained 0.1% (w/v) casamino acids and 0.5% (w/v) yeast extract in addition to MM. Strains were inoculated from -80°C glycerol stocks onto fresh CM plates and were allowed to grow and sporulate for 5-7 days at 30°C, prior to spore harvesting. Spores were harvested by addition of 15 mL of 0.9% (w/v) NaCl to CM spore plates and were carefully scraped from the surface with a cotton swab. In case of harvesting spore plates for bioreactor cultivations, 0.05% Tween-80 was added to the 0.9% (w/v) NaCl to prevent spore clumping. Spore solutions were poured over sterile cotton filters (Amplitude™ Ecocloth™ Wipes, Contec Inc., Spartanburg,

SC, USA) to remove large mycelial debris. Spore solutions were counted using Bio-Rad TC20™ Automated Cell Counter (Bio-Rad Laboratories, Inc. USA) using Counting Slides, Dual Chamber for Cell Counter (Cat#145-0011, Bio-Rad Laboratories, Inc. USA).

Table 1. All strains used in this study

Name	Genotype	Reference
N402	cspA1	Bos et al., 1988
AB4.1*ΔpclA*	cspA1, *pyrG⁻, ΔkexB::AOpyrG*	Punt et al., 2003
MA234.1	cspA1, *ΔkusA::DR-amdS-DR*	Park et al., 2016
TLF39	cspA1, *ΔkusA::DR-amdS-DR, ΔcrhA-G*	van Leeuwe et al., 2019
TLF69	cspA1, *ΔkusA::DR-amdS-DR, ΔcrhA-G, ΔkexB::hygB*	This study

2.2 Bioreactor cultivation

Controlled batch cultivations for *A. niger* strains N402 and the *ΔkexB* strain were performed in 6.6L BioFlo bioreactors (New Brunswick Scientific), as previously described (Jørgensen et al., 2010). A batch of 21 L MM containing 0.75% D-glucose was made by adding 1 L filter-sterilized (0.2 µm pore) glucose (15.75% w/v) solution to a freshly autoclaved volume of 20 L MM (no carbon source) as described above. Allowing 1 day of dissolving and a check for contamination, 5 L MM 0.75% glucose was added to each bioreactor directly after autoclaving. Temperature, acidity and stir speed were set to and kept at 30°C, pH 3 and 250 rpm, respectively. The pH was controlled by addition of titrants (2M NaOH and 1M HCl). Sparger aeration of 1 L/min was left on to allow oxygen saturation of the medium prior to inoculation. Next, aeration was set to headspace only and 1.5 mL 10% w/v Yeast Extract was added to the medium to promote homogeneous germination for the to-be-added spores. Subsequently, a total of $5x10^9$ (10^6 sp/mL) spores were added to the medium using a concentrated spore solution. Germination time of approximately 4-5h was maintained, preceding the addition of polypropylene glycol P2000 anti-foam agent, increasing agitation to 750 rpm and changing aeration from headspace to sparger only (1 L/min). Oxygen, base and acid consumption were monitored and samples were taken at regular intervals to obtain biomass, culture filtrate and microscopy samples. Biomass was harvested by applying a vacuum over Whatman™ Glass Microfiber Filter (GF/C™) (diameter 47 mm, CAT No.1822-047, Buckinghamshire, UK). Samples were all quickly frozen in liquid nitrogen prior to storage at -80°C. Biomass accumulation through time was gravimetrically determined by lyophilizing designated samples from the corresponding broth culture mass.

2.3 Biofilm cultivations

Biofilm cultivations were performed in a 4 stirred-tank mini-bioreactors platform (DASGIP DASbox Reactor SR0250ODLS, Eppendorf AG, Hamburg, Germany). For promoting biofilm formation, stirring device was completely removed in order to leave space to two sheets of stainless-steel 316L wire gauze. These metal sheets were used as support promoting biofilm growth. Each bioreactor was filled with 200 mL of MM and operated at 30°C. The pH level was maintained

at 5 or 6 depending on the experiment (controlled by the addition of NH_4OH or H_3PO_4) and the air flow rate was adjusted to 200 mL/min. Dissolved oxygen was measured using PSt1 optical sensors linked to an OXY-4 oxygen meter (Presens Precision Sensing, Regensburg, Germany). Each bioreactor was initially inoculated with spores in order to reach 10^6 sp/mL. At the end of the cultivation, metal sheets were removed from the bioreactor for estimating the biofilm wet (in this case, the sheets were left for 30 minutes in a beaker for removing excess of liquid before mass measurement) and dry (estimated after keeping the sheets at 105°C for 24 hours) weight.

2.4 Microscopy

Pellet morphology samples were taken at 100% biomass and visualized in a Zeiss Observer confocal laser-scanning microscope (Zeiss, Jena, Germany). Images were processed and analyzed using FIJI (ImageJ) software (Schindelin et al., 2012).

2.5 Cell wall isolation and chitin analysis

Cell wall samples were isolated as previously described (van Leeuwe et al., 2020b). In short, dried mycelium was frozen in liquid N_2 and were ground to break open the cells. Samples were washed to remove intracellular debris and proteins, three times with 1M NaCl and three times with MilliQ ultrapure water (MQ). Supernatant was carefully discarded prior to the next washing step. Cell wall samples were lyophilized after washing steps for 48h. Cell wall isolation, hydrolysis and chitin content analysis, measured as total glucosamine, have been performed as described previously (van Leeuwe et al., 2020b). Cell wall glucosamine measurements from independent replicate experiments are expressed as means ± SE.

2.6 RNA isolation and RNA-sequencing

RNA was isolated from mycelial biomass samples obtained from batch cultivated *A. niger* strains N402 and *ΔpclA* (*ΔkexB*), using TRIzol (Invitrogen). RNA was purified afterwards with NucleoSpin RNA Clean-up kit (Macherey-Nagel) with DNase treatment. Concentration and quality of the RNA was determined using a NanoDrop 2000 spectrophotometer (Thermo Scientific) and by gel-electrophoresis, respectively. RNA sample were sent to Genome Québec for sequencing using the HiSeq4000 technology. Sequencing data is available under GEO accession number GSE151618.

2.7 Transcriptomic analysis

Raw RNA-seq read sets were retrieved from the Génome Québec's Nanuq portal, and pre-processed with BBDuk from the BBTools package (https://sourceforge.net/projects/bbmap) to trim sequencing adapters and remove reads derived from PhiX and ribosomal RNA. The transcriptome of *A. niger* NRRL3 (v. 20140311) was retrieved from the *jgi* Genome portal (Aguilar-Pontes et al., 2018), and the raw reads were mapped to the transcriptome using Salmon v0.14.1 (Patro et al., 2017). The libraries were imported in RStudio 1.2.5001 (RStudio: Integrated Development for R. RStudio, Inc., Boston, 2016) running R 3.6.1 (R Development Core Team 3.6.1., 2019) using txtimport v.1.12.3 (Soneson et al., 2016). Differential gene expression was assessed

via pairwise comparisons using DESeq2 v1.24.0 (Love et al., 2014), using the design ~ mutation (*p*adj ≤ 0.05). Updated gene length data for the NRRL3 genome was retrieved from the *jgi* Genome portal. The full code is available at https://github.com/gabrifc/rnaseq_analysis_kexB.

2.8 Single gene knockouts of *kexB*

A deletion of *kexB* was introduced in the seven-fold *crh* knockout strain (TLF39) using a split marker approach. TLF39 (Table 1) was transformed after protoplastation as described previously (Arentshorst et al., 2012). Using the split marker approach for single gene knockouts, entire ORFs were deleted by replacement with the hygromycin B selection marker (Arentshorst et al., 2015). Flanks were generated via PCR using N402 genomic DNA as template and primers as described in Primer Table. *AOpyrG* fragments were obtained from plasmid pAN7-1 (Punt et al., 1987) with primers as described in Primer Table. Fusion PCR was used to generate split marker fragments containing *AOpyrG.* Approximately 2 µg of DNA per flank was added to protoplasts for transformation. Transformation plates were incubated on MMS for 6 days at 30°C. Transformed colonies were single streaked on MM twice for purification and were genotyped using diagnostic PCR (data not shown).

2.9 Cell wall sensitivity assays

Cell wall disturbing compounds Calcofluor White (CFW), Congo Red (CR), Caspofungin (CA), sodium dodecyl sulfate (SDS, 0.004% and 0.005%), were added to MM plates. Spores were harvested as described above, counted, serially diluted into 2000, 200, 20 and 2 spores/µL and 5 µL of respective dilutions were spotted on MM plates containing cell wall disturbing compounds. Plates were incubated for 3-5 days at 30°C.

3. RESULTS

3.1 Disruption of *kexB* shows a pH-dependent phenotype between pH 5.0 and pH 6.0 in fermenters

The deletion of *kexB* in *A. niger* is known to result in a pH dependent morphological phenotype on solid medium (Jalving et al., 2000). On pH 6.0 buffered agar plates, the *ΔkexB* strain displays a hyper-branching and compact phenotype whereas at pH 5.0 is growth like wild type (Jalving, 2005). To analyze the effect of the pH on the morphology during stirred submerged growth, we cultivated both parental strain (N402) and *ΔkexB* at pH 5.0, pH 5.5 and pH 6.0. Batch cultivations were performed at pH-controlled conditions using 0.75% glucose as carbon source. Dry weights were used to determine both the maximal specific growth rate (µmax) and maximum biomass, which are listed in Table 2. At pH 5.0, both the growth rate ($0.200 \cdot h^{-1}$) and maximum biomass ($4.15\ g_{DW} \cdot kg^{-1}$) of the *ΔkexB* strain were found to be similar to the wild type ($0.187 \cdot h^{-1}$, $3.66\ g_{DW} \cdot kg^{-1}$). The hyphal morphology of the *ΔkexB* strain shows a wild type-like phenotype at pH 5.0, although the *ΔkexB* strain showed a slightly more open pellet morphology (Figure 1). Submerged growth at pH 5.5 showed slightly shorter hyphae and increased branching in case of the *ΔkexB*

strain compared to wild type, as can be seen in Figure 1. The growth rate and maximum acquired biomass at pH 5.5 for the *ΔkexB* strain (0.194 · h^{-1}, 4.19 g_{DW} · kg^{-1}) was similar to wild type (0.175 · h^{-1}, 3.68 g_{DW} · kg^{-1}) and also similar to the conditions at pH 5.0. When grown at pH 6.0, the *ΔkexB* strain again showed a similar growth rate (0.211 · h^{-1}) and maximum biomass accumulation (4.31 g_{DW} · kg^{-1}) as at other pH conditions, but importantly, showed a very clear compact pellet phenotype (Figure 1). Cultivation of N402 at pH 6.0 resulted in severe biofilm formation on the walls of the fermenters. As a result, submerged biomass samples represented an incorrect measurement of both the submerged growth rate (0.063 · h^{-1}) and amount of in-broth maximum biomass (0.64 g_{DW} · kg^{-1}). Microscopic analysis of the N402 pellets at pH 6.0 was similar hyphal morphology compared to pH 5.0 and pH 5.5. In general, base consumption to maintain the desired culture pH in all cultures was largely similar, as was also already published earlier for N402 (Niu et al., 2016).

Table 2. Growth parameters of wild type and *ΔkexB*. Growth is shown as maximum growth rate per hour (μmax) and maximum biomass (gDW · kg^{-1}) at different pH-controlled batch-cultivations.

	Wild type		*ΔkexB*	
pH condition	**μmax (h^{-1})**	**max biomass (g_{DW} · kg^{-1})**	**μmax (h^{-1})**	**max biomass (g_{DW} · kg^{-1})**
pH 5.0	0.187	3.66	0.200	4.15
pH 5.5 (1)	0.175	3.68	0.194	4.19
pH 5.5 (2)	0.167	3.54	0.180	4.30
pH 6.0	0.063	0.64	0.211	4.31

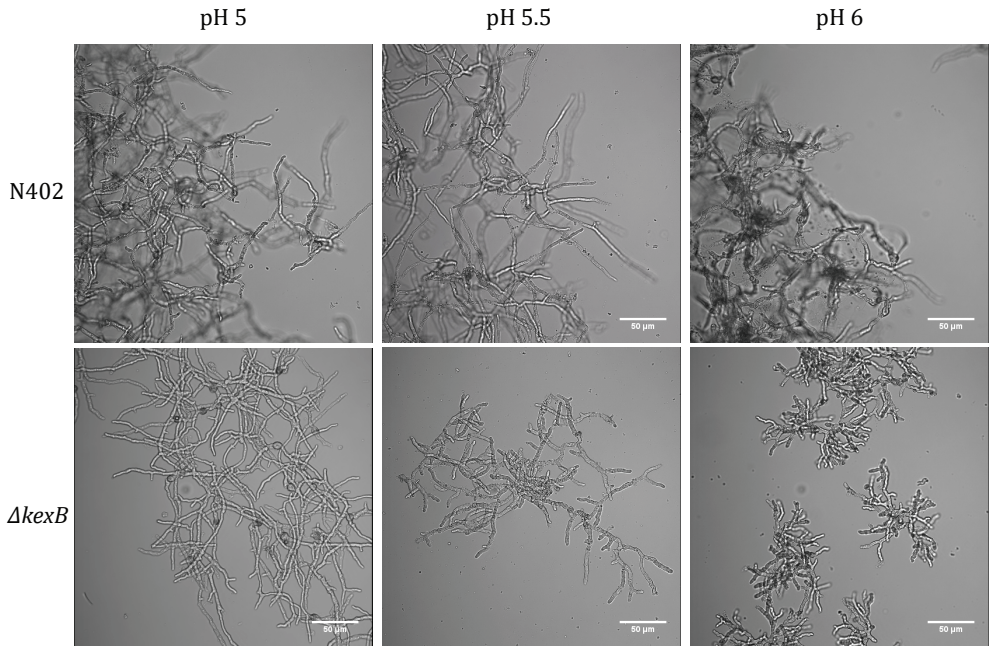

Figure 1. Pellet morphology of pH-controlled batch cultivations Wild type (N402) and *ΔkexB* strain microscopy samples taken at maximum biomass under different pH conditions: pH 5.0, pH 5.5 and pH 6.0.

3.2 Disruption of *kexB* displays reduced biofilm formation and more compact biofilm structure

As observed in the previous section, classical filamentous growth (i.e., without hyper-filamentation) displayed by wild type (N402) strain leads to severe biofilm proliferation on bioreactor walls. It seems thus that the hyper-filamentous phenotype exhibited by *ΔkexB* strain did not promote biofilm formation. In order to challenge this hypothesis, both strains have been cultivated in biofilm reactor at two different pH values (i.e., 5 and 6). This cultivation mode involves a standard lab-scale bioreactor where the mechanical stirring device has been removed and replaced by two sheets made of stainless-steel wire gauze (Figure 2A). This device has been evaluated for the cultivation of *Aspergillus oryzae* in a previous study and observations have pointed out the fact that fungal growth occurs exclusively on the metal sheets in this cultivation device (Zune et al., 2015), making the growth process fully dependent on the adhesion capacity of the strains. Qualitatively, wild type strain (N402) at both pH level and *ΔkexB* strain at pH 5 displayed similar biofilm morphologies, i.e. mycelium with relatively low ramification frequency. On the other hand, at pH 6 displayed a totally different biofilm morphology with, this one being composed of several hyper-ramified mycelial clumps instead of a continuous layer of mycelium (see microscopy images at figure 2A).

The two strains exhibited also differences at the quantitative level (Figure 2B), with biofilm dry weight for wild type strain (N402) cultivated at pH 5 and 6 were of 2.95 and 2.39 respectively (mean values), whereas mean dry weight of 1.74 and 1.31 respectively were observed for the *ΔkexB* strain. The pH-dependent hyper-filamentation phenotype of the *ΔkexB* strain is thus also observed in biofilm mode of cultivation, leading to reduced attachment on the metal supports and a much thicker biofilm structure with reduced water sorption capacity (Figure 2C).

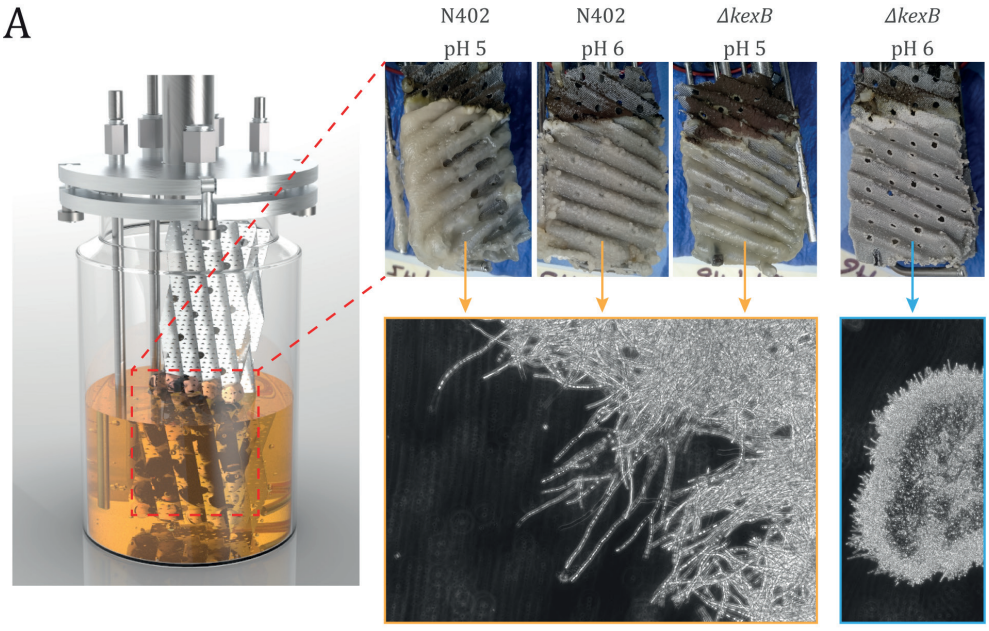

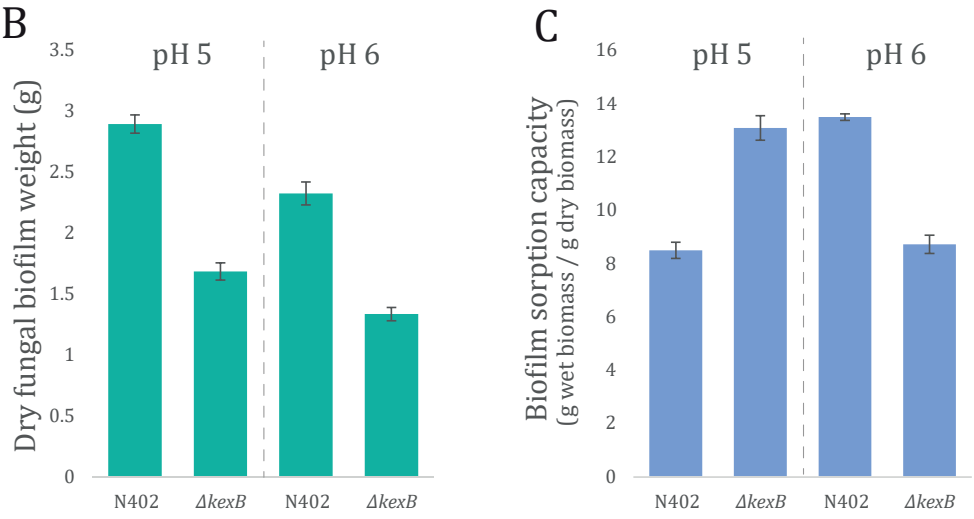

Figure 2. **Submerged biofilm reactor cultivations of wild type (N402) and *ΔkexB*.** (A) Scheme of the biofilm reactor set-up used in this work and pictures displaying biofilm layer for each strain at two pH levels. Representative microscopy pictures (brightfield, 20x) are displayed for each type of biofilm structure. (B) Dry fungal biomass weight developed on the stainless-steel sheets in biofilm reactor and biofilm water sorption capacity (n = 2). Biofilm (water) sorption capacity is the difference between biofilm wet and dry weight.

3.3 Cell wall chitin content is increased in *ΔkexB* irrespective of morphology

To assess the relation of different hyphal branching morphologies at pH 5.0, pH 5.5 and pH 6.0 and cell wall chitin content, we isolated cell walls from maximum biomass samples that were obtained from bioreactor cultivations described above. Cell wall samples were hydrolyzed in triplicate and total glucosamine content was assessed using a colorimetric assay (section 2.5). Results of glucosamine measurements are shown in Figure 3. During all cultivations, the *ΔkexB* strain displayed an increase in chitin content compared to the wild type. The increase in percentage of cell wall glucosamine for the *ΔkexB* strain compared to the wild type were found to be 35.0 ± 13.3%, 27.3 ± 5.51% and 29.6 ± 6.62% at pH 5.0, pH 5.5 and pH 6.0, respectively. Looking at absolute numbers of cell wall glucosamine per cell wall dry weight, we find that total glucosamine levels increase proportionally with the culture medium pH for both strains. Hence, cell wall glucosamine increases with increasing pH with about 20% between pH 5.0 and pH 6.0 and at all pH values the chitin content of the *ΔkexB* strain is about 30% higher compared the wild type.

3.4 Genome-wide expression profiling reveals changes in expression of cell wall biosynthetic genes

To gain better insight to transcriptomic responses in relation to cell wall biosynthetic changes occur as a result of lacking KexB, we decided to look into the transcriptome by performing RNA-sequencing on RNA extracted form wild type and the *ΔkexB* mutant grown at pH 5.5. A pH of

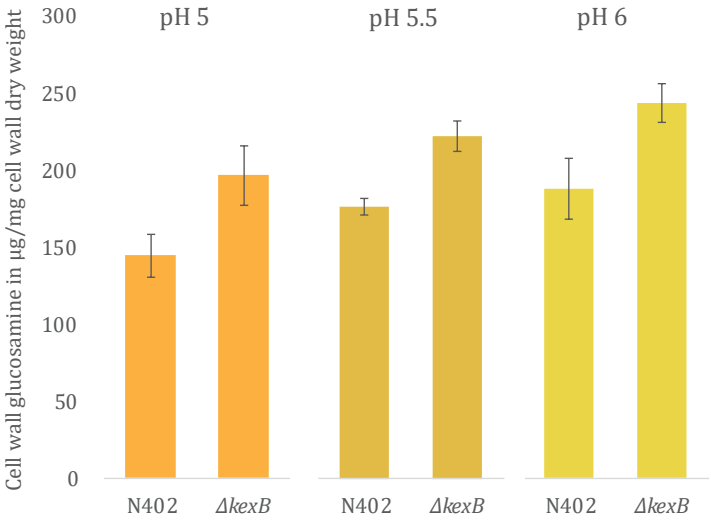

Figure 3. Cell wall glucosamine content of wild type (N402) and *ΔkexB* from pH-controlled batch cultivations. Cell wall glucosamine content maximum biomass samples that originate from single bioreactor cultivations, run at either pH 5.0, pH 5.5 (1) or pH 6.0. Measurements were performed in technical triplicates (n=3); error bars are the standard error (SE) and represent the variation of technical replicates.

5.5 resulted the most comparable growth conditions for both wild type and the *ΔkexB* strain. To obtain biological duplicates, additional bioreactor cultivations at pH 5.5 were performed and resulted in similar growth rates and maximum biomass accumulation as shown before for both wild type (0.167 · h^{-1}, 3.54 g_{DW} · kg^{-1}) and the *ΔkexB* strain (0.180 · h^{-1}, 4.30 g_{DW} · kg^{-1}) (Table 2). RNA was isolated from culture samples in the exponential growth phase at 90% of the maximum attained biomass. Duplicate batch-culture cultivations for both wild type and mutant were used to obtain a total of 4 RNA-sequencing samples. Following DeSeq2 analysis (section 2.7), we found 2461 transcripts (1163 up, 1298 down)—approximately 21% of the 11846 total transcripts—to be differentially expressed between the mutant strain and the wild type (adjusted p-value ≤ 0.05) (Expression data in Table S1).

For this study, we focused our interest to investigate to what extent cell wall biosynthesis was affected by deletion of *kexB*. To assess this, we checked for differential expression of all genes involved in 82 cell wall biosynthesis in *A. niger* as reported by Pel et al, 2007. Table 3 summarizes all cell wall related genes that were differentially expressed in the *ΔkexB* strain compared to N402. Differential expression was found for 29 out of 82 cell wall related genes involved in synthesis of all major components of the cell well, including α-glucan, β-glucan and chitin, and the modification thereof (Table 3, Table S1, expression data). The results on increased cell wall chitin (Figure 3) were corroborated by transcriptional upregulation of gene encoding the rate limiting step in chitin precursor synthesis (UPD-*N*-acetylglucosamine), *gfaA* (FC 1.19) and *gfaB* (FC 6.22). Other genes involved in the synthesis of UPD-*N*-acetylglucosamine (*gnaA*, *pcmA* and *ugnA*) were not differentially expressed. Additionally, five chitin synthases were found to be upregulated in the *ΔkexB* strain (*chsB*, *chsC*, *chsD*, *chsE* and *chsG*), whereas four out of seven putative chitin-to-glucan crosslinking enzymes were found to be differentially expressed (*crhA,* and *crhD* upregulated; and *crhB* and *crhF* downregulated) along with four differentially expressed chitinases (*cfcD* and NRRL3_09653 upregulated; and *cfcG* and NRRL3_04221 downregulated).

Table 3. Differentially expressed cell wall biosynthesis genes in *Aspergillus niger*. 29 genes were differentially expressed (Padj ≤ 0.05) based on all 82 cell wall biosynthesis genes described by Pel et al., 2007.

CBS513.88 ID	NRRL3 ID	Gene description	Gene	Wild type (normalized read counts)	*ΔkexB* (normalized read counts)	FC	up or down regulated	Padj
α-glucan biosynthesis and modification								
An12g02460	NRRL3_09001	Putative GPI-anchored amylase-like protein (GH13-family) with possible function in alpha1,3-1,4-glucan processing	*agtB*	30	1114	38.06	up	1.43E-69
An12g02450	NRRL3_09002	Putative catalytic subunit alpha1,3-glucan synthase complex; SpAgs1-like	*agsC*	64	1688	26.48	up	5.91E-67
An04g09890	NRRL3_07454	Putative catalytic subunit alpha1,3-glucan synthase complex; SpAgs1-like	*agsA**	104	574	5.52	up	8.90E-25
An08g09610	NRRL3_11494	Putative alpha-1,3-glucanase GH71; member of the SpAgn1-family	*agnD*	1496	6544	4.37	up	1.55E-71
β-glucan biosynthesis and modification								
An09g00670	NRRL3_00054	Predicted GPI-anchored protein. Putative 1,3-β-glucanosyltransferase GH72; member of the Gel-family	*gelD*	40	920	22.95	up	3.83E-73
An03g05290	NRRL3_08399	Predicted GPI-anchored protein. Putative beta-1,3-glucanosyltransferase GH17; member of the AfBgt1-family	*bgtB*	20956	29235	1.40	up	7.26E-04
An01g12450	NRRL3_02657	Putative exo-beta-1,3-glucanase (GH55-family); related to *Coniothyrium minitans* exo-1,3-glucanase (Cmg1)	*bxgA**	4743	6407	1.35	up	8.95E-03
An06g01550	NRRL3_11624	Putative catalytic subunit beta1,3-glucan synthase complex; ScFks1-like	*fksA*	18189	23402	1.29	up	6.29E-04
An07g04650	NRRL3_04586	Putative beta-1,3-glucanosyltransferase GH17; member of the AfBgt1-family	*bgtC*	1161	847	-1.37	down	2.46E-03

Table 3. Differentially expressed cell wall biosynthesis genes in *Aspergillus niger*. 29 genes were differentially expressed (Padj ≤ 0.05) based on all 82 cell wall biosynthesis genes described by Pel et al., 2007. (Continued)

CBS513.88 ID	NRRL3 ID	Gene description	Gene	Wild type (normalized read counts)	*ΔkexB* (normalized read counts)	FC	up or down regulated	Padj
α-glucan biosynthesis and modification								
An10g00400	NRRL3_06317	Predicted GPI-anchored protein. Putative 1,3-β-glucanosyltransferase GH72*; A. fumigatus* Gel1-like	*gelA**	14085	9570	-1.47	down	4.10E-08
An03g06220	NRRL3_08332	Predicted GPI-anchored protein. Putative 1,3-β-glucanosyltransferase GH72; member of the Gel-family	*gelE*	2008	192	-10.50	down	6.04E-120
An19g00090	NRRL3_01223	Putative exo-beta-1,3-glucanase (GH55-family); related to *Coniothyrium minitans* exo-1,3-glucanase (Cmg1)	*bgxC*	1101	102	-10.83	down	3.28E-50
Chitin biosynthesis and modification								
N/A	NRRL3_09653	Putative chitinase (N402 specific)	-	17	336	19.52	up	2.11E-17
An12g10380	NRRL3_02932	Putative chitin synthase ClassIII; EnChsB-like	*chsE**	3764	6517	1.73	up	1.35E-15
An08g05290	NRRL3_11152	Putative chitin synthase ClassVI;	*chsG*	147	252	1.71	up	4.56E-03
An14g00650 An14g00660	NRRL3_00641	Putative chitin synthase ClassI; EnChsC-like	*chsC*	2398	3814	1.59	up	2.44E-07
An11g01540	NRRL3_10021	Putative transglycosidase of GH16-family involved in cell wall biosynthesis; ScCrh1-like	*crhA*	737	1097	1.49	up	8.45E-04
An01g11010	NRRL3_02532	Predicted GPI-anchored protein. Putative transglycosidase of GH16-family involved in cell wall biosynthesis; member of the ScCrh1-family	*crhD**	3637	5234	1.44	up	7.65E-04
An09g02290	NRRL3_00179	Putative chitin synthase ClassIV; EnChsD-like	*chsD*	2278	3104	1.36	up	1.99E-03
An09g04010	NRRL3_00331	Putative chitin synthase ClassIII; EnChsB-like	*chsB**	6774	8553	1.26	up	5.98E-03
An01g05360	NRRL3_02063	Putative ClassV Chitinase (GH18); ScCts2-like	*cfcD*	1384	818	-1.69	down	3.96E-05

Table 3. Differentially expressed cell wall biosynthesis genes in *Aspergillus niger*. 29 genes were differentially expressed (Padj ≤ 0.05) based on all 82 cell wall biosynthesis genes described by Pel et al., 2007. (Continued)

CBS513.88 ID	NRRL3 ID	Gene description	Gene	Wild type (normalized read counts)	*ΔkexB* (normalized read counts)	FC	up or down regulated	Padj
Chitin biosynthesis and modification								
An16g02850	NRRL3_07085	Putative transglycosidase of GH16-family involved in cell wall biosynthesis; member of the ScCrh1-family	*crhF*	1468	812	-1.81	down	4.92E-08
An07g07530	NRRL3_04809	Predicted GPI-anchored protein. Putative transglycosidase of GH16-family involved in cell wall biosynthesis; ScCrh2-like	*crhB*	2205	988	-2.23	down	1.53E-09
N/A	NRRL3_04221	Putative chitinase (N402 specific)	-	174	58	-2.99		3.09E-03
An19g00100	NRRL3_01224	Putative ClassV Chitinase (GH18); ScCts2-like	*cfcG*	415	2	-197.88		8.05E-20
GH76 family proteins								
An11g01240	NRRL3_10041	Putative endo-mannanase (GH76-family) with a possible role in GPI-CWP incorporation; ScDfg5-like	*dfgH*	289	1103	3.82	up	2.58E-35
An14g03520	NRRL3_00897	Predicted GPI-anchored protein. Putative endo-mannanase (GH76-family) with a possible role in GPI-CWP incorporation; ScDfg5-like	*dfgC**	1133	1996	1.76	up	6.95E-10
An16g08090	NRRL3_06700	Predicted GPI-anchored protein. Putative endo-mannanase (GH76-family) with a possible role in GPI-CWP incorporation; ScDfg5-like	*dfgE*	886	1169	1.32	up	2.14E-02
An02g02660	NRRL3_06048	Putative endo-mannanase (GH76-family) with a possible role in GPI-CWP incorporation; ScDfg5-like	*dfgG*	2587	1693	-1.53	down	3.75E-05

Table 3. Differentially expressed cell wall biosynthesis genes in *Aspergillus niger*. 29 genes were differentially expressed (Padj ≤ 0.05) based on all 82 cell wall biosynthesis genes described by Pel et al., 2007. (Continued)

CBS513.88 ID	NRRL3 ID	Gene description	Gene	Wild type (normalized read counts)	*ΔkexB* (normalized read counts)	FC	up or down regulated	Padj
Rho-GAPs								
An18g06730	NRRL3_10703	Putative Cdc42-GTPase Activating protein (GAP) with similarity to ScBem3p	*capB*	1379	1783	1.29	up	5.54E-03
An13g00850	NRRL3_01500	Putative Rho1-GTPase Activating protein (GAP) with strong similarity to ScRgd2	*rapE*	2256	2755	1.22	up	1.91E-02
CWI signaling								
An04g10140	NRRL3_07436	Putative plasma membrane sensor required for cell wall integrity signaling; ScMtl1like	*mtlB*	93	575	6.16	up	6.51E-22
An07g04070	NRRL3_04545	Putative plasma membrane sensor-transducer of the stress-activated PKC1-MPK1 kinase pathway involved in maintenance of cell wall integrity; ScWsc1-like	*wscB**	2073	2963	1.43	up	4.60E-05
An18g02400	NRRL3_10351	Protein kinase C with putative function in CWI signaling	*pkcA*	3602	4518	1.25	up	5.43E-03
An08g10670	NRRL3_11584	MAPK with putative function in Pheromone response/pseudohyphal growth pathway; ScFus3-like	*fusC*	2269	2808	1.24	up	1.39E-02

*Identified as induced upon cell wall stress (Meyer et al., 2007; Park et al., 2016)

Next to upregulation of chitin related transcripts, we observed the upregulation of *agsA* (FC 5.52), a gene known to be induced upon activation of the cell wall integrity (CWI) pathway in an RlmA dependent manner (Damveld et al., 2005). We checked for upregulation of additional genes involved in the CWI response, as previously published (Meyer et al., 2007; Park et al., 2016). Many of the reported genes were found to be represented in the differential dataset including *bxgA*, *gelA*, *chsE*, *crhD*, *chsB*, *dfgC* and *wscB* (highlighted by asterisks in Table 3). However, some cell wall stress-related genes, such as chitin synthesis genes *gfaA* and *gfaB*, are not listed in this table. Taken together, the transcription data corroborate the observed increase in cell wall chitin and indicated that most of the CWI pathway is induced in a *ΔkexB* strain.

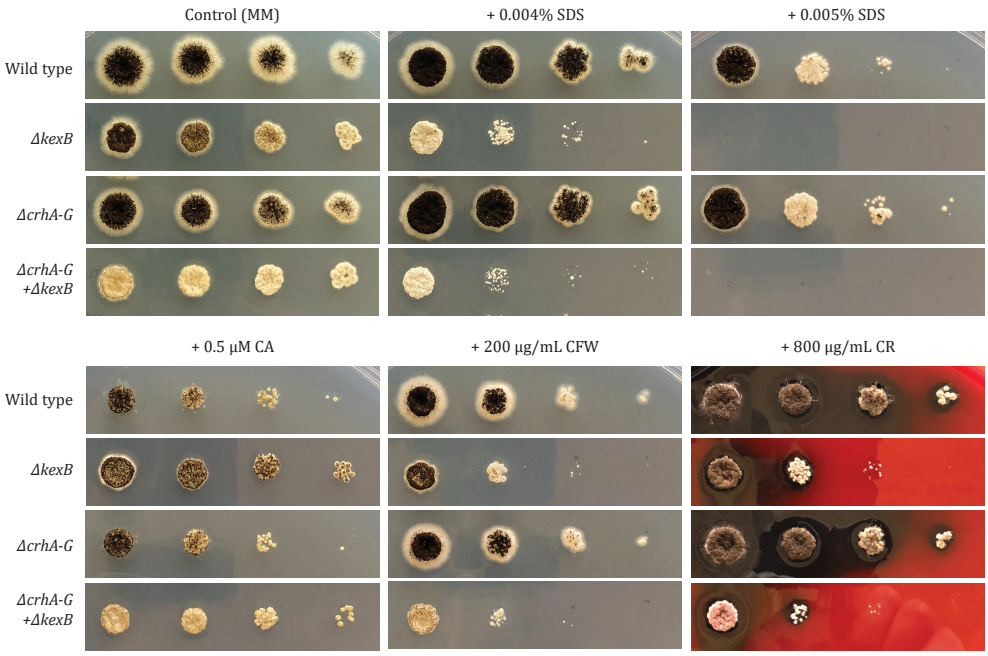

Figure 4. Susceptibility against cell wall disturbing compounds. Strains wild type (N402), *ΔkexB, ΔcrhA-G* and *ΔcrhA-G* + *ΔkexB* were grown on a cell wall sensitivity assay (section 2.9) using minimal medium (MM), pH 6.0 as base medium with additions of either SDS, Caspofungin (CA), CalcoFluor White (CFW) and Congo Red (CR). The number of spores plated, from left to right, are 10^4, 10^3, 10^2 and 10^1 spores, respectively. Strains were allowed to grow at 30°C for 96h prior to prior to recordings, whereas the control was incubatd for 65h.

3.5 Cell wall integrity is affected by disruption of *kexB*

To test whether a deletion of *kexB* affects the integrity of the cell wall, we exposed both the parental strain (N402) and *ΔkexB* to a series of cell wall disturbing compounds around pH 6.0 on plates—where the growth effect of *ΔkexB* is most prominent—that respond to changes in chitin content: Sodium dodecyl Sulfate (SDS), Caspofungin (CA), CalcoFluor White (CFW) and Congo Red (CR). As can be seen from Figure 4, the *ΔkexB* strain is more sensitive to SDS, CalcoFluor White (CFW) and Congo Red (CR) than the wild type, while slight resistance towards CA was observed for the *ΔkexB* strain in this assay.

In addition to an increase in chitin content for the *ΔkexB* strain, the transcriptional response showed differential expression for the majority of the chitin-to-glucan crosslinking *crh* family (Table 3). To investigate the importance of these enzymes in the construction and modification of existing chitin in the cell walls of the *ΔkexB* strain, we opted to knockout *kexB* in an existing seven-fold *crh* deletion (van Leeuwe et al., 2020c). We found that deleting *kexB* in the seven-fold *crh* deletion strain resulted sporulation deficiency. Despite the impact on sporulation, we neither observed a vegetative growth deficiency nor did we find a significant exacerbation of sensitivity towards any of the tested compounds when *ΔcrhA-G* and *ΔkexB* were combined (Figure 4).

4. DISCUSSION

In this study we invoked the impact of deleting *kexB* in *A. niger* on hyphal morphology and cell wall composition by performing phenotypic, cell wall and transcriptomic analysis. We show that the characteristic hyper-branching pH-dependent phenotype of the *ΔkexB* strain, as reported on solid agar plates, is also prevalent in submerged solid support growth and submerged pH-controlled batch cultivations at pH 6.0. The phenotypic plasticity of the *ΔkexB* strain transitions between pH 5.0 and pH 6.0; pH-controlled conditions revealed that the *ΔkexB* strain morphology resembles wild type at pH 5.0, shows slightly shorter hyphae and smaller pellets at pH 5.5, and shows severe hyper-branching and tiny pellets at pH 6.0 (Figure 1). Despite the differences in morphology, both the growth rate and maximum biomass of the *ΔkexB* strain were not impaired and even slightly higher than the wild type across all pH conditions. It is interesting to note, however, that wild type growth at pH 6.0 resulted in severe biofilm formation at the fermenter walls whereas the *ΔkexB* strain did not.

To extend on the observation that *kexB* may be involved in surface attachment (i.e. biofilm formation), we grew both wild type and *ΔkexB* in specific biofilm reactors. Under these very specific cultivation conditions, it has been shown before that fungal growth occurs only on the metal sheets and not (or in very limited amount) in the liquid phase (Khalesi et al., 2014; Zune et al., 2015). On these metal sheets, the *ΔkexB* strain showed reduced biofilm formation compared to the wild type at both pH 5.0 and pH 6.0. These observations showed that a deletion of *kexB* limits the proliferation of the fungal biomass on the metal support. Additionally, we found that the hyper-branching phenotype of the *ΔkexB* strain was only observed at pH 6.0 and is very similar to the batch cultivation conditions at pH 6.0. Also, the biofilm of the *ΔkexB* strain produced at pH 6.0 is of a totally different structure than the one observed for the wild type, as well as for the *ΔkexB* strain at pH 5.0. This mycelial layer of hyper-branching phenotype growing on the metal support is more compact and displayed reduced water sorption capacity. It is important to take note that it remains unknown to what extent the morphology and biofilm composition will affect secretion and total production parameters and may be topics of future research. Despite these different mycelial properties of the hyper-branching morphology, a deletion of *kexB* reduced the ability to form biofilms at both pH conditions compared to the wild type. Furthermore, the increase in

pH from 5.0 and 6.0 appeared to affect both wild type and *ΔkexB* as a similar percentual drop in biofilm dry weight was observed between pH 5.0 and pH 6.0 (Figure 2B). Taken together, these data show that the *kexB* deletion shows a pH-dependent morphology at pH 6.0 without affecting growth rate or maximum biomass formation under submerged batch cultivation conditions. Additionally, the hyper-branching morphology showed less mycelial clumping and will reduce the stirring viscosity due to tinier pellets. As such, a deletion of *kexB* may provide a valuable industrial candidate strain for fermentation in near neutral pH conditions. Additionally, we observed that the *kexB* deletion resulted in visibly thicker cell walls that could be used as an added-value post-fermentation product.

Next, we investigated the cell wall composition of the *ΔkexB* strain and found an increase in cell wall chitin compared to the wild type; a trait that is often coupled to activation of the cell wall integrity to increase the strength of the cell wall (Fortwendel et al., 2010; Heilmann et al., 2013; Ram et al., 2004; van Leeuwe et al., 2020b, 2020a; Walker et al., 2015, 2008), and increased susceptibility towards CFW and resistance towards CA (Ram and Klis, 2006; Walker et al., 2015, 2013, 2008). The observed increase in chitin content from bioreactor cultivations was corroborated by the transcriptional upregulation of *gfaA*, and its paralogue *gfaB*, that are required for chitin precursor (UDP-*N*-acetylglucosamine) synthesis, known as the rate-limiting step for chitin synthesis (Lagorce et al., 2002; Ram et al., 2004). In addition, upregulation of multiple chitin synthases and downregulation of chitinases *cfcD*, *cfcG* and the N402 lineage-specific chitinase NRRL3_04221 were found. This transcriptional response is similar to that of the UDP-galactopyranose mutase A (*ugmA*) cell wall mutant, lacking cell wall galactofuranose, that also has increased cell wall chitin and chitin modifications by upregulation of *gfaA* and *gfaB, chsB* and *chsE* and severe downregulation of chitinase *ctcA* (Damveld et al., 2008; Park et al., 2016).

Aside from increased chitin synthesis in the *ΔkexB* strain, chitin-modifying enzymes also appear to play a role in the response to KexB-deficiency, as be inferred from the upregulation of *crhA* and *crhD*, and downregulation of *crhB* and *crhF* (Table 3). However, a combined deletion of all *crh* genes and *kexB* did not result in increased susceptibility to cell wall disturbing compounds. We did observe reduced sporulation, an effect that was also observed when a deletion of the seven-fold *crh* family and *ugmA* were combined (**Chapter 3**). In case of the *ugmA* strain, it has clearly been described that the CWI pathway is activated. Here, also the *ΔkexB* strain showed a large number of differentially expressed cell wall biosynthetic genes that are known to be upregulated during the CWI response. Moreover, the *kexB* deletion has been reported to induce the CWI response pathway by means of MAPK phosphorylation in *A. oryzae* and *A. fumigatus* (Mizutani et al., 2004; Te Biesebeke et al., 2005; Wang et al., 2015). In addition, the *Aspergillus oryze kexB* (*AOkexB*) deletion has been reported to cause hyper-branching similar to *A. niger*, and increased amylase and protease production (Te Biesebeke et al., 2005). In *A. fumigatus*, a *kexB* deletion strain showed increased sensitivity towards CFW and CR, similar to our observations for the *ΔkexB* strain here (Figure 3). The sensitivity towards these compounds comined with the genome-wide expression profile confirm activation of the CWI pathway in *ΔkexB* strains.

The observed changes in cell wall chitin content in the *A. niger ΔkexB* strain are in congruence with *A. oryzae*, where a deletion of *kexB* was shown to increase cell wall chitin along with a reduction of α-glucan. This reduction in cell wall α-glucan was suggested to be caused by lack of KexB-processed α-glucan synthases (Mizutani et al., 2016). In this study, we did not analyze cell wall content for levels of α-glucan, however we did observe a very strong positive transcriptional response for both *agsA* (5.52 FC) and *agsC* (26.48 FC) in the *ΔkexB* strain. Similar to upregulation of chitin modifying enzymes, we found increased transcriptional expression of *agnD*, an alpha-1,3-glucanase (Meyer et al., 2009), and *agtB*, an α-glucan glycanosyl transferase (Levin et al., 2007; Yuan et al., 2008) in conjunction with the two α-glucan synthases. Upregulation of α-glucan metabolism may either indicate an attempted compensatory response to a lack of correctly processed α-glucan synthases (Yoshimi et al., 2017), or as a sign of general cell wall stress resulting from other improperly processed (cell wall) enzymes. Previously, we showed the relevance of proper α-glucan deposition in the cell wall for integrity; when α-glucan synthases *agsA* and *agsE* are disrupted in *A. niger* we showed that *crh*-facilitated chitin-β-glucan crosslinking genes become important for maintenance of cell wall integrity, while these genes are redundant when α-glucan synthesis is undisturbed (**Chapter 3**). Interestingly, α-glucan has also been described in relation to pathogenesis and hyphal aggregation for filamentous fungi (Yoshimi et al., 2017), by showing conidial and hyphal pellet clumping in α-glucan synthase knockouts of *A. fumigatus*, *A. oryzae* and *A. nidulans* (Henry et al., 2012; Miyazawa et al., 2018; Yoshimi et al., 2013). Hyphal aggregation of the *A. niger ΔkexB* strain appeared to be reduced across all three pH conditions (Figure 1) which may be related cell wall α-glucan levels. Further analysis of α-glucan dependent hyphal aggregation and biofilm formation may be a topic of future research.

Next to upregulation of α-glucan and chitin metabolism, *fksA*, the sole β-1,3-glucan synthase in *A. niger* was also found to be upregulated. Along with *fksA*, differential expression of glucanases and glucanosyltransferases (Table 2) were observed that are predicted to cause rearrangements of β-1,3-glucan polymer length and branching. This transcriptional response in *A. niger* is very similar to that observed in the *kexB* deletion in *A. fumigatus* that also resulted in upregulation of *gel* glucanosyltransferases (Wang et al., 2015), and results described on the β-1,3-glucan composition in *A. oryzae* where the *AOΔkexB* strain showed a higher degree of β-glucan polymerization combined with slightly less branching (Mizutani et al., 2016). Together with the overall cell wall biosynthetic gene response, a deletion of *kexB* appears to bring about major cell wall content and compositional changes for all major constituents of the cell wall.

This study shows that the cell wall integrity of the *ΔkexB* strain is clearly affected, however without impairing growth rate or the maximally attained biomass during submerged batch cultivations. Contrarily, we did observe that *kexB* is important in formation of biofilms, as this mode of cultivation in biofilm reactors led to a reduction of the ability of to colonize the metal support. For now, understanding the characteristic phenotype of the *ΔkexB* strain during growth at pH 5.5 and 6 seems a consequence of pleiotropic effects of several hitherto unrelated responses. The morphology at pH 5.5/6.0 is possibly the result of loss of polarity due to the inability to synthesize

or modify the cell wall correctly. Many possible cell wall synthesis or cell wall modifying enzymes could be targets of KexB processing. Explanations for the pH-dependent effect have been postulated and suggest that at lower pH , other proteases can perform KexB-like dibasic processing (Jalving, 2005). In yeast, yapsins, aspartic proteolytic enzymes involved in processing cell wall proteins including Scw4p, Utr2p, Pir4p and Gas1p (Gagnon-Arsenault et al., 2008; Grbavac et al., 2017; Miller et al., 2010), show a pH dependent dependency to kex2. For Scw4p, it was shown that only at a neutral pH (7.0), but not at acidic pH (4.0), Kex2p is required for correct processing of the cell wall protein prior to yapsin processing, in order to activate the protein (Grbavac et al., 2017). It is likely that such a pH-dependent dependency on KexB may relationship of pro-protein processing that also exist in *A. niger*. Here, we showed that—despite the clear morphological changes in liquid between pH 5.0 and pH 6.0—the respective increase in cell wall chitin compared to wild type was observed across all pH conditions. From this we infer that the increase of chitin content is unlikely to dictate cell shape, however we cannot rule out chitin modifying enzymes to still play a role in the distinct phenotype. Taken together, the transcriptional data suggests activation of the CWI pathway that results in cell wall compositional rearrangements. Despite these findings, it remains to be elucidated how and if the KexB-dependent cell wall modifications are related to the pH dependent growth phenotype.

Acknowledgement

We would like to thank Prof. Dr. Bruno M. Moerschbacher for the coordination of the FunChi project.

Funding

This work is part of the “FunChi” ERA-IB project with project number ERA-IB-15-080, which is (partly) financed by the Dutch Research Council (NWO).

Availability of data and materials

The DNA reads described in this study will be deposited in the short read archive upon request. All other data are available on request by contacting Dr. Arthur F.J. Ram.

Supplemental information descriptions

Table S1. Expression data of differentially expressed genes. Includes a tab of expression levels of all cell wall biosynthetic genes, as described by Pel et al., 2007.

CHAPTER 7

General Discussion

Filamentous fungi are intensively used in industrial biotechnology for the production of various enzymes, antibiotics, organic acids and other metabolites (Meyer et al., 2020). As exploitation of fungi to produce these (natural) products will continue to expand, so will the demand for large-scale fermentations. To make these high-value products, fungi are fed a diet of sugars, nitrogen and other essential organic elements such as phosphorous, potassium, sulfur and magnesium along with trace elements of other metal ions. In turn, the fungus grows to form biomass and secretes of large amounts of a desired product that can be harvested. During biomass formation, the supplied sugars are partially converted into glucan and chitin, the two main polymers that constitute the fungal cell wall. The cell wall is an essential structure for the fungus as it provides mechanical strength to withstand turgor pressure, but is also important under natural circumstances for the protection against external penetration and protection against environmental attack (Gow et al., 2017). In terms of mass, the cell wall accounts for approximately 50-80% of the mycelial dry weight, depending on fungal species (Isaza-Pérez et al., 2020). As such, the cell wall takes up a considerable part of the supplied sugars that are not available for the production of the desired fermentation product (e.g. acids or proteins). Post-fermentation, the mycelial biomass that has accumulated during the production process is generally disposed of and potentially precious polymeric sugars are lost. To recover and recycle these polymeric sugars from post-fermentation biomass waste into an added-value product, the fungal chitosan (FunChi) project set out to optimize extraction and production of the polymeric sugars chitin and chitosan from the fungal cell wall. The research described in this thesis addressed both production of chitin and provided insight into the way that chitin is attached to the cell wall. The findings from this work are discussed in this chapter and help to lay the foundations for profitable utilization of chitin and chitosan from fungal cell walls.

Chitin and its de-acetylated derivative, chitosan, are of high industrial interest due to the wide range of applications. The field of application of chitin/chitosan depends their properties such as molecular weight, oligomer length, degree of acetylation and patterns of acetylation (Dhillon et al., 2012; El Gueddari et al., 2014). As chitin/chitosan is not encountered in plant or human tissue, it often acts as an elicitor to plant and animal immune responses in order to fight off possible impending fungal infections. The application of both chitin and chitosan oligomers have been shown to prime plants against infection. Additionally, chitin and chitosan have been shown to benefit healthy plants in drought protection and may also promote total biomass accumulation (reviewed in Das et al., 2015; Hidangmayum et al., 2019; Orzali et al., 2017). During this project, the FunChi partners in Germany and Spain have focused on the chitin and chitosan

composition from fungal cell walls and their effects on the plant immune response, respectively. Our contribution to the FunChi project focused on i) increasing production of chitin in fungal cell walls and ii) removal of covalent cross-links of chitin to the cell wall that would allow for easier, environmentally friendly and cheaper extraction. of chitin We have taken a fundamental approach to tackle these two applied research challenges. To increase chitin production, we have screened an existing *Aspergillus niger* cell wall mutant strain library for mutants with a high chitin content. The research that is presented in this thesis both unravels the previously unknown involvement of three genes that dictate the amount of chitin deposition (described in **Chapters 4, 5 and 6**). Furthermore, we assessed the impact of removing the covalent cross-link between chitin and glucan (**Chapters 2 and 3**). In an attempt to modify chitin cross-linking, we set out to disrupt the seven-membered chitin cell wall crosslinking enzyme encoding gene family in *A. niger* that was considered to be responsible for the covalent cross-links between β-1,3-glucan and chitin. In the yeast *Saccharomyces cerevisiae*, the deletion of the genes encoding these glucan-chitin crosslinking enzymes result is a Congo Red hypersensitive (*CRH*) phenotype which have given the name to this gene family. The *A. niger* mutant in which all seven *crh* genes were deleted, was screened for phenotypic and transcriptomic alterations as a proxy for cell wall integrity.

Because the cell wall is such an important, complex and dynamic structure, many paralogues are found in the gene families that contribute to its construction, modification, fortification and degradation/recycling (Muszewska et al., 2018; Pel et al., 2007). The *crh* gene family in *A. niger* has putative involvement in cell wall construction and/or fortificaton and constitutes seven paralogues that have not been studied before. In contrast, the *S. cerevisiae* genome harbors three *CRH* genes, only two of which are active during vegetative growth. The role of these *CRH* genes have been extensively studied in relation to cell wall biosynthesis (Blanco et al., 2015; Cabib et al., 2008, 2007; Rodríguez-Peña et al., 2000a). Because redundancy in cross-linking of chitin to β-1,3-glucan was demonstrated for *CRH1* and *CRH2*, a likely scenario of redundancy in *A. niger* required the knockout of all seven *crh* genes. The construction of a seven-fold knockout presented a practical constraint with the available state-of-the-art transformation techniques at the start of the FunChi project.

1. Dealing with technical challenges for strain construction: CRISPR/Cas9 for gene editing

Over the years, advances in molecular techniques have allowed easier and more efficient construction of single gene knockouts in *A. niger* (Arentshorst et al., 2012; Carvalho et al., 2010). A major step in gene knockout efficiency has been through disruption of the Non-Homologous End-Joining (NHEJ) DNA repair pathway, leaving only homologous recombination (HR) as the default DNA repair pathway. In the wild type *A. niger* strain, the efficiency of HR is approximately 7% using the bipartite or "split marker" approach for gene knockouts, whereas disruption of the NHEJ pathway (through a *kusA* gene knockout; *ku70* homolog) boosted to HR efficiency to >80% (Arentshorst et al., 2015; Meyer et al., 2007). Two downsides of *kusA* disruption are (i) the

reduction in the ability to repair broken DNA and (ii) the increase in sensitivity towards radiation (Meyer et al., 2007a). To avoid permanent disruption of *kusA*, a clever *amdS*-based loop-out mechanism was devised to allow restoration *kusA* after transformation (Arentshorst et al., 2012).

The construction of an entire gene family knockout, such as the seven-membered *crh* gene family, poses additional challenges to knockout efficiency. To analyze the impact of a single gene deletion, the split marker technique relies on the integration of a selection marker at the gene of interest (GOI) which is easy to use and quick to generate. However, when multiple knockouts are desired in a single strain, the split marker technique can become time-consuming and problematic in its use. In the first place, the number of available selection markers for *A. niger* is limited (Niu et al., 2016b). Additionally, the use of integrative selection markers restricts the use of any selection markers that may be required for complementation studies. Some of the available markers are recyclable (Arentshorst et al., 2012; Carvalho et al., 2010), but this approach is laborious and requires counter-selective compounds that can be of mutagenic nature, such as 5'-FOA (Wellington et al., 2006). Moreover, even more problematic is that the expression of (auxotrophic) selection markers can be affected by the site of integration, described as "position effects", that compromise conclusions of gene function (Miki et al., 2009). This has specifically been shown for *pyrG/pyr4/URA3* auxotrophic markers in *Aspergillus nidulans*, *Aspergillus flavus*, *Neurospora crassa* and *Candida albicans* (Bok et al., 2006; Greenstein et al., 2006; Lay et al., 1998; Luo et al., 2016; Miki et al., 2009; Oestreicher et al., 2008; Robellet et al., 2010; Staab and Sundstrom, 2003). In this thesis, we also observed a similar "position effect" for the *Aspergillus oryzae pyrG* (*AOpyrG*) selection marker in a split-marker knockout experiment for both *crhE* and *crhG* (**Chapter 2**). Integration of the *AOpyrG* selection marker gene at these loci showed uridine-dependent growth-retardation phenotype, most likely due to aberrant expression. Similar to *crhG*, we observed

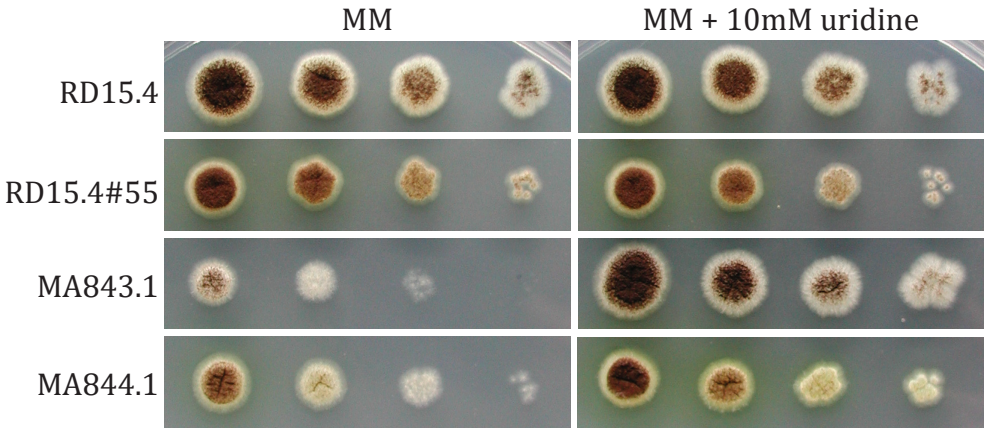

Figure 1. Growth on either minimal medium (MM) or MM with 10mM uridine. Parental strain and mutant (RD15.4#55) and single knockouts of *agsC* (MA843.1) and *cwcA* (MA844.1). MA843.1 and MA844.1 show a reduced growth phenotype on MM, but the growth phenotype is completely complemented upon supplementation of uridine. This indicates that the phenotype on MM in MA843.1 and MA844.2 is caused by uridine/uracil deficiency.

this "position effect" in **Chapter 4** for the knockout of *agsC* (MA843.1), and to a lesser extent for *cwcA* (MA844.1), where *AOpyrG* was used as in integrative selection marker to create single knockouts (Figure 1.) In both cases, a reduced growth phenotype was observed on selective medium, whereas these phenotypes were fully complemented by supplementation of uridine to the medium.

In **Chapter 2**, we describe a CRISPR/Cas9-based approach that circumvents the integrative selection marker problem mentioned above, by removing the reliance on integration of selection markers altogether. Instead, a gene knockout now requires a non-integrative plasmid, harboring a constitutively expressed Cas9 gene, a GOI-specific sgRNA and a hygromycin (*hph*) resistance cassette, along with a PCR-generated selection marker-free repair DNA fragment. This DNA repair fragment—homologous to flanks on either side of a GOI—was shown to successfully repair a Cas9-induced double strand break (DSB), effectively removing the gene through HR (**Chapter 2**). As such, CRISPR/Cas9-based gene editing still requires disruption of *kusA* for high HR efficiency. After desired gene editing, we showed that the Cas9/sgRNA plasmids can be easily cured by removal of selection pressure. This consequently permits the recycling of the same selection marker-containing plasmid—using a different GOI-specific sgRNA—for subsequent gene editing steps. Moreover, up to three plasmids—identical apart from the GOI-specific sgRNA—can be transformed to *A. niger* simultaneously, along with their respective PCR-generated repair DNA fragments, to generate a triple knockout. This strategy drastically improves the speed of which multiple knockouts can be made; in about one-third of the time of 5'-FOA induced *AOpyrG* recycling which is based on an estimation of the required construction time for a seven-fold knockout using either CRISPR/Cas9 recycling (73 days) or *AOpyrG* recycling (214 days), as mentioned in **Chapter 2**.

Next to the quick, easy and seamless construction of a seven-fold knockout strain in **Chapter 2**, we have also demonstrated that our CRISPR/Cas9 procedure works well to carry out precise gene-editing of single nucleotides, as described in **Chapter 4** and **Chapter 5**. In these chapters, we describe the identification of phenotype-responsible SNPs for two separate mutants and, importantly, prove single SNP involvement. This was done by re-creating these mutations in wild type backgrounds, at the endogenous locus of the relevant alleles in both RD15.8#16 (*gdiA* and NRRL3_05482) and RD15.4#55 (*cwcA*), a feat that is more difficult using traditional gene editing methods. Traditional methods either introduce a mutant allele ectopically, through HR with a selection marker (Arentshorst et al., 2015) or as large DNA constructs that contain mutant alleles fused to a selection maker that require to fully integrate into the genome at the endogenous locus. In either case, the expression levels of ectopically introduced genes have the potential to bring out "position effects" as described above. These possible side-effects can now be avoided altogether by using CRISPR/Cas9-based gene editing.

Aside from the advancements in multiplex gene editing, the current state-of-the-art CRISPR/Cas9-based gene editing leaves some to be desired. In particular, we encountered that in some cases (as in the case of NRRL3_05482) sgRNA design was somewhat limited by the lack of suitable

PAM sites to guide the Cas9 for gene editing. Many efforts have been made to design strategies that allow (almost) unrestricted use of Cas9-based gene editing to counter this constraint in the future. These efforts include protein engineering to alter PAM-recognition sites of current Cas9 enzymes (Liu et al., 2019; Miller et al., 2020; Nishimasu et al., 2018), usage of alternative Cas9-like enzymes that naturally contain different PAM-recognition sites, such as Cpf1 (Zetsche et al., 2015) (PAM site on 5' end of the guide RNA as 5' – TTTN – 3'), MAD7 (Inscripta, Inc, Boulder Colorado) and engineered variations thereof (Bin Moon et al., 2018; Gao et al., 2017) or engineered sgRNA structures (Kocak et al., 2019). Lastly, CRISPR/Cas9-based gene editing works very well in NHEJ deficient strains, but remains inefficient and unpredictable in existing strains with a wild type *kusA.* The inefficiency of CRISPR/Cas9-based gene restoration in strains with wild type *kusA* became evident in **Chapter 4**, where the *cwcA* mutant allele was restored to a wild type allele in RD15.4#55. A possible way to negotiate this hurdle is by temporal knock down of *kusA* through RNA silencing mechanisms, such as with small interfering RNAs (siRNA). Ideally, these would either be co-transformed as siRNAs together with CRIPSR/Cas9 plasmids and repair DNA fragments or siRNA expressing constructs can be integrated and expressed from CRISPR/Cas9 plasmids directly. Short hairpin RNAs (shRNA) have effectively been shown to be expressed from a vector and silence genes in different fungi (Dang et al., 2011). As such, implementation of a *kusA* targeting shRNA cassette on Cas9/sgRNA expressing vectors may provide an elegant solution absolve dependability on NHEJ deficient mutants by default in the future. Such an approach may be of particular relevance if transformation of industrial strains is desired, as these strains are usually not NHEJ deficient. The findings listed above, ongoing work and future plans on CRISPR systems continue to expand the genome editing toolkit and, in the foreseeable future, are likely enable any type of genetic alteration, anywhere in the genome.

2. Chitin attachment in the fungal cell wall

Chitin is known to be cross-linked to the fungal cell wall. Based on *S. cerevisiae* studies it was shown that Crh enzymes facilitate chitin cross-linking to both β-1,3-glucan and β-1,3-glucan branches of β-1,6-glucan (Cabib et al., 2008, 2007; Kollár et al., 1997; Rodríguez-Peña et al., 2000b). Absence of the Crh enzymes Crh1p and Crh2p resulted in complete loss of these covalent links between chitin and β-1,3-glucan, and an increased susceptibility towards Congo Red (CR) and Calcofluor White (CFW). In **Chapter 2,** we describe the construction of an *A. niger* strain in which all seven *crh* genes have been deleted. Surprisingly, we found that this seven-fold *A. niger* mutant did not show increased susceptibility to either CR or CFW and only showed slightly more compact colonies on plates under all tested conditions. Neither did we find differences in sensitivity towards other cell wall disturbing compounds nor in growth rate in batch-fed cultivations. Even more strikingly, both extensive in-depth analysis on transcriptomic level and cell wall composition of the seven-fold *crh* deletion strain revealed only minor differences compared to the wild type strain (**Chapter 3**). Consequently, we conclude that the effect on the cell wall of *CRH* gene family knockout in *S. cerevisiae* does not translate to the effect of a *crh* gene family knockout in *A. niger*. When looking

into detail, the relative cell wall composition of *A. niger* is different from *S. cerevisiae* and contains additional polysaccharides, such as α-glucan and galactomannan. In **Chapter 3**, we present evidence suggesting that these polymers compensate for the loss of *crh* gene function. Due to the interactions that exist between chitin and α-1,3-glucans—the core structure of what provides rigidity to the cell wall of filamentous fungi (Kang et al., 2018)—we hypothesized that the chitin cross-links and α-glucan act redundantly in tethering chitin to the cell wall. In correspondence to that, we have found that partial removal of *A. niger* α-glucan synthesis (by deleting *agsA* and *agsE*), in addition to the seven-fold *crh* family knockout, resulted in disturbed cell wall integrity that was demonstrated by increased sensitivity towards CR and CFW. Separately, knockouts of either *agsA* and/or *agsE* or *crhA-G* did not show the same effect and suggests that the interaction

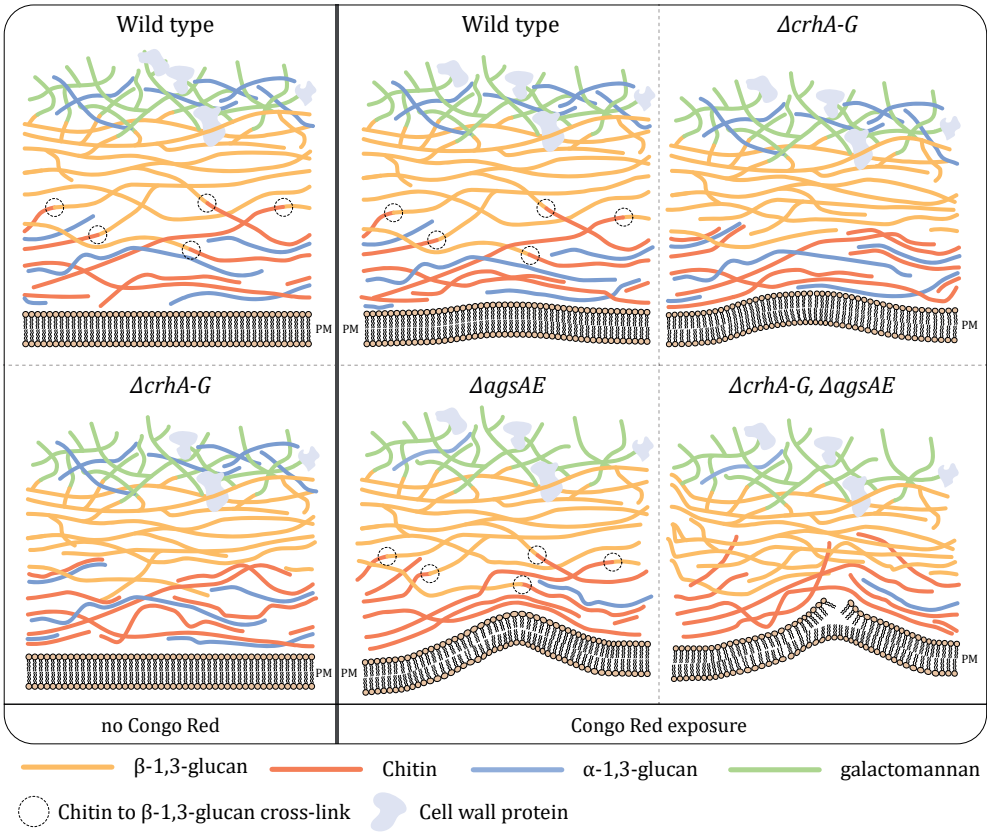

Figure 2. Schematic representation of the cell wall and the role of chitin crosslinks and α-glucan during cell wall stress in filamentous fungi. The left panel shows both the wild type and *ΔcrhA-G* cell wall and plasma membrane (PM) under normal conditions. Congo Red (CR) CR is thought to disrupt chitin and β-glucan assembly by which it weakens the cell wall (Klis et al., 2007), the effect of which is shown for both the wild type and three mutants (*ΔcrhA-G*, *ΔagsAE* and *ΔcrhA-G* + *ΔagsAE*) in the right panel. In the wild type, addition of CR causes slight bulging of the PM. Similarly, removal of the *crh* genes (*crhA-G*) does not affect cell wall integrity under CR-induced cell wall stress. Disruption of alpha-glucan synthases *agsA* and *agsE* reduces the total cell wall alpha-glucan and, in the presence of CR, weakens the cell wall even more, shown by the effects on cell membrane deformation. A combined knockout of the *crh* gene family and *agsAE* causes significant weakening to the cell wall resulting in lysis of the PM when CR is added.

between these two polymers acts as a redundancy mechanism for chitin-to-cell-wall anchorage. A schematic representation of how the knockouts of *crhA-G* and *ags* genes may affect the cell wall when exposed to CR-induced cell wall stress is shown in Figure 2.

Because the levels of cell wall α-glucan were not assessed in the *ΔcrhA-G*, *ΔagsAE* and *ΔcrhA-G* + *ΔagsAE* mutants, it remains unknown to what extent cell wall α-glucan is reduced, as *agsB*, *agsC* and *agsD* are still present. As α-glucan is present in two parts of the cell wall, namely the mobile outer layer and the hydrophobic inner layer, our hypothesis would suggest that the remaining α-glucan of the *ΔagsAE*-mutants resides in the more mobile outer layer, not interacting with chitin. A five-fold α-glucan synthase knockout would be required to study this in more detail. In case of other *Aspergillus* species, α-glucan synthase family knockouts were not found to be lethal, but do show phenotypic effects, such as reduced conidial aggregation, resulting in more dispersed submerged growth (Yoshimi et al., 2017). These are likely effects that result from loss in α-glucan from the outer mobile layer of the cell wall. However, it is worth noting that in *Aspergillus fumigatus* the loss of all α-glucan synthases resulted in a compensatory increase of both β-glucan and chitin (Henry et al., 2012), suggesting that total loss of α-glucan synthases affects more than the outer layer of α-glucan. With special regard to the FunChi project goals, it would be highly interesting as a future project to obtain both an α-glucan synthase family knockout and a α-glucan synthase family knockout combined with the seven-fold *crh* deletion strain, to assess cell wall composition and chitin extraction efficiency.

In the light the reported findings, it remains difficult to explain why there are so many *crh* genes in *A. niger* and other filamentous fungi (Arroyo et al., 2016). Apparently, natural selection has allowed the diversification and maintenance of multiple *crh* genes in the genome. It is not the first encounter where an attempted gene family knockout—orthologous to yeast—did not result in a significant phenotype in a filamentous fungus. Deletion of 11 mannosyltransferases responsible for establishing α-1,6 and α-1,2-mannose linkages in *A. fumigatus* did not affect mannan content in the mycelial cell wall, but only the conidial cell wall, despite highly conserved protein sequence with yeast (Henry et al., 2016). Later it was found that two other orthologs, with a different function in yeast, were important for this mannan polymerization in mycelial walls (Henry et al., 2019). In another study of cell wall enzymes, the GH76 family, responsible for the insertion of galactomannan into the cell wall, was recently investigated in *A. fumigatus*. Here, a disruption of only one out of the seven genes *dfg3* (*defective in filamentous growth*) displayed significant growth phenotypes and loss of cell wall galactomannan, whereas both single and multiple knockouts of other *GH76* members did not show any aberrant growth phenotypes (Muszkieta et al., 2019). Similar to the eleven-membered mannosyltransferases, seven-membered *dfg* family, the number for other cell wall biosynthesis genes found in *A. niger* is also high, e.g. five alpha-glucan synthases, ten chitin synthases, seven β-1,3-glucanosyltransferases, thirteen chitinases and ten mannosyltransferases (Pel et al., 2007). A similar "lack of effect" as in the studies described above could actually be the case for the GH16 *crh* gene family. A recent study characterized the five-membered *crh* gene family in *A. fumigatus.* The authors revealed the chitin to glucan cross-linking ability of those Crh enzymes, but single and multiple knockouts failed to show a

clear cell wall sensitivity phenotype (Fang et al., 2019), similar to our own observations for *A. niger*. Apparently, the cell wall permits the loss of cell wall biosynthesis related gene families with high paralog numbers, without a clear phenotype.

If filamentous fungi possess an α-glucan-chitin-interaction redundancy mechanism that renders that *crh* gene family dispensable, why do filamentous fungi contain more *crh* copies than yeast-like fungi that do not possess α-glucan? What is the evolutionary advantage that drove the duplication to attain so many *crh* genes? A possible explanation for the high number of *crh* paralogs is the diversity in developmental stages of filamentous fungi compared to unicellular growth. It is true that multi-condition expression data analysis showed differential expression of *crh* genes during different developmental conditions (Table 4, **Chapter 3**). Nevertheless, lack of Crh enzymes did not seem to affect cell wall integrity, vegetative growth, growth rate, sporulation or even formation of sclerotia. Therefore, it is difficult to see the morphological differentiation of filamentous fungi as an argument to explain the existence of so many *crh* genes, especially if α-glucan interactions with chitin suffice for structural cell wall integrity. However, it is worth noting that the evolution of cell wall α-glucan is considered to have emerged after the introduction of the *crh*-facilitated β-glucan to chitin transglycosylation (Kiss et al., 2019); possibly allowing selection pressure to drive the diversification of Crh enzymes during different growth conditions before the occurrence of α-glucan. The subsequent evolution of α-glucan—already recognized as an important virulence factor for pathogenic fungi and conidial aggregation factor in non-pathogenic species (Yoshimi et al., 2017)—may thus have gained an additional benefit as a chitin-interacting polymer that creates an additional layer of cell wall integrity.

If α-glucan provides such a beneficial role, this would mean one of two things for the *crh* gene family: i) The *crh* genes have become obsolete in all filamentous fungi that also possess α-glucan in their cell walls. Therefore, one would expect either gene loss or detrimental effects such as digression into pseudogenes, but no such detrimental effects are observed as active sites and substrate binding pockets are conserved. It is therefore likely that Crh enzymes still perform a relevant function. ii) There is still a benefit of having the *crh* gene family, but the benefit may be unclear under laboratory testing conditions. Singular phenotypic assessments may hamper the interpretation of the biological relevance of this multi-paralog gene family. In other words, we might fail to see how the disruption of (what we see as) one process, is actually not just a standalone component. Instead, the process of cell wall cross-linking has become an integral part of cell wall construction in conjunction with its other elements. This means that selection pressure for cell wall integrity may not occur at the level of individual components per se, but rather on the cell wall as a whole. To put this in context, the natural habitat of *A. niger* is the soil which poses a nutrient poor and competitive environment that is filled with hostile organisms competing over nutrients. These competitors possess an arsenal of various biological weapons that include chitinases and other putative cell wall destructive enzymes, and may attack the cell wall at structurally different levels. As such, having multiple layers of redundant mechanisms to maintain cell wall integrity makes a bit more sense from a biological perspective.

3. Exploitation of cell wall mutants for increased chitin production

Chitin consists of poly-β-1,4-linked *N*-acetyl-glucosamine that makes up a significant fraction (~16%) of the cell wall of *A. niger* (Isaza-Pérez et al., 2020). To synthesize chitin, UDP-*N*-acetyl-glucosamine monomers are assembled into a chitin chain by chitin synthases. At the cytosolic side of the plasma membrane, chitin synthases add UDP-*N*-acetyl-glucosamine monomers to the non-reducing end of an existing chitin chain in a β(1→4) fashion, a process in which UDP is cleaved off. Because chitin synthases reside in the plasma membrane, the chitin chain is protruded from the cytosol, through the chitin synthase, into the periplasmic space where it becomes part of the cell wall. Once in the cell wall, chitin can either be cross-linked to β-1,3-glucan or remain un-linked as "free" chitin. Chitin can also be remodeled through change of acetylation patterns or degree of polymerization by chitin deacetylases and chitinases/chitosinases, respectively. Break-down can either lead to chitooligosaccharides (COS) or *N*-acetylglucosamine/glucosamine monomers that can be reused in the chitin biosynthesis pathway (Figure 3). Because the length of and rate

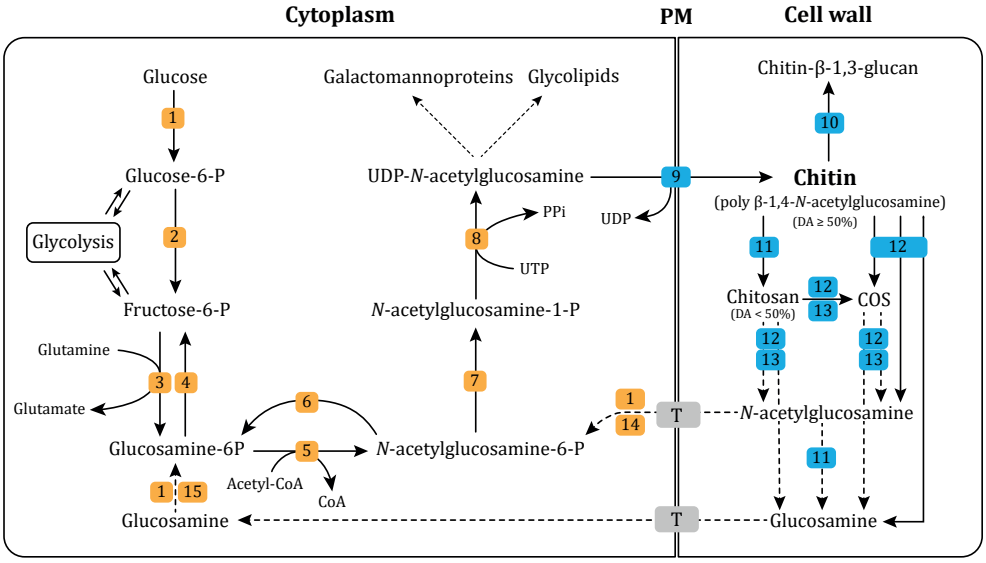

Figure 3. Chitin synthesis, cell wall incorporation and recycling in filamentous fungi. Glucose is converted to glucose-6-phosphate by a hexokinase (1) and is either used for glycolysis or converted to fructose-6-phosphate by glucose-6-phosphate isomerase (2). Fructose-6-phosphate can also either be used in glycolysis or branches off to the chitin biosynthesis pathway. Next, fructose-6-phosphate receives an amino group from glutamine that results in glucosamine-6-phosphate (GlcN-6-P), catalyzed by a glutamine-fructose-6-phosphate amidotransferase (3). Reversion can be facilitated by a glucosamine-6-phosphate deaminase (4). Chitin synthesis continues by the addition of an acetyl group to GlcN-6-P via donation of acetyl-CoA, catalyzed by glucosamine-6-phosphate acetyltransferase (5), resulting in *N*-acetylglucosamine-6-phosphate (GlcNAc-6-P). Also, the reverse reaction is possible here following the deacetylation of GlcNAc-6-P via the *N*-acetylglucosamine deacetylase (6). To continue chitin synthesis, GlcNAc-6-P goes on to be altered to *N*-acetylglucosamine-1-phosphate (GlcNAc-1-P) by a phosphoacetylglucosamine mutase (7). GlcNAc-1-P is then uridinylated by UDP- *N*-acetylglucosamine pyrophosphorylase (8), using UTP as a donor molecule, yielding UDP- *N*-acetylglucosamine (UDP-GlcNAc). UDP-GlcNAc is the precursor molecule that is used by the transmembrane-spanning chitin synthases (9) that remove UDP and add GlcNAc to the non-reducing end of a nascently formed β-1,4-linked GlcNAc polymer, called chitin. As such, chitin synthases protrude chitin chains

across the plasma membrane (PM) into the cell wall. Subsequently, cell wall chitin can either be cross-linked to β-1,3-glucan by chitin transglycosylases (10) or remain as "free" non-covalently interacting polymer in the cell wall. Chitin remains defined as chitin as long as the degree of acetylation (DA) is equal to or higher than 50% (i.e. GlcNAc ≥ GlcN). Below 50% acetylation (i.e. GlcNAc < GlcN), the polymer is referred as chitosan. Chitin deacetylases (11) actively contribute to the deacetylation of chitin and facilitate formation of chitosan. Both chitin and chitosan can be degraded by endo- and exo-acting chitinases (12) and chitosinases (13), resulting in either monomers of GlcNAc/GlcN or chitooligosaccharides (COS). Both GlcNAc and GlcN can putatively be transported into the cell via either specific GlcNAc/GlcN transporters or by promiscuous hexose transporters (T). Here, the GlcNAc/GlcN building blocks can be reintegrated into the chitin biosynthesis pathway via phosphorylation by hexokinases (1) or specific GlcNAc and GlcN kinases, respectively (14, 15). Solid lines define established in literature routes, dashed lines represent putative routes and frequently interspaced dashed lines depict alternative biosynthetic pathways using UDP-GlcNAc. Respective genes in *Aspergillus niger* that correspond to steps 1-8, 14 and 15 (yellow) are shown in Table 1, and steps 9-13 (blue) are shown in Supplementary table 1.

of which the chitin polymers are synthesized is dictated by the available concentration of UDP-*N*-acetyl-glucosamine (Kang et al., 1984; Keller and Cabib, 1971; Orlean and Funai, 2019; Peter, 1987; Sburlati and Cabib, 1986), the synthesis of UDP-*N*-acetyl-glucosamine is considered a primary rate-limiting step in chitin biosynthesis (Merzendorfer, 2011). UDP-*N*-acetyl-glucosamine synthesis shares part of the glycolysis pathway and splits off when fructose-6-phosphate is converted to glucosamine-6-phosphate via a glutamine-fructose-6-phosphate-amidotransferase, at the expense of glutamine (donating an amino-group which converts glutamine to glutamate). Glucosamine-6-phosphate is then acetylated to *N*-acetyl-glucosamine-6-phosphate, using acetyl-CoA as a substrate, and converted to *N*-acetyl-glucosamine-1-phosphate prior to becoming UDP-*N*-acetyl-glucosamine via donation of a UTP molecule. The UDP-*N*-acetylglucosamine is used for the synthesis of chitin. As mentioned above, chitin is remodeled and can be broken down in the cell wall. The resultant products, glucosamine and *N*-acetylglucosamine, can be taken up by hexosamine transporters into the cytosol. Glucosamine and *N*-acetylglucosamine can either be reused for chitin synthesis or they are catabolized to fructose-6-phosphate where they can be re-routed into glycolysis to provide energy for the cell. The required proteins for chitin catabolism, a *N*-acetylglucosamine transporter, *N*-acetylglucosamine deacetylase and a glucosamine-6-phosphate deaminase, are all found in the same gene cluster. This cluster also harbors two putative transcription factors (An16g08990 (*farB*) and An16g09150), a glucose-methanol-choline (GMC) oxidoreductase (An16g09050), a dehydrogenase (An16g09060), a protease (An16g09010) and a *N*-acetyl transferase (An16g09090). All enzymes that are involved in the chitin biosynthetic and catabolic pathways of *A. niger* are shown in Table 1 (and in more detail in Supplementary table 1), and are schematically shown in Figure 3.

The expression of *A. niger gfaA* (glutamine-fructose-6-phosphate-amidotransferase A) was shown to be first rate-limiting step in chitin synthesis (Ram et al., 2004). Additionally, *gfaA* expression was increased together with an elevated levels of chitin content upon activation of the cell wall integrity (CWI) pathway in *A. niger* (Ram et al., 2004). The CWI pathway s highly conserved among fungi, triggered by either disruption or misconstruction of the cell wall (Dichtl et al., 2016). Next to *A. niger*, activation of the CWI pathway has also been shown to cause increased cell wall chitin deposition in other fungi (Fortwendel et al., 2010; Heilmann et al., 2013; Walker et al., 2015,

2008). Aside from expression of *gfaA*, *agsA* (α-glucan synthase A) has also been shown to be induced upon cell wall stress (Damveld et al., 2005b) in *A. niger*, suggesting that simultaneous expression of both *agsA* and *gfaA* upon cell wall stress is relevant for fortifying the cell wall structure. This evidence was recently corroborated by a detailed study of intact *A. fumigatus* cell walls. It was shown that chitin and α-glucan tightly interact, non-covalently, deep inside the cell wall, forming a hydrophobic core that is of structural importance for cell wall integrity (Kang et al., 2018).

In a previous study of our lab, a positive screening method was constructed in an attempt to

Table 1. Enzymes involved in the chitin biosynthetic and catabolic pathways of *Aspergillus niger*. Enzymes are related to steps in Figure 3. In those cases where the corresponding genes have not been named and/or linked to a gene identifier in *Aspergillus niger,* n.a. (not available) is indicated.

Step	Enzyme action	Enzyme entry	gene	CBS513.88 ID	NRRL3_ID
1	Glucokinase	EC 2.7.1.1	*glkA*	An12g08610	NRRL3_03068
	Hexokinase		*hxkA*	An02g14380	NRRL3_05100
	Putative hexokinase		-	An13g00510	NRRL3_01532
	Putative hexokinase		-	An06g00380	NRRL3_11729
2	Glucose-6-P isomerase	EC 5.3.1.9	*pgiA*	An16g05420	NRRL3_06888
3	Glutamine-fructose-6-phosphate amidotransferase (GFAT)	EC 2.6.1.16	*gfaA*	An18g06820	NRRL3_10711
			gfaB	An03g05940	NRRL3_08347
4	Glucosamine-6-P (GlcN-6-P) deaminase	EC 3.5.99.6	-	An16g09070	NRRL3_06624
5	GlcN-6-P acetyltransferase	EC 2.3.1.4	*gnaA*	An12g07840	NRRL3_03114
6	*N*-acetylglucosamine (GlcNAc) deacetylase	EC 3.5.1.25	-	An16g09040	NRRL3_06627
7	Phosphoacetylglucosamine mutase	EC 5.4.2.3	*pcmA*	An18g05160 An18g05170	NRRL3_10581
8	UDP-GlcNAc pyrophosphorylase	EC 2.7.7.23	*ugnA*	An12g00480	NRRL3_09173
9	Chitin synthase	EC 2.4.1.16	10	**	**
10	Chitin transglycosylase	EC 3.2.1.-/ 2.4.1.-	7	**	**
11	Chitin deacetylase/chitooligo deacetylase	EC 3.5.1.41/3.5.1.-	8	**	**
12	Chitinase (endo)/GlcNAc glucosaminidase (exo-chitinase)	EC 3.2.1.14/ 3.2.1.52	13*	**	**
13	Chitosinase (exo/endo)	EC 3.2.1.132	2	**	**
14	GlcNAc kinase	EC 2.7.1.59	n.a.	n.a.	n.a.
15	GlcN kinase	EC 2.7.1.8	n.a.	n.a.	n.a.
T	Putative GlcNAc transporter	n.a.	n.a.	An16g09020	NRRL3_06628
	Putative UDP-GlcNAc transporter	n.a.	n.a.	An03g06940	NRRL3_08261

*Number of (putative) chitinases is 13 for CBS513.88 and 14 for NRRL3. Between the two strains, five chitinases are not shared, i.e. there are no corresponding orthologues (and gene IDs) present.

**See Supplementary table 1 for details on gene IDs

identify genes that are required for correct cell wall biosynthesis, lack of which would cause loss of cell wall integrity. At the time, the reported 20-fold induction of *agsA* expression during cell wall stress was exploited in a UV-mutagenesis screen to find mutants with a continuous state of cell wall stress (Damveld et al., 2008). This system yielded 240 cell wall mutant strains with a constitutively activated CWI pathway, based on *agsA* expression. Several mutants from this collection been characterized over the last few years and include a *ΔtupA* (general transcription repressor) mutant (Schachtschabel et al., 2013), the *ΔugmA* (galactofuranose synthesis) strain (Damveld et al., 2008), a deletion of which absolves cell wall galactofuranose and results in increased chitin content (El-Ganiny et al., 2008 and own observations), along with a verified upregulation of *gfaA* during transcriptomic analysis (Park et al., 2016). Other mutants that were isolated and characterized from this UV-screen are *vmaD* (vacuolar H(+)-ATPase (V-ATPase) subunit d) and *ugeA* (galactofuranose synthesis), but were not tested for cell wall chitin content, though *ΔvmaD* did not show increased CFW staining (Park et al., 2014; Schachtschabel et al., 2012).

Using the same cell wall mutant library as listed above, we screened for mutants with increases in cell wall chitin content, as described in **Chapter 4**. From this screen two candidates were selected with an increased chitin content, RD15.4#55 and RD15.8#16, which were separately characterized in **Chapter 4** and **Chapter 5**, respectively. Characterization of both mutants RD15.4#55 and RD15.8#16 resulted in the identification of two genes that were previously unknown to be involved in the CWI pathway, *cwcA* and *gdiA*. The former gene was named after the cell wall chitin (*cwcA*) increase and encodes a putative repressor of which we postulate that, under non-inducing conditions, represses the activation of the CWI pathway (**Chapter 4**). The latter gene (*gdiA*), Rab GDP dissociation inhibitor (GDI) A, regulates the balance of GTPase cycling between GDP and GTP bound states. GTP-bound, a GTPase is active and interacts with effector proteins, transports vesicles, assists in cargo selection, forms vesicles from membranes and assist fusion of vesicles with the target membranes (Oesterlin et al., 2014). Post-effector interaction, the active GTP-bound GTPase is hydrolyzed to its inactive GDP-bound form, a process which prevents further effector-interaction. Rab GDIs specifically bind the GDP-bound form and solubilize the inactive GTPases from membranes into the cytosol, preventing direct turnover of GDP to GTP (Pfeffer and Aivazian, 2004; Schalk et al., 1996; Ullrich et al., 1993). As such, GDIs act as negative regulators of GTPase cycling between active and inactive form. We identified that a full knockout of the *gdiA* gene is lethal, but that reduced levels of correct transcript result in a chitin increase in the cell wall (**Chapter 5**).

The genes *cwcA* and *gdiA* can, together with other identified mutated genes from the cell wall mutant library, *tupA*, *ugmA*, *ugeA* and *vmaD*, be effectively categorized into three specific functional groups:

i) Both *ugmA* and *ugeA* are involved in the **synthesis** of galactofuranose (Gal*f*), a principle component that is important for the integrity of the cell wall. Gal*f*-conjugates can be found in parts of the galactomannan fraction, *N*-glycan moiety of extracellular glycoproteins and in glycosylinositolphosphoceramides (Tefsen et al., 2012). It remains unknown to what extent

disruption of either one these elements contributes to the activation of the CWI pathway specifically or whether they all contribute equally.

ii) Enzymes VmaD and GdiA are both involved in the **transport** of other enzymes through the secretory pathway. The subunit d of the V-ATPase complex that *vmaD* encodes, is required for a functional V-ATPase that helps acidify intracellular compartments, including vacuoles, endosomes and late Golgi compartments. Organelle acidification has been shown to be important in protein sorting, in biosynthetic and endocytic pathways, proteolytic activation of zymogen precursors and transmembrane transport (Forgac, 2007; Nishi et al., 2003). A full gene disruption of *vmaD* showed a more severe phenotype than the original conditional mutant (RD6.13#15). Similarly, as described above, for *gdiA*, only a conditional mutant with reduced transcription levels was viable, whereas a full knockout was lethal, suggesting that both VmaD and GdiA play an important role in the secretory pathway, possibly for the transport of cell wall biosynthesis proteins and/or the synthesis and secretion of galactomannan or (galactomannoproteins) in the secretory system.

iii) A final class of enzymes acts on a higher regulatory level, encompassing *cwcA* and *tupA*, which both act as **transcriptional repressors** of the CWI pathway. Both deletions of *cwcA* and *tupA* caused pleiotropic effects which can be expected for regulatory genes, among which is the production of differently colored pigments that often related activation of secondary metabolite clusters. It is known that secondary metabolite gene clusters can be activated by the CWI pathway (Valiante, 2017), but does not appear to be universally induced—at least not to the same extent—in the cell wall mutants studied in our work.

Together, the different classes of cell wall mutants derived from this screen are involved in **precursor synthesis, protein transport** or **transcriptional repression**, but no enzymes directly involved in the synthesis of cell wall elements have been identified, such as chitin or glucan synthases. Clearly, the recurrent observations of 17 *tupA* mutants (Schachtschabel et al., 2013) and 4 *ugmA* mutants (Damveld et al., 2008) suggests saturation of this screen. Contrarily, only one mutant was identified for *ugeA*, also involved in Gal*f* synthesis and showing a similar colony phenotype to *ΔugmA*. This suggests that certain mutations may be more likely to occur in this screen even if they are part of the same (synthesis) process.

In **Chapter 6** we assessed the effects of a *kexB* deletion which also resulted in a higher chitin content and found transcriptional upregulation of both *agsA* and *gfaA* for the *ΔkexB* strain. The *ΔkexB* strain was selected separately from the UV-mutant screen based on its morphology and thicker cell walls (Jalving et al., 2000; Punt et al., 2003). Cell wall analysis showed increased chitin deposition which corroborated the observed expression levels for *agsA* and *gfaA*. The KexB enzyme is present on the membranes of the secretory pathway—mainly inside the Golgi apparatus by means of a Golgi retention signal (Jalving, 2005)—and may be categorized as a **transport** related class of cell wall mutants, similar to VmaD and GdiA. Its function is related the correct sorting or zymogenic activation of certain (cell wall biosynthesis) proteins. However, whether lack of KexB is directly related to activation of the CWI pathway as a consequence for the incorrect processing and sorting of cell wall biosynthesis proteins remains unknown.

4. Outlook and future perspectives

The FunChi project set out to optimize the process of chitosan extraction from fungal biomass waste. In order to increase the total yield, two different strategies were employed: removal of covalent cross-links of chitin to the cell wall and increase overall chitin composition. To this end, we analyzed an existing cell wall mutant collection that was previously obtained using a forward genetics screen for mutants with increased alpha-glucan synthase A (*agsA*) expression. The approach has led to the identification of a GdiA mutant strain that produces approximately 60% more cell wall chitin (26% of the cell wall dry weight) than its parental strain (16% of the cell wall dry weight), shown in **Chapter 5**. However, it remains unknown if this is the maximum attainable increase in cell wall chitin content and, if this would already represent an economic feasibility. If further increase is desired, it is also important to gauge the effect on primary product yields. The primary purpose of large-scale fermentations is generally to produce a desired compound in the most efficient way possible with an optimal conversion of energy (glucose) into the production of, for example, citric acid. Because glucose is also required for the synthesis of the cell wall, including chitin (Figure 3), an increase in chitin content directly competes with the available sugars for the desired product, which could be considered as an unfavorable outcome. Consequently, it may only be feasible to increase chitin content if, for example, cell wall α-glucans and β-glucans levels are reduced to compensate for increased chitin content. Alternatively, the extra chitin yield may provide additional value that offsets the loss in e.g. citric acid production. These considerations are outside the scope of this thesis, but are worth investigating if the commercial production of fungal-derived chitosans is to take off in order to compete with the current crustacean chitosan supply.

Instead of focusing on increasing chitin production, it may actually also be very interesting to find clever and cheaper ways to extract chitins and chitosans from fungal mycelial waste. Part of the work described in this thesis (**Chapter 2** and **Chapter 3**) set out in this direction by removing the Crh enzymes that were expected to facilitate covalent links of chitin to the cell wall. Our discoveries have led to the conclusion that removal of these Crh enzymes does not appear to weaken the cell wall at all. These observations can be explained by the possibility that chitin also interacts with α-glucan. We showed that only the knockout of the entire *crh* gene family combined with α-glucan synthase knockouts weakened the cell wall, whereas either knockouts of α-glucan synthases or all *crh* genes alone did not. Therefore, a lot more may be gained by removing all α-glucan synthases in conjunction with the removal of the *crh* gene family to enhance extraction of chitin from cell walls. In addition, removal of α-glucan is expected to reduce both mycelial clumping—causing more dispersed growth as seen in other *Aspergilli* (Yoshimi et al., 2017)—and reducing stirring viscosity, another problem in large scale fermentations (Cai et al., 2014; Papagianni, 2004). In fact, the disruption of *agsE* has already been explored for industrial purposes to increase production yields (van Peij et al., 2014). Reduction in stirring viscosity is also worth exploring further for the *kexB* deletion strain. The *kexB* disruption showed some of these reduced viscosity characteristics next to an increased cell wall chitin content, and the *kexB* deletion has already been combined

with the *crh* gene family knockout (**Chapter 6**), and now requires further investigation for its economic feasibility in industrial application.

There are alternatives ways to screen for mutants with increase chitin content in the cell wall of fungi. A logical experiment would be to create a similar reporter strain for a forward genetic screen that does not rely on *agsA* expression, but rather on chitin precursor synthesis directly, i.e. *gfaA* (or its paralog *gfaB*, Table 1). In this way, one looks directly to gene expression for the synthesis of UDP-*N*-acetyl-glucosamine instead of coincidental expression with *agsA*, which does not occur in all cell wall mutants as seen in **Chapter 4**. The use of the *gfaA* promoter was initially considered for the construction of the UV-mutant library, but was less favorable due to the relatively high baseline expression under non-cell wall stress conditions (Damveld et al., 2008). However, *gfaB* shows relatively low expression levels under non-cell wall stress conditions, similar to those of *agsA* (expression data of wild type in **Chapter 3** and **Chapter 6**) and was strongly induced in the *ΔugmA* strain (FC 119) (Park et al., 2016), and induced in the *ΔkexB* strain (FC 6.21), described in **Chapter 6**. In addition to reporter-based screening, one could also employ adaptive evolution in the presence of cell wall disturbing compounds such as caspofungin, a known echinocandin to induce cell wall chitin deposition through activation of the CWI pathway (Walker et al., 2015, 2008). Because both adaptive evolution and reporter-based screening techniques typically yield loss of function mutations, one might also consider a more directed strain engineering approach to increase chitin content in fungal cell walls. As such, overexpression of both of *gfaA* and *gfaB* may improve the total concentration of cytosolic UDP-*N*-acetyl-glucosamine. Additionally, again with the rise the CRISPR/Cas9 era, it will be much easier to generate strains with overexpression of all genes involved in the chitin biosynthesis pathway from the first hexokinase step, down to last UDP-*N*-acetyl-glucosamine pyrophosphorylase reaction (Table 1). Overexpression of putative regulatory elements for chitin synthesis or chitin synthase genes may be less favorable, as chitin synthases are under different transcriptional regulation and the mRNA transcript levels do not necessarily correlate to chitin synthase activity or chitin content due to post-transcriptional and post-translational modifications (Rogg et al., 2012). In similar multi-gene strategies, one could include the selective elimination of chitinases, with a possible caveat that disruption of all chitinases may hamper germination or hyphal growth (Takaya et al., 1998).

The way forward in either screening or designing mutant strains that produce more cell wall chitin ultimately depends on the requirements versus the trade-offs attached to each approach. The issues imposed by the FunChi project were to both increase chitin production and enhance extractability of chitin from fungal cell walls, through strain optimization. In this thesis, three mutants were described with increased cell wall chitin deposition as a result of cell wall stress. Next to determination of cell wall chitin content, the entire cell wall composition of all three mutants, *cwcA, gdiA* and *kexB,* is currently being analyzed in detail, using the monosaccharide analysis as described in **Chapter 3**. Additionally, fractionated cell wall samples of the three chitin mutants are being tested for their effect on the plant immune response. Both these cell wall content and efficacy tests are absolutely essential to assess whether the cell walls of these mutants

can be turned into an applied plant bio-stimulant. Additionally, it is required to know how these mutations would translate to the phenotype of an industrial strain and how they affect production parameters. With the exception of *ΔkexB*, it remains unknown whether these mutations affect growth rate. During the FunChi project, it was opted to introduce cell wall mutations in industrial strains which are notoriously difficult to transform. Successful knockouts have been introduced in an industrial strain using the CRISPR/Cas9 approach described in this thesis, demonstrating the system's effectiveness. Lastly, as mentioned above, we have obtained new insights in chitin to cell wall cross-linking. We showed evidence that suggests chitin-α-glucan interactions may act as a level of redundancy in cell wall integrity for α-glucan containing filamentous fungi. These novel observations pave the road towards directed strain design that would allow easier extraction from fungal cell walls in the future. The findings presented here and the ongoing work by the FunChi partners all contribute to the common project goal of valorizing spent fungal biomass.

Supplementary table 1. Enzymes involved in the chitin biosynthesis pathway.

Step	Enzyme action	Enzyme entry	CAZy entry	Gene	Annotation	CBS513.88_ID	NRRL3_ID
1	Hexokinase	EC 2.7.1.1	n.a.	*glkA*	Glucokinase	An12g08610	NRRL3_03068
				hxkA	Hexokinase	An02g14380	NRRL3_05100
				-	Putative hexokinase	An13g00510	NRRL3_01532
				-	Putative hexokinase	An06g00380	NRRL3_11729
2	Glucose-6-P isomerase	EC 5.3.1.9	n.a.	*pgiA*	Putative glucose-6-phosphate isomerase	An16g05420	NRRL3_06888
3	Glutamine-fructose-6-phosphate amidotransferase (GFAT)	EC 2.6.1.16	n.a.	*gfaA*	GFAT	An18g06820	NRRL3_10711
				gfaB	GFAT	An03g05940	NRRL3_08347
4	Glucosamine-6-P (GlcN-6-P) deaminase	EC 3.5.99.6	n.a.	-	GlcN-6-P deaminase	An16g09070	NRRL3_06624
5	GlcN-6-P acetyltransferase	EC 2.3.1.4	n.a.	*gnaA*	GlcN-6-P acetyltransferase	An12g07840	NRRL3_03114
6	*N*-acetylglucosamine (GlcNAc) deacetylase	EC 3.5.1.25	n.a.	-	Putative GlcNAc deacetylase	An16g09040	NRRL3_06627
7	Phosphoacetylglucosamine mutase	EC 5.4.2.3	n.a.	*pcmA*	Phosphoacetylglucosamine mutase	An18g05160 An18g05170*	NRRL3_10581
8	UDP-GlcNAc pyrophosphorylase	EC 2.7.7.23	n.a.	*ugnA*	UDP-GlcNAc pyrophosphorylase	An12g00480	NRRL3_09173

Supplementary table 1. Enzymes involved in the chitin biosynthesis pathway. (Continued)

Step	Enzyme action	Enzyme entry	CAZy entry	Gene	Annotation	CBS513.88_ID	NRRL3_ID
9	Chitin synthase	EC 2.4.1.16	GT2	*chsA*	Chitin synthase	An07g05570	NRRL3_04653
				chsB	Chitin synthase class III	An09g04010	NRRL3_00331
				-	Chitin synthase class II	An08g04350	NRRL3_11077
				chsD	Chitin synthase class IV	An09g02290	NRRL3_00179
				chsE	Chitin synthase class III	An12g10380	NRRL3_02932
				chsG	Chitin synthase class VI	An08g05290	NRRL3_11152
				chsL (csmB)	Chitin synthase class VII/class V myosin motor domain	An02g02340	NRRL3_06067
				chsM (csmA)	Chitin synthase class VII/class V myosin motor domain	An02g02360	NRRL3_06066
				chsF	Chitin synthase class III	An03g06360	NRRL3_08320
				chsC	Chitin synthase class I	An14g00650 An14g00660*	NRRL3_00641
10	Chitin transglycosylase	EC 3.2.1.-/2.4.1.-	GH16	*crhA*	GH16_2	An11g01540	NRRL3_10021
				crhB	GH16_2	An07g07530	NRRL3_04809
				crhC	GH16_2	An07g01160	NRRL3_04315
				crhD	GH16_2	An01g11010	NRRL3_02532
				crhE	GH16_2	An13g02510	NRRL3_01365
				crhF	GH16_2	An16g02850	NRRL3_07085
				crhG	GH16_2	An15g05350	NRRL3_03998

Supplementary table 1. Enzymes involved in the chitin biosynthesis pathway. (Continued)

Step	Enzyme action	Enzyme entry	CAZy entry	Gene	Annotation	CBS513.88_ID	NRRL3_ID
11	Chitin deacetylase/chitooligo deacetylase	EC 3.5.1.41/3.5.1.-	CE4	*cdaA*	Putative chitin deacetylase	An04g07110	NRRL3_07680
				cdaB	Putative chitin deacetylase	An12g04480	NRRL3_03397
				cdaC	Putative chitin deacetylase	An11g00920	NRRL3_10065
				cdaD	Putative chitin deacetylase	An18g04560	NRRL3_10540
				cdaE	Putative chitin deacetylase	An02g13530	NRRL3_05169
				cdaF	Putative chitin deacetylase	An08g09290	NRRL3_11464
				cdaG	Putative chitin deacetylase	An01g13340	NRRL3_02724
				cdaH	Putative chitin deacetylase	An15g00280	NRRL3_03591
12	Chitinase (endo)	EC 3.2.1.14	GH18	*cfcA*	Putative endochitinase, class V	An02g07020	NRRL3_05709
				chiD/ cfcB	Putative chitinase	An08g09030	NRRL3_11445
				cfcC	Putative chitinase	An04g04670	NRRL3_07862
				cfcD	Putative chitinase	An01g05360	NRRL3_02063
				cfcE	Putative chitinase	An15g00840	NRRL3_03643
				cfcF	Putative chitinase	An11g01160	NRRL3_10047
				cfcG	Putative chitinase	An19g00100	NRRL3_01224
				cfcH	Chitinase; endochitinase	An14g07420	n.a.
				cfcI	Endochitinase	An02g13580	NRRL3_05164
				cfcJ	Hydrolase activity	An11g05860	NRRL3_09665
				cfcK	Putative chitinase	An12g05330	n.a
				ctcA	GPI-anchored chitinase	An09g06400	NRRL3_00523
				-	Putative chitinase	n.a.	NRRL3_01212
				ctcB	Putative chitinase	An09g05920	NRRL3_00478
				-	Putative chitinase	n.a.	NRRL3_04221
				-	Putative chitinase	n.a.	NRRL3_09653

Supplementary table 1. Enzymes involved in the chitin biosynthesis pathway. (Continued)

Step	Enzyme action	Enzyme entry	CAZy entry	Gene	Annotation	CBS513.88_ID	NRRL3_ID
12	GlcNAc glucosaminidase (exo-chitinase)	EC 3.2.1.52	GH20	*nagA*	Putative *N*-acetylglucosaminidase	An09g02240	NRRL3_00174
				-	Putative *N*-acetyl glucosaminidase	An03g02960	NRRL3_08564
				-	Putative *N*-acetylglucosaminidase	An01g01920	NRRL3_01790
13	Chitosinase (exo/endo)	EC 3.2.1.132	GH75/ GH46	-	Putative chitosinase	An03g05260	NRRL3_08400
				-	Putative chitosinase	An04g04530	NRRL3_07870
14	GlcNAc kinase	EC 2.7.1.59	n.a.	n.a.	n.a.	n.a.	n.a.
15	GlcN kinase	EC 2.7.1.8	n.a.	n.a.	n.a.	n.a.	n.a.
T	(UDP-)GlcNAc transporter	n.a.	n.a.	n.a.	Putative GlcNAc transporter	An16g09020	NRRL3_06628
				n.a.	Putative UDP-GlcNAc transporter	An03g06940	NRRL3_08261

7

References

Abenza, J.F., Galindo, A., Pantazopoulou, A., Gil, C., De Los Ríos, V., Peñalva, M.A., 2010. *Aspergillus* RabB^{Rab5} integrates acquisition of degradative identity with the long distance movement of early endosomes. Mol. Biol. Cell 21, 2756–2769. https://doi.org/10.1091/mbc.E10-02-0119

Achstetter, T., 1989. Regulation of alpha-factor production in *Saccharomyces cerevisiae*: a-factor pheromone-induced expression of the MF alpha 1 and STE13 genes. Mol. Cell. Biol. 9, 4507–4514. https://doi.org/10.1128/mcb.9.10.4507

Adeyeye, S.A.O., 2016. Fungal mycotoxins in foods: A review. Cogent Food Agric. 2. https://doi.org/10.1080/23311932.2016.1213127

Aebi, M., Hornig, H., Weissmann, C., 1987. 5′ cleavage site in eukaryotic pre-mRNA splicing is determined by the overall 5′ splice region, not by the conserved 5′ GU. Cell 50, 237–246. https://doi.org/10.1016/0092-8674(87)90219-4

Afroz, S., El-Ganiny, A.M., Sanders, D.A.R., Kaminskyj, S.G.W., 2011. Roles of the *Aspergillus nidulans* UDP-galactofuranose transporter, UgtA in hyphal morphogenesis, cell wall architecture, conidiation, and drug sensitivity. Fungal Genet. Biol. 48, 896–903.

Aguilar-Pontes, M. V., Brandl, J., McDonnell, E., Strasser, K., Nguyen, T.T.M., Riley, R., Mondo, S., Salamov, A., Nybo, J.L., Vesth, T.C., Grigoriev, I. V., Andersen, M.R., Tsang, A., de Vries, R.P., 2018. The gold-standard genome of *Aspergillus niger* NRRL3 enables a detailed view of the diversity of sugar catabolism in fungi. Stud. Mycol. 91, 61–78. https://doi.org/10.1016/j.simyco.2018.10.001

Akcapinar, G.B., Kappel, L., Sezerman, O.U., Seidl-Seiboth, V., 2015. Molecular diversity of LysM carbohydrate-binding motifs in fungi. Curr. Genet. 61, 103–113. https://doi.org/10.1007/s00294-014-0471-9

Aleksenko, I. Nikolaev, Y. Vinetski, A.J.C., 1996. Gene expression from replicating plasmids in *Aspergillus nidulans*. Mol. Genet. Genomics 253, 242–246.

Andersen, M.R., Lehmann, L., Nielsen, J., 2009. Systemic analysis of the response of *Aspergillus niger* to ambient pH. Genome Biol. 10, R47. https://doi.org/10.1186/gb-2009-10-5-r47

Aranaz, I., Mengibar, M., Harris, R., Panos, I., Miralles, B., Acosta, N., Galed, G., Heras, A., 2009. Functional Characterization of Chitin and Chitosan. Curr. Chem. Biol. 3, 203–230. https://doi.org/10.2174/2212796810903020203

Arentshorst, M, Lagendijk, E.L., Ram, A.F.J., 2015. A new vector for efficient gene targeting to the *pyrG* locus in *Aspergillus niger*. Fungal Biol. Biotechnol. 2, 2. https://doi.org/10.1186/s40694-015-0012-4

Arentshorst, M., Niu, J., Ram, A.F.J., 2015. Efficient generation of *Aspergillus niger* knock out strains by combining NHEJ mutants and a split marker approach., in: van den Berg, M.A., Maruthachalam, K. (Eds.), Genetic Transformation Systems in Fungi Vol .1. Springer International Publishing, pp. 263–272. https://doi.org/10.1007/978-3-319-10142-2_25

Arentshorst, M., Ram, A.F.J., 2018. Parasexual crossings for bulk segregant analysis in *Aspergillus niger* to facilitate mutant identification via whole genome sequencing, in: Methods in Molecular Biology. Humana Press, New York, NY, pp. 277–287. https://doi.org/10.1007/978-1-4939-7804-5_22

Arentshorst, M., Ram, A.F.J., Meyer, V., 2012. Using non-homologous end-joining-deficient strains for functional gene analyses in filamentous fungi. Methods Mol. Biol. 835, 133–150. https://doi.org/10.1007/978-1-61779-501-5_9

Ariyoshi, M., Schwabe, J.W.R., 2003. A conserved structural motif reveals the essential transcriptional repression function of Spen proteins and their role in developmental signaling. Genes Dev. 17, 1909–20. https://

doi.org/10.1101/gad.266203

Arroyo, J., Farkaš, V., Sanz, A.B., Cabib, E., 2016. "Strengthening the fungal cell wall through chitin-glucan cross-links: effects on morphogenesis and cell integrity". Cell. Microbiol. 18, 1239–1250. https://doi.org/10.1111/cmi.12615

Aurich, A., Specht, R., Müller, R.A., Stottmeister, U., Yovkova, V., Otto, C., Holz, M., Barth, G., Heretsch, P., Thomas, F.A., Sicker, D., Giannis, A., 2012. Microbiologically produced carboxylic acids used as building blocks in organic synthesis. Subcell. Biochem. 64, 391–423. https://doi.org/10.1007/978-94-007-5055-5_19

Badawy, M.E.I., Rabea, E.I., Taktak, N.E.M., 2014. Antimicrobial and inhibitory enzyme activity of N-(benzyl) and quaternary N-(benzyl) chitosan derivatives on plant pathogens. Carbohydr. Polym. 111, 670–682. https://doi.org/10.1016/j.carbpol.2014.04.098

Baker, L.G., Specht, C.A., Lodge, J.K., 2011. Cell wall chitosan is necessary for virulence in the opportunistic pathogen *Cryptococcus neoformans*. Eukaryot. Cell 10, 1264–8. https://doi.org/10.1128/EC.05138-11

Bell, A.A., Hubbard, J.C., Liu, L., Michael Davis, R., Subbarao, K. V., 1998. Effects of chitin and chitosan on the incidence and severity of *Fusarium* yellows of celery. Plant Dis. 82, 322–328. https://doi.org/10.1094/PDIS.1998.82.3.322

Bennett, J.W., 2010. An Overview of the Genus *Aspergillus*. Machida, M. and Gomi, K., Eds., *Aspergillus*: Molecular Biology and Genomics.

Bentley, R., Thiessen, C.P., 1957. Biosynthesis of itaconic acid in *Aspergillus terreus*. I. Tracer studies with C14-labeled substrates. J. Biol. Chem. 226, 673–687.

Bin Moon, S., Lee, J.M., Kang, J.G., Lee, N.E., Ha, D.I., Kim, D.Y., Kim, S.H., Yoo, K., Kim, D., Ko, J.H., Kim, Y.S., 2018. Highly efficient genome editing by CRISPR-Cpf1 using CRISPR RNA with a uridinylate-rich 3′-overhang. Nat. Commun. 9, 1–11. https://doi.org/10.1038/s41467-018-06129-w

Blanco, N., Sanz, A.B., Rodríguez-Peña, J.M., Nombela, C., Farkaš, V., Hurtado-Guerrero, R., Arroyo, J., 2015. Structural and functional analysis of yeast *CRH*1 and *CRH*2 transglycosylases. FEBS J. 282, 715–731. https://doi.org/10.1111/febs.13176

Boeke, J.D., La Croute, F., Fink, G.R., 1984. A positive selection for mutants lacking orotidine-5′-phosphate decarboxylase activity in yeast: 5-fluoro-orotic acid resistance. Mol. Gen. Genet. MGG 197, 345–346. https://doi.org/10.1007/BF00330984

Bok, J.W., Noordermeer, D., Kale, S.P., Keller, N.P., 2006. Secondary metabolic gene cluster silencing in *Aspergillus nidulans*. Mol. Microbiol. 61, 1636–1645. https://doi.org/10.1111/j.1365-2958.2006.05330.x

Bos, C.J., Debets, A.J.M., Swart, K., Huybers, A., Kobus, G., Slakhorst, S.M., 1988. Genetic analysis and the construction of master strains for assignment of genes to six linkage groups in *Aspergillus niger*. Curr. Genet. 14, 437–443. https://doi.org/10.1007/BF00521266

Bose, I., Reese, A.J., Ory, J.J., Janbon, G., Doering, T.L., 2003. A Yeast under Cover: the Capsule of *Cryptococcus neoformans*. Eukaryot. Cell 2, 655. https://doi.org/10.1128/EC.2.4.655-663.2003

Braaksma, M., Smilde, A.K., van der Werf, M.J., Punt, P.J., 2009. The effect of environmental conditions on extracellular protease activity in controlled fermentations of *Aspergillus niger*. Microbiology 155, 3430–3439. https://doi.org/10.1099/mic.0.031062-0

Breslow, D.K., Cameron, D.M., Collins, S.R., Schuldiner, M., Stewart-Ornstein, J., Newman, H.W., Braun, S., Madhani, H.D., Krogan, N.J., Weissman, J.S., 2008. A comprehensive strategy enabling high-resolution functional analysis of the yeast genome. Nat. Methods 5, 711–8. https://doi.org/10.1038/nmeth.1234

Brown, J.L., Bussey, H., 1993. The yeast KRE9 gene encodes an O glycoprotein involved in cell surface beta-glucan assembly. Mol. Cell. Biol. 13, 6346–6356. https://doi.org/10.1128/mcb.13.10.6346

Brul, S., King, A., Van Der Vaart, J.M., Chapman, J., Klis, F., Verrips, C.T., 1997. The incorporation of mannoproteins in the cell wall of *S. cerevisiae* and filamentous Ascomycetes. Antonie van Leeuwenhoek, Int. J. Gen. Mol. Microbiol. 72, 229–237. https://doi.org/10.1023/A:1000429208049

Bryant, N.J., Stevens, T.H., 1997. Two separate signals act independently to localize a yeast late Golgi membrane protein through a combination of retrieval and retention. J. Cell Biol. 136, 287–297. https://doi.org/10.1083/jcb.136.2.287

Burset, M., Seledtsov, I.A., Solovyev, V. V, 2000. Analysis of canonical and non-canonical splice sites in mammalian genomes. Nucleic Acids Res. 28, 4364–4375. https://doi.org/10.1093/nar/28.21.4364

Cabib, E., 2009. Two novel techniques for determination of polysaccharide cross-links show that Crh1p and Crh2p attach chitin to both beta(1-6)- And beta(1-3)glucan in the saccharomyces *cerevisiae* cell wall. Eukaryot. Cell 8, 1626–1636. https://doi.org/10.1128/EC.00228-09

Cabib, E., Blanco, N., Grau, C., Rodríguez-peña, J.M., Arroyo, J., 2007. Crh1p and Crh2p are required for the cross-linking of chitin to b(1-6)glucan in the *Saccharomyces cerevisiae* cell wall. Mol. Microbiol. 63, 921–935. https://doi.org/10.1111/j.1365-2958.2006.05565.x

Cabib, E., Farkas, V., Kosík, O., Blanco, N., Arroyo, J., Mcphie, P., 2008. Assembly of the Yeast Cell Wall. Crh1p and Crh2p Act as Transglycosylases in vivo and in vitro. J. Biol. Chem. 283, 29859–29872. https://doi.org/10.1074/jbc.M804274200

Cai, H., Kauffman, S., Naider, F., Becker, J.M., 2006. Genomewide screen reveals a wide regulatory network for di/tripeptide utilization in *Saccharomyces cerevisiae*. Genetics 172, 1459–76. https://doi.org/10.1534/genetics.105.053041

Cai, J., Yang, J., Du, Y., Fan, L., Qiu, Y., Li, J., Kennedy, J.F., 2006. Enzymatic preparation of chitosan from the waste *Aspergillus niger* mycelium of citric acid production plant. Carbohydr. Polym. 64, 151–157. https://doi.org/10.1016/j.carbpol.2005.11.004

Cai, M., Zhang, Ying, Hu, W., Shen, W., Yu, Z., Zhou, W., Jiang, T., Zhou, X., Zhang, Yuanxing, 2014. Genetically shaping morphology of the filamentous fungus *Aspergillus glaucus* for production of antitumor polyketide aspergiolide A. Microb. Cell Fact. 13, 73. https://doi.org/10.1186/1475-2859-13-73

Cairns, T.C., Nai, C., Meyer, V., 2018. How a fungus shapes biotechnology: 100 years of *Aspergillus niger* research. Fungal Biol. Biotechnol. 5, 13. https://doi.org/10.1186/s40694-018-0054-5

Carvalho, N.D.S.P., Arentshorst, M., Kwon, M.J., Meyer, V., Ram, A.F.J., 2010. Expanding the ku70 toolbox for filamentous fungi: establishment of complementation vectors and recipient strains for advanced gene analyses. Appl. Microbiol. Biotechnol. 87, 1463. https://doi.org/10.1007/S00253-010-2588-1

Choi, W.J., Sburlati, A., Cabib, E., 1994. Chitin synthase 3 from yeast has zymogenic properties that depend on both the CAL1 and the CAL3 genes. Proc. Natl. Acad. Sci. U. S. A. 91, 4727–30. https://doi.org/10.1073/pnas.91.11.4727

Cole, G.T., 1996. Basic Biology of Fungi, Medical Microbiology. University of Texas Medical Branch at Galveston.

Corsi, B., Riccioni, L., Forni, C., 2015. In vitro cultures of Actinidia deliciosa (A. Chev) C.F. Liang & A.R. Ferguson: a tool to study the SAR induction of chitosan treatment. Org. Agric. 5, 189–198. https://doi.org/10.1007/s13165-014-0087-x

Damveld, R.A., Arentshorst, M., VanKuyk, P.A., Klis, F.M., Van Den Hondel, C.A.M.J.J., Ram, A.F.J., 2005a. Characterisation of CwpA, a putative glycosylphosphatidylinositol-anchored cell wall mannoprotein in the filamentous fungus *Aspergillus niger*. Fungal Genet. Biol. 42, 873–885. https://doi.org/10.1016/j.fgb.2005.06.006

Damveld, R.A., Franken, A., Arentshorst, M., Punt, P.J., Klis, F.M., Van Den Hondel, C.A.M.J.J., Ram, A.F.J., 2008. A novel screening method for cell wall mutants in *Aspergillus niger* identifies UDP-galactopyranose mutase as an important protein in fungal cell wall biosynthesis. Genetics 178, 873–881. https://doi.org/10.1534/

genetics.107.073148

Damveld, R.A., VanKuyk, P.A., Arentshorst, M., Klis, F.M., Cees A.M.J.J. van den Hondel, A.F.J.R., 2005b. Expression of *agsA*, one of five 1,3-α-D-glucan synthase-encoding genes in *Aspergillus niger*, is induced in response to cell wall stress. Fungal Genet. Biol. 42, 165–177. https://doi.org/10.1016/j.fgb.2004.11.006

Dang, Y., Yang, Q., Xue, Z., Liu, Y., 2011. RNA interference in fungi: Pathways, functions, and applications. Eukaryot. Cell. https://doi.org/10.1128/EC.05109-11

Das, S.N., Madhuprakash, J., Sarma, P.V.S.R.N., Purushotham, P., Suma, K., Manjeet, K., Rambabu, S., Gueddari, N.E. El, Moerschbacher, B.M., Podile, A.R., 2015. Biotechnological approaches for field applications of chitooligosaccharides (COS) to induce innate immunity in plants. Crit. Rev. Biotechnol. https://doi.org/10.3109/07388551.2013.798255

de Castro, E., Sigrist, C.J.A., Gattiker, A., Bulliard, V., Langendijk-Genevaux, P.S., Gasteiger, E., Bairoch, A., Hulo, N., 2006. ScanProsite: detection of PROSITE signature matches and ProRule-associated functional and structural residues in proteins. Nucleic Acids Res. 34, W362–W365. https://doi.org/10.1093/nar/gkl124

De Groot, P.W.J., Ruiz, C., De Vázquez Aldana, C.R., Duenas, E., Cid, V.J., Rey, F. Del, Rodríquez-Peña, J.M., Pérez, P., Andel, A., Caubín, J., Arroyo, J., García, J.C., Gil, C., Molina, M., García, L.J., Nombela, C., Klis, F.M., 2001. A genomic approach for the identification and classification of genes involved in cell wall formation and its regulation in *Saccharomyces cerevisiae*. Comp. Funct. Genomics 2, 124–142. https://doi.org/10.1002/cfg.85

de Nobel, H., Ruiz, C., Martin, H., Morris, W., Brul, S., Molina, M., Klis, F.M., 2000. Cell wall perturbation in yeast results in dual phosphorylation of the Slt2/Mpk1 MAP kinase and in an Slt2-mediated increase in FKS2-*lacZ* expression, glucanase resistance and thermotolerance. Microbiology 146, 2121–2132. https://doi.org/10.1099/00221287-146-9-2121

de Ruiter-Jacobs, Y.M.J.T., Broekhuijsen, M., Unkles, S.E., Campbell, E.I., Kinghorn, J.R., Contreras, R., Pouwels, P.H., van den Hondell, C.A.M.J.J., 1989. A gene transfer system based on the homologous *pyrG* gene and efficient expression of bacterial genes in *Aspergillus oryzae*. Curr. Genet. 16, 159–163. https://doi.org/10.1007/BF00391472

Delley, P.A., Hall, M.N., 1999. Cell wall stress depolarizes cell growth via hyperactivation of RHO1. J. Cell Biol. 147, 163–174. https://doi.org/10.1083/jcb.147.1.163

Deng, M.-D., McMullin, T.W., Grund, A.D., 2005. Metabolic engineering for enhanced production of chitin and chitosan in microorganisms.

Dhillon, G.S., Kaur, S., Brar, S.K., Verma, M., 2012. Green synthesis approach: extraction of chitosan from fungus mycelia. Crit. Rev. Biotechnol. 33, 1–25. https://doi.org/10.3109/07388551.2012.717217

Dhillon, G.S., Kaur, S., Sarma, S.J., Brar, S.K., 2013. Integrated process for fungal citric acid fermentation using apple processing wastes and sequential extraction of chitosan from waste stream. Ind. Crops Prod. 50, 346–351.

Dichtl, K., Samantaray, S., Wagener, J., 2016. Cell wall integrity signalling in human pathogenic fungi. Cell. Microbiol. 18, 1228–1238. https://doi.org/10.1111/cmi.12612

Dijkgraaf, G.J.P., Brown, J.L., Bussey, H., 1996. The KNH1 gene of *Saccharomyces cerevisiae* is a functional homolog of KRE9. Yeast 12, 683–692. https://doi.org/10.1002/(SICI)1097-0061(19960615)12:7<683::AID-YEA959>3.0.CO;2-8

Dong, H., Zheng, J., Yu, D., Wang, B., Pan, L., 2019. Efficient genome editing in *Aspergillus niger* with an improved recyclable CRISPR-HDR toolbox and its application in introducing multiple copies of heterologous genes. J. Microbiol. Methods 163, 105655. https://doi.org/10.1016/J.MIMET.2019.105655

Dyer, P.S., O'Gorman, C.M., 2012. Sexual development and cryptic sexuality in fungi: Insights from *Aspergillus* species. FEMS Microbiol. Rev. https://doi.org/10.1111/j.1574-6976.2011.00308.x

El-Ganiny, A.M., Sanders, D.A.R., Kaminskyj, S.G.W., 2008. *Aspergillus nidulans* UDP-galactopyranose mutase, encoded by *ugmA* plays key roles in colony growth, hyphal morphogensis, and conidiation. Fungal Genet. Biol. 45, 1533–1542. https://doi.org/10.1016/j.fgb.2008.09.008

El Gueddari, N.E., Kolkenbrock, S., Schaaf, A., Chilukoti, N., Brunel, F., Gorzelanny, C., Fehser, S., Chachra, S., Bernard, F., Nampally, M., Kalagara, T., Ihmor, P., Moerschbacher, B.M., 2014. Chitin and chitosan modifying enzymes: versatile novel tools for the analysis of structure-function relationship of partially acetylaed chitosans., in: Adv Chitin Sci. pp. 40–7.

Elson, L.A., Morgan, W.T.J., 1934. A Colorimetric Method for the Determination of N-acetylglucosamine and N-acetylchondrosamine. Biochem J. 28, 988–995. https://doi.org/10.1042/bj0280988

Ene, I. V., Walker, L. a., Schiavone, M., Lee, K.K., Martin-Yken, H., Dague, E., Gow, N. a R., Munro, C. a., Brown, A.J.P., 2015. Cell wall remodeling enzymes modulate fungal cell wall elasticity and osmotic stress resistance. MBio 6, 1–15. https://doi.org/10.1128/mBio.00986-15

Fang, W., Sanz, A.B., Bartual, S.G., Wang, B., Ferenbach, A.T., Farkaš, V., Hurtado-Guerrero, R., Arroyo, J., van Aalten, D.M.F., 2019. Mechanisms of redundancy and specificity of the *Aspergillus fumigatus* Crh transglycosylases. Nat. Commun. 10. https://doi.org/10.1038/s41467-019-09674-0

Feliziani, E., Landi, L., Romanazzi, G., 2015. Preharvest treatments with chitosan and other alternatives to conventional fungicides to control postharvest decay of strawberry. Carbohydr. Polym. 132, 111–117. https://doi.org/10.1016/j.carbpol.2015.05.078

Fiedler, M.R., Lorenz, A., Nitsche, B.M., van den Hondel, C.A., Ram, A.F., Meyer, V., 2014. The capacity of *Aspergillus niger* to sense and respond to cell wall stress requires at least three transcription factors: RlmA, MsnA and CrzA. Fungal Biol. Biotechnol. 1. https://doi.org/10.1186/s40694-014-0005-8

Finger, F.P., Novick, P., 1997. Sec3p is involved in secretion and morphogenesis in *Saccharomyces cerevisiae*. Mol. Biol. Cell 8, 647–662. https://doi.org/10.1091/mbc.8.4.647

Fontaine, T., Simenel, C., Dubreucq, G., Adam, O., 2000. Molecular organization of the alkali-insoluble fraction of *Aspergillus fumigatus* cell wall. J. Biol. Chem. 275, 27594–27607.

Fonzi, W.A., 1999. PHR1 and PHR2 of *Candida albicans* encode putative glycosidases required for proper cross-linking of beta-1,3- and beta-1,6-glucans. J. Bacteriol. 181, 7070–9.

Forgac, M., 2007. Vacuolar ATPases: Rotary proton pumps in physiology and pathophysiology. Nat. Rev. Mol. Cell Biol. https://doi.org/10.1038/nrm2272

Fortwendel, J.R., Juvvadi, P.R., Perfect, B.Z., Rogg, L.E., Perfect, J.R., Steinbach, W.J., 2010. Transcriptional regulation of chitin synthases by calcineurin controls paradoxical growth of *Aspergillus fumigatus* in response to caspofungin. Antimicrob. Agents Chemother. 54, 1555–63. https://doi.org/10.1128/AAC.00854-09

Free, S.J., 2013. Fungal Cell Wall Organization and Biosynthesis, 1st ed, Advances in Genetics. Elsevier Inc. https://doi.org/10.1016/B978-0-12-407677-8.00002-6

Frieman, M.B., McCaffery, J.M., Cormack, B.P., 2002. Modular domain structure in the *Candida glabrata* adhesin Epa1p, a β1,6 glucan-cross-linked cell wall protein. Mol. Microbiol. 46, 479–492. https://doi.org/10.1046/j.1365-2958.2002.03166.x

Frisvad, J.C., Petersen, L.M., Lyhne, E.K., Larsen, T.O., 2014. Formation of Sclerotia and Production of Indoloterpenes by *Aspergillus niger* and Other Species in Section Nigri. PLoS One 9, e94857. https://doi.org/10.1371/journal.pone.0094857

Fuller, R.S., Brake, A., Thorner, J., 1989. Yeast prohormone processing enzyme (KEX2 gene product) is a Ca^{2+}-dependent serine protease. Proc. Natl. Acad. Sci. https://doi.org/10.1073/pnas.86.5.1434

Gagnon-Arsenault, I., Parisé, L., Tremblay, J., Bourbonnais, Y., 2008. Activation mechanism, functional role and shedding of glycosylphosphatidylinositol-anchored Yps1p at the *Saccharomyces cerevisiae* cell surface.

Mol. Microbiol. 69, 982–993. https://doi.org/10.1111/j.1365-2958.2008.06339.x

Gaiser, O.J., Piotukh, K., Ponnuswamy, M.N., Planas, A., Borriss, R., Heinemann, U., 2006. Structural basis for the substrate specificity of a Bacillus 1,3-1,4-β-glucanase. J. Mol. Biol. 357, 1211–1225. https://doi.org/10.1016/j.jmb.2006.01.014

Gao, L., Cox, D.B.T., Yan, W.X., Manteiga, J.C., Schneider, M.W., Yamano, T., Nishimasu, H., Nureki, O., Crosetto, N., Zhang, F., 2017. Engineered Cpf1 variants with altered PAM specificities. Nat. Biotechnol. 35, 789–792. https://doi.org/10.1038/nbt.3900

Garcia-Rubio, R., de Oliveira, H.C., Rivera, J., Trevijano-Contador, N., 2020. The Fungal Cell Wall: *Candida*, *Cryptococcus*, and *Aspergillus* Species. Front. Microbiol. https://doi.org/10.3389/fmicb.2019.02993

Garrett, M.D., Zahner, J.E., Cheney, C.M., Novick, P.J., 1994. *GDI1* encodes a GDP dissociation inhibitor that plays an essential role in the yeast secretory pathway. EMBO J. 13, 1718–1728. https://doi.org/10.1002/j.1460-2075.1994.tb06436.x

Geoghegan, I., Steinberg, G., Gurr, S., 2017. The Role of the Fungal Cell Wall in the Infection of Plants. Trends Microbiol. https://doi.org/10.1016/j.tim.2017.05.015

Gherbawy, Y., Elhariry, H., Kocsubé, S., Bahobial, A., Deeb, B. El, Altalhi, A., Varga, J., Vágvölgyi, C., 2015. Molecular characterization of black *Aspergillus* species from onion and their potential for ochratoxin A and fumonisin B2 production. Foodborne Pathog. Dis. 12, 414–423. https://doi.org/10.1089/fpd.2014.1870

Ghormade, V., Pathan, E.K., Deshpande, M.V., 2017. Can fungi compete with marine sources for chitosan production? Int. J. Biol. Macromol. 1–7. https://doi.org/10.1016/j.ijbiomac.2017.01.112

Gómez-Esquer, F., Rodríguez-Peña, J.M., Díaz, G., Rodriguez, E., Briza, P., Nombela, C., Arroyo, J., 2004. CRR1, a gene encoding a putative transglycosidase, is required for proper spore wall assembly in *Saccharomyces cerevisiae*. Microbiology 150, 3269–3280. https://doi.org/10.1099/mic.0.27314-0

Gow, N.A.R., Latge, J.-P., Munro, C.A., 2017. The Fungal Cell Wall: Structure, Biosynthesis, and Function. Microbiol. Spectr. 5. https://doi.org/10.1128/microbiolspec.funk-0035-2016

Grbavac, A., Čanak, I., Stuparević, I., Teparić, R., Mrša, V., 2017. Proteolytic processing of the *Saccharomyces cerevisiae* cell wall protein Scw4 regulates its activity and influences its covalent binding to glucan. Biochim. Biophys. Acta - Mol. Cell Res. 1864, 507–515. https://doi.org/10.1016/j.bbamcr.2016.12.009

Greenstein, S., Shadkchan, Y., Jadoun, J., Sharon, C., Markovich, S., Osherov, N., 2006. Analysis of the *Aspergillus nidulans* thaumatin-like *cetA* gene and evidence for transcriptional repression of *pyr4* expression in the *cetA*-disrupted strain. Fungal Genet. Biol. 43, 42–53. https://doi.org/10.1016/j.fgb.2005.10.001

Grün, C.H., Hochstenbach, F., Humbel, B.M., Verkleij, A.J., Sietsma, J.H., Klis, F.M., Kamerling, J.P., Vliegenthart, J.F.G., 2004. The structure of cell wall α-glucan from fission yeast. Glycobiology 15, 245–257. https://doi.org/10.1093/glycob/cwi002

Guest, G.M., Lin, X., Momany, M., 2004. *Aspergillus nidulans* RhoA is involved in polar growth, branching, and cell wall synthesis. Fungal Genet. Biol. 41, 13–22. https://doi.org/10.1016/J.FGB.2003.08.006

Guo, W., Roth, D., Walch-Solimena, C., Novick, P., 1999. The exocyst is an effector for Sec4p, targeting secretory vesicles to sites of exocytosis. EMBO J. 18, 1071–1080. https://doi.org/10.1093/emboj/18.4.1071

Hahn, M., Olsen, O., Politz, O., Borriss, R., Heinemann, U., 1995. Crystal structure and site-directed mutagenesis of Bacillus macerans endo- 1,3-1,4-β-glucanase. J. Biol. Chem. 270, 3081–3088. https://doi.org/10.1074/jbc.270.7.3081

Hammer, P.E., Carr, B., 2006. Methods for production of chitin and chitosan.

Hanes, S.D., Shank, P.R., Bostian, K.A., 1989. Sequence and mutational analysis of *ESS1*, a gene essential for growth in *Saccharomyces cerevisiae*. Yeast 5, 55–72. https://doi.org/10.1002/yea.320050108

Hartland, R.P., Fontaine, T., Debeaupuis, J.P., Simenel, C., Delepierre, M., Latgé, J.P., 1996. A novel beta-(1-3)-glucanosyltransferase from the cell wall of *Aspergillus fumigatus*. J. Biol. Chem. 271, 26843–9. https://doi.org/10.1074/jbc.271.43.26843

Hartland, R.P., Vermeulen, C.A., Sietsma, J.H., Wessels, J.G.H., Klis, F.M., 1994. The linkage of (1–3)-β-glucan to chitin during cell wall assembly in *Saccharomyces cerevisiae*. Yeast 10, 1591–1599. https://doi.org/10.1002/yea.320101208

Heilmann, C.J., Sorgo, A.G., Mohammadi, S., Sosinska, G.J., de Koster, C.G., Brul, S., de Koning, L.J., Klis, F.M., Sosinsk, G.J., de Koster, C.G., Brul, S., de Koning, L.J., Klis, F.M., 2013. Surface stress induces a conserved cell wall stress response in the pathogenic fungus *Candida albicans*. Eukaryot. Cell 12, 254–264. https://doi.org/10.1128/EC.00278-12

Heiman, M.G., Engel, A., Walter, P., 2007. The Golgi-resident protease Kex2 acts in conjunction with Prm1 to facilitate cell fusion during yeast mating. J. Cell Biol. 176, 209–222. https://doi.org/10.1083/jcb.200609182

Henry, C., Fontaine, T., Heddergott, C., Robinet, P., Aimanianda, V., Beau, R., Beauvais, A., Mouyna, I., Prevost, M.C., Fekkar, A., Zhao, Y., Perlin, D., Latgé, J.P., 2016. Biosynthesis of cell wall mannan in the conidium and the mycelium of *Aspergillus fumigatus*. Cell. Microbiol. 18, 1881–1891. https://doi.org/10.1111/cmi.12665

Henry, C., Latgé, J.P., Beauvais, A., 2012. α-1,3 glucans are dispensable in *Aspergillus fumigatus*. Eukaryot. Cell 11, 26–29. https://doi.org/10.1128/EC.05270-11

Henry, C., Li, J., Danion, F., Alcazar-Fuoli, L., Mellado, E., Beau, R., RémiJouvion, G., Latgé, J.P., Fontainea, T., 2019. Two KTR mannosyltransferases are responsible for the biosynthesis of cell wall mannans and control polarized growth in *Aspergillus fumigatus*. MBio 10. https://doi.org/10.1128/mBio.02647-18

Hidangmayum, A., Dwivedi, P., Katiyar, D., Hemantaranjan, A., 2019. Application of chitosan on plant responses with special reference to abiotic stress. Physiol. Mol. Biol. Plants. https://doi.org/10.1007/s12298-018-0633-1

Hochstenbach, F., Klis, F.M., Van Ende, H. Den, Van Donselaar, E., Peters, P.J., Klausner, R.D., 1998. Identification of a putative alpha-glucan synthase essential for cell wall construction and morphogenesis in fission yeast. Proc. Natl. Acad. Sci. U. S. A. 95, 9161–9166. https://doi.org/10.1073/pnas.95.16.9161

Horn, B.W., Moore, G.G., Carbone, I., 2009. Sexual reproduction in *Aspergillus flavus*. Mycologia 101, 423–429. https://doi.org/10.3852/09-011

Hossain, A.H., Li, A., Brickwedde, A., Wilms, L., Caspers, M., Overkamp, K., Punt, P.J., 2016. Rewiring a secondary metabolite pathway towards itaconic acid production in *Aspergillus niger*. Microb. Cell Fact. 15, 130. https://doi.org/10.1186/s12934-016-0527-2

Isaza-Pérez, F., Ramírez-Carmona, M., Rendón-Castrillón, L., Ocampo-López, C., 2020. Potential of residual fungal biomass: a review. Environ. Sci. Pollut. Res. https://doi.org/10.1007/s11356-020-08193-6

Ja'afaru, M.I., 2013. Screening of fungi isolated from environmental samples for xylanase and cellulase production. ISRN Microbiol. 2013, 283423. https://doi.org/10.1155/2013/283423

Jalving, R., 2005. Proteolytic processing in the secretory pathway of *Aspergillus niger*. Ph.D. thesis.

Jalving, R., Van De Vondervoort, P.J.I.I., Visser, J., Schaap, P.J., 2000. Characterization of the kexin-like maturase of *Aspergillus niger*. Appl. Environ. Microbiol. 66, 363–368. https://doi.org/10.1128/AEM.66.1.363-368.2000

Johansson, P., Brumer, H., Baumann, M.J., Kallas, Å.M., Henriksson, H., Denman, S.E., Teeri, T.T., Jones, T.A., 2004. Crystal structures of a poplar xyloglucan endotransglycosylase reveal details of transglycosylation acceptor binding. Plant Cell 16, 874–886. https://doi.org/10.1105/tpc.020065

Jørgensen, T.R., Burggraaf, A.-M., Arentshorst, M., Schutze, T., Lamers, G., Niu, J., Kwon, M.J., Park, J., Frisvad,

J.C., Nielsen, K.F., Meyer, V., Hondel, C.A.M.J.J. van den, Dyer, P.S., Ram, A.F.J., 2020. Identification of SclB, a Zn(II)2Cys6 transcription factor involved in sclerotium formation in *Aspergillus niger*. Fungal Genet. Biol.

Jørgensen, T.R., Nielsen, K.F., Arentshorst, M., Park, J.H., van den Hondel, C.A., Frisvad, J.C., Ram, A.F., 2011a. Submerged conidiation and product formation by *Aspergillus niger* at low specific growth rates are affected in aerial developmental mutants. Appl. Environ. Microbiol. 77, 5270–5277. https://doi.org/10.1128/AEM.00118-11

Jørgensen, T.R., Nitsche, B.M., Lamers, G.E., Arentshorst, M., Van Den Hondel, C.A.M.J.J., Ram, A.F.J., 2010. Transcriptomic insights into the physiology of *Aspergillus niger* approaching a specific growth rate of zero. Appl. Environ. Microbiol. 76, 5344–5355. https://doi.org/10.1128/AEM.00450-10

Jørgensen, T.R., Park, J., Arentshorst, M., van Welzen, A.M., Lamers, G., VanKuyk, P.A., Damveld, R.A., van den Hondel, C.A.M.J.J., Nielsen, K.F., Frisvad, J.C., Ram, A.F.J., 2011b. The molecular and genetic basis of conidial pigmentation in *Aspergillus niger*. Fungal Genet. Biol. 48, 544–553. https://doi.org/10.1016/j.fgb.2011.01.005

Kang, M.S., Elango, N., Mattia, E., Au-Young, J., Robbins, P.W., Cabib, E., 1984. Isolation of chitin synthetase from *Saccharomyces cerevisiae*. Purification of an enzyme by entrapment in the reaction product. J. Biol. Chem. 259, 14966–14972.

Kang, X., Kirui, A., Muszyński, A., Widanage, M.C.D., Chen, A., Azadi, P., Wang, P., Mentink-Vigier, F., Wang, T., 2018. Molecular architecture of fungal cell walls revealed by solid-state NMR. Nat. Commun. 9, 2747. https://doi.org/10.1038/s41467-018-05199-0

Kapitzky, L., Beltrao, P., Berens, T.J., Gassner, N., Zhou, C., Wüster, A., Wu, J., Babu, M.M., Elledge, S.J., Toczyski, D., Lokey, R.S., Krogan, N.J., 2010. Cross-species chemogenomic profiling reveals evolutionarily conserved drug mode of action. Mol. Syst. Biol. 6. https://doi.org/10.1038/msb.2010.107

Kapteyn, J.C., Montijn, R.C., Vink, E., De La Cruz, J., Llobell, A., Douwes, J.E., Shimoi, H., Lipke, P.N., Klis, F.M., 1996. Retention of *Saccharomyces cerevisiae* cell wall proteins through a phosphodiester-linked β-1,3-/β-1,6-glucan heteropolymer. Glycobiology 6, 337–345. https://doi.org/10.1093/glycob/6.3.337

Karaffa, L., Kubicek, C.P., 2003. *Aspergillus niger* citric acid accumulation: do we understand this well working black box? Appl. Microbiol. Biotechnol. 61, 189–196. https://doi.org/10.1007/s00253-002-1201-7

Katayama, T., Nakamura, H., Zhang, Y., Pascal, A., Fujii, W., Maruyama, J.-I., 2019. Forced Recycling of an AMA1-Based Genome-Editing Plasmid Allows for Efficient Multiple Gene Deletion/Integration in the Industrial Filamentous Fungus *Aspergillus oryzae*. Appl. Environ. Microbiol. 85, e01896-18. https://doi.org/10.1128/AEM.01896-18

Kaur, S., Dhillon, G.S., 2014. The versatile biopolymer chitosan: potential sources, evaluation of extraction methods and applications. Crit. Rev. Microbiol. 40, 155–175. https://doi.org/10.3109/1040841X.2013.770385

Keitel, T., Simon, O., Borriss, R., Heinemann, U., 1993. Molecular and active-site structure of a Bacillus 1,3-1,4-β-glucanase, in: Proceedings of the National Academy of Sciences of the United States of America. pp. 5287–5291. https://doi.org/10.1073/pnas.90.11.5287

Keller, F.A., Cabib, E., 1971. Chitin and yeast budding. Properties of chitin synthetase from *Saccharomyces* carlsbergensis. J. Biol. Chem. 246, 160–166.

Khalesi, M., Zune, Q., Telek, S., Riveros-Galan, D., Verachtert, H., Toye, D., Gebruers, K., Derdelinckx, G., Delvigne, F., 2014. Fungal biofilm reactor improves the productivity of hydrophobin HFBII. Biochem. Eng. J. 88, 171–178. https://doi.org/10.1016/j.bej.2014.05.001

Kinkelin, K., Wozniak, G.G., Rothbart, S.B., Lidschreiber, M., Strahl, B.D., Cramer, P., 2013. Structures of RNA polymerase II complexes with Bye1, a chromatin-binding PHF3/DIDO homolog. Proc. Natl. Acad. Sci. U. S. A. 110, 15277–82. https://doi.org/10.1073/pnas.1311010110

Kiss, E., Hegedüs, B., Virágh, M., Varga, T., Merényi, Z., Kószó, T., Bálint, B., Prasanna, A.N., Krizsán, K., Kocsubé, S., Riquelme, M., Takeshita, N., Nagy, L.G., 2019. Comparative genomics reveals the origin of fungal hyphae and multicellularity. Nat. Commun. 10. https://doi.org/10.1038/s41467-019-12085-w

Klis, F.M., Ram, A.F.J., De Groot, P.W.J., 2007. A Molecular and Genomic View of the Fungal Cell Wall, in: Biology of the Fungal Cell. Springer Berlin Heidelberg, pp. 97–120. https://doi.org/10.1007/978-3-540-70618-2_4

Knorr, D., 1991. Recovery and utilization of chitin and chitosan in food processing waste management. Food Technol. 45, 114–122.

Kocak, D.D., Josephs, E.A., Bhandarkar, V., Adkar, S.S., Kwon, J.B., Gersbach, C.A., 2019. Increasing the specificity of CRISPR systems with engineered RNA secondary structures. Nat. Biotechnol. 37, 657–666. https://doi.org/10.1038/s41587-019-0095-1

Kollár, R., Reinhold, B.B., Petráková, E., Yeh, H.J.C., Ashwell, G., Drgonová, J., Kapteyn, J.C., Klis, F.M., Cabib, E., 1997. Architecture of the yeast cell wall: β(1→6)glucan interconnects mannoprotein, β(1→3)-glucan, and chitin. J. Biol. Chem. 272, 17762–17775. https://doi.org/10.1074/jbc.272.28.17762

Kolodziej, P.A., Yeh Jan, L., Nung Jan, Y., 1995. Mutations that affect the length, fasciculation, or ventral orientation of specific sensory axons in the *Drosophila* embryo. Neuron 15, 273–286. https://doi.org/10.1016/0896-6273(95)90033-0

Kowalski, B., Terry, F.J., Herrera, L., Peñalver, D.A., 2006. Application of soluble chitosan in vitro and in the greenhouse to increase yield and seed quality of potato minitubers. Potato Res. 49, 167–176. https://doi.org/10.1007/s11540-006-9015-0

Krijgsheld, P., Bleichrodt, R., van Veluw, G.J., Wang, F., Müller, W.H., Dijksterhuis, J., Wösten, H.A.B., 2013. Development in *Aspergillus*. Stud. Mycol. 74, 1–29. https://doi.org/10.3114/sim0006

Krijgsheld, Pauline, Nitsche, B.M., Post, H., Levin, A.M., Müller, W.H., Heck, A.J.R., Ram, A.F.J., Altelaar, A.F.M., Wösten, H.A.B., 2013. Deletion of flbA results in increased secretome complexity and reduced secretion heterogeneity in colonies of *Aspergillus niger*. J. Proteome Res. 12, 1808–1819. https://doi.org/10.1021/pr301154w

Krogh, A., Larsson, B., Von Heijne, G., Sonnhammer, E.L.L., 2001. Predicting transmembrane protein topology with a hidden Markov model: Application to complete genomes. J. Mol. Biol. 305, 567–580. https://doi.org/10.1006/jmbi.2000.4315

Kuivanen, J., Wang, Y.-M.J., Richard, P., 2016. Engineering *Aspergillus niger* for galactaric acid production: elimination of galactaric acid catabolism by using RNA sequencing and CRISPR/Cas9. Microb. Cell Fact. 15, 210. https://doi.org/10.1186/s12934-016-0613-5

Kumaresapillai, N., Basha, R.A., Sathish, R., 2011. Production and evaluation of chitosan from *Aspergillus niger* MTCC strains. Iran. J. Pharm. Res. 10, 553–558. https://doi.org/10.22037/ijpr.2011.1003

Kupfer, D.M., Drabenstot, S.D., Buchanan, K.L., Lai, H., Zhu, H., Dyer, D.W., Roe, B.A., Murphy, J.W., 2004. Introns and splicing elements of five diverse fungi. Eukaryot. Cell 3, 1088–1100. https://doi.org/10.1128/EC.3.5.1088-1100.2004

Labun, K., Montague, T.G., Gagnon, J.A., Thyme, S.B., Valen, E., 2016. CHOPCHOP v2: a web tool for the next generation of CRISPR genome engineering. Nucleic Acids Res. 44, W272–W276. https://doi.org/10.1093/nar/gkw398

Lafontaine, P.J., Benhamou, N., 1996. Chitosan treatment: An emerging strategy for enhancing resistance of greenhouse tomato plants to infection by *Fusarium oxysporum* f.sp. *radicis-lycopersici*. Biocontrol Sci. Technol. 6, 111–124. https://doi.org/10.1080/09583159650039575

Lagorce, A., Berre-Anton, V. Le, Aguilar-Uscanga, B., Martin-Yken, H., Dagkessamanskaia, A., François, J., 2002. Involvement of GFA1, which encodes glutamine-fructose-6-phosphate amidotransferase, in the activation

of the chitin synthesis pathway in response to cell-wall defects in *Saccharomyces cerevisiae*. Eur. J. Biochem. 269, 1697–1707. https://doi.org/10.1046/j.1432-1327.2002.02814.x

Latgé, J.-P., 2007. The cell wall: a carbohydrate armour for the fungal cell. Mol. Microbiol. 66, 279–290. https://doi.org/10.1111/j.1365-2958.2007.05872.x

Lay, J., Henry, L.K., Clifford, J., Koltin, Y., Bulawa, C.E., Becker, J.M., 1998. Altered Expression of Selectable Marker *URA3* in Gene-Disrupted *Candida albicans* Strains Complicates Interpretation of Virulence Studies, Infection and Immunology.

Le Marquer, M., San Clemente, H., Roux, C., Savelli, B., Frei Dit Frey, N., 2019. Identification of new signalling peptides through a genome-wide survey of 250 fungal secretomes. BMC Genomics. https://doi.org/10.1186/s12864-018-5414-2

Lee, J.-H., Skalnik, D.G., 2012. Rbm15-Mkl1 interacts with the Setd1b histone H3-Lys4 methyltransferase via a SPOC domain that is required for cytokine-independent proliferation. PLoS One 7, e42965. https://doi.org/10.1371/journal.pone.0042965

Leibowitz, M.J., Wickner, R.B., 1976. A chromosomal gene required for killer plasmid expression, mating, and spore maturation in *Saccharomyces cerevisiae*. Proc. Natl. Acad. Sci. U. S. A. 73, 2061–2065. https://doi.org/10.1073/pnas.73.6.2061

Levin, A.M., De Vries, R.P., Conesa, A., De Bekker, C., Talon, M., Menke, H.H., Van Peij, N.N.M.E., Wösten, H.A.B., 2007. Spatial differentiation in the vegetative mycelium of *Aspergillus niger*. Eukaryot. Cell 6, 2311–2322. https://doi.org/10.1128/EC.00244-07

Levin, D.E., 2005. Cell Wall Integrity Signaling in *Saccharomyces cerevisiae*. Microbiol Mol Biol Rev 69, 262–291. https://doi.org/10.1128/MMBR.69.2.262

Leynaud-Kieffer, L.M.C., Curran, S.C., Kim, I., Magnuson, J.K., Gladden, J.M., Baker, S.E., Simmons, B.A., 2019. A new approach to Cas9-based genome editing in *Aspergillus niger* that is precise, efficient and selectable. PLoS One 14. https://doi.org/10.1371/journal.pone.0210243

Liu, H., Tian, W., Li, B., Wu, G., Ibrahim, M., Tao, Z., Wang, Y., Xie, G., Li, H., Sun, G., 2012. Antifungal effect and mechanism of chitosan against the rice sheath blight pathogen, *Rhizoctonia solani*. Biotechnol. Lett. 34, 2291–2298. https://doi.org/10.1007/s10529-012-1035-z

Liu, R., Xu, C., Zhang, Q., Wang, S., Fang, W., 2017. Evolution of the chitin synthase gene family correlates with fungal morphogenesis and adaption to ecological niches. Sci. Rep. 7, 44527. https://doi.org/10.1038/srep44527

Liu, R.M., Liang, L.L., Freed, E., Chang, H., Oh, E., Liu, Z.Y., Garst, A., Eckert, C.A., Gill, R.T., 2019. Synthetic chimeric nucleases function for efficient genome editing. Nat. Commun. 10. https://doi.org/10.1038/s41467-019-13500-y

Lizárraga-Paulín, E.G., Miranda-Castro, S.P., Moreno-Martínez, E., Lara-Sagahón, A.V., Torres-Pacheco, I., 2013. Maize seed coatings and seedling sprayings with chitosan and hydrogen peroxide: Their influence on some phenological and biochemical behaviors. J. Zhejiang Univ. Sci. B 14, 87–96. https://doi.org/10.1631/jzus.B1200270

Lord, A.K., Vyas, J.M., 2019. Host Defenses to Fungal Pathogens. Clin. Immunol. 413-424.e1. https://doi.org/10.1016/B978-0-7020-6896-6.00029-6

Love, M.I., Huber, W., Anders, S., 2014. Moderated estimation of fold change and dispersion for RNA-seq data with DESeq2. Genome Biol. 15, 550. https://doi.org/10.1186/s13059-014-0550-8

Lu, C.F., Kurjan, J., Lipke, P.N., 1994. A pathway for cell wall anchorage of *Saccharomyces cerevisiae* alpha-agglutinin. Mol. Cell. Biol. 14, 4825–4833. https://doi.org/10.1128/mcb.14.7.4825

Lu, C.F., Montijn, R.C., Brown, J.L., Klis, F., Kurjan, J., Bussey, H., Lipke, P.N., 1995. Glycosyl phosphatidylinosi-

tol-dependent cross-linking of α-agglutinin and β1,6-glucan in the *Saccharomyces cerevisiae* cell wall. J. Cell Biol. 128, 333–340. https://doi.org/10.1083/jcb.128.3.333

Luo, X., Affeldt, K.J., Keller, N.P., 2016. Characterization of the Far Transcription Factor Family in *Aspergillus flavus*. https://doi.org/10.1534/g3.116.032466

Ma, Z., Atencio, D., Barnes, C., DeFiglio, H., Hanes, S.D., 2012. Multiple roles for the Ess1 prolyl isomerase in the RNA polymerase II transcription cycle. Mol. Cell. Biol. 32, 3594–607. https://doi.org/10.1128/MCB.00672-12

MacKenzie, D.A., Guillemette, T., Al-Sheikh, H., Watson, A.J., Jeenes, D.J., Wongwathanarat, P., Dunn-Coleman, N.S., Peij, N. van., Archer, D.B., 2005. UPR-independent dithiothreitol stress-induced genes in *Aspergillus niger*. Mol. Genet. Genomics 274, 410–418. https://doi.org/10.1007/s00438-005-0034-3

Maghsoodi, V., Razavi, J., Yaghmaei, S., 2009. Production of Chitosan by Submerged Fermentation from *Aspergillus niger*, Transactions C: Chemistry and Chemical Engineering.

Magnuson, J.K., Lasure, L.L., 2004. Organic Acid Production by Filamentous Fungi, in: Advances in Fungal Biotechnology for Industry, Agriculture, and Medicine. Springer US, pp. 307–340. https://doi.org/10.1007/978-1-4419-8859-1_12

Martin, S.H., Wingfield, B.D., Wingfield, M.J., Steenkamp, E.T., 2011. Causes and consequences of variability in peptide mating pheromones of ascomycete fungi. Mol. Biol. Evol. 28, 1987–2003. https://doi.org/10.1093/molbev/msr022

Mazáň, M., Blanco, N., Kováčová, K., Firáková, Z., Řehulka, P., Farkaš, V., Arroyo, J., 2013. A novel fluorescence assay and catalytic properties of *CRH1* and *CRH2* yeast cell wall transglycosylases. Biochem. J. 455, 307–318. https://doi.org/10.1042/BJ20130354

Merzendorfer, H., 2011. The cellular basis of chitin synthesis in fungi and insects: Common principles and differences. Eur. J. Cell Biol. 90, 759–769. https://doi.org/10.1016/j.ejcb.2011.04.014

Meyer, V., Andersen, M.R., Brakhage, A.A., Braus, G.H., Caddick, M.X., Cairns, T.C., de Vries, R.P., Haarmann, T., Hansen, K., Hertz-Fowler, C., Krappmann, S., Mortensen, U.H., Peñalva, M.A., Ram, A.F.J., Head, R.M., 2016. Current challenges of research on filamentous fungi in relation to human welfare and a sustainable bio-economy: a white paper. Fungal Biol. Biotechnol. 3, 6. https://doi.org/10.1186/s40694-016-0024-8

Meyer, V., Arentshorst, M., El-Ghezal, A., Drews, A.C., Kooistra, R., van den Hondel, C.A.M.J.J., Ram, A.F.J., 2007a. Highly efficient gene targeting in the *Aspergillus niger kusA* mutant. J. Biotechnol. 128, 770–775. https://doi.org/10.1016/j.jbiotec.2006.12.021

Meyer, V., Basenko, E.Y., Benz, J.P., Braus, G.H., Caddick, M.X., Csukai, M., de Vries, R.P., Endy, D., Frisvad, J.C., Gunde-Cimerman, N., Haarmann, T., Hadar, Y., Hansen, K., Johnson, R.I., Keller, N.P., Kraševec, N., Mortensen, U.H., Perez, R., Ram, A.F.J., Record, E., Ross, P., Shapaval, V., Steiniger, C., van den Brink, H., van Munster, J., Yarden, O., Wösten, H.A.B., 2020. Growing a circular economy with fungal biotechnology: a white paper. Fungal Biol. Biotechnol. 7, 5. https://doi.org/10.1186/s40694-020-00095-z

Meyer, V., Damveld, R. a., Arentshorst, M., Stahl, U., Van Den Hondel, C.A.M.J.J., Ram, A.F.J., 2007b. Survival in the presence of antifungals: Genome-wide expression profiling of *Aspergillus niger* in response to sublethal concentrations of caspofungin and fenpropimorph. J. Biol. Chem. 282, 32935–32948. https://doi.org/10.1074/jbc.M705856200

Meyer, V., Wu, B., Ram, A.F.J., 2011. *Aspergillus* as a multi-purpose cell factory: Current status and perspectives. Biotechnol. Lett. https://doi.org/10.1007/s10529-010-0473-8

Miki, B., Abdeen, A., Manabe, Y., MacDonald, P., 2009. Selectable marker genes and unintended changes to the plant transcriptome. Plant Biotechnol. J. 7, 211–218. https://doi.org/10.1111/j.1467-7652.2009.00400.x

Miller, K.A., Didone, L., Krysan, D.J., 2010. Extracellular secretion of overexpressed glycosylphosphatidylinositol-linked cell wall protein Utr2/Crh2p as a novel protein quality control mechanism in *Saccharomyces*

cerevisiae. Eukaryot. Cell 9, 1669–1679. https://doi.org/10.1128/EC.00191-10

Miller, S.M., Wang, T., Randolph, P.B., Arbab, M., Shen, M.W., Huang, T.P., Matuszek, Z., Newby, G.A., Rees, H.A., Liu, D.R., 2020. Continuous evolution of SpCas9 variants compatible with non-G PAMs. Nat. Biotechnol. https://doi.org/10.1038/s41587-020-0412-8

Miyazawa, K., Yoshimi, A., Kasahara, S., Sugahara, A., Koizumi, A., Yano, S., Kimura, S., Iwata, T., Sano, M., Abe, K., 2018. Molecular Mass and Localization of α-1,3-Glucan in Cell Wall Control the Degree of Hyphal Aggregation in Liquid Culture of *Aspergillus nidulans*. Front. Microbiol. 9. https://doi.org/10.3389/fmicb.2018.02623

Miyazawa, K., Yoshimi, A., Zhang, S., Sano, M., Nakayama, M., Gomi, K., Abe, K., 2016. Increased enzyme production under liquid culture conditions in the industrial fungus *Aspergillus oryzae* by disruption of the genes encoding cell wall α-1,3-glucan synthase. Biosci. Biotechnol. Biochem. 80, 1853–1863. https://doi.org/10.1080/09168451.2016.1209968

Mizutani, O., Nojima, A., Yamamoto, M., Furukawa, K., Fujioka, T., Yamagata, Y., Abe, K., Nakajima, T., 2004. Disordered cell integrity signaling caused by disruption of the *kexB* gene in *Aspergillus oryzae*. Eukaryot. Cell 3, 1036–1048. https://doi.org/10.1128/EC.3.4.1036-1048.2004

Mizutani, O., Shiina, M., Yoshimi, A., Sano, M., Watanabe, T., Yamagata, Y., Nakajima, T., Gomi, K., Abe, K., 2016. Substantial decrease in cell wall α-1,3-glucan caused by disruption of the *kexB* gene encoding a subtilisin-like processing protease in *Aspergillus oryzae*. Biosci. Biotechnol. Biochem. 8451, 1–11. https://doi.org/10.1080/09168451.2016.1158632

Mol, P.C., Wessels, J.G.H., 1987. Linkages between glucosaminoglycan and glucan determine alkali-insolubility of the glucan in walls of *Saccharomyces cerevisiae*. FEMS Microbiol. Lett. 41, 95–99. https://doi.org/10.1111/j.1574-6968.1987.tb02148.x

Mouyna, I., Fontaine, T., Vai, M., Monod, M., Fonzi, W.A., Diaquin, M., Popolo, L., Hartland, R.P., Latgé, J.P., 2000. Glycosylphosphatidylinositol-anchored glucanosyltransferases play an active role in the biosynthesis of the fungal cell wall. J. Biol. Chem. 275, 14882–9. https://doi.org/10.1074/jbc.275.20.14882

Muñoz, G., Valencia, C., Valderruten, N., Ruiz-Durántez, E., Zuluaga, F., 2015. Extraction of chitosan from *Aspergillus niger* mycelium and synthesis of hydrogels for controlled release of betahistine. React. Funct. Polym. 91–92, 1–10.

Muszewska, A., Piłsyk, S., Perlińska-Lenart, U., Kruszewska, J.S., 2018. Diversity of cell wall related proteins in human pathogenic fungi. J. Fungi 4. https://doi.org/10.3390/jof4010006

Muszkieta, L., Fontaine, T., Beau, R., Mouyna, I., Vogt, M.S., Trow, J., Cormack, B.P., Essen, L.-O., Jouvion, G., Latgé, J.-P., 2019. The Glycosylphosphatidylinositol-Anchored DFG Family Is Essential for the Insertion of Galactomannan into the β-(1,3)-Glucan–Chitin Core of the Cell Wall of *Aspergillus fumigatus*. mSphere 4. https://doi.org/10.1128/msphere.00397-19

Muzzarelli, R.A.A., 1973. Natural chelating polymers; alginic acid, chitin, and chitosan, in: International Series of Monographs on Analytical Chemistry. Pergamon Press, Oxford, New York.

Naveed, M., Phil, L., Sohail, M., Hasnat, M., Baig, M.M.F.A., Ihsan, A.U., Shumzaid, M., Kakar, M.U., Mehmood Khan, T., Akabar, M.D., Hussain, M.I., Zhou, Q.G., 2019. Chitosan oligosaccharide (COS): An overview. Int. J. Biol. Macromol. https://doi.org/10.1016/j.ijbiomac.2019.01.192

Newport, G., Kuo, A., Flattery, A., Gill, C., Blake, J.J., Kurtz, M.B., Abruzzo, G.K., Agabian, N., 2003. Inactivation of Kex2p diminishes the virulence of *Candida albicans*. J. Biol. Chem. 278, 1713–1720. https://doi.org/10.1074/jbc.M209713200

Nielsen, H., 2017. Predicting Secretory Proteins with SignalP. Humana Press, New York, NY, pp. 59–73. https://doi.org/10.1007/978-1-4939-7015-5_6

Nishi, T., Kawasaki-Nishi, S., Forgac, M., 2003. Expression and Function of the Mouse V-ATPase d Subunit Iso-

forms. J. Biol. Chem. 278, 46396–46402. https://doi.org/10.1074/jbc.M303924200

Nishimasu, H., Shi, X., Ishiguro, S., Gao, L., Hirano, S., Okazaki, S., Noda, T., Abudayyeh, O.O., Gootenberg, J.S., Mori, H., Oura, S., Holmes, B., Tanaka, M., Seki, M., Hirano, H., Aburatani, H., Ishitani, R., Ikawa, M., Yachie, N., Zhang, F., Nureki, O., 2018. Engineered CRISPR-Cas9 nuclease with expanded targeting space. Science (80-.). https://doi.org/10.1126/science.aas9129(2018)

Niu, J., Arentshorst, M., Nair, P.D.S., Dai, Z., Baker, S.E., Frisvad, J.C., Nielsen, K.F., Punt, P.J., Ram, A.F.J., 2016a. Identification of a classical mutant in the industrial host *Aspergillus niger* by systems genetics: LaeA is required for citric acid production and regulates the formation of some secondary metabolites. G3 Genes, Genomes, Genet. 6, 193–204. https://doi.org/10.1534/g3.115.024067

Niu, J., Arentshorst, M., Seelinger, F., Ram, A.F.J., Ouedraogo, J.P., 2016b. A set of isogenic auxotrophic strains for constructing multiple gene deletion mutants and parasexual crossings in *Aspergillus niger*. Arch. Microbiol. 1–8. https://doi.org/10.1007/s00203-016-1240-6

Nødvig, C.S., Hoof, J.B., Kogle, M.E., Jarczynska, Z.D., Lehmbeck, J., Klitgaard, D.K., Mortensen, U.H., 2018a. Efficient oligo nucleotide mediated CRISPR-Cas9 gene editing in Aspergilli. Fungal Genet. Biol. 115, 78–89. https://doi.org/10.1016/J.FGB.2018.01.004

Nødvig, C.S., Hoof, J.B., Kogle, M.E., Jarczynska, Z.D., Lehmbeck, J., Klitgaard, D.K., Mortensen, U.H., 2018b. Efficient oligo nucleotide mediated CRISPR-Cas9 gene editing in Aspergilli. Fungal Genet. Biol. https://doi.org/10.1016/j.fgb.2018.01.004

Nødvig, C.S., Nielsen, J.B., Kogle, M.E., Mortensen, U.H., 2015. A CRISPR-Cas9 System for Genetic Engineering of Filamentous Fungi. PLoS One 10, e0133085. https://doi.org/10.1371/journal.pone.0133085

Novick, P., Brennwald, P., Walworth, N.C., Kabcenell, A.K., Garrett, M., Moya, M., Roberts, D., Müller, H., Govindan, B., Bowser, R., 1993. The cycle of SEC4 function in vesicular transport. Ciba Found. Symp.

Novodvorska, M., Hayer, K., Pullan, S.T., Wilson, R., Blythe, M.J., Stam, H., Stratford, M., Archer, D.B., 2013. Tranciptional landscape of *Aspergillus niger* at breaking of conidial dormancy revealed by RNA-sequencing. BMC Genomics 14. https://doi.org/10.1186/1471-2164-14-246

NRC, N.R.C., 1983. Underutilized Resources as Animal Feedstuffs, Underutilized Resources as Animal Feedstuffs. National Academies Press. https://doi.org/10.17226/41

Nwe, N., Stevens, W.F., 2004. Effect of urea on fungal chitosan production in solid substrate fermentation. Process Biochem. 39, 1639–1642. https://doi.org/10.1016/S0032-9592(03)00301-7

Oesterlin, L.K., Pylypenko, O., Goud, B., 2014. Effectors of Rab GTPases: Rab Binding Specificity and Their Role in Coordination of Rab Function and Localization, in: Ras Superfamily Small G Proteins: Biology and Mechanisms 2. Springer International Publishing, Cham, pp. 39–66. https://doi.org/10.1007/978-3-319-07761-1_3

Oestreicher, N., Ribard, C., Scazzocchio, C., 2008. The nadA gene of *Aspergillus nidulans*, encoding adenine deaminase, is subject to a unique regulatory pattern. Fungal Genet. Biol. 45, 760–775. https://doi.org/10.1016/J.FGB.2007.10.015

Orlean, P., Funai, D., 2019. Priming and elongation of chitin chains: Implications for chitin synthase mechanism. Cell Surf. 5, 100017. https://doi.org/10.1016/J.TCSW.2018.100017

Orzali, L., Corsi, B., Forni, C., Riccioni, L., 2017. Chitosan in Agriculture: A New Challenge for Managing Plant Disease, in: Biological Activities and Application of Marine Polysaccharides. InTech. https://doi.org/10.5772/66840

Orzali, L., Forni, C., Riccioni, L., 2014. Effect of chitosan seed treatment as elicitor of resistance to *Fusarium* graminearum in wheat. Seed Sci. Technol. 42, 132–149. https://doi.org/10.15258/sst.2014.42.2.03

Osmani, A.H., Oakley, B.R., Osmani, S.A., 2006. Identification and analysis of essential *Aspergillus nidulans*

genes using the heterokaryon rescue technique. Nat. Protoc. 1, 2517–2526. https://doi.org/10.1038/nprot.2006.406

Paege, N., Jung, S., Schäpe, P., Müller-Hagen, D., Ouedraogo, J.-P., Heiderich, C., Jedamzick, J., Nitsche, B.M., Hondel, C.A. van den, Ram, A.F., Meyer, V., 2016. A Transcriptome Meta-Analysis Proposes Novel Biological Roles for the Antifungal Protein AnAFP in *Aspergillus niger*. PLoS One 11, e0165755. https://doi.org/10.1371/JOURNAL.PONE.0165755

Papagianni, M., 2004. Fungal morphology and metabolite production in submerged mycelial processes. Biotechnol. Adv. https://doi.org/10.1016/j.biotechadv.2003.09.005

Pardini, G., De Groot, P.W.J., Coste, A.T., Karababa, M., Klis, F.M., De Koster, C.G., Sanglard, D., 2006. The *CRH* family coding for cell wall glycosylphosphatidylinositol proteins with a predicted transglycosidase domain affects cell wall organization and virulence of *Candida albicans*. J. Biol. Chem. 281, 40399–40411. https://doi.org/10.1074/jbc.M606361200

Park, J., Hulsman, M., Arentshorst, M., Breeman, M., Alazi, E., Lagendijk, E.L., Rocha, M.C., Malavazi, I., Nitsche, B.M., van den Hondel, C.A.M.J.J., Meyer, V., Ram, A.F.J., 2016. Transcriptomic and molecular genetic analysis of the cell wall salvage response of *Aspergillus niger* to the absence of galactofuranose synthesis. Cell. Microbiol. 18, 1268–1284. https://doi.org/10.1111/cmi.12624

Park, J., Tefsen, B., Arentshorst, M., Lagendijk, E., van den Hondel, C.A., van Die, I., Ram, A.F., 2014. Identification of the UDP-glucose-4-epimerase required for galactofuranose biosynthesis and galactose metabolism in *A. niger*. Fungal Biol. Biotechnol. 1, 1–12. https://doi.org/10.1186/s40694-014-0006-7

Patel, P.K., Free, S.J., 2019. The Genetics and Biochemistry of Cell Wall Structure and Synthesis in *Neurospora crassa*, a Model Filamentous Fungus. Front. Microbiol. https://doi.org/10.3389/fmicb.2019.02294

Patro, R., Duggal, G., Love, M.I., Irizarry, R.A., Kingsford, C., 2017. Salmon provides fast and bias-aware quantification of transcript expression. Nat. Methods 14, 417–419. https://doi.org/10.1038/nmeth.4197

Pel, H.J., de Winde, J.H., Archer, D.B., Dyer, P.S., Hofmann, G., Schaap, P.J., Turner, G., de Vries, R.P., Albang, R., Albermann, K., Andersen, M.R., Bendtsen, J.D., Benen, J.A.E., van den Berg, M., Breestraat, S., Caddick, M.X., Contreras, R., Cornell, M., Coutinho, P.M., Danchin, E.G.J., Debets, A.J.M., Dekker, P., van Dijck, P.W.M., van Dijk, A., Dijkhuizen, L., Driessen, A.J.M., d'Enfert, C., Geysens, S., Goosen, C., Groot, G.S.P., de Groot, P.W.J., Guillemette, T., Henrissat, B., Herweijer, M., van den Hombergh, J.P.T.W., van den Hondel, C.A.M.J.J., van der Heijden, R.T.J.M., van der Kaaij, R.M., Klis, F.M., Kools, H.J., Kubicek, C.P., van Kuyk, P.A., Lauber, J., Lu, X., van der Maarel, M.J.E.C., Meulenberg, R., Menke, H., Mortimer, M.A., Nielsen, J., Oliver, S.G., Olsthoorn, M., Pal, K., van Peij, N.N.M.E., Ram, A.F.J., Rinas, U., Roubos, J.A., Sagt, C.M.J., Schmoll, M., Sun, J., Ussery, D., Varga, J., Vervecken, W., van de Vondervoort, P.J.J., Wedler, H., Wösten, H.A.B., Zeng, A.-P., van Ooyen, A.J.J., Visser, J., Stam, H., 2007. Genome sequencing and analysis of the versatile cell factory *Aspergillus niger* CBS 513.88. Nat. Biotechnol. 25, 221–231. https://doi.org/10.1038/nbt1282

Peter, O., 1987. Two Chitin Synthases in *Saccharomyces cerevisiae*. J. Biol. Chem. 262, 5732–5739.

Pfeffer, S., Aivazian, D., 2004. Targeting Rab GTPases to distinct membrane compartments. Nat. Rev. Mol. Cell Biol. https://doi.org/10.1038/nrm1500

Pfeffer, S.R., 1992. GTP-binding proteins in intracellular transport. Trends Cell Biol.

Pierleoni, A., Martelli, P., Casadio, R., 2008. PredGPI: a GPI-anchor predictor. BMC Bioinformatics 9, 392. https://doi.org/10.1186/1471-2105-9-392

Pillai, C.K.S., Paul, W., Sharma, C.P., 2009. Chitin and chitosan polymers: Chemistry, solubility and fiber formation. Prog. Polym. Sci. 34, 641–678. https://doi.org/10.1016/j.progpolymsci.2009.04.001

Pinskaya, M., Ghavi-Helm, Y., Mariotte-Labarre, S., Morillon, A., Soutourina, J., Werner, M., 2014. PHD and TFIIS-Like Domains of the Bye1 Transcription Factor Determine Its Multivalent Genomic Distribution. PLoS One 9, 102464.

Pir, P., Gutteridge, A., Wu, J., Rash, B., Kell, D.B., Zhang, N., Oliver, S.G., 2012. The genetic control of growth rate: a systems biology study in yeast. BMC Syst. Biol. 6, 4. https://doi.org/10.1186/1752-0509-6-4

Pochanavanich, P., Suntornsuk, W., 2002. Fungal chitosan production and its characterization. Lett. Appl. Microbiol. 35, 17–21. https://doi.org/10.1046/j.1472-765X.2002.01118.x

Pontecorvo, G., Roper, J.A., Forbes, E., 1953. Genetic recombination without sexual reproduction in *Aspergillus niger*. J. Gen. Microbiol. 8, 198–210. https://doi.org/10.1099/00221287-8-1-198

Punt, P.J., Drint-Kuijvenhoven, A., Lokman, B.C., Spencer, J.A., Jeenes, D., Archer, D.A., Van Den Hondel, C.A.M.J.J., 2003. The role of the *Aspergillus niger* furin-type protease gene in processing of fungal proproteins and fusion proteins: Evidence for alternative processing of recombinant (fusion-) proteins. J. Biotechnol. 106, 23–32. https://doi.org/10.1016/j.jbiotec.2003.09.005

Punt, P.J., Oliver, R.P., Dingemanse, M.A., Pouwels, P.H., van den Hondel, C.A.M.J.J., 1987. Transformation of *Aspergillus* based on the hygromycin B resistance marker from *Escherichia coli*. Gene 56, 117–124. https://doi.org/10.1016/0378-1119(87)90164-8

Punt, P.J., Seiboth, B., Weenink, X.O., Van Zeijl, C., Lenders, M., Konetschny, C., Ram, A.F.J., Montijn, R., Kubicek, C.P., Van Den Hondel, C.A.M.J.J., 2001. Identification and characterization of a family of secretion-related small GTPase-encoding genes from the filamentous fungus *Aspergillus niger* : a putative SEC4 homolog is not essential for growth. Mol. Microbiol. 41, 513–525. https://doi.org/10.1046/j.1365-2958.2001.02541.x

Punt, P.J., van Biezen, N., Conesa, A., Albers, A., Mangnus, J., van den Hondel, C., 2002. Filamentous fungi as cell factories for heterologous protein production. Trends Biotechnol. 20, 200–206. https://doi.org/10.1016/S0167-7799(02)01933-9

Punt, P.J., van den Hondel, C.A.M.J.J., 1992. Transformation of filamentous fungi based on hygromycin b and phleomycin resistance markers. Methods Enzymol. 216, 447–457. https://doi.org/10.1016/0076-6879(92)16041-H

R Development Core Team 3.6.1., 2019. A Language and Environment for Statistical Computing. R Found. Stat. Comput.

Ram, A.F.J., Arentshorst, M., Damveld, R.A., vanKuyk, P.A., Klis, F.M., van den Hondel, C.A.M.J.J., 2004. The cell wall stress response in *Aspergillus niger* involves increased expression of the glutamine: Fructose-6-phosphate amidotransferase-encoding gene (*gfaA*) and increased deposition of chitin in the cell wall. Microbiology 150, 3315–3326. https://doi.org/10.1099/mic.0.27249-0

Ram, A.F.J., Klis, F.M., 2006. Identification of fungal cell wall mutants using susceptibility assays based on Calcofluor white and Congo red. Nat. Protoc. 1, 2253–2256. https://doi.org/10.1038/nprot.2006.397

Reglinski, T., Elmer, P.A.G., Taylor, J.T., Wood, P.N., Hoyte, S.M., 2010. Inhibition of Botrytis cinerea growth and suppression of botrytis bunch rot in grapes using chitosan. Plant Pathol. 59, 882–890. https://doi.org/10.1111/j.1365-3059.2010.02312.x

Rep, M., Duyvesteijn, R.G.E., Gale, L., Usgaard, T., Cornelissen, B.J.C., Ma, L.J., Ward, T.J., 2006. The presence of GC-AG introns in *Neurospora crassa* and other euascomycetes determined from analyses of complete genomes: Implications for automated gene prediction. Genomics 87, 338–347. https://doi.org/10.1016/j.ygeno.2005.11.014

Ribeiro, M.P., Espiga, A., Silva, D., Baptista, P., Henriques, J., Ferreira, C., Silva, J.C., Borges, J.P., Pires, E., Chaves, P., Correia, I.J., 2009. Development of a new chitosan hydrogel for wound dressing. Wound Repair Regen. 17, 817–824. https://doi.org/10.1111/j.1524-475X.2009.00538.x

Ribeiro, M.S., Paula, R.G. De, Voltan, A.R., Castro, R.G. De, Jos, L., Assis, D., Jos, C., Monteiro, V.N., 2019. *Trichoderma harzianum* Participates in Cell Wall Biogenesis but Is Not Essential for Antagonism Against Plant Pathogens. Biomolecules 9, 1–17. https://doi.org/10.3390/biom9120781

Ricard, C.S., Jakubowski, J.M., Verbsky, J.W., Alejandro Barbieri, M., Lewis, W.M., Esteban Fernandez, G., Vogel,

M., Tsou, C., Prasad, V., Stahl, P.D., Waksman, G., Cheney, C.M., 2001. *Drosophila* rab GDI mutants disrupt development but have normal rab membrane extraction. Genesis 31, 17–29. https://doi.org/10.1002/gene.10000

Rinaudo, M., 2006. Chitin and chitosan: Properties and applications. Prog. Polym. Sci. 31, 603–632. https://doi.org/10.1016/j.progpolymsci.2006.06.001

Robellet, X., Oestreicher, N., Guitton, A., Vélot, C., 2010. Gene silencing of transgenes inserted in the *Aspergillus nidulans alcM* and/or *alcS* loci. Curr Genet 56, 341–348. https://doi.org/10.1007/s00294-010-0303-5

Roberts, G.A.F., 1992. Chitin chemistry. Macmillan press, Ltd, London.

Rodríguez-Peña, J.M., Cid, V.J., Arroyo, J., Nombela, C., 2000a. A novel family of cell wall-related proteins regulated differently during the yeast life cycle. Mol. Cell. Biol. 20, 3245–3255. https://doi.org/10.1128/MCB.20.9.3245-3255.2000

Rodríguez-Peña, J.M., Cid, V.J., Arroyo, J., Nombela, C., Rodriguez-Pena, J.M., Cid, V.J., Arroyo, J., Nombela, C., 2000b. A novel family of cell wall-related proteins regulated differently during the yeast life cycle. Mol. Cell. Biol. 20, 3245–3255. https://doi.org/10.1128/MCB.20.9.3245-3255.2000

Rodriguez-Peña, J.M., Rodriguez, C., Alvarez, A., Nombela, C., Arroyo, J., 2002. Mechanisms for targeting of the *Saccharomyces cerevisiae* GPI-anchored cell wall protein Crh2p to polarised growth sites. J. Cell Sci. 115, 2549–58.

Rogg, L.E., Fortwendel, J.R., Juvvadi, P.R., Steinbach, W.J., 2012. Regulation of expression, activity and localization of fungal chitin synthases. Med. Mycol. 50, 2–17. https://doi.org/10.3109/13693786.2011.577104

Roncero, C., Duran, A., 1985. Effect of Calcofluor White and Congo red on fungal cell wall morphogenesis: In vivo activation of chitin polymerization. J. Bacteriol. 163, 1180–1185. https://doi.org/10.1128/jb.163.3.1180-1185.1985

RStudio: Integrated Development for R. RStudio, Inc., Boston, M., 2016. RStudio Team.

Rudall, K.M., Kenchington, W., 1973. THE CHITIN SYSTEM. Biol. Rev. 48, 597–633. https://doi.org/10.1111/j.1469-185x.1973.tb01570.x

Ruiz-Herrera, J., Ortiz-Castellanos, L., 2019. Cell wall glucans of fungi. A review. Cell Surf. 5, 100022. https://doi.org/10.1016/j.tcsw.2019.100022

Samalova, M., Mélida, H., Vilaplana, F., Bulone, V., Soanes, D.M., Talbot, N.J., Gurr, S.J., 2017. The β-1,3-glucanosyltransferases (Gels) affect the structure of the rice blast fungal cell wall during appressorium-mediated plant infection. Cell. Microbiol. 19. https://doi.org/10.1111/cmi.12659

Santos, B., Snyder, M., 1997. Targeting of chitin synthase 3 to polarized growth sites in yeast requires Chs5p and Myo2p. J. Cell Biol. 136, 95–110. https://doi.org/10.1083/jcb.136.1.95

Sarkari, P., Marx, H., Blumhoff, M.L., Mattanovich, D., Sauer, M., Steiger, M.G., 2017. An efficient tool for metabolic pathway construction and gene integration for *Aspergillus niger*. Bioresour. Technol. 245, 1327–1333.

Sburlati, A., Cabib, E., 1986. Chitin synthetase 2, a presumptive participant in septum formation in *Saccharomyces cerevisiae*. J. Biol. Chem. 261, 15147–15152.

Schachtschabel, D., Arentshorst, M., Lagendijk, E.L., Ram, A.F.J., 2012. Vacuolar H +-ATPase plays a key role in cell wall biosynthesis of *Aspergillus niger*. Fungal Genet. Biol. 49, 284–293. https://doi.org/10.1016/j.fgb.2011.12.008

Schachtschabel, D., Arentshorst, M., Nitsche, B.M., Morris, S., Nielsen, K.F., Hondel, C.A.M.J.J. Van Den, Klis, F.M., Ram, A.F.J., 2013. The Transcriptional Repressor TupA in *Aspergillus niger* Is Involved in Controlling Gene Expression Related to Cell Wall Biosynthesis, Development, and Nitrogen Source Availability. PLoS One 8, 1–15. https://doi.org/10.1371/journal.pone.0078102

Schalk I, Zeng K, Wu SK, Stura EA, Matteson J, et al. 1996. Structure and mutational analysis of Rab GDP-dissociation inhibitor. Nature 381(6577):42–48 http://doi.org/10.1038/381042a0

Schäpe, P., Kwon, M.J., Baumann, B., Gutschmann, B., Jung, S., Lenz, S., Nitsche, B., Paege, N., Schütze, T., Cairns, T.C., Meyer, V., 2019. Updating genome annotation for the microbial cell factory *Aspergillus niger* using gene co-expression networks. Nucleic Acids Res. 47, 559–569. https://doi.org/10.1093/nar/gky1183

Schindelin, J., Arganda-Carreras, I., Frise, E., Kaynig, V., Longair, M., Pietzsch, T., Preibisch, S., Rueden, C., Saalfeld, S., Schmid, B., Tinevez, J.-Y., White, D.J., Hartenstein, V., Eliceiri, K., Tomancak, P., Cardona, A., 2012. Fiji: an open-source platform for biological-image analysis. Nat. Methods 9, 676–682. https://doi.org/10.1038/nmeth.2019

Shen, K.-T., Chen, M.-H., Chan, H.-Y., Jeng, J.-H., Wang, Y.-J., 2009. Inhibitory effects of chitooligosaccharides on tumor growth and metastasis. Food Chem. Toxicol. 47, 1864–1871. https://doi.org/10.1016/J.FCT.2009.04.044

Sietsma, J.H., Wessels, J.G.H., 1979. Evidence for covalent linkages between chitin and β-glucan in a fungal wall. J. Gen. Microbiol. 114, 99–108. https://doi.org/10.1099/00221287-114-1-99

Smith, M.E., Henkel, T.W., Rollins, J.A., 2015. How many fungi make sclerotia? Fungal Ecol. 13, 211–220. https://doi.org/10.1016/j.funeco.2014.08.010

Soneson, C., Love, M.I., Robinson, M.D., 2016. Differential analyses for RNA-seq: Transcript-level estimates improve gene-level inferences [version 2; referees: 2 approved]. F1000Research 4. https://doi.org/10.12688/F1000RESEARCH.7563.2

Song, L., Ouedraogo, J.-P., Kolbusz, M., Nguyen, T.T.M., Tsang, A., 2018. Efficient genome editing using tRNA promoter-driven CRISPR/Cas9 gRNA in *Aspergillus niger*. PLoS One 13, e0202868. https://doi.org/10.1371/journal.pone.0202868

Sonnhammer, E.L., von Heijne, G., Krogh, A., 1998. A hidden Markov model for predicting transmembrane helices in protein sequences. Proc. Sixth Int. Conf. Intell. Syst. Mol. Biol. 6, 175–182.

Sopko, R., Huang, D., Preston, N., Chua, G., Papp, B., Kafadar, K., Snyder, M., Oliver, S.G., Cyert, M., Hughes, T.R., Boone, C., Andrews, B., 2006. Mapping Pathways and Phenotypes by Systematic Gene Overexpression. Mol. Cell 21, 319–330. https://doi.org/10.1016/J.MOLCEL.2005.12.011

Staab, J.F., Sundstrom, P., 2003. *URA3* as a selectable marker for disruption and virulence assessment of *Candida albicans* genes. Trends Microbiol. https://doi.org/10.1016/S0966-842X(02)00029-X

Swart, K., Debets, A.J.M., Slakhorst, M., Holub, E.F., Hoekstra, R.F., Bos, C.J., 2001. Genetic analysis in the asexual fungus *Aspergillus niger*. Acta Biol. Hung. 52, 335–343. https://doi.org/10.1556/ABiol.52.2001.2-3.18

Takai, R., Hasegawa, K., Kaku, H., Shibuya, N., Minami, E., 2001. Isolation and analysis of expression mechanisms of a rice gene, EL5, which shows structural similarity to ATL family from Arabidopsis, in response to N-acetylchitooligosaccharide elicitor. Plant Sci. 160, 577–583. https://doi.org/10.1016/S0168-9452(00)00390-3

Takaya, N., Yamazaki, D., Horiuchi, H., Ohta, A., Takagi, M., 1998. Cloning and characterization of a chitinase-encoding gene (chia) from *Aspergillus nidulans*, disruption of which decreases germination frequency and hyphal growth. Biosci. Biotechnol. Biochem. 62, 60–65. https://doi.org/10.1271/bbb.62.60

Te Biesebeke, R., Record, E., Van Biezen, N., Heerikhuisen, M., Franken, A., Punt, P.J., Van Den Hondel, C.A.M.J.J., 2005. Branching mutants of *Aspergillus oryzae* with improved amylase and protease production on solid substrates. Appl. Microbiol. Biotechnol. 69, 44–50. https://doi.org/10.1007/s00253-005-1968-4

Teertstra, W.R., Tegelaar, M., Dijksterhuis, J., Golovina, E.A., Ohm, R.A., Wösten, H.A.B., 2017. Maturation of conidia on conidiophores of *Aspergillus niger*. Fungal Genet. Biol. 98, 61–70. https://doi.org/10.1016/j.fgb.2016.12.005

Tefsen, B., Ram, A.F.J., Die, I. Van, Routier, F.H., 2012. Galactofuranose in eukaryotes: aspects of biosynthesis and functional impact. Glycobiology 22, 456–469. https://doi.org/10.1093/glycob/cwr144

Touchot, N., Chardin, P., Tavitian, A., 1987. Four additional members of the ras gene superfamily isolated by an oligonucleotide strategy: molecular cloning of YPT-related cDNAs from a rat brain library. Proc. Natl. Acad. Sci. U. S. A. 84, 8210–8214. https://doi.org/10.1073/pnas.84.23.8210

Trilla, J.A., Durán, A., Roncero, C., 1999. Chs7p, a new protein involved in the control of protein export from the endoplasmic reticulum that is specifically engaged in the regulation of chitin synthesis in *Saccharomyces cerevisiae*. J. Cell Biol. 145, 1153–1163. https://doi.org/10.1083/jcb.145.6.1153

Tsai, H.F., Wheeler, M.H., Chang, Y.C., Kwon-Chung, K.J., 1999. A developmentally regulated gene cluster involved in conidial pigment biosynthesis in *Aspergillus fumigatus*. J. Bacteriol. 181, 6469–77.

Ullrich, O., Stenmark, H., Alexandrov, K., Huber, L.A., Kaibuchi, K., Sasaki, T., Takai, Y., Zerial, M., 1993. Rab GDP dissociation inhibitor as a general regulator for the membrane association of rab proteins. J. Biol. Chem. 268, 18143–18150.

Utsunomiya, N., Kinai, H., Matsui, Y., Takebayashi, T., 1998. The Effects of Chitosan Oligosaccharides Soil Conditioner and Nitrogen Fertilizer on the Flowering and Fruit Growth of Purple Passionfruit (Passiflora edulis Sims var. edulis). J. Japanese Soc. Hortic. Sci. 67, 567–571. https://doi.org/10.2503/jjshs.67.567

Valdivia, R.H., Schekman, R., 2003. The yeasts Rho1p and Pkc1p regulate the transport of chitin synthase III (Chs3p) from internal stores to the plasma membrane. Proc. Natl. Acad. Sci. U. S. A. 100, 10287–10292. https://doi.org/10.1073/pnas.1834246100

Valiante, V., 2017. The cell wall integrity signaling pathway and its involvement in secondary metabolite production. J. Fungi. https://doi.org/10.3390/jof3040068

van Leeuwe, T.M., Arentshorst, M., Ernst, T., Alazi, E., Punt, P.J., Ram, A.F.J., 2019. Efficient marker free CRISPR/Cas9 genome editing for functional analysis of gene families in filamentous fungi. Fungal Biol. Biotechnol. 6, 13. https://doi.org/10.1186/s40694-019-0076-7

van Leeuwen, M.R., Krijgsheld, P., Bleichrodt, R., Menke, H., Stam, H., Stark, J., Wösten, H.A.B., Dijksterhuis, J., 2013. Germination of conidia of *Aspergillus niger* is accompanied by major changes in RNA profiles. Stud. Mycol. 74, 59–70. https://doi.org/10.3114/sim0009

van Munster, J.M., Nitsche, B.M., Akeroyd, M., Dijkhuizen, L., Van Der Maarel, M.J.E.C., Ram, A.F.J., 2015. Systems approaches to predict the functions of glycoside hydrolases during the life cycle of *Aspergillus niger* using developmental mutants *ΔbrlA* and *ΔflbA*. PLoS One 10. https://doi.org/10.1371/journal.pone.0116269

van Peij, N.N.M.E., Beishuizen, M., van de Vondervoort, P.J.I., 2014. Agse-deficient strain. WO2014013074A1.

Viborg, A.H., Terrapon, N., Lombard, V., Michel, G., Czjzek, M., Henrissat, B., Brumer, H., 2019. A subfamily roadmap of the evolutionarily diverse glycoside hydrolase family 16 (GH16). J. Biol. Chem. 294, 15973–15986. https://doi.org/10.1074/jbc.RA119.010619

Wagner, J., Escher, C. and Wolf, Dieter H. (1987), Some characteristics of hormone (pheromone) processing enzymes in yeast, FEBS Letters, 218, doi: 10.1016/0014-5793(87)81012-8

Walker, L.A., Gow, N.A.R., Munro, C.A., 2013. Elevated chitin content reduces the susceptibility of *Candida* species to caspofungin. Antimicrob. Agents Chemother. 57, 146–154. https://doi.org/10.1128/AAC.01486-12

Walker, L.A., Lee, K.K., Munro, C.A., Gow, N.A.R.R., 2015. Caspofungin treatment of *Aspergillus fumigatus* results in ChsG-dependent upregulation of chitin synthesis and the formation of chitin-rich microcolonies. Antimicrob. Agents Chemother. 59, 5932–5941. https://doi.org/10.1128/AAC.00862-15

Walker, L.A., Munro, C.A., De Bruijn, I., Lenardon, M.D., McKinnon, A., Gow, N.A.R., 2008. Stimulation of chitin synthesis rescues *Candida albicans* from echinocandins. PLoS Pathog. 4, e1000040. https://doi.

org/10.1371/journal.ppat.1000040

Wang, J., Zhou, H., Lu, H., Du, T., Luo, Y., Wilson, I.B.H., Jin, C., 2015. Kexin-like endoprotease KexB is required for N-glycan processing, morphogenesis and virulence in *Aspergillus fumigatus*. Fungal Genet. Biol. 76, 57–69. https://doi.org/10.1016/j.fgb.2015.02.006

Weastra, S.R.O., 2011. Determination of market potential for selected platform chemicals Itaconic acid, Succinic acid, 2,5-Furandicarboxylic acid.

Webb, G.C., Zhang, J., Garlow, S.J., Wesp, A., Riezman, H., Jones, E.W., 1997. Pep7p provides a novel protein that functions in vesicle-mediated transport between the yeast Golgi and endosome. Mol. Biol. Cell 8, 871–895. https://doi.org/10.1091/mbc.8.5.871

Wellington, M., Kabir, M.A., Rustchenko, E., 2006. 5-Fluoro-orotic acid induces chromosome alterations in genetically manipulated strains of *Candida albicans*. Mycologia 98, 393–398. https://doi.org/10.3852/mycologia.98.3.393

White, S.A., Farina, P.R., Fulton, I., 1979. Production and isolation of chitosan from Mucor rouxii. Appl. Environ. Microbiol. 38, 323–8.

Wickham, H., 2017a. Easily install and load the "Tidyverse." Cran-R.

Wickham, H., 2017b. ggplot2 - Elegant Graphics for Data Analysis | Hadley Wickham | Springer. https://doi.org/10.1007/978-0-387-98141-3

Wiellette, E.L., Harding, K.W., Mace, K.A., Ronshaugen, M.R., Wang, F.Y., McGinnis, W., 1999. spen encodes an RNP motif protein that interacts with Hox pathways to repress the development of head-like sclerites in the *Drosophila* trunk. Development 126, 5373–5385.

Wilcox, C.A., Fuller, R.S., 1991. Posttranslational processing of the prohormone-cleaving Kex2 protease in the *Saccharomyces cerevisiae* secretory pathway. J. Cell Biol. 115, 297–307. https://doi.org/10.1083/jcb.115.2.297

Wösten, H.A.B., van Veluw, G.J., de Bekker, C., Krijgsheld, P., 2013. Heterogeneity in the mycelium: implications for the use of fungi as cell factories. Biotechnol. Lett. 35, 1155–64. https://doi.org/10.1007/s10529-013-1210-x

Wu, X., Rossettini, A., Hanes, S.D., 2003. The *ESS1* prolyl isomerase and its suppressor *BYE1* interact with RNA pol II to inhibit transcription elongation in *Saccharomyces cerevisiae*. Genetics 165, 1687–1702.

Xing, K., Zhu, X., Peng, X., Qin, S., 2015. Chitosan antimicrobial and eliciting properties for pest control in agriculture: a review. Agron. Sustain. Dev. https://doi.org/10.1007/s13593-014-0252-3

Xu, G., Amicucci, M.J., Cheng, Z., Galermo, A.G., Lebrilla, C.B., 2018. Revisiting monosaccharide analysis-quantitation of a comprehensive set of monosaccharides using dynamic multiple reaction monitoring. Analyst 143, 200–207. https://doi.org/10.1039/c7an01530e

Yoshikawa, K., Tanaka, T., Ida, Y., Furusawa, C., Hirasawa, T., Shimizu, H., 2011. Comprehensive phenotypic analysis of single-gene deletion and overexpression strains of *Saccharomyces cerevisiae*. Yeast 28, 349–361. https://doi.org/10.1002/yea.1843

Yoshimi, A., Miyazawa, K., Abe, K., 2017. Function and biosynthesis of cell wall α-1,3-glucan in fungi. J. Fungi 3. https://doi.org/10.3390/jof3040063

Yoshimi, A., Sano, M., Inaba, A., Kokubun, Y., Fujioka, T., Mizutani, O., Hagiwara, D., Fujikawa, T., Nishimura, M., Yano, S., Kasahara, S., Shimizu, K., Yamaguchi, M., Kawakami, K., Abe, K., 2013. Functional Analysis of the α-1,3-Glucan Synthase Genes *agsA* and *agsB* in *Aspergillus nidulans*: AgsB Is the Major α-1,3-Glucan Synthase in This Fungus. PLoS One 8. https://doi.org/10.1371/journal.pone.0054893

Young, M.D., Wakefield, M.J., Smyth, G.K., Oshlack, A., 2010. Gene ontology analysis for RNA-seq: accounting for

selection bias. Genome Biol. 11, R14. https://doi.org/10.1186/gb-2010-11-2-r14

Yousuf, B., Qadri, O.S., Srivastava, A.K., 2018. Recent developments in shelf-life extension of fresh-cut fruits and vegetables by application of different edible coatings: A review. LWT - Food Sci. Technol. https://doi.org/10.1016/j.lwt.2017.10.051

Zeng, D., Luo, X., 2012. Physiological Effects of Chitosan Coating on Wheat Growth and Activities of Protective Enzyme with Drought Tolerance. Open J. Soil Sci. 02, 282–288. https://doi.org/10.4236/ojss.2012.23034

Zetsche, B., Gootenberg, J.S., Abudayyeh, O.O., Slaymaker, I.M., Makarova, K.S., Essletzbichler, P., Volz, S.E., Joung, J., Van Der Oost, J., Regev, A., Koonin, E. V., Zhang, F., 2015. Cpf1 Is a Single RNA-Guided Endonuclease of a Class 2 CRISPR-Cas System. Cell 163, 759–771. https://doi.org/10.1016/j.cell.2015.09.038

Zhang, Y., Ouyang, L., Nan, Y., Chu, J., 2019. Efficient gene deletion and replacement in *Aspergillus niger* by modified in vivo CRISPR/Cas9 systems. Bioresour. Bioprocess. 6. https://doi.org/10.1186/s40643-019-0239-7

Zheng, X., Zheng, P., Zhang, K., Cairns, T.C., Meyer, V., Sun, J., Ma, Y., 2019. 5S rRNA Promoter for Guide RNA Expression Enabled Highly Efficient CRISPR/Cas9 Genome Editing in *Aspergillus niger*. ACS Synth. Biol. 8, 1568–1574. https://doi.org/10.1021/acssynbio.7b00456

Ziani, K., Ursúa, B., Maté, J.I., 2010. Application of bioactive coatings based on chitosan for artichoke seed protection. Crop Prot. 29, 853–859. https://doi.org/10.1016/j.cropro.2010.03.002

Zou, P., Yang, X., Wang, J., Li, Y., Yu, H., Zhang, Y., Liu, G., 2016. Advances in characterisation and biological activities of chitosan and chitosan oligosaccharides. Food Chem. 190, 1174–1181. https://doi.org/10.1016/J.FOODCHEM.2015.06.076

Zune, Q., Delepierre, A., Gofflot, S., Bauwens, J., Twizere, J.C., Punt, P.J., Francis, F., Toye, D., Bawin, T., Delvigne, F., 2015. A fungal biofilm reactor based on metal structured packing improves the quality of a Gla::GFP fusion protein produced by *Aspergillus oryzae*. Appl. Microbiol. Biotechnol. 99, 6241–6254. https://doi.org/10.1007/s00253-015-6608-z

R

Summary

The use of filamentous fungi for the production of numerous products dates far back into human history. Common examples are fermentation of soy and milk. Their long-lived role throughout human history is still continues on to this day and has expanded to a formidable array of products. Products such as antibiotics, enzymes and preservative acids that are produced on a massive scale. Production on a massive scale means that fungi are cultivated in (an often) liquid medium, inside containers that are called fermenters. These fermenters hold tens of thousands of liters of both fungal biomass and a desired product that these fungi secrete. After the required product is harvested, the post-fermentation biomass is considered as waste; a spent tool that served a means to an end. Because a lot of energy is invested in the assimilation of biomass in order to produce the desired compound, discarding the spent biomass can be considered as a missed opportunity to recover valuable resources.

The Fungal Chitosan (FunChi) project set out to repurpose the spent biomass by investigating its potential for the stimulation of plant growth. A considerable portion of this spent biomass is the fungal cell wall and constitutes up to 80% of the biomass dry weight. Specifically, chitin (and its derivative chitosan) are parts of the cell wall that are of particular interest due to their wide range of applications. Among these applications is the possibility to stimulate the plant immune system Because chitin and chitosan naturally occur in cell walls of many fungi, plants have adapted to respond by activating their immune system to combat an impending infection when they are exposed to these compounds. Thus, cell walls from spent biomass of filamentous fungi can provide a natural plant defense-priming agent that is of natural origin. In order to make the use of fungal cell walls economically feasible, two main issues are to be considered: (i) what is the chitin yield for fungal biomass and can this be increased? (ii) Can the extractability of chitin from the fungal cell wall be enhanced (or be made cheaper) by removing chitin-to-cell wall linkages? The work described in this thesis has taken a fundamental approach to tackle both of these problems individually. To bridge the gap between fundamental science and industry, we have used the organism *Aspergillus niger* that is widely used in laboratory environments for fundamental work, but is also used in industrial settings for the production of numerous enzymes and citric acid.

The yield of chitin and chitosan in the cell wall of the wild type *A. niger* was found to be ~15% of the total biomass dry weight. In the attempt to find candidate strains that have an increased chitin fraction, cell wall mutants with a constitutive state of cell wall stress were screened. When a strain experiences a state of cell wall stress, many cell wall changes can occur, among which is the upregulation of chitin production. A collection of cell wall mutants was screened for an increase in cell wall chitin content. Two main candidates, RD15.4#55 and RD15.8#16, showed an increase in chitin content compared to wild type of ~35% and ~60%, respectively. The causative mutations have been identified for each strain individually (see **Chapter 4** and **Chapter 5),** using a combination of genome sequencing, the parasexual cross, and co-segregation analysis.

Following the abovementioned approach, mutant strain RD15.4#55 was found to have a C-terminal truncation of a previously unknown negative regulator of transcription. A gene deletion of the putative transcriptional repressor was not lethal, and resulted in the same cell wall chitin phenotype as the C-terminally truncated version in RD15.4#55, suggesting full loss of function. No previous studies have reported on this repressor in *A. niger*. Therefore, we named this gene *cwcA* (***c***ell ***w***all ***c***hitin A) after its cell wall chitin phenotype. (**Chapter 4**). Mutant strain RD15.8#16, with ~60% increased cell wall chitin content, was identified to contain an intronic mutation in the Rab GDP dissociation inhibitor A (*gdiA*) that resulted in lower amounts of correctly spliced transcript, in addition to an unspliced intron 2, and two versions of alternatively spliced transcript (**Chapter 5**). We also observed that a full knockout of *gdiA* is lethal. From our results, we deduced that the intronic mutation likely causes a Rab GTPase GTP/GDP cycle imbalance that either directly or indirectly leads to a in chitin deposition in the cell wall.

Next to employing a forward genetic screen, we also considered an existing deletion strain (*kexB*) for cell wall investigation due to its visibly thicker cell walls and prominent hyperbranching phenotype. The latter trait is of additional industrial interest as it reduces viscosity at high biomass densities, which may lead to both increased energy consumption and inconsistent production yields. Notably, a deletion of *kexB* showed strong transcriptional signs of cell wall stress and upregulation of a series of enzymes involved in chitin synthesis. These data were corroborated by a ~20% increase in cell wall chitin content compared to the wild type. However, the increase was found to be irrespective of the hyperbranching phenotype. It was further shown that a deletion of *kexB* showed phenotypic plasticity between pH 5 and pH 6, displaying a wild type like phenotype at pH 5 and a hyperbranching phenotype at pH 6, with a clear transitioning phenotype at pH 5.5 (**Chapter 6**).

In our attempts to enhance the extractability of chitin and chitosan from the cell wall of *A. niger*, we set out to delete the *crh* gene family that is considered to be responsible for facilitating the cross-link of chitin to β-1,3-glucan in the cell wall. Because *A. niger* contains seven *crh* gene family members, the knockout of all genes posed a practical constraint. We solved this by designing a marker free CRISPR/Cas9 gene editing system that allowed the accurate and efficient knockout of all seven gene members of the *crh* family (**Chapter 2**). In addition to showing this system's efficiency, concurrent *crh* gene knockout construction using existing auxotrophic marker selection recycling (*AOpyrG*) showed that these selection markers caused occasional false-positive phenotypes due to locus-dependent-side-effects of poor auxotrophic marker expression (**Chapter 2**).

The impact of deleting the *crh* gene family was, surprisingly, not visible on cell wall integrity; several cell wall disturbing compounds did not show an effect on growth which contrasts yeast literature. Growth rates of both wild type and the sevenfold *crh* mutant were also identical in controlled batch fermentations, as was the case on a transcriptional level. Fractionated cell walls neither showed differences in cell wall composition nor shifts in glucan and chitin (**Chapter 2** and **Chapter 3**). As such the *crh* genes appear dispensable, however we showed that the *crh* genes

are important when other cell wall components, such as galactomannan or α-glucan are absent. Interestingly, as α-glucan is absent in yeast, the discrepancy in effect of deleting the *crh* genes between yeast and *A. niger* may be explained by α-glucan. In line with our results, the lack of effect on the cell wall in absence of all *crh* genes has also been observed for *A. fumigatus*. Taken together, from these results we conclude that the interaction between chitin and α-glucan may play a pivotal role in anchoring chitin to the cell wall in addition to the chitin-β-1,3-glucan crosslinks of α-glucan containing filamentous fungi.

In addition to the results obtained in our research, we discuss alternative approaches to increase chitin production than the ones presented in this thesis. In relation to the FunChi project, the most important results and conclusions are discussed and ideas for future implementation are proposed (**Chapter 7**).

Nederlandse Samenvatting

Het gebruik van filamenteuze schimmels voor het maken van voedingsmiddelen is terug te vinden in de historie van de beschaafde wereld; bekende voorbeelden hiervan zijn de fermentatie van sojasaus en melk. Naast het feit dat deze technieken nog steeds worden toegepast, zijn de toepassingen van schimmels alleen nog maar verder gegroeid. Zo worden schimmels tegenwoordig gebruikt om een verscheidenheid aan producten te maken zoals antibiotica, enzymen en organische zuren, zoals citroenzuur. Deze producten worden op grote schaal geproduceerd wat inhoudt dat schimmels worden gekweekt in een (meestal) vloeibare voedingsbron. Containers die deze voedingsbron (meestal medium genoemd) en de schimmel bevatten, worden fermentoren genoemd en zijn bedoeld om de schimmelgroei zo optimaal mogelijk te maken. Deze fermentoren kunnen zeer omvangrijk zijn en bevatten soms wel tienduizenden liters medium. Nadat het benodigde product dat de schimmel produceert is geoogst, wordt de schimmelbiomassa na fermentatie als afval beschouwd; vanuit dit perspectief heeft de biomassa enkel als middel gediend om een doel te bereiken. Echter, omdat veel van de energie uit het medium wordt geïnvesteerd in de productie van biomassa, kan het weggooien van die biomassa worden beschouwd als een gemiste kans om waardevolle componenten terug te winnen.

Het Fungal Chitosan (FunChi)-project, waar dit promotieonderzoek een onderdeel van uitmaakt, is opgezet om te onderzoeken of de gebruikte biomassa nuttig kan worden gebruikt in plaats van weggegooid. Hierbij is onderzocht of bepaalde componenten van deze biomassa toe te passen zijn als natuurlijke gewassenbeschermingsmiddelen. De gebruikte biomassa bestaat voor een aanzienlijk deel uit de schimmelcelwand die tot wel 80% van het drooggewicht van de biomassa uitmaakt. Een belangrijk component van de celwand is chitine en zijn derivaat chitosan, twee polymeren die van bijzonder belang zijn vanwege toepassing om het immuunsysteem van planten te stimuleren. Chitine en chitosan komen van nature in celwanden voor van veel verschillende schimmels, en uit onderzoek is gebleken dat planten de aanwezigheid van schimmels detecteren via deze polymeren. Wanneer planten blootgesteld worden aan deze polymeren, reageren ze door hun immuunsysteem te activeren om zo een dreigende schimmelinfectie te bestrijden. Extracten van de celwanden uit gebruikte biomassa van filamenteuze schimmels zouden dus kunnen worden toegepast als activator om op een natuurlijke manier resistentie tegen schimmelinfecties op te roepen. Om het gebruik van celwanden van schimmels voor dit doel economisch haalbaar te maken, moeten twee hoofdpunten worden bekeken: (i) wat is de chitine-opbrengst uit schimmelbiomassa en kan deze worden verhoogd? (ii) Kan de extraheerbaarheid van chitine uit de schimmelcelwand worden verbeterd (of goedkoper gemaakt) door natuurlijke chitine-celwandverbindingen te verwijderen? Het werk dat in dit proefschrift wordt beschreven, heeft een fundamentele benadering gekozen om beide problemen afzonderlijk aan te pakken. Voor deze studie is het organisme *Aspergillus niger* gebruikt; een filamenteuze schimmel die veel wordt gebruikt in industriële omgevingen voor de productie van talrijke enzymen en citroenzuur,

maar ook in fundamenteel onderzoek van universitaire laboratoriumomgevingen wordt gebruikt.

De totale opbrengst aan chitine en chitosan in de celwand van het wildtype *A. niger* bleek ~15% van het celwanddrooggewicht te zijn. Om een *A. niger* stam te vinden die meer celwand chitine kan aanmaken, werden *A. niger* celwandmutanten—afkomstig uit eerder uitgevoerd onderzoek met een zogenaamde 'forward genetics screen'—met een constitutieve toestand van celwandstress nader onderzocht. Wanneer een stam een toestand van celwandstress ervaart, kunnen er veel celwandveranderingen optreden, waaronder de activatie van de chitineproductie. Een verzameling celwandmutanten werd zodanig gescreend op een toename van het celwandchitine-gehalte. Twee van deze celwandmutanten, RD15.4#55 en RD15.8#16, vertoonden een toename van het chitinegehalte vergeleken met wildtype van respectievelijk ~35% en ~60% (zie **Hoofdstuk 4** en **Hoofdstuk 5**). De verantwoordelijke mutaties voor dit fenotype zijn geïdentificeerd met behulp van genoomsequencing, parasexuele kruisingen en co-segregatieanalyse.

De stam RD15.4#55 bleek een C-terminaal deel te missen van een voorheen onbekende transcriptionele repressor, *cwcA*. Een complete deletie van deze vermeende transcriptionele repressor *cwcA* resulteerde in hetzelfde celwand-chitinefenotype als de C-terminaal ingekorte versie de transcriptionele repressor in RD15.4#55. Deze vondst wijst er dan ook op dat het missen van het C-terminale deel van *cwcA* leidt tot volledig functieverlies. Er zijn geen eerdere studies gerapporteerd over deze repressor in *A. niger* en wij hebben dit gen *cwcA* (*c*ell *w*all *c*hitin A) genoemd naar het celwand-chitinefenotype (**Hoofdstuk 4**). Van mutant RD15.8#16, met ~60% verhoogd chitinegehalte in de celwand werd vastgesteld dat het om een mutatie in de Rab GDP dissociation inhibitor A (*gdiA*) gaat. De gevonden mutatie, in het tweede intron van het *gdiA* gen, resulteerde zowel in lagere hoeveelheden van het correct geprocesste transcript als incorrecte trasnscripten (**Hoofdstuk 5**). Ook hebben wij gevonden dat een complete knock-out van *gdiA* niet levensvatbaar was. Uit deze resultaten concludeerden wij dat de mutatie in het tweede intron van *gdiA* waarschijnlijk leidt tot een te lage hoeveelheid actieve Rab GDP dissociation inhibitor. Dit heeft als gevolg dat er een onbalans is in de Rab GTPase GTP/GDP-cyclus die, ofwel direct ofwel indirect, leidt tot extra chitine-afzetting in de celwand.

Naast het gebruik van een forward genetics screen, werd ook een *kexB*-deletiestam meegenomen voor celwandonderzoek. Het gen *kexB* codeert voor het protease dat als functie dient om eiwitten in de cellulaire secretieroute te activeren. Verlies van dit eiwit resulteert bovendien in een fenotype met dikkere celwanden en prominente hyper-vertakking van de hyphen. Hyper-vertakking van hyphen kan de viscositeit verlagen bij hoge biomassadichtheden in fermentoren. Hoge viscositeit is normaliter onlosmakelijk verbonden aan de manier van filamenteuze groei en kan leiden tot zowel een hoger energieverbruik als inconsistente productieopbrengsten in schimmelfermentaties. Analyse van het transcriptoom van de *kexB*-deletie stam vertoonde sterke signalen van celwandstress, maar ook positieve activatie van genen die betrokken zijn bij de chitinesynthese. Deze toename in genexpressie was terug te vinden in de ~20% verhoging van het chitinegehalte in de celwand. Een verrassende vondst daarbij was dat de toename in celwand chitine onafhankelijk bleek van het hyper-vertakte fenotype. Dit hyper-vertakte fenotype van de

kexB-deletie stam was overigens alleen zichtbaar bij pH 6 en vertoonde fenotypische plasticiteit tussen pH 5 en pH 6. Bij pH 5 was het fenotype vrijwel identiek aan de wild type *A. niger* stam, terwijl bij pH 6 het hyper-vertakte fenotype duidelijk zichtbaar was (**Hoofdstuk 6**).

Om de extraheerbaarheid van chitine en chitosan uit de celwand van *A. niger* te verbeteren, hebben we ook onderzoek gedaan naar de rol van een familie van genen wordt verantwoordelijk geacht voor het faciliteren van de cross-link tussen chitine en β-1,3-glucaan in de celwand, de zogenaamde *crh*-genfamilie. Omdat *A. niger* zeven *crh*-genfamilieleden bezit, vormde het uitschakelen van alle genen een praktisch probleem. De oplossing diende zich aan door voor *A. niger* een methode van gen-editing op de zetten met behulp van CRISPR/Cas9. Deze methode is onafhankelijk van het gebruik van selectiemarkers om genen te inactiveren en wij hebben laten zien dat nauwkeurige en efficiënte uitschakeling van alle zeven gen-leden van de *crh*-familie mogelijk was (**Hoofdstuk 2**). Naast het aantonen van de efficiëntie van dit systeem, toonde parallel uitgevoerde uitschakeling van de *crh* genen aan—met behulp van bestaande auxotrofe markerselectierecycling—dat gebruik van de selectiemarker gebaseerde methode regelmatig vals-positieve fenotypen opleverden. Dit negatieve effect is hoogstwaarschijnlijk toe te wijzen aan locus-afhankelijke effecten van ontoereikende expressie van het auxotrofe selectiemarker gen (**Hoofdstuk 2**).

De impact van het verwijderen van de complete *crh*-genfamilie had verrassend genoeg geen noemenswaardig effect of de celwandsamenstelling en ook niet op de celwandintegriteit. In contrast met wat bekend is uit de literatuur voor (de aan schimmels verwante) gisten, veroorzaakten verschillende celwand-verstorende verbindingen geen ander effect op de groei van de mutant in vergelijking met het wildtype. De groeisnelheid voor zowel wildtype als de zevenvoudige *crh*-mutant was hetzelfde bij gecontroleerde batch-fermentaties en ook de mRNA transcriptiepatronen waren bijna identiek. Celwand fracties vertoonden geen verschillen in polymeer samenstelling zoals glucanen en chitine (**Hoofdstuk 2** en **Hoofdstuk 3**). Als zodanig lijken de *crh* genen dus verwerpelijk te zijn, maar we hebben toch kunnen laten zien dat de *crh* genen belangrijk zijn wanneer andere celwandcomponenten, zoals galactomannaan of α-glucaan afwezig zijn. Aangezien α-glucaan van nature afwezig is in gisten, zou de discrepantie in het effect van het verwijderen van de *crh* genen in gist en *A. niger* dus kunnen worden verklaard door de aan/afwezigheid van α-glucanen. Het ontbreken aan effect op de celwand bij het verwijderen van alle *crh* genen is ook waargenomen voor een andere schimmel, *A. fumigatus*. Dit ondersteunt onze resultaten verder dat er een verschil is tussen filamenteuze schimmels en gist wat betreft het belang van de *crh* genen voor celwandintegriteit. We veronderstellen dus dat in filamenteuze schimmels naast de chitine-β-1,3-glucaan-crosslinks ook de interactie tussen chitine en α-glucaan een cruciale rol kan spelen bij het verankeren van chitine aan de celwand.

Naast een overzicht van resultaten die we in ons onderzoek hebben verkregen, bespreken we in **Hoofdstuk 7** ook alternatieve benaderingen om de chitineproductie in schimmelcelwanden te verhogen. Met betrekking tot het FunChi-project worden de belangrijkste resultaten en conclusies besproken en worden ideeën voor toekomstige implementatie voorgesteld.

Curriculum Vitae

Tim Marijn van Leeuwe was born on the 2nd of February, 1990 in Haarlem, The Netherlands. After finishing high school with the minimum required grades in 2008, Tim took a break from any form of education to figure out what to do next. In 2009, after failing the tests to become an F-16 fighter pilot, he enrolled for the BSc Industrial Design at Delft University only to figure out that this was not his calling. Spurred-on by his unwillingness to work yet another year as a full-time HEMA employee, he enrolled for the bachelor program of Biology at Leiden university after some convincing words of Tonny Regensburg. Despite the initial interest in ecology and evolution, Tim soon developed his interest in molecular biology and microbiology. After studying abroad in Sweden during the final year of his bachelor degree, Tim enjoyed performing microbial research in the group of Dr. Bert van der Zaal under Dr. Martijn Rolloos' supervision. Following graduation in 2012, Tim assisted Tonny Regensburg during lab practicals for first year BSc Biology students at Leiden University. Next, a job at a probiotics company kept Tim busy for the next months before deciding to enroll for the MSc program Microbial Biotechnology and Health at Leiden University in 2013. During his first research internship, Tim combined his interest of evolution with microbiology in the group of Dr. Daniel Rozen. Tim's second internship was at the University of California, Berkeley in the group of Prof. N. Louise Glass, under supervision of Dr. Trevor Starr. This is where Tim discovered his fascination for filamentous fungi. It developed his determination and passion for research and he graduated *cum laude* in 2015. Six months later, at the start of 2016, Tim was offered a position as PhD student by Dr. Arthur Ram to work on the cell walls of the filamentous fungus *Aspergillus niger*. The work performed as a PhD student is described in this Thesis. After four successful publications during his contractual time and after having enjoyed the (research) environment during his PhD, Tim decided not to pursue an academic career. Instead, he has decided to explore other talents and skills in a different environment. As such, Tim is now enrolled in the military program to become a Fighter Controller for the Royal Netherlands Airforce.

Publications

van Leeuwe, T.M., Wattjes, J., Niehues, A., Forn-Cuni, G., Arentshorst, M., Geoffrion, N., Melida, H., Molina, A., Tsang, A., Meijer, A.H., Moerschbacher, B.M., Punt, P.J., Ram A.F.J., A seven-membered cell wall related transglycosylase gene family in *Aspergillus niger* is relevant for cell wall integrity in cell wall mutants with reduced α-glucan or galactomannan. The Cell Surface (2020). *In press.* doi: 10.1016/j.tcsw.2020.100039

van Leeuwe, T.M., Arentshorst, M., Punt, P.J., Ram A.F.J., Interrogation of the cell wall integrity pathway in *Aspergillus niger* identifies a putative negative regulator in transcription involved in chitin deposition. (2020) Gene X 5, 100028. doi: 10.1016/j.gene.2020.100028

van Leeuwe, T.M., Gerritsen A., Arentshorst, M., Punt, P.J., Ram A.F.J., Rab GDP-dissociation inhibitor *gdiA* is an essential gene required for chitin deposition in *Aspergillus niger.* (2020) Fungal Genet. Biol. 136, 103319. doi:10.1016/j.fgb.2019.103319

van Leeuwe, T.M., Arentshorst, M., Ernst, T. Alazi, E., Punt, P.J., Ram, A.F.J., Efficient marker free CRISPR/Cas9 genome editing for functional analysis of gene families in filamentous fungi. Fungal Biol Biotechnol 6, 13 (2019) doi: 10.1186/s40694-019-0076-7

Westhoff S*, **van Leeuwe T.M.***, Qachach O, Zhang Z, van Wezel GP, Rozen DE. The evolution of no-cost resistance at sub-MIC concentrations of streptomycin in *Streptomyces coelicolor.* ISME J. 2017;11(5):1168–1178. doi: 10.1038/ismej.2016.194

*Authors contributed equally